







Maastricht University

universiteit  
▶▶ hasselt

2014 | Faculty of Medicine and Life Sciences

DOCTORAL DISSERTATION

# Development of a suitable bioreceptor for C-reactive protein: Aptamer selection, validation & sensor development

Doctoral dissertation submitted to obtain the degree of doctor  
of Biomedical Science, to be defended by:

**Jeroen Vanbrabant**

Promoter: Prof. Dr Luc Michiels

Co-promoter: Dr Veronique Vermeeren

D/2014/2451/36

universiteit  
▶▶ hasselt

BIOMED  
BIOMEDISCH  
ONDERZOEKINSTITUUT



Dissertation presented in fulfillment of the requirements for the degree of Doctor in Biomedical Science.

Member of the Jury:

Prof. Dr. Ivo Lambrechts, chair

Prof. Dr. Luc Michiels, promotor  
Dr. Veronique Vermeeren, co-promotor

Prof. Dr. Patrick Wagner  
Prof. Dr. Veerle Somers  
Prof. Dr. Marcel Ameloot  
Prof dr. Aye Mu Myint (Maastricht University)  
Prof. Dr. Jeroen Lammertyn (KU Leuven)  
Prof. Dr. Peter Dubrueel (Ugent)

June 2014



"Most people think of nucleic acids as information holders, not globular things like proteins...what our work proved is that when you do SELEX...you get molecules that, even though they're chemically made out of nucleic acid, are more like proteins than nucleic acids"

Dr. Larry Gold

## Preface

This is it; the result of 4 years research in the exciting world of biosensors. It has been a wonderful exploration for me, as this work has learnt me that there is still a lot to be learned about these interesting pieces of technology that biosensors are.

This work would not have been possible without the help of several people. I have got a tremendous amount of opportunities from my supervisor, Luc Michiels. You have provided me with ideas and with real hands-on experience of state-of-the-art technologies. Thank you for the chances you have given and still give me.

To my former colleagues of the biosensor-club, Katrijn, Nathalie, Evi, Lotte, Karolien, Veronique and Kaushik, thank you for the nice atmosphere and good scientific discussions we have had. In good and bad times, I think we have managed well as a team.

I would also like to thank colleagues of other research groups for their efforts in our collaborations. Bart, Bram, Mohammed and Patrick from IMO, thank you for your help on the  $R_{Th}$  set-up and for providing me with NCD-samples. Marcel and Nick, your efforts on the fluorescence measurements have not passed unnoticed. My gratitude also goes out to the colleagues in Leuven from the MeBioS Lab. Jeroen, Dragana, Kris and Karen, thank you for sharing your expertise with me.

It is the last straw that breaks the camel's back. Therefore I would like to thank all my new colleagues at PharmaDiagnostics NV. You have given me extra motivation to end this thesis and have renewed my enthusiasm with your passion for nano.

The manuscript of this thesis has substantially improved by the useful comments of the jury. Thank you for your thorough reading and good suggestions.

Last but definitely not least, I would like to thank my parents for always listening and providing me with the opportunities that I have got and off course my girlfriend Floor for being a true fellow traveler along this journey, for listening, for your love and for helping me where-ever you could.



## **Abstract**

Not many research areas are as evolving as biosensor research. Started in the fifties, it is now expanded to a technology-driven, multidisciplinary field with large impact on society and hence commercial interest. A myriad of applications exists for a device that very specifically and sensitively measures the presence and concentration of a target molecule of choice, e.g. in environmental monitoring (contaminants, pesticides), food analysis (pathogens, antibiotics) and especially in healthcare. Diagnostics of disease specific markers is one of the main but not the only application in the field of medicine. High-end technologies deliver biosensor devices that measure the interaction of bioreceptors or biomolecules of choice with other analytes in very high detail. These technologies provide information on affinity and moreover, on the rate of interaction. Therefore, therapeutic applications as biological activity evaluation of drugs, protein-DNA or protein-protein interactions and compound screening for new drug development have increased the performance of this research field even more.

Biosensors are true examples of the multidisciplinary approach: a biological target binding element (molecular biology) on a binding signal transducing material (physics and chemistry) and the resulting biochemical or biophysical signal that is translated to a quantifiable value (engineering). The research presented in this dissertation is focused on the biological receptor element of the biosensor and on one type in particular: aptamers or selected synthetic DNA that binds very specifically to a target of choice.

This dissertation starts at the onset of the development of a new biosensing application, the selection procedure. Suitable aptamers are selected that bind C-reactive protein (CRP), an acute-phase protein and inflammation marker. By performing a selected and optimized SELEX procedure (Systematic Evolution of Ligands by Exponential Enrichment) nanomolar affinity aptamer candidates are selected and pitfalls of the SELEX selection procedure are addressed. By increasing the number of negative selection steps, reducing the number of amplification cycles and addition of non-specific single-stranded DNA (ssDNA), frequently encountered problems as non-specific binding and introduction of amplification bias are untangled. The research presented shows it is of utter importance to carefully monitor and test the applied selection conditions (target immobilization procedure, buffer compositions and applied SELEX design), preferably by different methods. An interesting tool for monitoring the selection progress is explored in this dissertation. By performing remelting curve analysis

(rMCA) on the selection pools of three different SELEX set-ups, the method is proven to be very useful for monitoring SELEX conditions and dynamics in the DNA selection pool. By applying the real-time DNA amplification analysis as suggested here, the SELEX procedure and conditions are tailored in more detail, monitored and made more efficient.

Detailed binding analysis of the selected aptamers is performed on different platforms, ranging from standard immunosorbent-like techniques to high-end instrumentations such as surface plasmon resonance (SPR) analysis. This has shown high affinity (nanomolar) of the aptamers for CRP when applied as they were selected: unmodified with reporter molecules and in solution over the target. This proves aptamer functionality but also the high demands aptamers have for the proper binding conditions. This limits the versatility of the selected bioreceptors and the possible biosensor designs using this receptor to label-free homogeneous assays. The experiments performed on different read-out systems show that it is possible to optimize the aptamer functionality after the SELEX procedure with detailed binding condition optimizations on highly informative read-out systems as SPR. More ideally, aptamer versatility and flexible functionality is obtained during the selection procedure, by changing the selection conditions or by modifying a priori part of the selection library.

The selected aptamers for CRP and another well validated aptamer sequence for thrombin are also used in this dissertation to test the applicability of aptamers in a recently developed read-out platform. This new platform measures the change in heat-transfer resistance over a solid-liquid interface when the binding event takes place on that interface. The experiments performed here show that the binding of the target or the selected aptamers does not result in a measurable insulation signal change in the prototype set-up. Nevertheless, indications from the work with DNA hybridization and denaturation show that target induced strand displacement is an interesting option to get this read-out system operational for aptamer applications.

## Samenvatting

Niet veel onderzoeksgebieden zijn zo snel evoluerend als biosensoronderzoek, begonnen in de jaren vijftig en uitgegroeid tot een technologie-gedreven, multidisciplinair onderzoeksveld met grote impact op de maatschappij en dus met commercieel belang. Vele toepassingen zijn mogelijk voor een instrument dat de aanwezigheid en concentratie van een relevant molecuule zeer specifiek en nauwkeurig meet, bijvoorbeeld in milieuonderzoek (vervuiling, pesticiden), in voedselanalyse (pathogenen, antibiotica) en vooral in de gezondheidszorg. Diagnose van ziekte-specifieke merkers is één van de belangrijkste maar niet de enige toepassing in de geneeskunde. Hoogtechnologische instrumenten meten zeer gedetailleerd de interactie tussen biomoleculen, met informatie over de sterkte of affiniteit en de snelheid van de binding. Daarom hebben therapeutische toepassingen zoals de evaluatie van de biologische activiteit van geneesmiddelen, eiwit - DNA of eiwit - eiwitinteracties en drug screening voor de ontwikkeling van nieuwe geneesmiddelen de performantie van dit onderzoeksgebied nog doen toenemen.

Biosensoren zijn echte voorbeelden van een multidisciplinaire aanpak: een biologische receptor of bindend element (moleculaire biologie) op een signaal geleidend materiaal (fysica/chemie) en het daaruit voortvloeiende biochemische of biofysische signaal dat wordt gemeten en vertaald naar een meetbare waarde (ingenieurswetenschappen). Het in dit proefschrift beschreven onderzoek is gericht op het biologische receptorelement van de biosensor en op één type in het bijzonder: aptameren of geselecteerd synthetisch gemaakt DNA dat zeer specifiek bindt op een doelwitmolecuule naar keuze.

Dit proefschrift begint bij de start van de ontwikkeling van een nieuwe biosensortoepassing, de selectieprocedure. Geschikte aptameren worden geselecteerd die C - reactief proteïne (CRP) binden, een acute - fase eiwit en tevens een merker voor ontsteking en hartfalen. Door het uitvoeren van een geoptimaliseerde SELEX (Systematic Evolution of Ligands by Exponential Enrichment) procedure voor enkelstrengig DNA (ssDNA), worden aptamer kandidaten met hoge affiniteit voor CRP geselecteerd en worden mogelijke problemen en valkuilen van de SELEX procedure behandeld. Door het opvoeren van het aantal negatieve selectiestappen, een daling van het aantal amplificatiecycli en de toevoeging van niet-specifieke ssDNA worden vaak voorkomende problemen als niet - specifieke binding en het invoeren van amplificatieartefacten aangepakt. Het hier gepresenteerde onderzoek toont aan dat het van het grootste belang is om de toegepaste selectiecondities (immobilisatieprocedure van het target molecuule, buffercomposities en het ontwerp van de SELEX procedure) zorgvuldig te controleren en testen, bij voorkeur door verschillende methoden. Een interessante methode voor het

opvolgen van de voortgang van de aptameerselectie wordt voorgesteld in dit proefschrift. Door het uitvoeren van de zogenaamde dubbele smeltcurveanalyse op de selectiepools van drie onafhankelijke SELEX procedures voor verschillende targets, is deze methode zeer nuttig gebleken voor het monitoren van selectiecondities en van de dynamiek in de verschillende selectiepools. Door het toepassen van de real-time DNA amplificatieanalyse zoals ze hier wordt voorgesteld, kan de selectiecondities en - procedure in meer detail worden geoptimaliseerd en efficiënter worden gemaakt.

Gedetailleerde bindingsanalyse van de geselecteerde aptameren wordt uitgevoerd op verschillende uitleesplatformen, variërend van standaard immunosorbent-achtige technieken tot hoogtechnologische instrumentatie zoals surface plasmon resonance (SPR) analyse. Hieruit blijkt een hoge affiniteit (nanomolair) van de aptameren voor CRP, indien ze worden toegepast zoals ze zijn geselecteerd: niet gewijzigd met reporter-moleculen en in oplossing gemeten. Dit illustreert de functionaliteit van de geselecteerde aptameren, maar ook de hoge eisen die de aptameren stellen voor de juiste bindingscondities. Hierdoor zijn de veelzijdigheid van de geselecteerde bioreceptoren en eventuele toepassingen met deze receptor beperkt tot labelvrije, homogene tests. De experimenten uitgevoerd op verschillende uitleessystemen laten zien dat het mogelijk is om de functionaliteit van aptameren te optimaliseren na voltooiing van de SELEX procedure, met behulp van zeer gedetailleerde en informatieve systemen zoals SPR. Idealiter wordt de veelzijdigheid en flexibele functionaliteit van de aptameren al verkregen tijdens de selectieprocedure zelf, door het afwisselen van selectiecondities of door het vooraf wijzigen van de DNA selectiebibliotheek.

De geselecteerde aptameren voor CRP en een ander goed beschreven aptameer voor thrombine worden gebruikt om de toepasbaarheid van aptameren te testen in een nieuw ontwikkeld uitleesplatform. Dit toestel meet de verandering in de weerstand van warmteoverdracht ofwel isolatie over een interface van vaste stof naar een vloeistof in een meetcel, wanneer binding van het biologisch target molecule plaatsvindt op deze interface. De uitgevoerde experimenten tonen aan dat de binding van het target molecule of van de geselecteerde aptameren op de interface niet leidt tot een meetbare verandering van de isolatie in dit prototype instrument. Toch duiden verschillende aanwijzingen uit DNA denaturatie-experimenten erop dat zogenaamde displacement assays, waarbij een dubbelstrengige aptameer sequentie enkelstrengig wordt onder invloed van het target, een interessante optie zijn om dit toestel operationeel te krijgen met aptameren.

## Abbreviations

AES	aptameric enzyme sub-unit
ALISA	aptamer-linked immobilized sorbent assay
AMD	age-related macular degeneration
AP	alkaline phosphatase
AptaBID	aptamer-facilitated biomarker discovery
ATP	adenosine tri phosphate
BMI	body mass index
BSA	bovine serum albumin
Bp	base pairs
CRP	C-reactive protein
CE	capillary electrophoresis
cDNA	complementary deoxyribonucleic acid
C <sub>t</sub>	threshold cycle value (number of qPCR cycles that are performed before a threshold fluorescence value is measured in qPCR analysis)
Da	Dalton
dCRP	decameric form of CRP
-dF/dT	First negative derivative of fluorescence (F), generated by SYBR Green in real-time PCR analysis. This denotes the decrease in Fluorescence or dsDNA melting or denaturation with increasing temperature (T) during real-time PCR analysis.
DiStRO	diversity standard of random oligonucleotides

DNA	deoxyribonucleic acid
dsDNA	double-stranded DNA
DPV	differential pulse voltammetry
ECEEM	equilibrium capillary electrophoresis of equilibrium mixtures
ECL	electrogenerated chemiluminescence
EDC	1-ethyl-3-(3-dimethylaminopropyl)carbodiimide
EDTA	ethylenediaminetetraacetic acid
EIS	electrochemical impedance spectroscopy
ELAA	enzyme-linked aptamer assay
ELAST	ELISA amplification system
ELISA	enzyme-linked immunosorbent assay
ELONA	enzyme-linked oligonucleotide assay
EMSA	electrophoretic mobility shift assay
F	fluorescence, generated by SYBR Green in real-time PCR measurements
Fab	fragment antigen-binding
FAM	6-carboxyfluorescein
FDA	Food and Drug Administration
FIS	faradic impedance spectroscopy
FITC	fluorescein isothiocyanate
FO-SPR	fiber-optic surface plasmon resonance
FRET	fluorescence resonance energy transfer

GE	gel electrophoresis
h	hours
HBS	4-(2-hydroxyethyl)-1-piperazineethanesulfonic acid buffered saline
HEPES	4-(2-hydroxyethyl)-1-piperazineethanesulfonic acid
HER3	human epidermal growth factor receptor 3
HRP	horse radish peroxidase
HS-ssDNA	herring sperm single stranded DNA
IL-1	Interleukin 1
IL-6	Interleukin 6
$K_a$	equilibrium association constant
$K_d$	equilibrium dissociation constant
$k_a$	association rate constant
$k_d$	dissociation rate constant
kDa	kilo Dalton
LBA	lysozyme binding aptamer
LSPR	localized surface plasmon resonance
mAB	monoclonal antibody
MCA	melting curve analysis
MES	2-(N-morpholino)ethanesulfonic acid
min	minutes

MIP	molecular imprinted polymer
mRNA	messenger ribonucleic acid
mCRP	monomeric C-reactive protein
NCD	nanocrystalline diamond
NDA	neutralizer displacement assays
NECEEM	non-equilibrium capillary electrophoresis of equilibrium mixtures
NGS	next-generation sequencing
NHS	N-hydroxyl succinimide ester
NP-EMSA	nanoparticle-based electrophoretic mobility shift assay
NSB	non-specific binding
Nt	nucleotides
OD	optical density @ certain wavelength
PAGE	polyacrylamide gel electrophoresis
PBS	phosphate buffered saline
PCR	polymerase chain reaction
pCRP	pentameric C-reactive protein
PEG	poly-ethylene glycol
pI	isoelectric point
pKa	acid dissociation constant
PLA	proximity ligation assay
PRR	pattern recognition receptor



qPCR	quantitative polymerase chain reaction
$R_{Th}$	heat-transfer resistance
rMCA	remelting curve analysis
RNA	ribonucleic acid
Rpm	rotations per minute
RT-PCR	real-time polymerase chain reaction
RU	response units
s	seconds
SA	streptavidin
SAM	self-assembled monolayer
SDS	sodium dodecyl sulfate
SELEX	systematic evolution of ligands by exponential enrichment
SI	silica
SNP	single nucleotide polymorphism
SPR	surface plasmon resonance
SPRi	surface plasmon resonance imaging
SSC	sodium chloride/sodium citrate
ssDNA	single-stranded DNA
$T_a$	annealing temperature
$T_m$	melting temperature
TAE	Tris acetate EDTA
TBA	thrombin binding aptamer

TEG	tetra-ethylene glycol
TGK	Tris glycine potassium phosphate
TID	target-induced dissociation / displacement mode
TISS	target-induced structure switching mode
TMB	3,3',5,5'-tetramethylbenzidine
TNF	tumor necrosis factor
UV	ultraviolet
VGEF	vascular endothelial growth factor

## Table of Contents

<b>Abstract</b> .....	<b>iii</b>
<b>Abbreviations</b> .....	<b>vii</b>
<b>Contents</b> .....	<b>xiii</b>
<b>1. General introduction</b> .....	<b>1</b>
<b>1.1. Biosensors and their applications</b> .....	<b>1</b>
<b>1.2. Promising bio-receptors: aptamers</b> .....	<b>4</b>
<b>1.3. SELEX – Darwinian selection of high affinity oligonucleotides</b> .....	<b>10</b>
1.3.1. SELEX step 1: DNA library and target incubation and binding .....	11
1.3.2. SELEX step 2: relevant binder separation .....	11
1.3.3. SELEX step 3: relevant binder amplification .....	11
1.3.4. SELEX step 4: conditioning for the next selection round	12
<b>1.4. Aptamer characterization: binding studies and affinity analysis</b> .....	<b>15</b>
1.4.1. Aptamer binding interaction mechanisms .....	15
1.4.2. Affinity and kinetic analysis of binding interactions .....	16
1.4.3. Binding assays for affinity and kinetic analysis .....	18
<b>1.5. Application of aptamers in aptasensors</b> .....	<b>21</b>
1.5.1. Immunosorbent-like assays: ELAA and ALISA .....	21
1.5.2. PCR assays .....	22
1.5.3. Fluorescence assays .....	23
1.5.4. Electrochemical assays.....	24
1.5.5. Surface plasmon resonance .....	25
1.5.6. Application of aptamers in aptasensors .....	26
<b>1.6. Aims and objectives of this thesis</b> .....	<b>28</b>

## **2. Modified SELEX procedure for CRP aptamer selection ..... 31**

<b>2.1.</b>	<b>Introduction</b> .....	<b>31</b>
	2.1.1. Target properties and characteristics.....	31
	2.1.2. Optimizing the SELEX protocol for pCRP selection .....	34
<b>2.2.</b>	<b>Experimental section</b> .....	<b>36</b>
	2.2.1. ssDNA library construction and amplification .....	36
	2.2.2. Target immobilization .....	37
	2.2.3. General SELEX design .....	38
	2.2.4. Cloning and sequencing .....	38
<b>2.3.</b>	<b>Results &amp; discussion</b> .....	<b>39</b>
	2.3.1. SELEX design optimizations.....	39
	2.3.2. Sequence and structure analysis of selected aptamer candidates .....	44
<b>2.4.</b>	<b>Conclusions and recommendations</b> .....	<b>48</b>

## **3. reMelting Curve Analysis as a tool for enrichment monitoring in the SELEX process ..... 51**

<b>3.1.</b>	<b>Introduction</b> .....	<b>51</b>
<b>3.2.</b>	<b>Experimental section</b> .....	<b>54</b>
	3.2.1. Enrichment simulation in random starting libraries.....	54
	3.2.2. Plate SELEX for CRP aptamers .....	54
	3.2.3. Bead SELEX for 17 $\beta$ -estradiol aptamers.....	55
	3.2.4. CE-SELEX for peptide X aptamers .....	55
<b>3.3.</b>	<b>Results &amp; discussion</b> .....	<b>56</b>
	3.3.1. reMelting Curve Analysis after short reannealing (rMCA) .....	56
	3.3.2. rMCA analysis of simulated enrichment.....	57
	3.3.3. rMCA of different SELEX procedures - general applicability.....	59

3.3.4.	Optimizing and monitoring the SELEX progress – SELEX design and contamination detection .....	67
3.3.5.	Importance of DNA quantity for rMCA.....	68
<b>3.4.</b>	<b>Conclusions and future prospects .....</b>	<b>69</b>
<b>4.</b>	<b>Binding assays for selected aptamers .....</b>	<b>71</b>
<b>4.1.</b>	<b>Introduction .....</b>	<b>71</b>
<b>4.2.</b>	<b>Experimental section .....</b>	<b>77</b>
4.2.1.	Modified aptamer sequences for immobilization and detection .....	77
4.2.2.	Sandwich assays: ALISA and ELAA.....	77
4.2.3.	Quantitative PCR assays .....	79
4.2.4.	Fluorescence assays.....	79
4.2.5.	Surface Plasmon Resonance .....	79
<b>4.3.</b>	<b>Results and discussion .....</b>	<b>81</b>
4.3.1.	Sandwich assays: ALISA and ELAA.....	81
4.3.2.	Quantitative PCR assays .....	83
4.3.3.	Fluorescence microscopy .....	84
4.3.4.	Surface Plasmon Resonance.....	85
<b>4.4.</b>	<b>Conclusions and future recommendations .....</b>	<b>95</b>
<b>5.</b>	<b>Application of aptamers in a new label-free read-out system .....</b>	<b>97</b>
<b>5.1.</b>	<b>Introduction .....</b>	<b>97</b>
<b>5.2.</b>	<b>Experimental section .....</b>	<b>100</b>
5.2.1.	Design of the sensor cell and the thermal read-out system .....	100
5.2.2.	Aptamer immobilization and direct CRP binding detection .....	101
5.2.3.	Aptamer immobilization, target binding and detection of conformational changes at increasing temperature.....	102

5.2.4.	CRP capture and aptamer binding detection .....	104
<b>5.3.</b>	<b>Results and discussion .....</b>	<b>106</b>
5.3.1.	Direct detection of the CRP binding event by heat-transfer resistance measurements .....	106
5.3.2.	Aptamer immobilization, target binding and detection of conformational changes at increasing temperature.....	109
5.3.3.	CRP capture and aptamer binding detection .....	111
<b>5.4.</b>	<b>Conclusions and future recommendations .....</b>	<b>120</b>
<b>6.</b>	<b>General discussion, conclusions and perspectives .....</b>	<b>123</b>
6.1.	Synopsis .....	123
6.2.	Future considerations and perspectives .....	125
	<b>References .....</b>	<b>131</b>
	<b>Appendix A: Figures .....</b>	<b>143</b>
	<b>Appendix B: Buffer and reagent list .....</b>	<b>153</b>







# 1

## General introduction

*In this chapter, biosensors and aptamers are defined and the numerous possibilities for future applications are illustrated. General aptamer selection protocols and validation assays are introduced as some difficulties of aptasensor applications are explained. To end this introduction, the objectives and a structural overview of this dissertation are presented.*

### 1.1. Biosensors and their applications

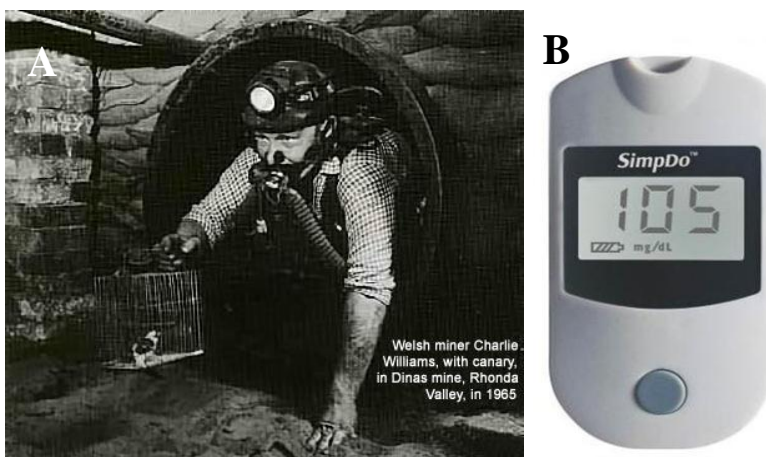


**Fig. 1.1. (A) Most probably one of the first biosensors in use: canaries in the mines as warning systems for oxygen depletion (B) Biosensors today: the SimpDo™ blood glucose monitoring system shows fast and accurate glucose level results in less than 10 seconds (Rapha Diagnostics®)**

In this introducing chapter, the omnipresence of biosensors in our daily life is illustrated. The term biosensor is broadly defined and then concretized in more specific examples and applications of biosensors. The general definition of biosensors was firstly described in Turner *et al.* (1987) as "a compact analytical device incorporating a biological/biologically derived sensing element with a

physicochemical transducer. The usual aim of a biosensor is to produce either discrete or continuous digital electronic signals which are proportional to a single analyte or a related group of analytes. "

In other words, a biosensor consists of two crucial elements in spatial proximity; a biological recognition element or receptor, able to interact with a specific target, and a transducing element, converting the recognition event to a measurable signal (Fig. 1.2). In a biosensor, this signal is then processed by associated electronics or signal processors for the display of the results in a user-friendly way. Biosensors are a special case of bioassays, since the detection and analysis of interaction is possible at the moment this takes place, without any extra procedures or handling. This characteristic makes biosensors attractive devices for real-time, portable diagnostic applications or so called point-of-care devices (Kumar & Arrowsmith, 2006).

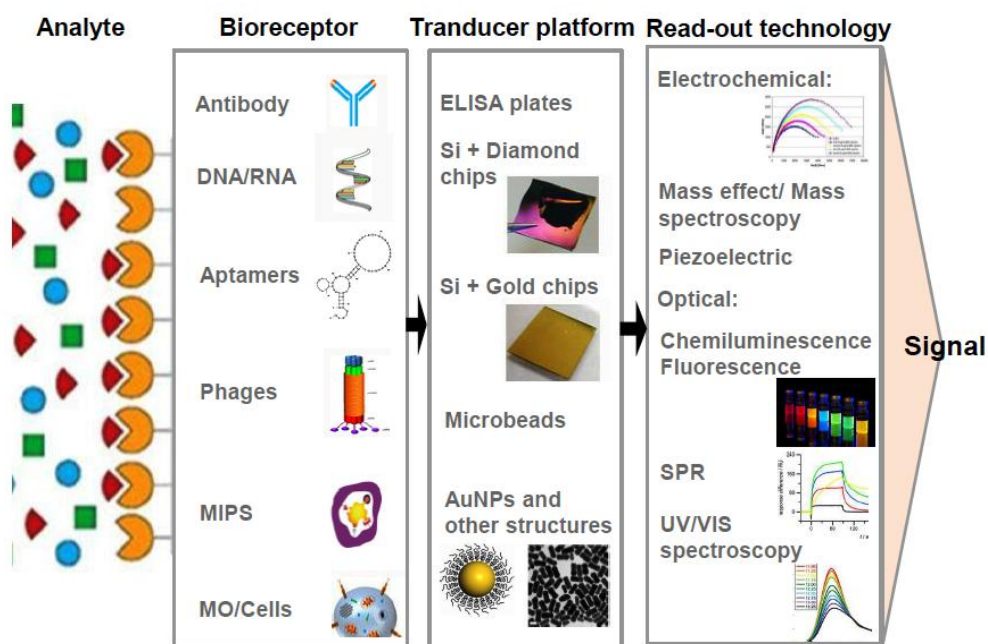


**Fig. 1.2. General scheme of a biosensor design. (Adapted from Scheller et al., 2001)**

Alcohol- and drug tests, pregnancy tests and point-of-care measuring devices such as blood glucose meters are only few of the many illustrations of the applications and performance of biosensors in many fields;

*Healthcare* (Vo-Dinh & Cullum, 2000): Monitoring of health-relevant targets and markers in cells, tissues and body fluids (e.g. glucose sensor) is important for disease treatment and evaluation. Biomarker diagnostics and disease-specific

identification of markers allows disease detection and risk assessment. Moreover, detailed interaction analysis of metabolites and chemical compounds with disease-related molecules is used in therapeutics for drug screening and biological activity evaluation.

*Environment* (Rodriguez-Mozaz *et al.*, 2004a): Detection of pesticides, water contaminants and pathogens allows environmental monitoring and risk assessment. Detection of toxic metabolites before and after bioremediation is used to evaluate remediation efficiency in polluted industrial sites and river shores.

*Security and food analysis* (Serna-Cock & Perenguez-Verdugo, 2011): Detection of pathogens and toxic substances is important for security reasons in harbors, airports and mail order services. Remote sensing of bacteria, drugs, toxins, explosives and even people is globally applied by the custom services of all countries. Detection and identification of drug residues, antibiotics, allergens and growth promoters in food analysis is used to control the food producing industries. Moreover, redox sensors and bacterial detection protects the consumers against health risks of degenerated food.

The broad range of biosensors can be classified according to the signal transduction modes or to the target recognition elements or receptors (Rodriguez-Mozaz *et al.*, 2004b) (Table 1.1). The selective receptors are coupled to a transducing element, translating the binding event to a measurable signal, processed in a specified read-out platform.

**Table 1.1. Biosensor types classified according to the method of signal transduction and according to the biorecognition element or bioreceptor.**

<b>Signal transduction</b>	
<b>Electrochemical</b>	amperometric, potentiometric conductimetric, impedimetric
<b>Optical</b>	UV/Vis absorption bio/chemiluminescence fluorescence/phosphorescence reflectance, Raman scattering, refractive index and plasmon resonance changes
<b>Mass sensitive</b>	acoustic wave cantilever
<b>Thermometric</b>	Calorimetry
<b>Bioreceptor</b>	
<b>Antibodies</b>	mono/polyclonal
<b>Protein receptors</b>	metabotropic/ ionotropic receptors
<b>Whole cells</b>	tissue, mammalian cells, microbial receptors
<b>Nucleic acids</b>	Hybridization
<b>Enzymes</b>	Biocatalysis
<b>Biomimetic receptors</b>	
<b>Molecular Imprinted Proteins (MIPs)</b> <b>Peptides</b> <b>Aptamers</b> <b>Fab fragments</b>	

## 1.2. Promising bioreceptors: aptamers

The biorecognition elements of biosensors can be classified in natural biological receptor elements like antibodies and enzymes and half and fully synthetic binding molecules that mimic the characteristics of the biological ones, the biomimetic receptors (Table 1.1; completed from Giovannoli *et al.*, 2008). One example of these molecules are aptamers, synthesized DNA and RNA oligonucleotides that are selected for their very specific and selective binding to any target of interest (Scheller *et al.* 2001). They consist of nucleotide sequences that are capable of adopting three-dimensional structures which interact precisely and specifically with a target molecule. Dependent on the target functional groups, hydrogen bonds, electrostatic interactions, stacking interactions and hydrophobic effects are the driving forces, which are commonly involved in the molecule binding to the aptamer (Smuc *et al.*, 2013).

In 1990, two research groups independently developed *in vitro* selection and amplification procedures for the isolation of RNA sequences that could

specifically bind to target molecules such as T4 DNA polymerase (Tuerk & Gold, 1990) and various organic dyes (Ellington & Szostak, 1990). These functional RNA oligonucleotides were termed aptamers, derived from the Latin *aptus*, meaning "to fit" and the Greek *meros*, "particle". Later, DNA-based aptamers were also developed (Ellington & Szostak, 1992). The general *in vitro* selection method for aptamers was termed Systematic Evolution of Ligands by Exponential Enrichment or SELEX (Tuerk & Gold, 1990). Only a few years later, the first selected nucleic acid ligands were applied in a biosensor design, detecting human  $\alpha$ -thrombin (Potyrailo *et al.*, 1998) by means of a fluorescently labeled anti-thrombin aptamer attached to a glass support and measuring changes in fluorescence anisotropy upon target binding.

Although aptamers are synthetically manufactured, natural aptamers also exist in the form of riboswitches, regulating segments of messenger RNA that bind small molecules or cofactors, resulting in a change of the production of the protein encoded by this mRNA (Nudles & Mironov, 2004). In this way, riboswitches are parts of mRNA that regulate the mRNA activity.

Since aptamers are synthetic oligonucleotides which are selected *in vitro*, they have some characteristic advantages over other bio-receptor molecules (Keefe *et al.*, 2010):

Aptamers are produced chemically in a readily scalable process, which is not prone to viral or bacterial contamination. Furthermore, aptamers usually seem to be low-immunogenic and low-toxic molecules, because nucleic acids are not typically recognized by the human immune system as foreign agents (Song *et al.*, 2012).

Aptamers can be selected for and against a variety of specific targets and against cell-surface targets. In contrast to antibodies, pathogenic and toxic targets can also be targeted. Moreover, aptamers show a high affinity and specificity for some ligands that cannot be recognized by antibodies, such as ions or small molecules. Some aptamers even show chiral specificity (Song *et al.*, 2012). In addition to this high selectivity, aptamers bind to their targets with high affinity, particularly with macromolecules (*e.g.* proteins), which often possess dissociation constants ( $K_d$ ) ranging from picomolar to nanomolar (Song *et al.*, 2008).

The phosphodiester bond is extremely chemically stable, which makes aptamers resistant to high temperatures. They can be reversibly denatured. In this case, tools using aptamers are re-usable. Conjugation chemistries for the attachment of dyes or functional groups are orthogonal and can be readily introduced during synthesis. Their smaller size allows more efficient entry into biological compartments and integration in nanoscale sensor applications.

Aptamers can be tailored and optimized for activity and persistence under physiological conditions during selection or after during structure–activity relationship and medicinal chemistry studies (Guo *et al.*, 2008a). Furthermore, addition of conjugation partners such as poly-ethylene glycol (PEG) can increase circulating half-life in complex media (Healy *et al.*, 2004) and chemical modifications (Fig. 1.3) incorporated into the sugars or internucleotide phosphodiester linkages enhance nuclease resistance, duplex stability or allows specific functionalization of selected aptamers for attachment or detection (Burmeister *et al.*, 2006).

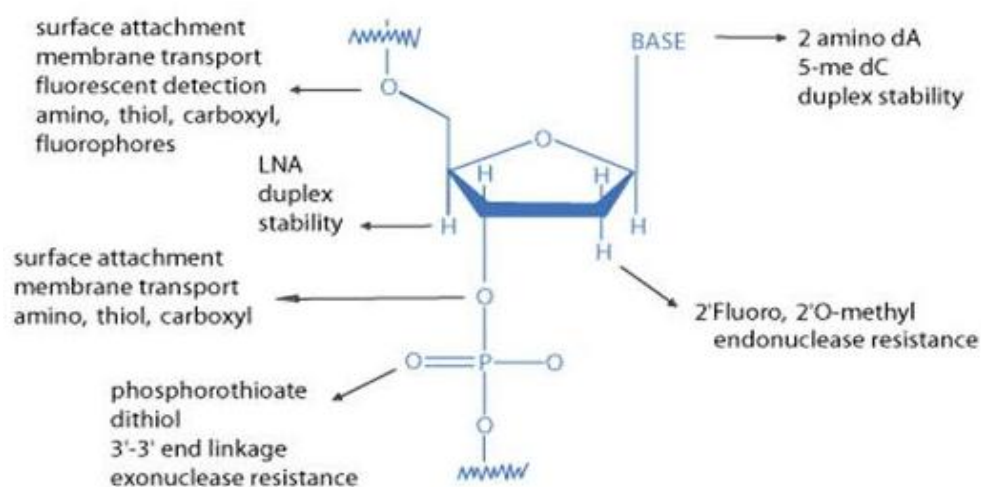


**Fig. 1.3. A partial overview of possible nucleotide base modifications and their effects (Genelink Duplex Stability V3.1)**

There are many fields to which aptamers may be applied, as illustrated in Fig. 1.4. (Song *et al.*, 2012). Aptamers have been studied as a bio-material in numerous investigations concerning their use as a biosensing probe and in the development of new drugs and drug delivery systems. There have been attempts to search for aptamers that are specific to targets involved in various diseases, such as cancer and viral infection. By means of aptamer-facilitated biomarker identification (aptaBID), new biomarkers and highly specific aptamers for those markers can be identified and developed (Berezovski *et al.*, 2008).

Aptamers have been studied primarily for applications as diagnostic or therapeutic tools (Keefe *et al.*, 2010). In 2004, the approval by the Food and Drug Administration (FDA) of Macugen (Pfizer, Eyetech®) or Pegaptanib, a vascular endothelial growth factor (VEGF)-specific aptamer, for the treatment of neovascular (wet) age-related macular degeneration (AMD), is a prominent

landmark in the application of aptamers (Gragoudas *et al.*, 2004; Bunka and Stockley, 2006). Most therapeutically useful aptamers tend to inhibit protein-protein interactions, such as receptor-ligand interactions, and thereby function as antagonists. Many aptamers that are selected to bind to a specific protein also inhibit its function.

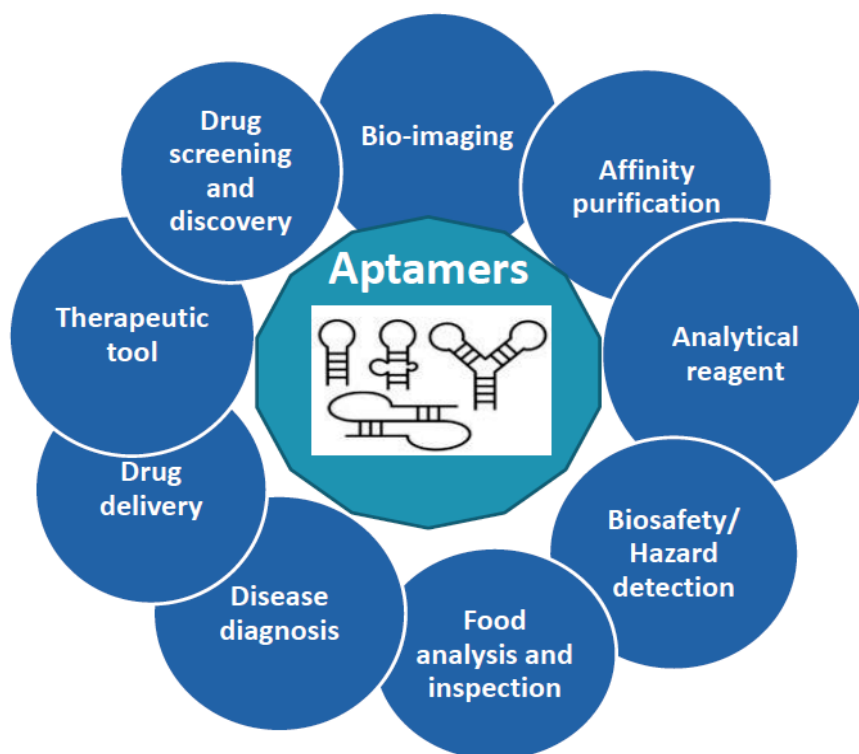


**Fig. 1.4. Aptamers and their fields of applications**

This is possibly because protein active sites offer more functional groups for hydrogen bonding and other interactions. Another explanation is that aptamers have a limited number of interactions that they can make with a protein target, and therefore aptamers that 'fit' into a crevice on a protein, such as an active site, are more likely to be selected (the so-called homing principle). However, at least some aptamers have been shown to have agonist-like activities as well *e.g.* aptamers isolated against the extracellular domain of the protein human epidermal growth factor receptor 3 (HER3) can promote oligomerization (Chen *et al.*, 2003).

For therapeutic applications, aptamers are frequently in competition with small molecules and antibodies. Aptamers exhibit significant advantages relative to

protein therapeutics in terms of size, synthetic accessibility and modification flexibility by medicinal chemistry. Despite all these promising properties, aptamers are slow to reach the marketplace and commercial applications, with only one aptamer-based drug receiving approval so far. A series of aptamers (Table 1.2.) currently in development may change how nucleic acid therapeutics is perceived. It is likely that in the future, aptamers will increasingly find use with other therapeutic molecules.

Until now, aptamers have been selected toward a broad range of targets, including metal ions (*e.g.*,  $K^+$ ,  $Hg^{2+}$  and  $Pb^{2+}$ ), small organic molecules (*e.g.*, amino acids, ATP, antibiotics, vitamins and cocaine) organic dyes, peptides and proteins (*e.g.*, thrombin, growth factors and HIV-associated peptides) and even whole cells or microorganisms (*e.g.*, bacteria) (Song *et al.*, 2008). Importantly, the availability of such a large pool of aptamers makes it possible to develop novel bioassay tools covering the diagnostic and therapeutic areas and the other fields of applications illustrated in Fig. 1.4. as well.



**Table 1.2. Aptamers for therapeutic targets in clinical trial stages (modified from Keefe *et al.*, 2010)**

<b>Name (company)</b>	<b>Composition</b>	<b>Target</b>	<b>Indication</b>	<b>Current phase</b>
<b>Pegaptanib sodium/ Macugen (Pfizer/Eyetechn)</b>	2'-O-methyl purine/2'-fluoropyrimidine w. two 2'-ribose purines conjugated to 40kDa PEG. 3' inverted dT	VEGF	AMD	Approved in US & EU
<b>AS1411/AGRO001 (Antisoma)</b>	G-rich DNA	Nucleolin	Acute myeloid leukemia	Phase II
<b>REG1/RB006 (Regado Biosciences)</b>	2'-ribose purine/2'-fluoropyrimidine to 40 kDa PEG	Coagulation factor IXa	Percutaneous coronary intervention	Phase II
<b>NU172 (ARCA biopharma)</b>	Unmodified DNA aptamer	Thrombin	Cardiopulmonary bypass	Phase II
<b>E10030 (Ophthotech)</b>	DNA and 2'-O-methyl 5'-conjugated to 40kDa PEG. 3' inverted dT	Platelet-derived growth factor	AMD	Phase I
<b>ARC1905 (Ophthotech)</b>	2'-ribose purine/2'-fluoropyrimidine conjugated to 40kDa PEG. 3' inverted dT	Complement component 5	AMD	Phase I
<b>Nox-A12 (Noxxon Pharma)</b>	L-RNA with 3'-PEG (Spiegelmer)	Chemokine CXCL12	Multiple myeloma & non-Hodgkin's lymphoma	Phase I

### 1.3. SELEX – “Darwinian” selection of high affinity oligonucleotides

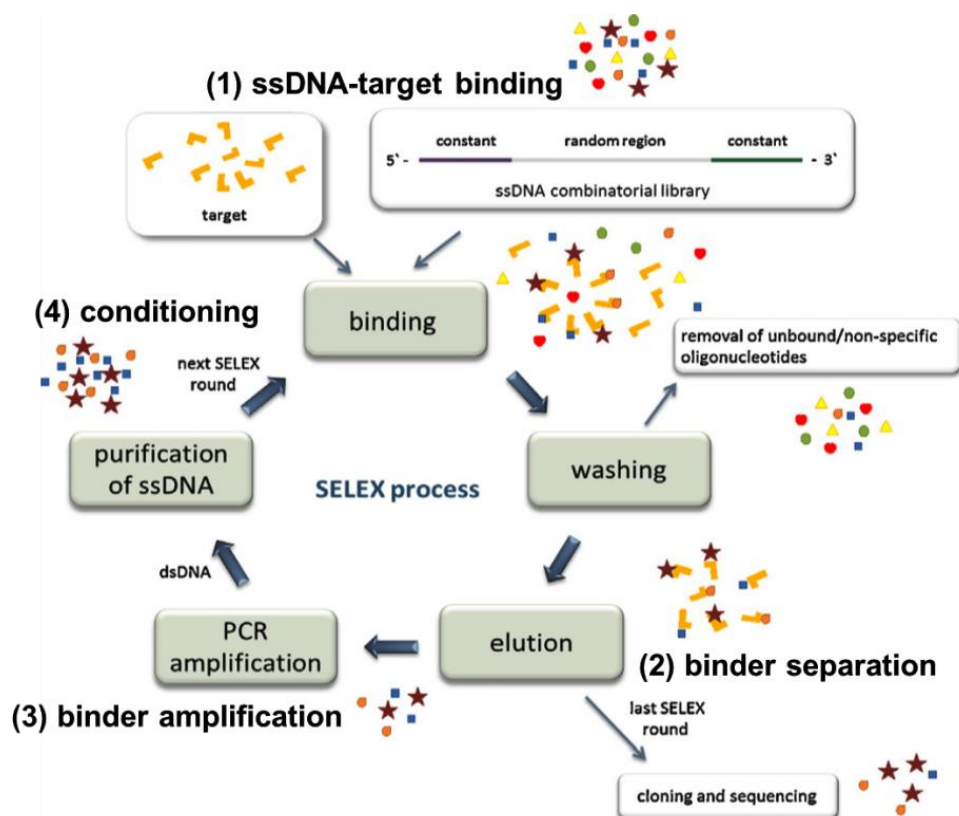


**Fig. 1.5. Schematic illustration of the main steps in the SELEX procedure (Adapted from Smuc *et al.*, 2013), where a specific target is put in contact with a highly diverse library of ssDNA oligonucleotides. During the SELEX procedure, the diversity of the ssDNA library is reduced to oligonucleotides that specifically and selectively bind the target.**

As mentioned in previous section, SELEX or *in vitro* selection is a standard technique used to isolate aptamers with high affinity for a given target from a random library, consisting of approximately  $10^{12}$ – $10^{15}$  combinatorial oligonucleotides. In general, the SELEX process is comprised of four general steps (Fig. 1.5). By iterative cycles of these steps the initial random oligonucleotide pool is reduced to relatively few sequence motifs with the highest affinity and specificity for the target. The number of rounds necessary depends on a variety of parameters, such as target features and concentration, design of the starting oligonucleotide library, selection conditions, ratio of target molecules to oligonucleotides and the efficiency of partitioning between bound and unbound oligonucleotides (Stoltenburg *et al.*, 2007).

### 1.3.1. SELEX step 1: DNA library and target incubation and binding

In the first step, a DNA library that consists of identical primer binding regions and 20-50mers randomized regions is put in contact with the target of choice, in a selected binding buffer. As the secondary structure of an oligonucleotide and its binding to the target are highly dependent on buffer characteristics, one should choose this buffer carefully. Other binding conditions such as temperature may influence structure formation and aptamer binding as well. In short, binding conditions in the SELEX procedure should mimic binding conditions in the eventual ligand application as close as possible. The choice of the selection parameters will tune the selection and determine the downstream use of the resulting aptamers (Hianik *et al.*, 2007). *E.g.* an aptamer for diagnostics in blood needs to be selected at the relevant pH, since this influences the target charge. If one tends to use the selected aptamers for therapeutic *in vivo* applications, the SELEX procedure needs to be performed at 37°C since temperature has influence on secondary structures of selected aptamers.

### 1.3.2. SELEX step 2: relevant binder separation

The selection or separation step is a crucial step of the SELEX procedure and separates unbound oligonucleotides from the bound nucleotides and the target. The immobilization of the target molecule on a particular matrix material allows an effective separation. In this case, the oligonucleotide library is incubated for binding with the immobilized target. Consecutively, the matrix material is washed in a washing step, and the specifically bound oligonucleotides are eluted from the target in a denaturing step. Common used matrix materials are affinity chromatography columns (Liu & Stormo, 2005) or magnetic beads (Stoltenburg *et al.*, 2005). Commonly used methods of separation without target immobilization are ultrafiltration by use of nitrocellulose filters (Bianchini *et al.*, 2001) and centrifugation (Rhie *et al.*, 2003). More advanced separation methods are Capillary Electrophoresis (Tang *et al.*, 2006), Electrophoretic Mobility Shift Assays (Tsai & Reed, 1998), Flow Cytometry (Yang *et al.*, 2003) and Surface Plasmon Resonance (Misono & Kumar, 2005).

### 1.3.3. SELEX step 3: relevant binder amplification

Because of the high complexity of the initial oligonucleotide library, it is expected to get only few functional oligonucleotides in result of the (first) selection steps. To maintain competition for binding to the target, these rare active molecules are amplified to be presented in the next selection round. This amplification step can also be applied to introduce extra variation or properties in the selection library. By means of modified primers, one can attach specific functional groups to part of the library. Furthermore, SELEX in combination with error-prone PCR (Gadwell & Joyce, 1994) or hypermutagenic PCR (Vartanian *et*

*al.*, 1996) introduces point mutations that may enhance desired binding or catalytic properties (McGinness *et al.*, 2002) at a frequency of  $\sim$  1–10% per base per PCR reaction (Bittker *et al.*, 2002).

Despite the need for amplification in most SELEX procedures, exponential amplification of random DNA libraries is reported to differ significantly from that of homogeneous samples. If not properly controlled, amplification could lead to non-desired PCR artifacts *e.g.* amplification products that convert to artifacts by DNA mismatching or oligomerization due to sub-optimal amplification conditions (Musheev & Krylov, 2006). Therefore, the Non-SELEX procedure involves repetitive steps of selection with no amplification steps between them. In these procedures, highly efficient affinity methods are used for partitioning such as Non-equilibrium capillary electrophoresis of equilibrium mixtures (NECEEM (Berezovski *et al.*, 2006).

#### 1.3.4. SELEX step 4: conditioning for the next selection round

The last step is the conditioning step that renders ssDNA oligonucleotides from the dsDNA amplicons after PCR and prepares the ssDNA SELEX pool for the next selection round. Strand separation can be done in several ways; bead capture of the tagged antisense strand (Naimuddin *et al.*, 2007), PAGE-separation of the normal sense strand and a prolonged or labeled antisense strand (Stoltenburg *et al.*, 2005), asymmetric PCR (Wu & Curran, 1999) or specific antisense exonuclease digestion (Avci-Adali *et al.*, 2010; Citartan *et al.*, 2011).

By iteratively executing the procedures of selection, amplification and conditioning during the SELEX process, the complexity of the original library is reduced and target binding candidates are enriched. As soon as the affinity of the enriched library cannot be increased any further, generally after 6–20 selection rounds, the nucleotide sequences of individual binding molecules are determined. For this purpose, the final pool is cloned into a bacterial vector and individual colonies are sequenced. Based on the alignment data, the aptamer clones with mostly identical sequences or sequence parts (motifs), different in only few single nucleotide positions, can be grouped. In recent studies, Next Generation Sequencing is applied to allow high-throughput screening of aptamer candidates in different SELEX rounds (Schütze *et al.*, 2011).

Additional steps can be introduced into each round of the SELEX process particularly with regard to the specificity of the oligonucleotides. Negative selection steps or subtraction steps are strongly recommended to minimize enrichment of unspecific binding oligonucleotides or to direct the selection to a specific epitope of the target. The affinity of the oligonucleotides to their target can be influenced by the stringency of the selection conditions. Typically, the stringency is progressively increased in the course of a SELEX process. This can be achieved by reducing the target concentration in later SELEX rounds or

changing the binding and washing conditions (buffer composition, volume, time) (Marshall & Ellington, 2000).

A major advantage of the SELEX procedure is the possibility to adapt the conditions of further applications already during the selection process. On account of this, numberless variations of the procedure originally established by Tuerk and Gold (1990) were described during the last years. Some of these methods were developed to increase affinity or specificity of the selecting aptamers, others to optimize the procedure (Table 1.3). A partial overview of the many SELEX variants is reviewed in Stoltenburg *et al.* (2007).

**Table 1.3. Variations and optimizations of the general SELEX procedure, specific method characteristics and their desired applications or outcomes (modified from Radom *et al.*, 2013).**

SELEX method	Method characteristics	Application
<b>Primer-free SELEX</b>	elimination of primers prior to selection step	elimination of the primer incorporated in the binding sequence
<b>Toggle SELEX</b>	change of targets during process	aptamers with different specificity levels
<b>Tailored SELEX</b>	use of libraries that lack fixed border sequences	smaller size aptamers
<b>Conditional SELEX</b>	selection in specific conditions (temperature, buffer)	binding depending on specific condition/molecule
<b>Mirror-image SELEX</b>	use of compound's enantiomers for selection	spiegelmer selection, aptamers specific for a compound's enantiomers
<b>Genomic SELEX</b>	use of libraries based on genomic sequences	selection of natural sequences binding molecules
<b>Cell SELEX</b>	whole cells are targets of selection	aptamers for unknown cellular markers

The expansion of the genetic alphabet on which selection takes place, in terms of oligonucleotide chemistry, has increased the versatility of SELEX procedures even more. As nucleotide modifications can increase aptamer stability by enhanced nuclease-resistance, recent advances have enabled SELEX with libraries that contain other chemical functionalities, yielding new aptamers to different targets and unseen specificity and selectivity (Keefe & Cload, 2008; Gold *et al.*, 2010).

Serious progress has been made in making the SELEX procedure standardized, high-throughput, parallel for multiple targets and even automated (Fig. 1.6) (Cox & Ellington, 2001; Eulberg *et al.*, 2005; Gold *et al.*, 2010). The combined automated forces of selection procedures and high-diversity library synthesis opens up interesting possibilities. This will expand the library of aptamers for

different targets and the repertoire of aptamers in analytical, diagnostic and therapeutic applications (Yang *et al.*, 2007).

The SELEX advances described above illustrate how aptamer technology is rapidly maturing from a research tool (with target-specific, manual selection) into a major technology with commercial potentials (multiplexed proteomic analysis and automated selection).

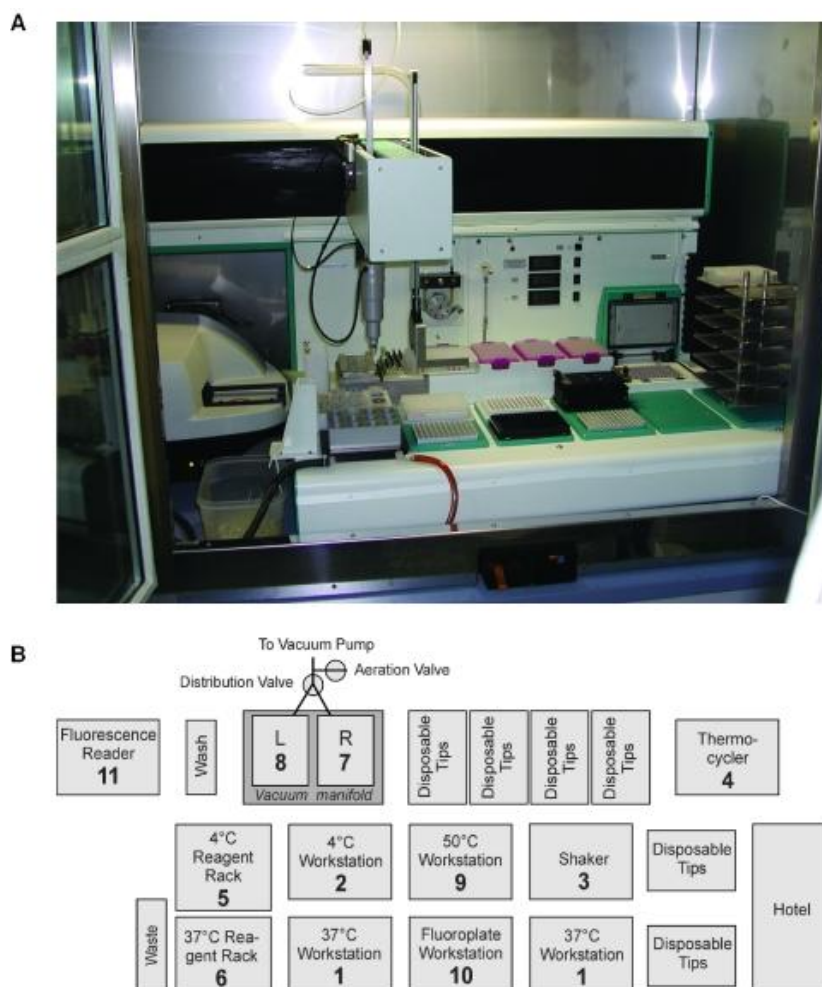


**Fig. 1.6. Automated selection robot. (A) Picture of the RoboAmp robot with accessories under a temperature-controlled hood. (B) Schematic presentation of the RoboAmp work surface used for the automated selection of aptamers consisting of temperature controlled work stations (1,2,9) and reagent racks (5,6), a shaker (3), a thermocycler (4) for PCR and a fluorescence reader (11) for binding assays (Eulberg *et al.* 2005)**

## **1.4. Aptamer characterization: binding studies and affinity analysis**

At the end of a SELEX procedure, sequencing analysis results in a batch of candidate aptamers for the target under the applied selection conditions. The number of candidates obtained depends on selection stringency and target characteristics, but usually varies between one and one million (Conrad *et al.*, 1995). When a lot of oligonucleotides are selected, aptamers are grouped and characterized by nucleotide sequence and secondary structure. In the next step, candidates are tested in binding studies with increasing complexity. As a result, the candidate pool is reduced to one to ten aptamers with high affinity and selectivity for the target under characterized binding conditions.

In silico characterization of the aptamer batch depends on nucleotide sequence information. Based on the alignment data, the aptamer clones with mostly identical sequences, different in only few single nucleotide positions, can be grouped. In some cases special sequence patterns or highly conserved regions can be identified among the aptamer groups. These regions are often involved in specific target binding of the aptamers (Stoltenburg *et al.*, 2007). Moreover, the mfold web server (<http://mfold.rna.albany.edu/>) performs a secondary structure prediction, under defined buffer conditions such as temperature and ionic strength (Zuker, 2003). This secondary structure analysis may indicate relevant structures for binding, and the corresponding sequence motifs, responsible for stabilizing this structure.

Binding studies for the determination of specificity and affinity of the selected aptamers usually follow. These studies are a very important part of aptamer selection since subsequent applications of aptamers depend on the exact assessment of specificity and affinity and optimal binding conditions. Binding assays come in different shapes and complexities, but also in different costs. The outcomes of these assays range from a binding or no-binding answer, to complex possibilities of binding characterization, concentration dependence and affinity analysis. When analyzing 100 candidates, it is useful to start with simple, high-throughput and relatively cheap assays, to have a preselection before continuing to more expensive, specialized techniques.

### 1.4.1. Aptamer binding interaction mechanisms

As DNA or RNA aptamers consist of a sequence of nucleotides, they will form secondary structures such as hairpins, helical arms and loops. Combination of these structures results in distinct tertiary structures of aptamers upon target recognition. By forming these structures, aptamers can bind to their target via van der Waals forces, hydrogen bonding and electrostatic interactions in hydrophilic and hydrophobic binding pockets (Smuc *et al.*, 2013, Song *et al.*,

2012) This results in a more stable aptamer-ligand complex, which has certain strength (binding affinity) and is formed and dissociated with a certain speed (binding kinetics).

#### 1.4.2. Affinity and kinetic analysis of binding interactions

Aptamer binding strength or affinity is influenced by the non-covalent intermolecular interactions between the aptamer and the target as described above and is expressed as the equilibrium dissociation constant ( $K_d$ ). This measures the proneness of the aptamer-target complex to dissociate or fall apart in equilibrium conditions, where sufficient amounts of aptamers (A) and target (B) are available and no constraints on complex (AB) formation are present (Fig. 1.7). The inverse, the association constant ( $K_a$ ) measures the proneness of the complex to be formed.

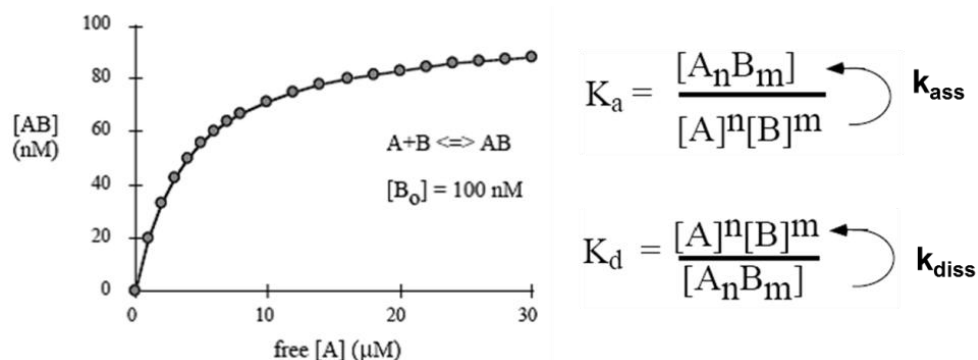


**Fig. 1.7. Equilibrium curve of a 1:1 interaction between interactant A and reagent B, where increasing concentrations of A are titrated to a constant concentration of B. The concentration of free [A] where the concentration of complex [AB] is half of the equilibrium concentration is the dissociation constant of the complex.**

If target binding is allowed until equilibrium distributions are reached ( $A + B <-> AB$ ), increasing amounts of reactant [A] can be titrated against a fixed amount of the reactant [B] and the equilibrium concentration of the product [AB] can be determined (Jing & Bowser, 2011). Moreover, this approach allows the determination of the equilibrium constants for dissociation ( $K_d$ ) in molar units as the concentration of free ligand [A] where the concentration of complex [AB] equals the concentration of free reactant [B] or the concentration of [A] at which half of the total molecules of reactant B are in complex with ligand A (Fig. 1.8., Goodrich & Kugel, 2007).

The smaller the dissociation constant, the more tightly bound the ligand is, or the higher the affinity between ligand and protein.

These equilibrium constants can also be written as the ratio of the kinetic rate constants of association ( $k_a = k_{ass} = d(AB)/dt$ ) and dissociation ( $k_d = k_{diss} = -$



$d(AB)/dt$ ), which are indicative of the speed of complex formation and disruption. In the onset of the reaction, the association rate ( $k_a[A][B]$ ) dominates and the dissociation rate ( $-k_d[AB]$ ) is small, since there is almost no complex. As more complexes are formed, the associations rate decreases and the dissociation rate increases until they are equal. At this point, the concentrations have a constant ratio,  $K_d$  that is called the equilibrium dissociation constant and equals  $k_d/k_a$  which equals  $[A][B]/[AB]$ .

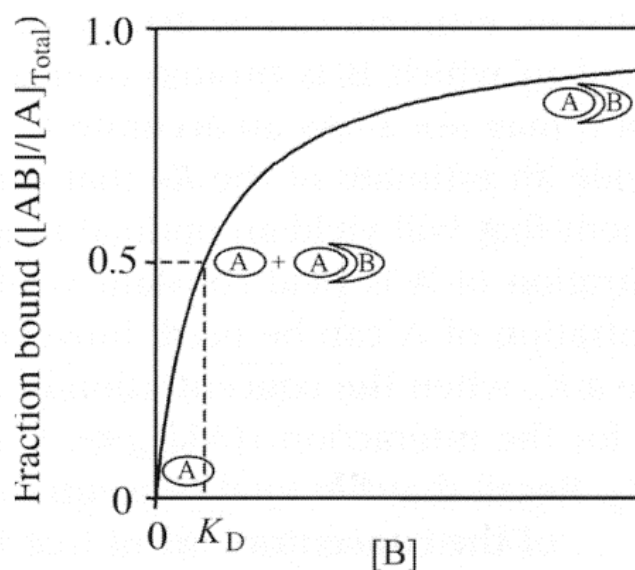


**Fig. 1.8. Determination of affinity dissociation constant ( $K_d$ ) in equilibrium. (Goodrich & Kugel, 2007). In practice,  $K_d$  is defined at the concentration of  $[B]$  needed to reach half of the equilibrium binding maximum of  $[AB]$ .**

Kinetic methods that allow determination of the distinct association and dissociation rate constants ( $k_a$  and  $k_d$ ) exceeds the classical steady-state analysis of biomolecules and gives information about the speed of complex formation and disruption. As illustrated in Fig. 1.9, this is more informative, as the same equilibrium dissociation constant can result from different association and dissociation rates.

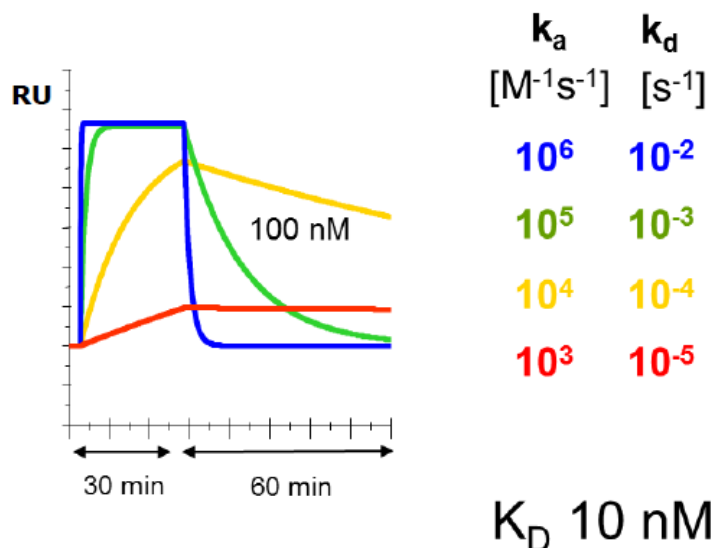


**Fig. 1.9. Different rates of association ( $k_a$  [ $M^{-1}s^{-1}$ ]) and dissociation ( $k_d$  [ $s^{-1}$ ]) still result in the same affinity dissociation constant ( $K_d$  [ $M$ ]) in a Biacore SPR analysis of 30 minutes association and 60 minutes dissociation. RU = Response Units (Biacore Technology Brochure).**

#### 1.4.3. Binding assays for affinity and kinetic analysis.

Binding assays can be classified in different ways. A first classification is label-free and labeled assays. Labeling the aptamer with fluorescent dyes, chemiluminescence enzymes or interaction tags such as biotin or streptavidin is necessary for signal generation and quantification or detection purposes. After reaching equilibrium, the interaction is measured and quantified by means of reporter labels that are attached to the target and/or the aptamer e.g. fluoresceins, radiolabels and affinity tags. However, complications may arise with the use of such labels which can lead to either high background noise or a decrease in aptamer specificity and functionality (Rowe *et al.*, 2009). These effects can all be tested by comparing label-free and labeled binding assays before selecting the aptamer(s) for sensor applications. A next classification is in solution or by covalent immobilization of the receptor or the target. This may be needed for signal generation or practical reasons to keep the receptor or target stationary under flow conditions (Balamurugan *et al.*, 2008). When the aptamer is immobilized, a linker is applied, to maintain aptamer functionality. Table 1.4 illustrates the array of analytical assay formats that makes use of biorecognition molecules immobilized to a solid surface.

**Table 1.4. Different analytical methods used for the detection of aptamer-protein interaction along with a respective substrate used in each method (Balamurugan *et al.*, 2008).**

Surface and related modifications	Analytical method
Gold, self-assembled monolayers on gold, biocoatings on gold	(localized-) surface plasmon resonance, electrochemical impedance/resistance, enzyme-linked aptamer assay, fluorescence microscopy, ellipsometry, surface acoustic wave, quartz crystal microbalance, cantilever, atomic force microscopy
Silica, silicon, or TiO <sub>2</sub> ; Al <sub>2</sub> O <sub>3</sub> , biocoatings on silica; carbohydrates on silica	fluorescence spectroscopy, capillary electrophoresis, atomic force microscopy, affinity chromatography, fluorescence microscopy fluorescence anisotropy
Biocoatings on polymers	High-performance liquid chromatography
Carbohydrate surfaces	fluorescence microscopy
Single-walled carbon nanotube	conductance, single-walled carbon nanotube field-effect transistor
Quantum dots	Photoluminescence

In separation-based assays that measure the interaction between the aptamer and the target in solution, the complex [AB] and free reagents [A] and [B] are physically separated before quantification. In dialysis, centrifugation and filtration experiments *e.g.*, this separation is purely based on size differences. Other separation techniques rely on the difference in electrophoretic mobility, due to size and charge differences between free aptamers or targets and their complexes. In EMSAs (Electrophoretic Mobility Shift Assay), free labeled DNA ligand and/or target and the complex give rise to distinct bands on the gel (Zhu *et al.*, 2008), provided that the dissociation rate constant of the interaction is small and the complex half-life is significantly longer than the separation time scale (Jing & Bowser, 2011). As an alternative, Capillary Electrophoresis (CE) separates analytes and complex in free solution based on their size and charge. As in EMSA, the protein and aptamer-protein complex generally have slower mobility than the unbound aptamer giving rise to distinct peaks. If a fluorescently labeled aptamer is titrated with increasing concentrations of protein, two peaks representing the complex and unbound aptamers are observed in the electropherogram (Fig. 1.10). The bound fraction can be calculated from the decrease in the intensity of the free ligand peak as increasing amounts of protein are added. This technique has been used to characterize aptamers selected via CE-SELEX, a process in which only nucleic acid sequences that stay bound to the target for approximately the same separation time would be collected to evolve aptamers.

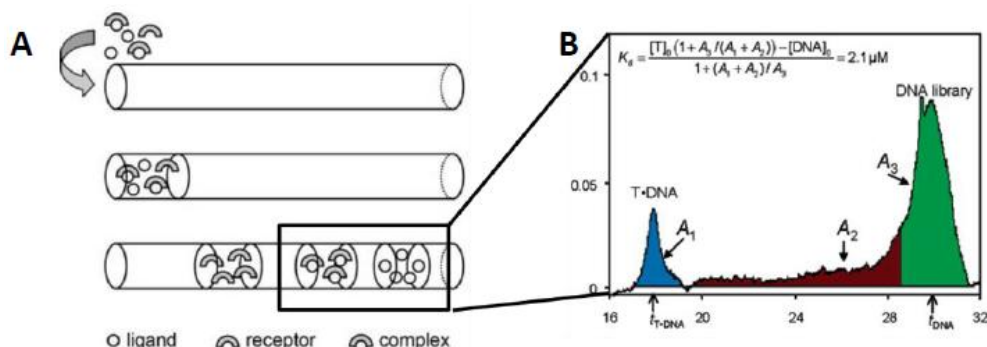


**Fig. 1.10. (A) CE separation of ligand, receptor and complex and (B) the resulting electropherogram with a clear peak for free DNA library at the right and Target-DNA complex at the left. Inset equation shows the equation for  $K_d$  determination by means of CE (Figure adapted from Giovannoli *et al.*, 2008 and Drabovich *et al.*, 2005).**

Krylov (2006) classifies separation-based methods by the way of separation (heterogeneous on a surface or homogeneous in solution) and their use, if they are used to determinate kinetic rate constants or not (Fig. 1.11).

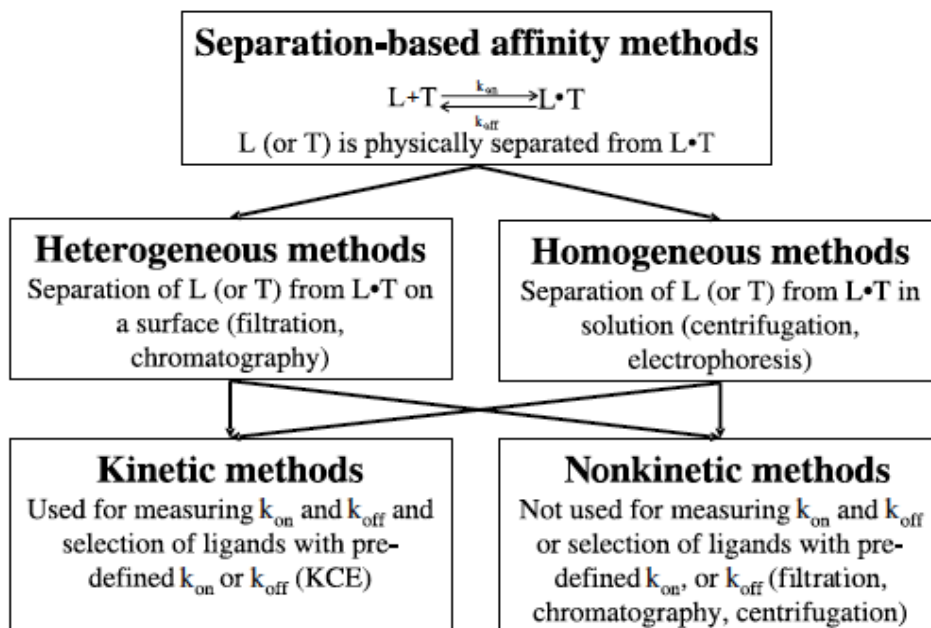


**Fig. 1.11. Classification of separation-based affinity methods (Krylov, 2006).**

Mixture based techniques on the other hand do not need separation of complex and other reagents (Jing & Bowser, 2011) and can be performed at equilibrium concentrations *e.g.* by in solution fluorescence measurements of fluorescently labeled aptamers and/or targets.

If the binding event does induce a change in fluorescence quantum yield of the fluorescein label, this signal can be used directly to estimate binding affinity. More complex techniques are Fluorescence anisotropy ( $\rho$ ) that measure the change in polarization or anisotropy of emitted light when a labeled aptamer binds the target it is selected for (Gokulrangan *et al.*, 2005) and Fluorescence Correlation Spectroscopy (FCS), based on the temporal fluctuations of measured fluorescence intensity occurring in a small observed volume, using confocal optics (Wiegraebe, 2000).

In the following section, a short overview of several types of aptamer binding assays and their characteristics are given. It is beyond the scope of this chapter to give a full review about them.

## 1.5. Aptamer binding assays and the application of aptamers in biosensor assays.

### 1.5.1. Immunosorbent-like assays: ELAA and ALISA

Immunosorbent assays make use of antibodies, specific for the target. They can serve as a capturing agent, as a detecting agent, or both in sandwich ELISAs. Following this idea, detection methods were developed in which the capture/reporting antibody/ protein of ELISA is substituted by aptamers, specific for targets of interest (Drolet *et al.* (1996), Kirby *et al.*, (2004).

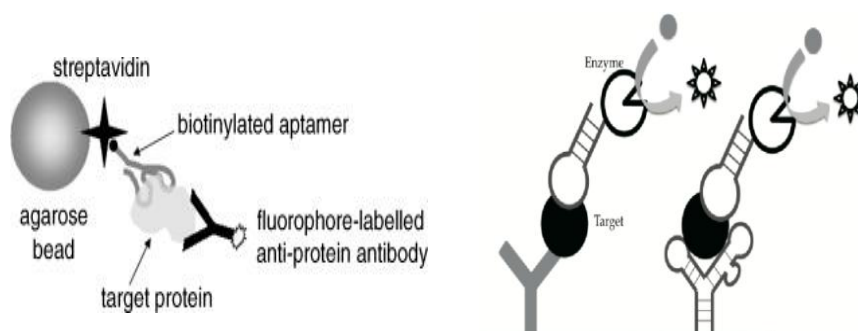


**Fig. 1.12. Left: Biotinylated aptamer is bound on Streptavidin beads and used as a capturing agent for in-solution target capture. (Kirby *et al.*, 2004). Right: Enzyme-linked aptamers are used as reporting agents in different set-ups (Abe & Ikebukuro, 2011).**

This is the case in the ALISA (aptamer-linked immobilized sorbent assay) that was applied to examine the specificity of an aptamer against an antigen associated with *Francisella tularensis*, causing rabbit fever (Vivekananda & Kiel, 2006). Enzyme-linked aptamer assays (ELAA) use aptamers directly conjugated

to signal generating and amplifying enzymes, such as HRP and AP. A list of conjugated enzymes and the types of detection that are used is given in Table 1.5 (Abe & Ikebukuro, 2011).

**Table 1.5. Enzyme list for signal amplification (modified from Abe & Ikebukuro, 2011)**

Enzyme name	Detection type
<b>Polymerase</b>	fluorescence
<b>Phi29 polymerase</b>	fluorescence or electrochemical
<b>Dehydrogenase</b>	electrochemical
<b>Peroxidase (HRP)</b>	electrochemical, chemiluminescence & fluorescence
<b>Alkaline phosphatase (AP)</b>	electrochemical, chemiluminescence & fluorescence
<b>Nuclease</b>	fluorescence
<b>Protease</b>	fluorescence or others

### 1.5.2. PCR assays

Since the development of immuno-PCR (Sano *et al.*, 1992), it is clear that DNA as such can serve as a signal amplifier. Aptamers are easily applicable to similar assays that use immuno-PCR. If the aptamer has sufficient length for primer binding, it can be amplified directly (Fischer *et al.*, 2008). Since a PCR reaction amplifies DNA exponentially, signal amplification by polymerase enables more sensitive detection than by ELISA. The limit of detection of a given ELISA is, in general, enhanced 100 to 10000-fold by the use of PCR as a signal amplification system (Adler *et al.*, 2003). Liao *et al.* demonstrated direct detection of the aptamer by means of RT-PCR (Fig. 1.13).

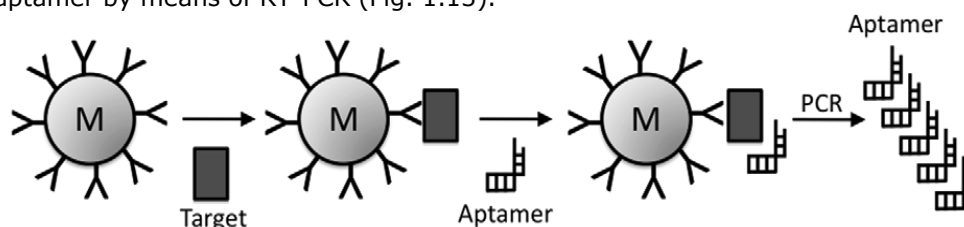


**Fig. 1.13. Direct aptamer detection by means of RT-PCR amplification (Liao *et al.* 2010)**

A similar technique uses the Proximity Ligation Assay (PLA) for sensitive protein detection. When two aptamers bind the same target on different epitopes, extended probes can be linked by an affinity probe. When these ends are linked, specific PCR amplification results in ultra-sensitive detection with the amplification of DNA as a signal generator (Fredriksson *et al.*, 2002).

### 1.5.3. Fluorescence assays

Fluorescent detection of the binding event is widely employed due to the ease of labeling aptamers with fluorescent dyes, the availability of many different fluorophores and quenchers, and the capability for real-time detection. Several strategies have been developed for converting aptamers into fluorescent signaling probes (Song *et al.*, 2008).

Aptamer-based molecular beacons have the aptamer sequence in a molecular beacon-like, hairpin structure, end-labeled with a fluorophore and a quencher (Yamamoto & Kumar, 2000). Other formats have a fluorophore-labeled aptamer in duplex with a quencher-labeled complementary strand (Fig. 1.14). Binding of the target disrupts the hairpin or the duplex formation, leading to fluorescence signals (Nutiu & Li, 2003). By using a fluorogenic competitor strand, one can perform optical binding studies without labeling the target or aptamer (Fig. 1.10) (Li, 2011).

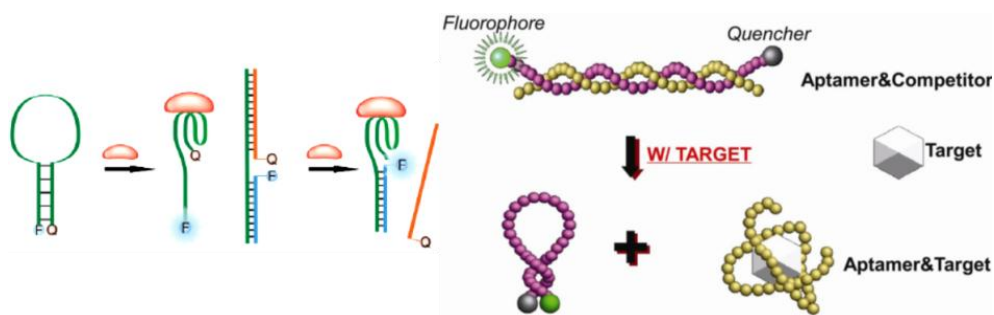


**Fig. 1.14. Left: Aptamer-based beacon formats (Song *et al.*, 2008); Right: 'Label-free' optical assay by using a fluorogenic competitor (Li, 2011).**

Alternative strategies rely on fluorescence resonance energy transfer (FRET) when two fluorescent donor and acceptor molecules come in proximity of each other. This can be achieved by dual labeling of the aptamer strand (Li *et al.*, 2008), or by measuring fluorescence intensity changes when aptamer- and target-functionalized fluorescent (nano)particles come in proximity (Wang *et al.*, 2011; Dausse *et al.*, 2011).

More specialized fluorescence spectroscopy techniques are fluorescence anisotropy (FA) and fluorescence correlation spectroscopy (FCS). Fluorescence anisotropy measurements are performed with an immobilized labeled aptamer (Potyrailo *et al.*, 2009) or by measuring the changes in fluorescence polarization of the aptamer in solution (Gokulrangan *et al.*, 2005). Anisotropy of the emission ( $r$ ) is calculated according to its definition (Lakowicz, 2006) for different concentrations of added target to a constant concentration of labeled aptamer.

Fluorescent Correlation Spectroscopy (FCS) identifies molecular interactions based on a changes of molecular mobility at the single molecule level and is

applied to determine the dissociation constant of a complex formed by a fluorescence-labeled target and its corresponding aptamer (Werner & Hahn, 2009).

#### 1.5.4. Electrochemical assays

Electrochemical assays measure the change in electron movement over an electrode surface. This means these types of assays always have one of the two binding agents immobilized to an electrode surface to generate the signal. When labeling target molecules with redox active compounds, they produce current when they come in contact with the aptamer-coated electrode's surface (Rowe *et al.*, 2009). Labeling the aptamer with redox active compounds also results in electrochemical changes when target binding causes conformational changes. Label-free assays, with no need for labeling the target or the aptamer, make use of so-called redox reporters (Song *et al.*, 2008) or neutralizer strands (Das *et al.*, 2012) that bind to the electrode via electrostatic interaction with the aptamer. Upon target binding, the reporters or neutralizers are displaced, which results in distinct electrochemical changes (Fig. 1.15).

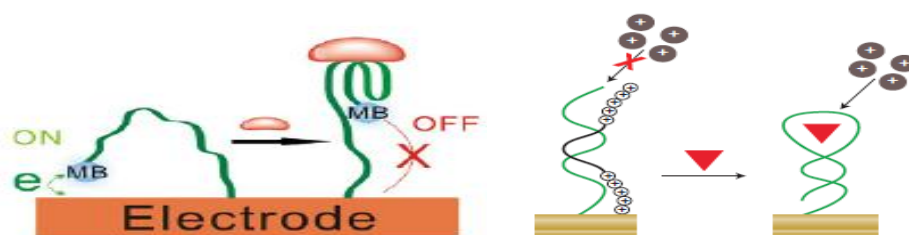


**Fig. 1.15. Left: 'Signal on-off' electrochemical assay with Methylene Blue labeled aptamer (Song *et al.*, 2008). Right: Label-free electrochemical measurements by means of neutralizer strand displacement (Das *et al.*, 2012)**

Electrochemical Impedance Spectroscopy (EIS) is another way of measuring binding events at a semiconductor surface, by measuring the response (current and its phase) of an electrochemical system to an applied oscillating potential as a function of the frequency. In Tran *et al.* (2011) EIS is applied to measure the changes in interfacial electrical properties that arise when an IgE aptamer-functionalized diamond surface is exposed to IgE solutions. The formation of aptamer-IgE complexes causes a significant change in the capacitance of the double-layer, in good correspondence with the IgE concentration. The detection limit of the aptasensor reached physiologically relevant concentrations (1.5  $\mu\text{M}$ ). By adding a redox-couple  $[\text{Fe}(\text{CN})_6]^{3-/4-}$  to the buffer solution and measuring on aptamer-coated gold nanoparticles, label-free detection of thrombin is achieved with a detection limit of 0.013 nM (Li *et al.*, 2011).



### 1.5.5. Surface plasmon resonance

Surface Plasmon Resonance (SPR) is a physical phenomenon that occurs on metal surfaces when plane-polarized light hits a metal film under total internal reflection conditions, resulting in an evanescent resonance plasmon wave (Nagata & Handa, 2000). In this wave, incident light is refracted in a certain resonance angle. When compounds bind to the metal surface, this resonance angle shifts due to changes in the refractive index of the dielectric medium at the metal interface. These shifts in resonance angle are concentration dependent and are translated into arbitrary Response Units (RU). The response is followed in real-time during association and dissociation on the coated metal surface, allowing ultra-sensitive interaction detection and determination of affinity constants ( $K_d$  and  $K_a$ ) and dissociation ( $k_d$ ) and association ( $k_a$ ) rate constants (Fig. 1.16).

There are different types of SPR configurations. Most configurations are prism-based, such as the Biacore Technology. Other configurations are Fiber Optic-SPR (FO-SPR) that uses the propagation of light in a multimode optical fiber only if it enters the fiber at certain discrete angles (Gupta & Verma, 2009).

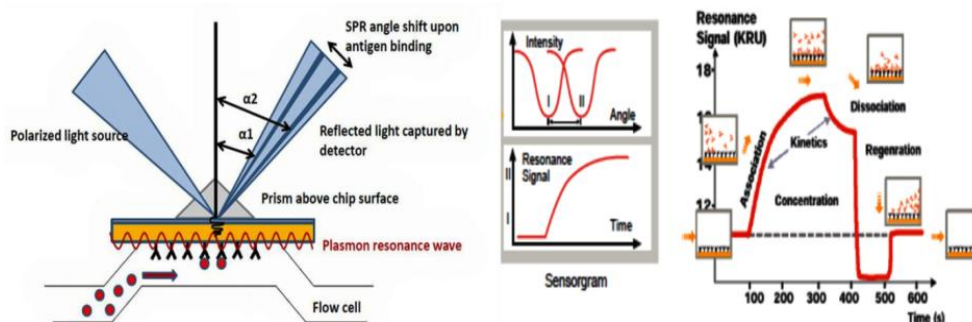


**Fig. 1.16. Left: Prism-based SPR Technology from Biacore allows real-time label-free interaction analysis by measuring resonance angle shifts upon binding on functionalized gold chips. Right: Typical binding sensorgram (Adapted from Biacore Technology brochure).**

Localized SPR (LSPR) is an optical phenomenon generated by collective oscillations of the electron gas in metal nanostructures surrounded by a dielectric, such as gold nanoparticles (AuNPs) and other nano-structures. Depending on the origin of LSPR changes, two types of sensors can be distinguished: aggregation sensors and refractive index sensors. Local refractive index changes such as those induced by biomolecular interactions at the surface of the nanostructures are monitored via the LSPR peak shift, which is proportional to the concentration of bound molecules (Fig. 1.17) (Sepulveda *et al.*, 2009). Aggregation sensors detect the presence of a target molecule by means of aggregation of nanoparticles in solution, resulting in a colorimetric

assay for target presence (Guo *et al.*, 2013). Recently, a plasmonic aptasensor for the detection of Bisphenol A is developed by measuring the disruption of nanoparticle dimers formed by hybridization between the selected aptamer and a complementary ssDNA strand. Upon addition of low concentrations of Bisphenol A, strand displacement results in a large LSPR peak shift upon dimer disruption (Kuang *et al.*, 2014).

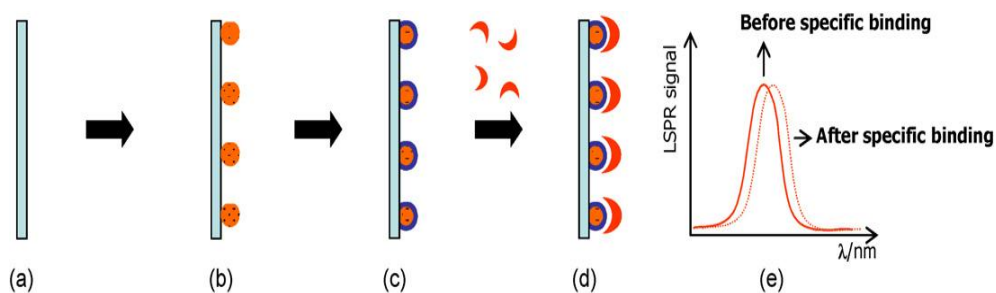


**Fig. 1.17. Schematic representation of a LSPR biosensor: (a) bare substrate (b) deposition of metal nanoparticles (c) functionalization of particles with receptor (d) specific binding of analyte (e) the binding event results in a LSPR peak shift to higher wavelengths.**

#### 1.5.6. Application of aptamers in aptasensors

The vast amount of binding assays developed for aptamers is not represented in the number of applied aptasensors for different applications (see 1.1). Point-of-care applications demand analyte detection within a very short period of time, ideally in the form of small hand-held devices, with clear, unambiguous representation of the results. At least three basic criteria should be met in an affinity sensor (Jayasena, 1999):

- (1) to transduce the binding event without addition of extra reagents
- (2) to detect and quantify the target, within the needed time period and concentration range
- (3) to have some turn-over capacity *i.e.* the possibility to make repeated measurements on the same transducer multiple times.

Immunosensors, sensor devices based on antibody-antigen recognition, have been used in clinical and environmental testing areas (Morgan *et al.*, 1996). Despite huge innovations and investments, however, the impact of immunosensors is limited. Obvious limitations are the cost to develop highly sensitive and specific antibodies and the non-reversible antibody-antigen binding, making them hard to reuse without loss of activity. Aptamers are much cheaper to produce once selected (Carlson B., 2007). Moreover, the ability to regenerate the function of immobilized aptamers by denaturation and renaturation allows for repeated measurements (Jayasena *et al.*, 1999). Other

advantages are the ease aptamers can be modified and labeled for immobilization and detection purposes, and the fact that they can be selected against toxic and pathogenic targets, which are highly relevant in point-of-care applications.

Due to the above advantages, aptamers are regarded as promising alternatives to antibodies in bioassay and biosensor related fields and have been applied in bio-molecule detection, cell collection and detection, imaging or other clinical treatments (Carlson B., 2007). Han *et al.* (2010) reviews design strategies for the fabrication and application of aptamer-based biosensors. Although the detection approaches (optical, electrochemical ...) or instruments may be different for various aptamer-based biosensors, the core of these four design strategies is somewhat similar:

- (a) *Target-induced structure switching mode (TISS)*: Conformational change by direct target binding induces changes of detectable characters.
- (b) *Sandwich or sandwich-like mode*: Analytes with dual binding sites are 'sandwiched' between two recognition elements: aptamers and/or antibodies.
- (c) *Target-induced dissociation or displacement mode (TID)*: Complementary sequences of aptamers, instead of the aptamers themselves, are employed as anchors to localize the aptamers. Target binding causes duplex disruption which leads to changes of detectable characters.
- (d) *Competitive replacement mode*: Competition assays with labeled target and native target, detecting the replacement of the labeled target by the native target for aptamer binding.

Aptamers can also be joined to nucleic acid enzymes (*e.g.*, ribozymes and deoxyribozymes) to create allosteric enzymes or so-called aptazymes (Cho *et al.*, 2009). An aptameric enzyme subunit (AES) is a DNA aptamer composed of an enzyme-inhibiting aptamer and a target-binding aptamer that can allosterically regulate the corresponding enzymatic activity upon binding to the target molecule (Han *et al.*, 2010). Incorporation of aptamer sequences with DNAzymes or RNAzymes enable catalytic activities to be measured upon target binding or complex disruption.

Despite the advantages of aptasensors and the potential of aptasensing technologies, their impact is very limited (Baird, 2010). This might be caused by the very specific nature of the aptamer performance, unique for each aptamer structure requiring specific binding conditions. Formation of the 3-D structures required for target binding is influenced by a range of variable parameters: immobilization strategy, buffer composition, temperature, labeling. In a case study on the effect of these parameters, TBA1 performance was seriously

affected by labeling and immobilization at the 5'- or 3'-ends. Incubation temperature and ionic strength had marked effects on aptamer structure stability (Baldrich *et al.*, 2004). Unlike antibody based assays, there are no general recommendations, which makes them hard to commercially develop and risky for industry to invest in. Although aptamers match antibodies in specificity or selectivity, and fill in other antibody shortcomings, several crucial factors have prevented their widespread distribution. A combination of patents prevented initial spread, and this suppression of the technology has allowed antibodies to become well ingrained in the medical industry. Many in the industry are reluctant to tear themselves away from well-supported and effective antibodies for the risky and still relatively underdeveloped aptamers (Baird, 2010).

## 1.6. Aims and objectives of this thesis

From this introduction it is clear that the whole spectrum of aptamer research is far beyond what one PhD dissertation can encompass. The research presented in this dissertation focusses on the basis of any biosensor, the bioreceptor molecule, in this case an aptamer. In the case of aptasensors, it is clear from the previous sections that proper characterization of the aptamer and its binding properties for the target are of the utmost importance. Nevertheless, this seems to be one of the flaws in aptamer research.

Despite the advantages of aptamers over antibodies, the latter are still the golden standard in receptor molecules for diagnostics (Baird, 2010). A condition for increased aptamer performance in the applications listed in section 1.2 and Fig. 1.4. is to have more insight in the characteristics of aptamer binding mechanisms, in order to formulate general rules and procedures for aptamer selection and binding assays for virtually any target. The main objective of this dissertation is to contribute to an increased understanding of aptamer binding interactions. This dissertation tries to identify pitfalls and to formulate recommendations for frequently encountered problems as reduced specificity and aptamer functionality in binding conditions that are deviant from the selection conditions, which are a serious threat for aptamer credibility and performance. This objective is aimed for by focusing on the selection procedure in Chapter 2 and 3, on a panel of existing binding assays in Chapter 4 and by the application of aptamers in a new read-out system in Chapter 5.

The first aim of this dissertation is a better understanding of the selection procedure. The performance of an aptamer directly depends on its selection procedure and the conditions it is allowed to bind in. General procedures for SELEX control and monitoring will contribute to more efficient aptamer selection under controlled conditions. By optimizing a SELEX procedure for aptamers specific for native C-reactive protein (CRP) in **Chapter 2**, general pitfalls of and

recommendations for general aptamer selection procedures are highlighted. CRP is an acute-phase protein and inflammation marker and hence an interesting prototype target for diagnostic aptamer applications. CRP is widely used at the clinic as biomarker and fast and sensitive measurement methods are already well established, therefore this is an interesting target to compare outcomes of the selection procedure to other receptors developed for CRP. Different SELEX designs, buffer conditions and selection steps are evaluated for this CRP specific aptamer selection. This chapter ends with a discussion about the manual selection procedure and how this process can be made more efficient. In **Chapter 3**, the need for concise SELEX monitoring is addressed by proposing a newly developed method for SELEX enrichment monitoring and SELEX conditioning. By applying this method to the CRP aptamer selection and to two other independent SELEX designs and targets ( $\beta$ -estradiol and a bacterial peptide) as well, SELEX monitoring by reMelting Curve Analysis (rMCA) is demonstrated to be a universal tool for following the selection procedure and outcome, regardless of target properties.

Following a successful selection of CRP aptamers, the second aim is to validate the selected aptamer candidates, in terms of selectivity and specificity for CRP. Testing the aptamer performances in various binding assay designs will increase understanding of the effects of aptamer labeling and immobilization and the effect of selection buffer conditions. In **Chapter 4**, the selected aptamer candidates are tested in a set of binding assays with ranging properties (RT-PCR, ALISA-ELAA, Fluorescence detection and SPR). This chapter explores assays with increasing complexities and costs, and highlights the challenges of using immobilized or labelled aptamers. Moreover, the importance of negative controls is highlighted when evaluating complex binding designs and specificity, selectivity and affinity of the selected aptamers for CRP is determined.

The third aim of this research is the application of the selected aptamer as a receptor or detector in a new label-free prototype read-out system. **Chapter 5** explores the application of the selected aptamer(s) and one other well validated aptamer for human  $\alpha$ -thrombin in a new label-free read-out system, measuring changes in heat-transfer resistance over an aptamer-coated surface upon target binding and vice versa. This method is proven to be useful in DNA denaturation experiments for SNP detection. Several assay designs are explored which highlights some key features of this read-out method and their consequences for sensitive protein detection on this platform by means of aptamers.

In a concluding **Chapter 6**, the obtained findings of this research will be summarized and evaluated. Suggestions are made for further implementation and for further improvements in the selection procedures, validation assays and applications of new aptamers.

The relation between the main objective, the aims and the different chapters of this dissertation is presented in Fig. 1.18.

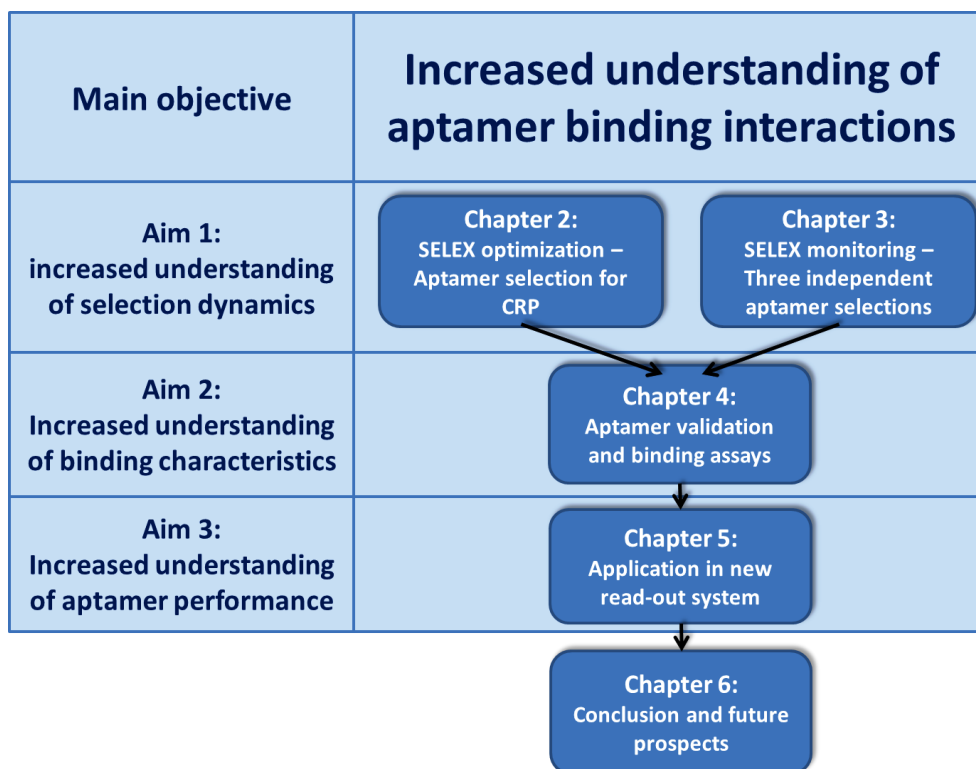


**Fig. 1.18. Structure overview of this dissertation**

# 2

## **Modified SELEX procedure for CRP aptamer selection**

*In this chapter, the SELEX procedure is optimized for aptamer selection for C - reactive protein (CRP). This optimization starts from random library optimizations to the selection of candidate aptamers for CRP. Different SELEX designs, buffer conditions and selection steps are evaluated for this specific CRP selection. Moreover, general recommendations and pitfalls of the SELEX procedure are discussed.*

### **2.1. Introduction**

The SELEX procedure is generally introduced and explained in chapter 1.3. Although the selection procedure is explained in general steps, there is no such thing as a general SELEX procedure. In this chapter, a selection platform for aptamer selection against C-reactive protein (CRP) is optimized and tested. Problems that arise during the selection process are discussed and solutions are proposed to mitigate these difficulties. This results in a detailed description of a modified, optimized aptamer selection procedure for this target. Since CRP levels are routinely measured in blood analysis as a marker for inflammation, this is an interesting target for diagnostic and other applications.

#### 2.1.1. Target properties and characteristics

CRP is a homopentameric oligoprotein of 125 kDa, composed of monomeric subunits that are each about 25 kDa (Fig. 2.1). It is an acute-phase protein as it is involved in several host defense related functions based on its ability to recognize foreign pathogens and damaged cells of the host and to initiate their elimination by interacting with humoral and cellular effector systems in the blood (Mantovani *et al.*, 2013). As part of the innate immune system, it was the first pattern recognition receptor (PRR) to be identified (Mantovani *et al.*, 2008). The level of this protein in plasma increases greatly during acute phase response to tissue injury, infection, or other inflammatory stimuli, as it is produced by hepatocytes in response to IL-6, IL-1 and TNF (Pepys & Hirschfield, 2003). Its concentration increases by as much as a 1000-fold in many pathological conditions, with a sharp rise within 6 h of induction and a maximum increase at approximately 48 hours (Mantovani *et al.*, 2013). CRP pentraxins are lectin-like

molecules (Fig. 2.1.) and interaction with sugars has been well characterized (Mantovani *et al.*, 2008). CRP binds a whole range of molecules (pathogens, growth factors, complement components and extracellular matrix proteins), mostly in a  $\text{Ca}^{2+}$ -dependent manner (Mantovani *et al.*, 2008).

CRP plasma levels are routinely measured as a marker for inflammation and for monitoring the state of a disease (Pepys & Hirschfield, 2003). Patients with elevated basal levels of CRP are reported to be at an increased risk of diabetes (Dehghan *et al.*, 2007) hypertension and cardiovascular disease, but since so many factors can cause basal level elevation; this is not a specific prognostic marker. There is also a strong association between basal CRP levels and BMI, and CRP levels decrease in response to low-fat diet or exercise (Pepys & Hirschfield, 2003). Recently, pre-operation levels of CRP are investigated as a predictor for complications after various treatments *e.g.* coronary artery bypass (Bařrakova *et al.*, 2013; Meyer *et al.*, 2013) and for survival *e.g.* in patients with a primary sarcoma of bone (Nakamura *et al.*, 2013). Moreover, high levels of CRP are associated with increasing lung cancer risk, elucidating the complex and possible role of inflammation in tumor biology (Xu *et al.*, 2013).

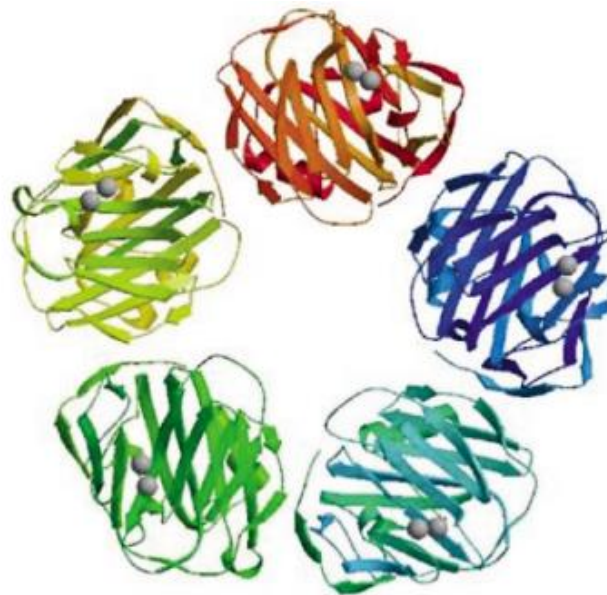


**Fig 2.1. Ribbon diagram of the crystal structure, showing the lectin fold and the two calcium atoms (spheres) in the ligand-binding site of each protomer (Thompson *et al.*, 1999)**

The correlation of circulating CRP concentrations with the severity, extent, and progression of a lot of different pathologies, and the prognostic significance of these associations, are consistent with CRP not just being a marker of disease but also contributing to pathogenesis (Pepys & Hirschfield, 2003). A definitive way to test this concept is the use of novel drugs that specifically block CRP



binding and its proinflammatory effect *in vivo* (Pepys, 1999). If these compounds are effective, they may find very broad therapeutic applicability. As aptamers are good therapeutic candidates, studies with CRP specific aptamers could lead to fully understand which systems are regulated by the protein and what disturbances are produced if the CRP is missing or overexpressed (Miramontes & Romero-Prado, 2013).

Standard analytical methods for CRP determination are agglutination and ELISA tests. High-sensitivity ELISA tests for CRP detection are readily available (e.g. from ApDia bvba, Turnhout). Recent advances in aptamer research has resulted in the selection of several aptamer sequences for CRP (Fig. 2.2) as well, both RNA (Bini *et al.*, 2008; Orito *et al.*, 2012) and DNA (Huang *et al.*, 2010). Though initially reported to bind native pentameric CRP, these sequences are shown to bind monomeric CRP (mCRP) and not the native form (Wang & Reed, 2012). While native, pentameric CRP (pCRP) is used in clinical assays to predict cardiovascular disease (CVD) risk, it is the monomeric isoform that is more strongly associated with pro-inflammatory and pro-atherogenic effects. Furthermore, mCRP has a greater influence on the development of vascular inflammation than pCRP (Khreiss *et al.*, 2004). Therefore, there is great potential for assays that can distinguish between the different forms of CRP and bind native pCRP as well. In 2013, a battery of patented aptamers is developed for detecting and/or measuring different forms of CRP (Miramontes & Romero-Prado, 2013).

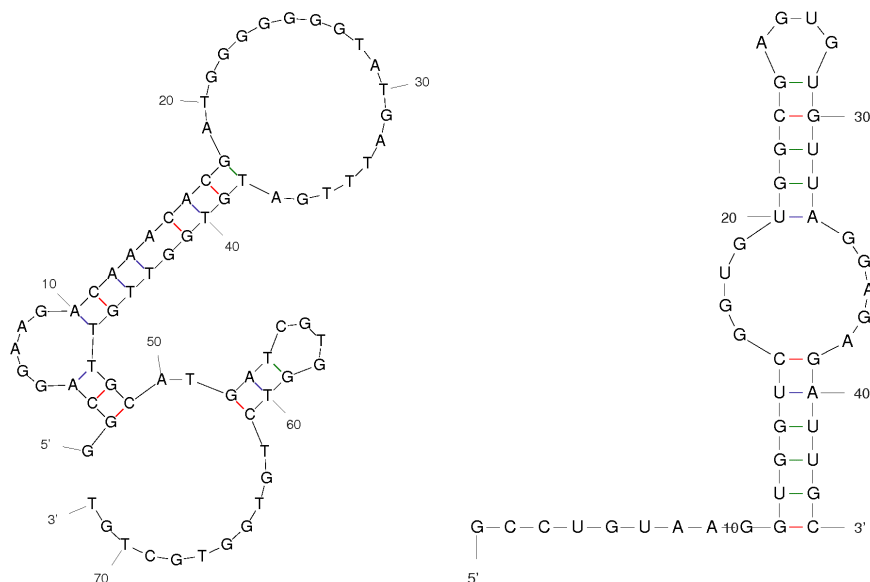


**Fig. 2.2. Graphic representations of the ssDNA aptamer (left, Huang *et al.*, 2010) and one of the RNA aptamers (right, Bini *et al.*, 2008) for CRP as illustrated at [www.aptagen.com](http://www.aptagen.com).**

### 2.1.2. Optimizing the SELEX protocol for pCRP selection

One of the first aspects to consider is the design of the random library and the primers, needed for amplification purposes. Standard SELEX libraries require two primers, one of each binding to one side of a central, random domain of 20 to 80 nucleotides (Stoltenburg *et al.*, 2007). Dependent on the size of the target, one could choose for a small or large random part of the library. Since a great number of selected aptamers are truncated down to a minimal functional sequence after the SELEX process, libraries with short randomized regions seem sufficient for a successful aptamer selection. Moreover, short libraries are better manageable and cost-effective in chemical synthesis. However, longer randomized regions give the libraries a greater structural complexity which may provide better opportunities for the identification of aptamers (Marshall & Ellington, 2000). The primer-binding regions, fixed sequences of 18 to 21 nucleotides, are subject of discussion as well. They cause non-specific binding by their DNA nature (leading to false-positive binding sequences) or interfere with the binding of random sequence parts to the target (Pan & Clawson, 2009). As these regions are constant, they decrease the random library diversity as well. However, Djordevic (2007) points out that the oligonucleotide library is so large, that it completely saturates the relevant sequence space. From a bio-informatical study of 2000 aptamers for 141 unique target ligands in the Aptamer Database (<http://www.aptamer.icmb.utexas.edu> (Lee *et al.*, 2004), it is clear that the constant, primer-binding regions do not, in general, contribute significantly to aptamer structures (Cowperthwaite & Ellington, 2008). Nevertheless, efforts have been made to come up with Primer-Free and Minimal-Primer selection protocols (Pan & Clawson, 2009).

The selection step includes the binding of the target with the oligonucleotide library, the subsequent partition of unbound oligonucleotides and the elution of bound oligonucleotides in relevant binding, washing and elution conditions. The selection library is put in close contact with the target in a binding buffer. Incubation conditions are the conditions in which the aptamer is selected and are crucial for aptamer performance. As pCRP is reported to slowly self-dissociate in the absence of calcium (Wang *et al.*, 2002), it is suggested to add small amounts of CaCl<sub>2</sub> to the binding buffer, to ensure CRP stays present in the native pentameric form. The selection design and separation technique for bound and unbound oligonucleotides greatly depends on the target properties and the techniques that are at hand. Immobilization of the target molecule on a particular matrix material allows effective separation. This approach seems appropriate for CRP, since this is a pentameric form. When immobilizing small, monomeric molecules, there is always a risk that the one epitope for aptamer binding is used or blocked by the immobilization strategy. Elution by denaturation is induced by heat or by adding denaturing components to the elution buffer.

The amplification of eluted sequence has to be as efficient as possible. After efficient separation of the bound oligonucleotides, efficient amplification is important, especially in the beginning of selection, with low amounts of retained specific oligonucleotides and high levels of randomness. Fundamental differences between PCR amplification of homogeneous and random DNA templates however call for extra PCR optimizations. In the amplification of random libraries, product formation reaches a maximum after 20 cycles (Fig. 2.3.) and products rapidly convert to by-products after only 5 additional amplification cycles. The loss of yield increases with the length of the DNA sequences to be amplified (Musheev & Krylov, 2006) and comes from primer-product and product-product hybridization. Emulsion PCR is proposed as a new efficient way to amplify random DNA libraries by means of compartmentalization of the PCR mix (Shao *et al.*, 2011).

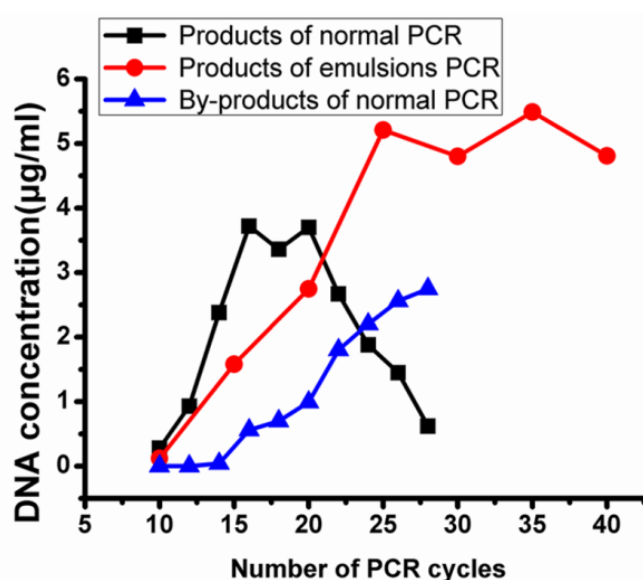


**Fig. 2.3. Product and by-product formation in conventional and emulsion PCR (Shao *et al.*, 2011)**

In the crowded pool of oligonucleotides, there are only a few sequence-specific binders to the target, due to hydrogen bonds and Van-der Waals interactions. Other oligonucleotides bind only due electrostatic interactions, and are sequence-non-specific (Djordjevic, 2007). Moreover, during the selection step, it is not possible to completely separate bound and non-bound sequences (*i.e.* background partitioning). Consequently, the number of non-specific binders is larger than the number of specific binders in the first rounds of selection. Furthermore, the library also contains sequence-specific binders to molecules that are part of the selection mix, but are not the target of selection. Changing the selection design and selection conditions during the SELEX process can

mitigate these problems. *E.g.* when selecting for the strongest binders from a large random pool, it is fundamental not to lose those sequences due to stochastic effects in the early rounds. Therefore, SELEX can start with higher amounts of proteins, but then gradually decreasing to increase the stringency of selection in the later SELEX rounds.

The following parts contain the optimization steps that were followed to come up with a selection platform for aptamer selection for CRP, which results in selection of multiple aptamer candidates for CRP, by performing a modified, optimized SELEX design and approach.

## 2.2. Experimental section

For full description of the generally applied buffers and reagents, please see the abbreviations and buffer composition list in the appendix of this dissertation. Specific buffer compositions are mentioned in text. Unless stated otherwise, buffers are made with reagents purchased from Sigma Aldrich (Bornem, Belgium).

### 2.2.1. ssDNA library construction and amplification.

A 40 *nt* (nucleotides) random library flanked by 18 *nt* primer binding regions together with corresponding primer sequences (Table 2.1) are purchased from Integrated DNA Technologies (IDT, Haasrode, Belgium). Primers are checked *in silico* for dimerization, hairpin formation and melting temperature with Oligo v.6 Primer Analysis Software (Molecular Biology Insights, Cascade, CO, USA).

**Table 2.1. ssDNA library and Forward and Reverse primers.**

<b>5'-GCACCAGCATATTCGATT-40N-GGCTAGTAGGTGCATCAG-3'</b>	
F: 5'- GCACCAGCATATTCGATT-3'	R <sub>(p)</sub> : 5'- CTGATGCACCTACTAGCC-3'

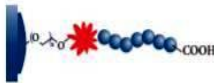
PCR amplification is optimized by gradient PCR with different Mg<sup>2+</sup> concentrations. PCR conditions are optimized as 50 µL reaction mixes, containing 1x PCR buffer (Roche, Merelbeke, Belgium); 2.5 mM extra Mg<sup>2+</sup>; 0.6 mM dNTP; 0.2 µM of each primer and 0.5 units Taq DNA Polymerase (Roche) and a three-step PCR procedure of 20 cycles with an annealing temperature of 60 °C.

### 2.2.2. Target immobilization

CRP is purchased from BBI Solutions (Cardiff, UK) and covalently coupled by Pierce™ EDC and NHS (Thermo Fisher Scientific, Erembodegem, Belgium) chemistry to magnetic beads. A carbodiimide is utilized to activate Dynabeads® MyOne™ Carboxylic Acid (Life Technologies™, Ghent, Belgium) for amide bonding with primary amines of the CRP pentamers. For this purpose, the 'Two-Step Coating Procedure using NHS', provided by the manufacturer is used (Dynabeads® website, 2013). CRP is delivered in CRP-buffer containing CaCl<sub>2</sub> and 50 µg CRP /mg of activated magnetic beads is coated in 25 mM MES, pH 6. Beads are covalently counter coated with 0.5 % of BSA and non-reacted activated carboxylic acid groups are quenched by 2 hours incubation with 100 mM ethanolamine in carbonate-bicarbonate buffer, pH 9.6. Washings are done with 1 x PBS + 0.1 % TWEEN® 20 (Sigma Aldrich). Beads are stored in SELEX binding buffer.

CRP is also covalently coupled to NucleoLink™ Immobilizer Plates (Thermo Fisher Scientific). The technology is based on the anthraquinone photo-coupling method (Jauho *et al.*, 2000) which provides a simple one-step procedure for covalently coupling bio-molecules. The photoprobe consists of 3 parts: The anthraquinone molecule, the ethylene glycol spacer and an electrophilic group. The density of the electrophilic groups and the spacer design is optimized for immobilizing peptides, proteins, or antibodies (Thermo Scientific Plate Guide, 2009). For the first SELEX rounds, 0.87 µM CRP is coated in carbonate-bicarbonate buffer, pH 9.6. Washings are performed with 1x TBS + 0.5 % TWEEN® 20 and the wells are inactivated with 100 mM ethanolamine in carbonate-bicarbonate buffer, pH 9.6.

Negative beads and wells for negative selections are prepared by following the same procedures, but omitting the target addition to the coating buffers. CRP coatings on both substrates are checked by chemiluminescence immunoassays using HRP- and AP-conjugated monoclonal CRP-antibodies (In house and purchased from BBI Solutions, Cardiff) after 1 h incubation in conjugation buffer and washing with corresponding washing buffers (according instructions provided by the manufacturer).

Surface	Structure	Binding Preference	Applications	Molecular Drawings
Immobilizer Amino	Reactive electrophile tethered by spacer arm	Proteins, nucleic acids with free NH <sub>2</sub> or SH groups	ELISA, Hybridization Assays	

**Fig. 2.4. NucleoLink™ Immobilizer 96-Well plate characteristics (Thermo Scientific Plate Guide, 2009)**

### 2.2.3. General selection design

Bead-SELEX is performed in Eppendorf tubes with selection steps in a rotor for mixing and magnetic separation in magnetic holders. Plate-SELEX steps are executed in the wells, with gentle mixing on a shaker at slow rpm.

In analogy with the RNA aptamer selection by Bini *et al.* (2008), 10 mM HEPES is chosen as the SELEX binding buffer, but with addition of 5 mM CaCl<sub>2</sub> and a physiological pH of 7.4. An amount of 10<sup>14</sup> oligonucleotides (1.6 μM) is diluted in binding buffer, predenatured at 94°C, put on ice and incubated for 1 h at room temperature with the target. Five min. washings are done three times in 1x PBS, pH 7.4. Bound oligonucleotides are collected from the target four times by addition of 1x TE + 2 M Urea of 80°C and two minutes incubation. Counter selections are performed on negative coated beads and wells. After incubation, the ssDNA in the supernatant is collected. ssDNA collections are extracted by Phenol-Chloroform extraction (Phenol:Chloroform:Isoamylalcohol 25:24:1, Sigma Aldrich), purified by cross-linked dextran gel filtration (Sephadex<sup>®</sup> G-100, Sigma Aldrich) and rediluted in 50 μL PCR reaction mixes for amplification.

DNA conditioning is tested in two ways: extra asymmetric amplification in 100x excess of Forward primer and anti-sense specific strand digestion by λ-exonuclease digestion according the instructions provided by the manufacturer (New England Biolabs, Frankfurt am Main, Germany). Therefore, PCR amplification is done with a 5'-phosphorylated Reverse primer, purchased from IDT. After Sephadex<sup>®</sup> purification, the ssDNA is rediluted in SELEX binding buffer.

An effort is put in following the ssDNA pool in terms of quantity, by measuring the DNA quantities after different selection steps and conditions. This is done by gel quantification, UV-Vis Spectrophotometry (NanoDrop ND-1000, NanoDrop Technologies inc., DE, USA) or by quantitative PCR on a Lightcycler<sup>®</sup> 1.5 Caroussel, using LightCycler<sup>®</sup> DNA Master SYBR Green I reaction mix (Roche). This is optimized as 35 amplification cycles of 5 s at 95 °C, 3 s at 60 °C and 4 s at 72 °C in a 20 μL reaction mix (1x SYBR; 3 mM Mg<sup>2+</sup> extra; 0.1 μM of each primer). A random library dilution series (8.3 nM - 0.083 pM) is ran as a DNA quantity standard.

### 2.2.4. Cloning and sequencing

After 16 rounds of selection, the collected ssDNA pools are amplified by PCR amplification with the non-phosphorylated reverse primer. The amplified dsDNA is transformed into a plasmid vector and cloned by means of the TOPO<sup>®</sup> TA Cloning<sup>®</sup> Kit for Subcloning with TOP10 chemically competent Cells (Life Technologies<sup>™</sup>, Ghent, Belgium) by following the instructions provided by the

manufacturer (Life Technologies™, 2012). Cells are grown overnight on Agar plates with 0.1 % Ampicillin. After DNA isolation and amplification of individual clones, the aptamer candidates are purified by following the ExoSAP-IT® For PCR Product Clean-Up procedure (Affymetrix, CA, USA). This enzymatic digestion of contaminants is performed as instructed with 50 ng dsDNA input (Affymetrix, 2011) to ensure correct and highly specific amplification and sequencing by means of the ABI Prism® BigDye® Terminator v3.1 Cycle Sequencing Kit (Life Technologies™) on a 310 Genetic Analyzer (Life Technologies™). Sequence analysis is performed in the software supplied by Applied Biosystems and Chromas Lite v2.1.1 (Technelysium Pty Ltd, Brisbane, Australia). Sequences are aligned and compared in the ClustalX2 Software (Larkin *et al.*, 2007).

## **2.3. Results & discussion**

### 2.3.1. Selection design optimizations

DNA quantity measurements elucidate some interesting features of the selection design. Gel Electrophoresis of the amplified ssDNA collections indicates there is severe loss of PCR product by by-product formation, leading to dimerization and further oligomerization of the DNA products (Fig. 2.5.). Limiting the amount of amplification cycles to 20 or even 15 cycles is not enough to cope with this effect as DNA smears appear after only two consecutive PCR amplifications with Sephadex® purification in between. Therefore, PCR amplicons are conditioned by size separation on a 4 % agarose (Sigma Aldrich) gel and cutting out the 76 bp dsDNA band. Agarose gel extraction in 1 mL Crush & Soak buffer is performed overnight in a rotor at 4 °C. Since amplification has such negative effect on by-product formation, λ-exonuclease digestion is chosen to be the way for generation of ssDNA after amplification. In a recent paper (Avci-Adali *et al.*, 2013), the PCR induced by-product formation is reported in a CELL-SELEX experiment and is explained by increased ssDNA template input as the selection procedure continues. Therefore, the amount of cell-binding aptamers is assessed by qPCR and the number of amplification cycles is adapted according the ssDNA quantity in the SELEX pool. Here, it is shown that GE separation and isolation of the PCR-product band efficiently addresses this problem, without the need for adjusting the amount of amplification cycles.

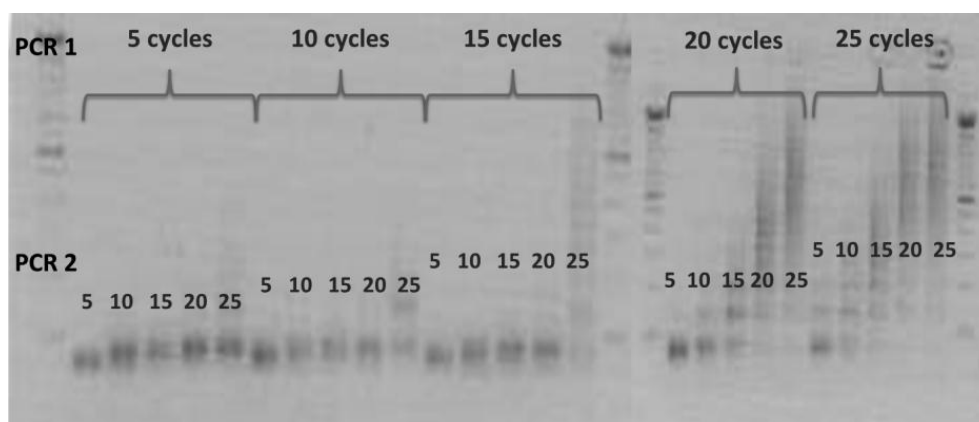


**Fig. 2.5. GE of amplicons after 2 consecutive PCR amplifications with 5-25 amplification cycles. Cycle number for PCR 1 is indicated above, cycle number for consecutive PCR 2 below. Concatemerization is clear in the conditions with too many consecutive cycles.**

In pilot studies of both positive and negative Bead-SELEX selections, ssDNA quantities were measured by UV-VIS Spectrophotometry (Fig. 2.6). The amounts of eluted ssDNA are very high and do not significantly decrease after 7 elutions. This indicates there is a high degree of undesired binding of the ssDNA to both negative and target beads, non-specifically by the nature of the DNA, specifically to compounds other than CRP or both. DNA LoBind® tubes (Eppendorf) are tested to reduce non-specific sticking of DNA to the tubes but this did not alter the outcomes of this test.

To cope with this effect, the SELEX design is modified by increasing the amount of counter selections and changing the timing of amplification. Each selection round (*i.e.* from GE separation to PCR amplification) now consists of multiple negative selections and one positive selection step without ssDNA pool amplification in between. This sequence of selections is chosen by reasoning that the ssDNA selection pool contains, especially in the onset of the procedure, more non-specifically binding sequences than specific binders that need to be purified from the selection pool before PCR amplification. For this reason, each selection round consists of an initial negative selection, a positive selection and another consecutive negative selection step. Furthermore, in the very first SELEX round, the procedure is started with 4 initial negative selection steps, to purify the selection library from non-specific binders.



## Random library ssDNA collections (NanoDrop)

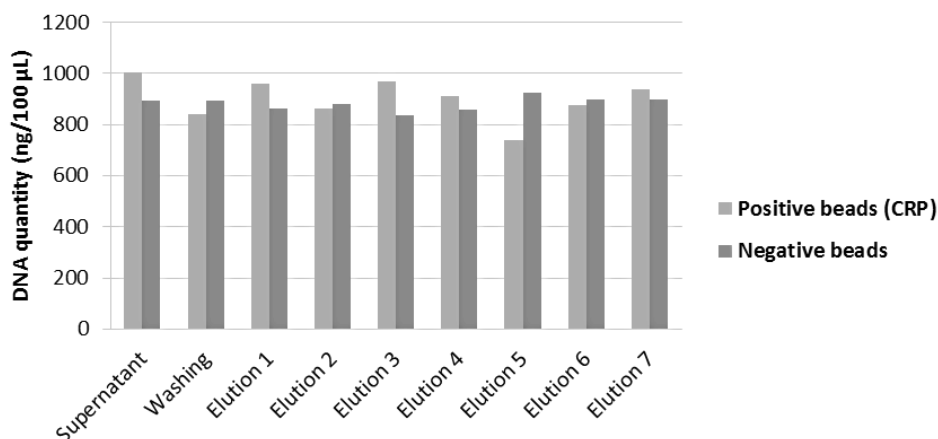


**Fig. 2.6. ssDNA quantities of collected fractions measured by UV/Vis Spectrophotometry (NanoDrop ND-1000) in a pilot selection step with 16 µM random library on positive and negative coated beads.**

By increasing the number of negative selection steps, the chance of losing specific binders to CRP by non-specific DNA adsorption increases. To address this risk, an excess of non-specific Herring Sperm ssDNA (HS-ssDNA, Sigma Aldrich), with extra sonication to a length of  $\approx 200$  nt, is added during the negative selection steps. Since this is present in excess, this will be lost first by non-specific sticking of DNA.

However, the presence of an excess of non-specific HS-ssDNA needs to be compatible with following PCR and GE purification protocols and may not block CRP epitopes for target recognition, as HS-ssDNA will still be present in the selection buffer during the positive selection step.

Target availability is checked by performing an ELISA assay on the used immobilization substrates as described above, with addition of different amounts of HS-ssDNA to the mAb conjugation buffer. A pilot study with quantitative PCR (Fig. 2.7) and GE-purification of various single oligonucleotide ssDNA templates (83 pM, 8.30 pM and 0.83 pM) and increasing proportions of HS-ssDNA:ssDNA (10:1, 50:1, 100:1, 250:1, 1000:1) is performed to determine the maximum proportion of specific ssDNA and non-specific HS-ssDNA.

From this study it is clear that the total bulk amount of DNA in the PCR reaction is the most important factor that determines PCR and GE-separation efficiency (Fig. 2.7). The inhibiting effect of HS-ssDNA on PCR efficiency decreases as the amount of template ssDNA decreases. With 83 pM input, addition of 50x excess HS-ssDNA has a large impact, as with 0.83 pM this seems to have a beneficial effect. GE-separation seems to be inhibited by high quantities of bulk DNA in the

gel as well with 100x excess of HS-ssDNA. A maximum proportion of 50:1 HS-ssDNA: ssDNA is set for negative selections, directly followed by PCR amplification and GE conditioning, and of 100:1 for negative selections followed by a consecutive positive selection. ELISA results confirm CRP epitope availability at both calculated levels of HS-ssDNA addition.

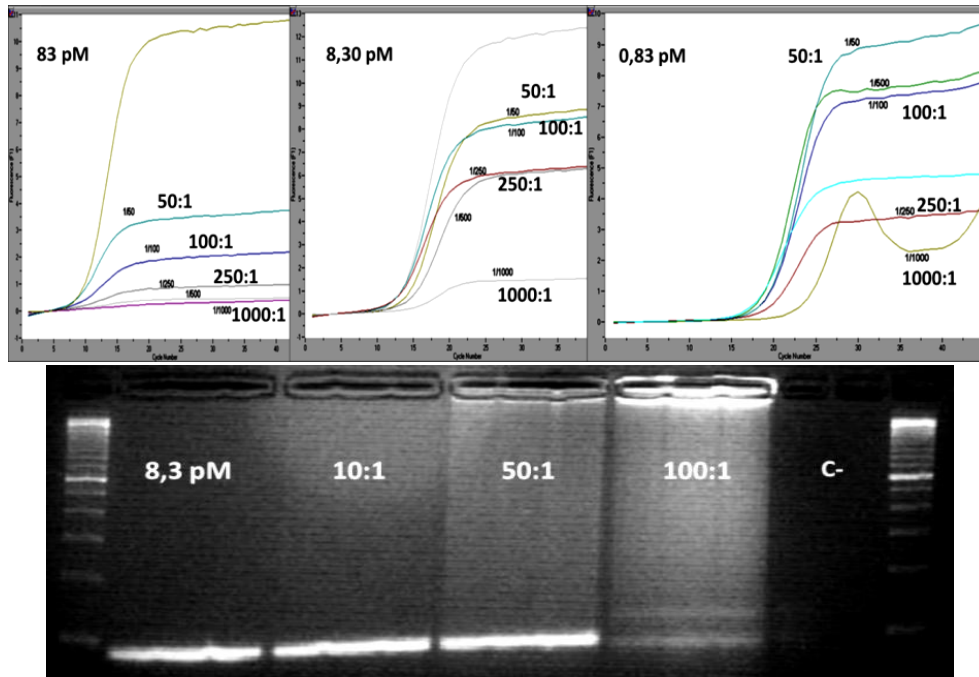


**Fig. 2.7. Top: qPCR of 83-0.83 pM of random library with increasing proportions (50-1000:1) of HS-ssDNA added (y-axis: F= fluorescence generated by SYBR Green; x-axis: number of cycles 0 – 40). Down: GE-separation of 8.3 pM template and different HS-ssDNA proportions**

In a last optimization, the magnetic separation approach with selection on functionalized Dynabeads® is omitted after Flow Cytometry (BD Biosciences, Erembodegem, Belgium) results of coated and uncoated beads. Forward and Side Scatter, indications of particle size and granulometry, are increased for CRP-coated magnetic beads (Fig. 2.8). The beads show not only low autofluorescence, they also aggregate upon CRP-functionalization which reduces target availability and selection efficiency in comparison to negative beads. This may be caused by monomerization of pCRP during the immobilization process and re-association of immobilized mCRP in selection buffer (10 mM HEPES + 5 mM CaCl<sub>2</sub>).

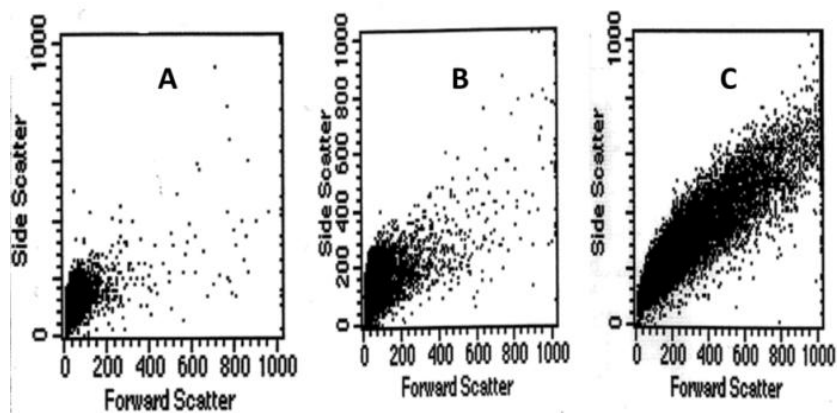


**Fig. 2.8. Flow Cytometry of (A) uncoated beads (B) BSA-ethanolamine beads: slightly increased forward and side scatter (C) CRP beads: high increase of forward and size scatter**

The optimized selection procedure is executed on NucleoLink™ Immobilizer plates and consists of multiple selection steps per SELEX round, as illustrated in Fig. 2.9.

As explained above, in the first SELEX round, the random ssDNA library is subjected to 4 initial negative selections to eliminate non-specific binding sequences out of the selection library before the first PCR amplification. Non-specific HS-ssDNA is added in 50x or 100x excess prior to the counter selection steps. Therefore, the selected ssDNA fractions are quantified by real-time PCR.

Stringency is increased throughout the SELEX progress by lowering the amount of target and decreasing the incubation time (1h → 30 min) during positive selection steps. The amount of washings is increased to five times and at a slightly increased temperature of 30°C. During positive selections, elutions are performed four times (E1-E4 in fig. 2.9) and analyzed separately by real-time PCR.

Amplification of the selected ssDNA fractions by PCR is set for 15 cycles to avoid by-product formation, followed by GE-separation and agarose extraction of the 76 bp dsDNA band. Amplified sense ssDNA library is generated by λ-exonuclease digestion of the antisense strand. After purification, this ssDNA selection pool is dissolved in SELEX binding buffer for the next SELEX round.

Assessment of recovered ssDNA quantities after positive and negative selection steps allows for quantitative monitoring of the SELEX progress. As explained in Chapter 3, a new qualitative method for SELEX monitoring in terms of DNA composition by remelting curve analysis (rMCA) after real-time PCR is developed. The results of these analyses are very useful in deciding when to stop selection and start sequencing of the ssDNA pools. Based on these results, the 4 separate elutions are pooled together in the first 10 SELEX rounds, but

kept separate for parallel SELEX afterwards. This results in differentiated selection in 4 SELEX fractions of different aptamers. After 16 SELEX rounds, minimum 40 sequences per SELEX fraction are analyzed and compared in Clustal X2.

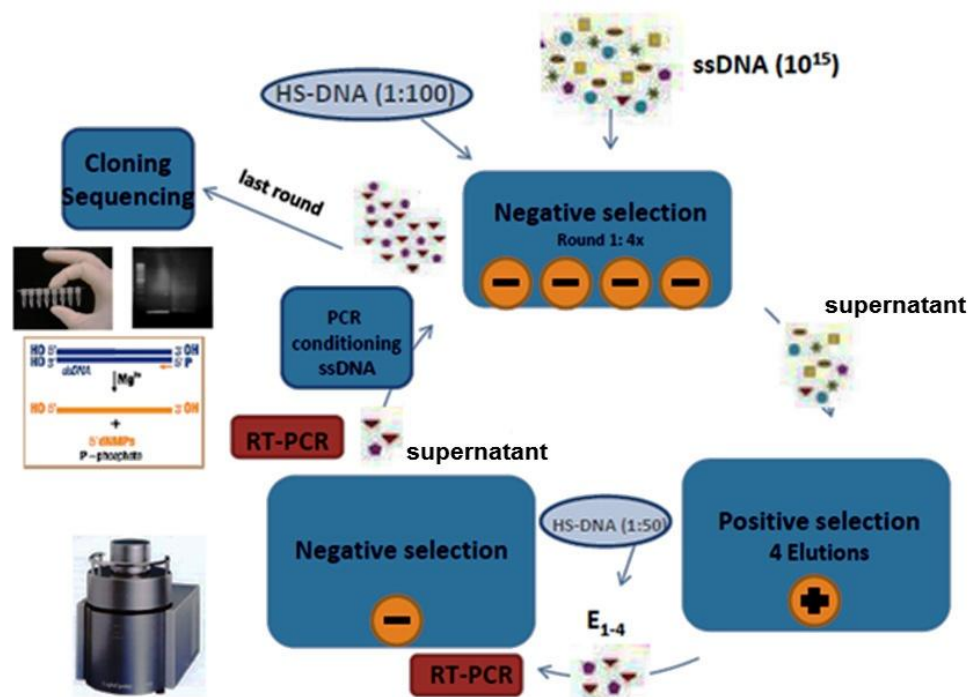


**Fig. 2.9. Optimized plate-SELEX procedure for aptamer selection for CRP.** Each SELEX round consists of a negative selection step (4 negative selection steps in the first round), followed by a positive selection step and an extra negative selection prior to PCR amplification. Before the negative selection steps, Herring Sperm ssDNA (HS-DNA) is added in 100x and 50x excess. In a full SELEX round, the ssDNA library is subjected to a negative selection and supernatant is subjected to a positive selection step in presence of CRP. Four elution fractions (E1-E4) are again subjected to a negative selection step before the supernatant is amplified by PCR, purified by GE and conditioned to ssDNA again by nuclease digestion. After each selection step, resulting ssDNA pools are analyzed by real-time PCR for quantitative analysis.

### 2.3.2. Sequence and structure analysis of selected aptamer candidates.

Sequence analysis indicates enrichment of oligonucleotide sequences in 4 fractions. This enrichment differs in term of numbers of enriched aptamers (Table 2.2). For every fraction, the sequence alignment is illustrated in appendix (Appendix Fig. 1 - 4) and the sequence information of the most enriched sequence in every fraction is given in Table 2.3. and Fig. 2.10. Structure analysis in mfold (Zuker, 2003) predicts the secondary structure of these aptamer candidates in the given buffer conditions ( $\text{Na}^+ = 140 \text{ mM}$ ) and

temperature (24 °C) and gives the Gibbs Energy value ( $\Delta G$  in kcal/mol) as a stability estimation of the structure.

**Table 2.2. Sequencing analysis of selected oligonucleotides for CRP confirms enrichment in four fractions. Table shows each fraction with the number of enriched oligonucleotides (# aptamer candidates) and their proportion of the total amount of analyzed sequences (n) for that fraction (e.g. in fraction 3 there is 1 enriched oligonucleotide that consists 90% of all 31 analyzed sequences).**

	<b>Fraction 1 (n = 43)</b>	<b>Fraction 2 (n = 27)</b>	<b>Fraction 3 (n = 31)</b>	<b>Fraction 4 (n = 17)</b>
<b>Number of enriched sequences</b>	5	2	1	4
<b>Proportion of enriched sequences (%)</b>	23, 16, 7, 7, 5	50 & 20	90	16 each

It is clear that the aptamer enriched in Fraction 4 (A4), correspondent with the last eluted fraction in SELEX round 10, has the greatest stability. The most enriched aptamer for Fraction 1 (A1) has the lowest stability. Whereas, several oligonucleotides returned in the analyzed sequences of all fractions, the most enriched aptamer was different for all 4 fractions. By dividing the SELEX pool of round 10 in 4 pools that were eluted with different stringencies, the aptamer outcome in these pools was differentiated as well, with the most stable aptamer structure in the fraction that was eluted with the highest stringency.

**Table 2.3. Sequence information for most enriched aptamer candidate in each fraction and the Gibbs Energy value for stability of the structure ( $\Delta G$ ).**

<b>A.1</b>	5' - GCA CCA GCA TAT TCG ATT GGA GGG GGG TAT TGA TTG ACA TAT TGA TCT TGT TTC TTG GGC TAG TAG GTG CAT CAG - 3'	<b><math>\Delta G = -2.56</math> kcal/mol</b>
<b>A.2</b>	5' - GCA CCA GCA TAT TCG ATT GTG GCG GGT TGT GAA GGG TGG AGT ATG GTC GTG TTG GTT GGG CTA GTA GGT GCA TCA G - 3'	<b><math>\Delta G = -2.85</math> kcal/mol</b>
<b>A.3</b>	5' - GCA CCA GCA TAT TCG ATT GGG AGC GCG GGG GAG AGT AGT GGG GAA CGG TGG AGA GTT GGG CTA GTA GGT GCA TCA G - 3'	<b><math>\Delta G = -3.02</math> kcal/mol</b>
<b>A.4</b>	5' - GCA CCA GCA TAT TCG ATT GGG AGG TGT GAA CGT TAT GTG GTA GAG AGA TGG GTG GTG GGG CTA GTA GGT GCA TCA G - 3'	<b><math>\Delta G = -4.35</math> kcal/mol</b>

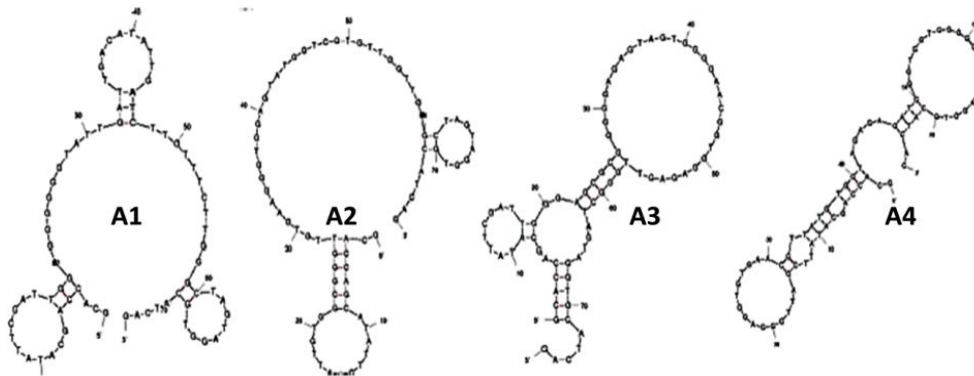


**Fig. 2.10. Secondary structure analysis of aptamer candidates A1 – A4.**

Comparison of the four selected aptamer candidates sequences (Fig. 2.11) to each other and the previously selected ssDNA aptamer (*apta2010*, Huang *et al.*) shows there are corresponding motifs with all aptamer sequences (red) and motifs that are only shared by some of the ssDNA aptamers (blue). Aptamers A1 and A2 have the largest similarity with *apta2010*, other motifs reoccur in A2, A3 & A4. High similarities are found within and right next to the primer binding regions (grey), implying that these sequences may participate in binding of CRP. Secondary structure analysis (Fig. 2.12) reveals most similarity with A3 & A4, in a double halter-like confirmation with a higher stability ( $\Delta G = -7.94$  kcal/mol) (Aptagen, 2013).

Sequence and structure similarities with another ssDNA aptamer for CRP which is now commercially available (Aptagen, 2013) may confirm specific aptamer selection for CRP. In the study of Huang *et al.* (2010), the aptamer is reported to bind pCRP with a 3.51 nM affinity, determined by SPR analysis. However, recently this aptamer is reported to be specific for mCRP and not pCRP (Wang & Reed, 2012) after performing a nanoparticle-based electrophoresis mobility shift assay (NP-EMSA) on reported RNA and DNA aptamers for CRP.



**Fig. 2.11. Sequence alignment (Clustal X2) of obtained aptamer candidates and *apta2010* (Huang *et al.*, 2010). Grey: Primer binding regions; Red: Corresponding motifs for all sequences; Blue: Corresponding motifs for some sequences.**

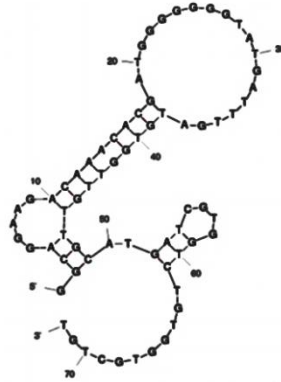


**Fig. 2.12. Secondary Structure prediction of apta(2010) as provided by AptaGen (2013).**

Okemefuna *et al.* (2010) reported about the transition between monomeric (mCRP) and pentameric CRP (pCRP). pCRP slowly dissociates to mCRP in  $\text{Ca}^{2+}$  depleted conditions and mCRP needs 2 mM  $\text{Ca}^{2+}$  and 140 mM NaCl for specific re-association, in low salt conditions non-specific aggregation is reported. As *apta2010* (Huang *et al.*, 2010) is selected and tested in 10 mM Tris buffer containing only 50 mM NaCl and 2 mM  $\text{CaCl}_2$ , there is a possibility *apta2010* is selected and tested against mCRP(-aggregates). As the SELEX binding buffer in the SELEX procedure reported here is chosen to be 10 mM HEPES containing 140 mM NaCl and 5 mM  $\text{CaCl}_2$ , pCRP integrity should be maintained or re-associated and aptamers should be selected against the native pentameric CRP. Furthermore, this study reported for the first time a  $\text{Ca}^{2+}$ -dependent pentamer-decamer equilibrium. Decamer formation is reported in presence of 2 mM of  $\text{Ca}^{2+}$  and decreases with increasing NaCl concentration. This implies that decamer formation is also possible in the applied selection binding buffers, by means of low-salt concentration in the buffer of Huang *et al.* (2010), or by high  $\text{CaCl}_2$  concentration in the HEPES buffer of this study. The buffer dependent aggregation or association of mCRP and pCRP can also explain the Dynabeads<sup>®</sup> aggregation upon CRP-coating detected by Flow Cytometry (BD Biosciences). The effect of SELEX buffer composition (concentration of salts and  $\text{CaCl}_2$ ) on the form of CRP that is selected for and on SELEX aptamer outcomes has not been evaluated in this dissertation. However, this could be a very interesting option to compare SELEX results of selection in various buffers in terms of selected aptamer diversity and in terms of binding affinities to different forms of CRP (mCRP, pCRP and dCRP).

In Chapter 4, the candidate aptamer sequences will be tested for pCRP binding in various validation assays. Affinity studies will be performed to determine their affinity constants ( $K_d$ ).

## 2.4. Conclusions and recommendations

The aim of this second chapter was the optimization of the general SELEX procedure and the specific application for the selection of aptamers for C-reactive protein. Different SELEX designs, buffer conditions and selection steps are evaluated for this purpose. Moreover, general recommendations and pitfalls of the SELEX procedure are discussed.

This optimized SELEX procedure for CRP aptamers has shown that monitoring of the effect that selection condition steps have on the ssDNA random library is of high importance for a successful SELEX procedure. Care must be taken not to introduce a bias during amplification or non-specific binding during selection (Bowser, 2005). To address these problems, the SELEX design was radically modified, with a significant increase of negative selection steps, reduced PCR amplifications and an extra conditioning of the ssDNA pool by GE separation. HS-ssDNA is added to the selection mix to reduce non-specific binding. Our findings point out that monitoring the effect of the applied selection conditions provides crucial information needed for efficient aptamer selection. Therefore, we need to improve the monitoring of the SELEX procedure and progression, not only in terms of DNA quantities, but also in terms of composition or diversity of the selected ssDNA pools. This is addressed in chapter three, where a new tool for monitoring the enrichment of ssDNA pools under selection is presented.

The research presented in this chapter also indicates the importance of prior target characterization in the applied selection conditions. The selection buffer is chosen to be 10 mM HEPES containing 140 mM NaCl and 5 mM CaCl<sub>2</sub>, although this Ca<sup>2+</sup> concentration could favor decamer formation of pCRP. This could explain the problems that occur upon CRP-coating of Dynabeads<sup>®</sup>. This bead aggregation can decrease target availability or is caused by changed target characteristics, so the magnetic separation approach is omitted in the selection procedure.

The high number of selection rounds (16), with each round consisting of multiple selections, indicates low separation efficiency between bound and unbound oligonucleotides. This can be expected when the selection is performed in 96-well plates, where the separation method is manually pipetting the selection buffers out of the well, which is not as efficient as magnetic separation, filtration or other separation methods. The possible decamer formation in the selection buffer can also explain the low selection efficiency of this aptamer, reducing epitope availability.

As this method is laborious and prone to manually induced bias, efforts need to be made to change the separation approach for higher efficiency e.g. by capillary electrophoresis or gel filtration approaches. Performing less selection



rounds in a more automated way can significantly decrease selection time and non-specific binding.

Despite the low separation efficiency, this procedure resulted in the selection of 4 clearly enriched aptamer candidates for CRP. Moreover, by dividing the SELEX pool into pools of different stringency, aptamer differentiation is possible. Similarities with a previously selected ssDNA CRP aptamer indicate specific selection of certain binding motifs, needed for binding. Validation studies will investigate how these aptamer candidates bind to CRP and what is their affinity.



# 3

## reMelting Curve Analysis as a tool for enrichment monitoring in the SELEX process.

This chapter is based on:

Vanbrabant J., Leirs K., Vanschoenbeek K., Lammertyn J. & Michiels L. (2014) reMelting Curve Analysis as a Tool for Enrichment Monitoring in the SELEX Process. *Analyst* **39**(3): 589-95.

DOI: 10.1039/C3AN01884A

*Current aptamer selection procedures enable limited control and transparency on how the DNA selection pool is evolving. Here, it is shown that real-time PCR provides a valuable tool for the follow-up of aptamer selection. Limited time, work and amount of amplified ssDNA make this an interesting instrument to set-up a SELEX design and monitor the enrichment of oligonucleotides. reMelting Curve Analysis (rMCA) after reannealing at stringent conditions provides information about enrichment, compared to a random library. Monitoring the SELEX process and optimizing conditions by means of the proposed methods can increase the selection efficiency in a controlled way.*

### 3.1. Introduction

Different iterative steps are involved in the selection of aptamers by means of SELEX: incubation with target or blocked surface in binding buffer, washing with wash buffer, elution by denaturation and amplification of the remaining ssDNA pool. Conditions of both positive and negative selections are essential for efficient selection of aptamers. Although the selection conditions are critical, they are to great extent documented trial and error. Only after a number of SELEX rounds (*i.e.* 6-15) the selected DNA pool is sequenced and checked for enrichment of target-specific oligonucleotides (Stoltenburg *et al.*, 2008). Monitoring the effect of separate selections under different binding and washing conditions on the DNA pool provides valuable information to increase selection efficiency. Monitoring of the progression is critical for the success of an *in vitro* selection experiment and the characteristics of the selected aptamers. This allows early intervention and adjustment of the selection pressure and

stringency to achieve the desired activities of the selected aptamers (Müller *et al.*, 2008). Up to date, both direct measurement of SELEX progression, in terms of affinity of the ssDNA pool for the target, and indirect measurements have been addressed.

Measuring the amount of target-binding nucleotides in selection pools offers a way of monitoring enrichment directly by assessing average affinity of the SELEX pool for the target. For example, ELISA-like assays enable comparison of different consecutive ssDNA selection pools. A fraction is labeled with a fluorophore or enzyme and incubated on a target-coated substrate. Binding is then visualized and quantified by fluorescence or chemiluminescence on a membrane by blotting (Yoshida *et al.*, 2009) or on magnetic beads to perform flow cytometry for fluorescence acquisition (Wang *et al.*, 2009; Cao *et al.*, 2009). Other studies use radiolabeling to visualize and quantify the bound DNA (Hwang & Lee, 2002). Non-equilibrium capillary electrophoresis of Equilibrium mixtures (NECEEM) has proven to be a good way to control and compare SELEX fractions for target binding and even determine affinity ( $K_d$ ) of the SELEX pools (Berezovski *et al.*, 2005). Another way of direct screening for affinity is the HAPIScreen (High throughput Aptamer Identification screen) methodology (Dausse *et al.*, 2011). Target and candidate fractions are coated on beads, which results in chemiluminescence when the beads come in proximity *i.e.* when there is interaction between them. As such, an arbitrary score for affinity is determined and only fractions with a high score are evaluated.

These described assays suffer from several limitations and drawbacks. They are time- and material-consuming and do not always offer the required resolution or sensitivity for concise SELEX monitoring. One needs a very sensitive and good assay to see the difference in binding capacity of consecutive SELEX pools, especially in the onset of selection, when there are still a lot of random, non-specific oligonucleotides present in the eluted fractions. These assays are also target and platform dependent and not applicable for all SELEX targets. For example, small molecules often lack functional groups that are needed for attachment of the target to the carriers needed in these assays. When they have a functional group, there is the risk of using the functional group the aptamer recognizes for binding. NECEEM measures in solution yet suffers from other limitations. Not all targets are suited for analysis by capillary electrophoresis. For example, when a target has a high pI, it is difficult to distinguish a complex peak. In another case, when the molecular weight of the target is highly similar to that of the ssDNA, it is difficult to distinguish the complex peak from the peak with free ssDNA (Tran *et al.*, 2013; Tran *et al.*, 2010). Moreover, these assays all involve labeling the ssDNA oligonucleotides with fluorophores, biotin or other functional groups. This labeling can change the characteristics, structure and hence binding properties of the ssDNA pools and decreases the power of these assays to assess enrichment and evolution in the selection process in a concise way. As stated by Rowe *et al.* (2009), complications may arise with the use of

labels, either by altering the protein chemistry or from interactions between tags and the target aptamers, which can lead to either high background noise or a decrease in aptamer specificity. Since direct monitoring of affinity is limited by the need for labels, signal enhancers or other functional groups, monitoring of progression needs to be done in other ways than directly measuring affinity of the SELEX pools for the target.

Monitoring the *in vitro* selection process can be achieved in terms of ssDNA quantities that are eluted during different SELEX rounds. Niazi *et al.* (2008) performed seven selection rounds until the ssDNA quantity (measured by UV/Vis spectrophotometry) in the eluted pools was 90 % of the ssDNA quantity that was added to the target. A more straightforward way of monitoring is assessing sequence diversity of the pools and the most informative but elaborate technique to do this is sequencing individual clones. However, this is expensive and one does not know how much clones to sequence. Furthermore, it is not applicable to the more random stages of the procedure. Müller *et al.* (2008) propose a method based on sequence diversity that enables monitoring of a SELEX procedure by employing denaturing high-performance liquid chromatography (dHPLC). The technique is useful for both analysis of the selection progression and separation of distinct sequences. Charlton and Smith (1999) reasoned that the sequence complexity of a ssDNA pool can be quantified by observing the renaturation rate of its double-stranded PCR product by performing a  $C_0t$  analysis. By deriving an equation for reannealing at a distinct temperature, the number of individual sequences in the pool can be determined.  $C_0t$  analysis was initially developed to measure the nucleotide complexity of genomes (Britten & Kohne, 1968). In addition, Amplicot analysis measures 'diversity', defined as the number of different full-length sequences in a PCR product. The annealing rates of the samples decrease as the diversity of their templates increases (Baum & McCune, 2006). However, this analysis appears impossible for libraries with diversities higher than  $10^6$ . Remelting curves following an annealing step are observed to be a better characteristic indicator for the analyzed diversity (Schütze *et al.*, 2010). On an increase of diversity, a decrease in melting temperature was detected, denoting the amount of imperfectly formed heteroduplex. The applied annealing temperature determines the resolution in a given diversity range. Using DiStRO (Diversity Standard of Random Oligonucleotides), population dynamics of an aptamer selection against daunomycin were analyzed and quantified.

Various attempts have been made to monitor the selection progress of target-specific ligands. Direct measurements of SELEX pool affinities for the target are prone to several limitations and need a target-specific approach. Therefore, indirect monitoring applies the characteristics of the DNA pool as such, ideally without the need for labeling and independent of the target characteristics. Diversity analysis of the recovered DNA pools is the most straightforward way to achieve this. In this study, melting curve analysis after a short reannealing step (rMCA) is proven to be a useful tool for diversity analysis of a given SELEX pool

and hence for enrichment monitoring, independent of extra DNA modifications, the SELEX target and design. The principle of rMCA monitoring is shown using an enrichment simulation procedure. Furthermore, rMCA is applied to different, independently executed SELEX strategies (plate based, bead based and capillary electrophoresis based SELEX) and using targets of ranging physical properties (C-reactive protein, 17 $\beta$ -estradiol and peptide X) to demonstrate the general applicability of the rMCA as a monitoring tool. The selection on peptide X is analyzed with the proposed method on a different real-time PCR platform. Monitoring different approaches in different labs demonstrates the robustness, reproducibility and ease of use of this method. This proves complexity analysis of SELEX pools to be very useful to evaluate the selection process steps and make the right decisions to increase efficiency, resulting in high-affinity aptamers.

## **3.2. Experimental section**

### 3.2.1. Enrichment simulation in random starting libraries

All used ssDNA libraries, primers and oligonucleotides were synthesized by Integrated DNA Technologies (IDT, Haasrode, Belgium). Two different starting libraries are spiked with increasing concentrations of aptamer sequence, from 0% enrichment to 100 % enrichment. The random library used for CE-SELEX is spiked with IgE aptamer, D 17.4. (Wiegand *et al.*, 1996). The random library used for CRP selection is artificially enriched with either one single oligonucleotide or a homogeneous mix of ten different oligonucleotides, extended with the primer binding sites of the corresponding applied random libraries to allow amplification. The analysis is performed on the Lightcycler<sup>®</sup> 1.5 carousel (Roche, Merelbeke, Belgium) with 20  $\mu$ L reaction mixes containing: 1x SYBR Mastermix (Roche), 100 nM of each primer, extra 2 mM MgCl<sub>2</sub>. 100 pM (for one oligonucleotide or the mix of ten) and 10 pM (for IgE aptamer) of enriched library is added. PCR protocol consists of 5 minutes of denaturation, followed by 35 cycles of 5 s at 95 °C, 3 s at primer annealing temperature and 4 s at 72 °C for elongation. Different reannealing temperatures and times are tested for rMCA. Reannealing is tested for 30 s, 1 and 2 minutes at 65 °C, 70 °C and 75 °C. The rate for melting from the reannealing temperature to 95 °C is set at 0.1 °C/s.

### 3.2.2. Plate SELEX for CRP aptamers

The optimized SELEX procedure for CRP is described in Chapter 2.

### 3.2.3. Bead SELEX for 17 $\beta$ -estradiol aptamers

A random 40 nt library is constructed, flanked by 21 nt primer-binding regions: GTCACCGTACTCAGCCTCTCA-40N-GATGTATTGCGAGAGTTTGGC. Primers used for amplification are F: GTCACCGTACTCAGCCTCTCA and R: GCCAAACTCTCGCAATACATC. Estradiol (E2) Sepharose<sup>®</sup> 6B affinity chromatography beads (Polysciences Inc., Eppelheim, Germany) are used for positive selections and nortestosterone Sepharose<sup>®</sup> 6B beads (Polysciences Inc.) are used for counter selections. All beads are blocked extra with a mix of 1 % BSA (Sigma Aldrich), 1 % marvel (Sigma Aldrich), 4 % synthetic blockerNB3025 (NOF corporation, Tokyo, Japan) and an excess of sonicated HS-ssDNA (Life Technologies). Each selection cycle consists of a counter selection step, a positive selection step and another counter selection step prior to amplification. This is done to avoid amplification of non-specific binders for E2 and to direct aptamer binding to a specific epitope of E2. Buffer for incubation is 10 mM HEPES, pH 7.4; washing buffer is 1x TBS, pH 7.4 and elution buffer is 1x TE-buffer + 3 M urea, pH 8 at 80 °C. Before counter selection steps, HS-ssDNA (Life Technologies) is added in a 50x excess to avoid losing E2 binding oligonucleotides by non-specific DNA absorption in counter selections. SELEX fractions are amplified and analyzed as described in Chapter 2, with a primer annealing temperature of 56 °C. Reannealing was set at 1 min at 72 °C.

### 3.2.4. CE-SELEX for peptide X aptamers

A random 40 nt library is constructed, flanked by 20 nt primer regions:

TCGCACATTCCGCTTCTACC-40N-CGTAAGTCCGTGTGTGCGAA

Primers used for amplification are F: TCGCACATTCCGCTTCTACC and R: TTCGCACACACGGACTTACG. The peptide X is synthesized by Eurogentec (Seraing, Belgium). Selection is performed using a P/ACE-MDQ capillary electrophoresis system (Beckman Coulter, Fullerton, USA) with an uncoated fused silica capillary (length: 40.2 cm, outer diameter: 375  $\mu$ m, inner diameter: 50  $\mu$ m). The 488 nm line of a 3 mW Argon-ion laser is used for excitation of the fluorescently labeled DNA. The emission is measured using a 520  $\pm$  10 nm band pass filter. Running buffer is TGK buffer (25 mM tris(hydroxyamino)methane, 192 mM glycine and 5 mM K<sub>2</sub>HPO<sub>4</sub>, pH 8.4). Samples are incubated in tris magnesium buffer solution (10 mM tris(hydroxyamino)methane and 1 mM MgCl<sub>2</sub>, pH 7.2). Separation is done at 15 kV under normal polarity. Free DNA sequences will move slower through the column so only complex is collected to use for the following SELEX round.

After each selection step, a fraction of the pool is amplified by real-time PCR (Rotor-Gene Q, Qiagen, Venlo, Netherlands) followed by rMCA. A 30  $\mu$ l reaction mix is prepared containing 1x AccuMelt<sup>TM</sup> HRM SuperMix (Quanta Biosciences,

Gaithersburg, USA), 67 nM of each primer and equal fractions SELEX pools. Before amplification, a denaturation step at 95 °C is performed for 10 minutes. This is followed by a two-step amplification process (5s at 95 °C and 30s at 60 °C) of 35 cycles. The amplification products are melted from 60°C to 95 °C by increasing the temperature. Reannealing is allowed at 70 °C for 1 minute followed by a second melting analysis from 70 °C till 95 °C at 0.5 °C/s.

### **3.3. Results and discussion**

#### 3.3.1. reMelting Curve Analysis after short reannealing (rMCA)

Annealing and melting kinetics of DNA is extensively studied since  $C_0t$  analysis (Britten & Kohne, 1968), from gene analysis (Britten *et al.*, 1974) and genome sequencing (Lamoureux *et al.*, 2005) to analysis of selection libraries. Schütze *et al.* (2010) created a diversity calibration standard (DiStRO) for the evaluation of DNA pools by analyzing remelting curves after an annealing step of 180 minutes. Remelting analysis is applied and optimized here for monitoring diversity changes during the SELEX procedure, regardless from design and target properties.

In a standard melting curve analysis, all amplified high-copy pools are slowly denatured, determining the average melting temperature of the pool as the temperature where fluorescence drops the most. In rMCA, a short reannealing step at high temperature is introduced after total denaturation. In this stringent reannealing phase, hetero- and homoduplexes are formed, completely depending on the sequence diversity. Melting curve analysis is then executed as before. As the diversity of SELEX pools decreases due to enrichment for target-binding ssDNA species, more homoduplexes will be formed in the reannealing phase and one can expect a shift in the obtained rMCA melting temperatures. Consequently, rMCA will provide crucial information on enrichment in terms of diversity.



### 3.3.2. rMCA analysis of simulated enrichment

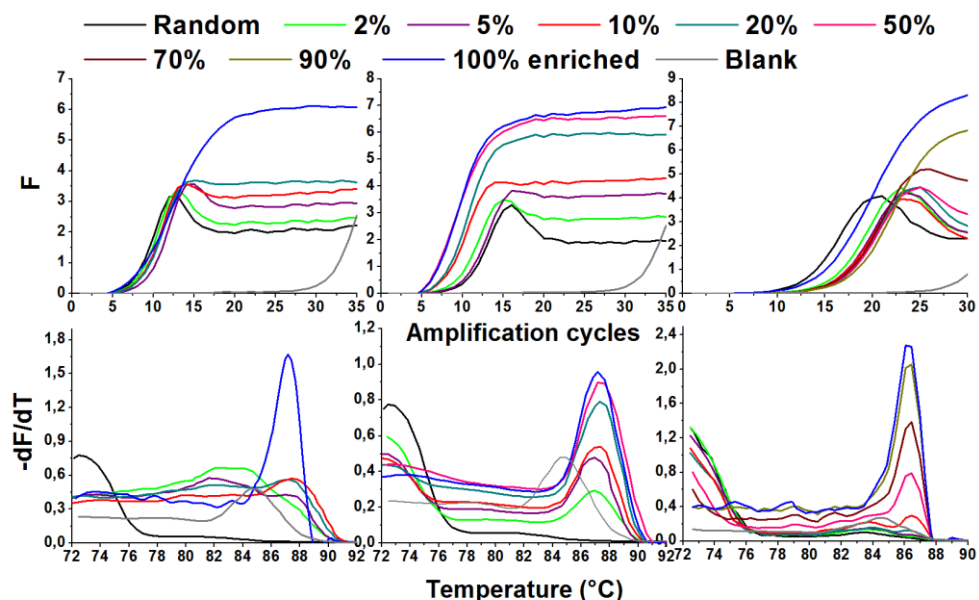


**Fig. 3.1. Amplification data (up) and rMCA (down) of three enrichment simulations with random library and 2-20 & 100 % enrichment of one oligonucleotide (left); random library and 2-50 & 100% enrichment of oligo mix (middle) and random library with 2-100 % enrichment of D 17.4 IgE aptamer (right) after 1 min reannealing at 70°C. (F = Fluorescence, generated by SYBR Green.  $-dF/dT$  = first negative derivative of F, denoting the decrease in Fluorescence or dsDNA melting with increasing temperature T)**

Simulation of enrichment in different libraries is performed to demonstrate the broad applicability of rMCA, studying amplification and melting behavior of complex DNA pools with different diversities. As shown in Figure 1, all three simulations show a similar trend in both amplification (Fig. 3.1up) and melting data (Fig. 3.1low). Where 100 % enriched fractions show the normal exponential amplification curves, 100 % random libraries show a drop in fluorescence (F) after reaching a maximum. This occurs after 12 amplification cycles for one oligo (Fig. 3.1 left), 15 for the oligo mix (Fig. 3.1 middle) and 20 cycles for D17.4 (Fig. 3.1 right). The amplification curves change along with increasing enrichment of spiked oligonucleotide(s). When diversity decreases, the drop in fluorescence is less pronounced and disappears in more enriched conditions. This can be explained by the same principle as the rMCA. At this drop, there is no more amplification (limitation of primers or dNTP) and fluorescence acquisition at 72 °C is performed after a reannealing phase. Random pools contain less stable duplexes at this temperature and fluorescence drops.

Remelting data also show an evolution from a gradual melting behavior of 100 % random library (broad melting zone from 70-75 °C) to a melting peak at the expected melting temperature of the spiked oligonucleotide or the average melting temperature of the oligo mix, which is reflected in a broader melting peak. This proves there is indeed a shift from a lower, broad remelting peak to a more distinct, higher remelting temperature as diversity decreases and enrichment occurs. Melting peaks at 72 °C gradually disappear and evolve to the (average) melting temperature of the more stable duplexes of the enriched oligonucleotide(s). The speed and form of this shift differs, depending on the library and enriched oligonucleotide(s). Blank amplifications (gray curves) show a rise in fluorescence after 30 amplification cycles and a melting peak which correlates with the formation and disruption of primer dimers after iterative heating and cooling of the mix.

Simulation also shows that reannealing goes very fast: reannealing 30 s gives the same empirical results as 2 min (Fig. 3.2). Shorter reannealing times increase stringency and reflect the differences in enrichment better whereas longer reannealing results in sharper melting peaks.

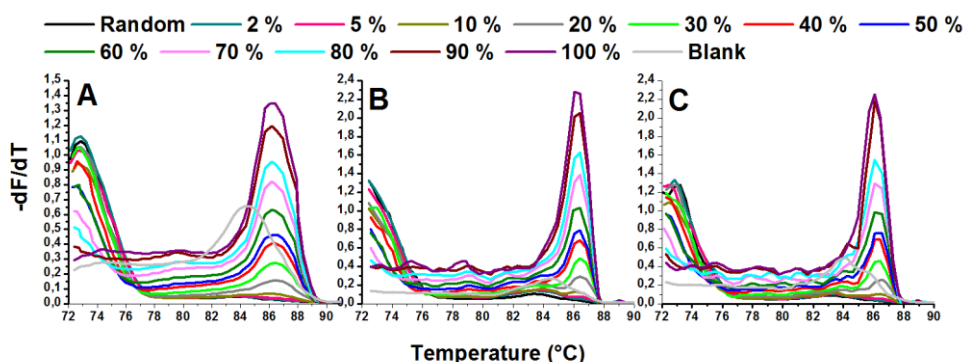


**Fig. 3.2. rMCA data of simulated D17.4 enrichment in random library. rMCA is compared after reannealing at 70 °C for 30 s (A), 1 min (B) and 2 min (C).**

Changing the reannealing temperature changes the window and resolution of rMCA. Reannealing at 70 °C allows formation of heteroduplexes and hence, there is a broad melting zone starting from this reannealing point in random or poorly enriched conditions. Reannealing at a higher temperature allows one to zoom in on enriched fractions. When reannealing at 75 °C, the melting peak of random library at 72-74 °C will not be formed and remelting starts at 75 °C (Fig. 3.3).

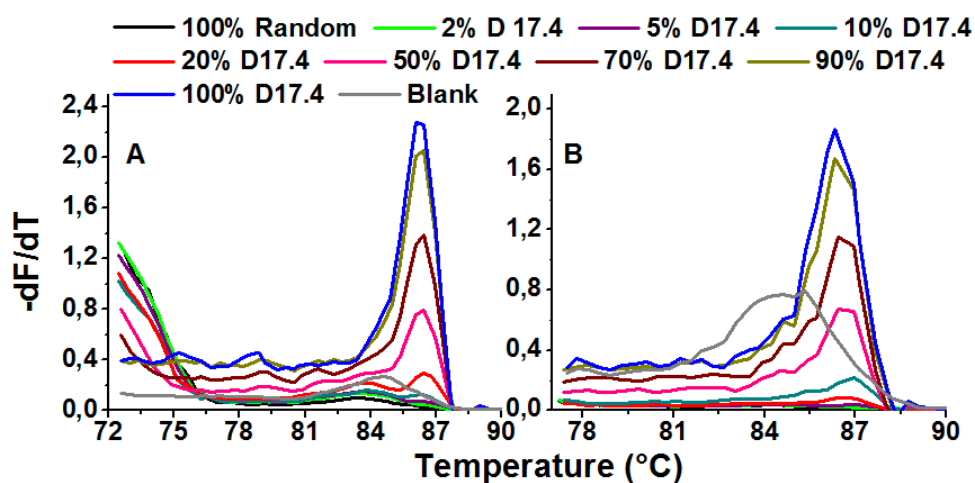


**Fig. 3.3.** rMCA of simulated 2-100% enrichment of D17.4 in random library analyzed after 1 min at 70°C reannealing (A) and 1 min at 75 °C reannealing (B).

### 3.3.3. rMCA of different SELEX procedures – general applicability

rMCA is applied successfully in three different selection procedures for different targets. It is demonstrated to be applicable for different SELEX designs (plate based, bead based and CE-SELEX) and targets of various physical properties, a macroprotein (CRP, 115 kDa, pI 5.3-7.4) (Tsujimoto *et al.*, 1983), a steroid (17 $\beta$ -estradiol, 272 Da, pKa 10.7) (O’Neil, 2006) and a peptide (X, 1.6 kDa, pI 11).

In the plate SELEX protocol for CRP, four elution fractions are collected in the positive selections which are separately analyzed by rMCA. Before round 10, all four fractions show similar melting peaks. After round 10, there is a clear differentiation in DNA composition of separate fractions, indicated by different melting peaks (Fig. 3.4).

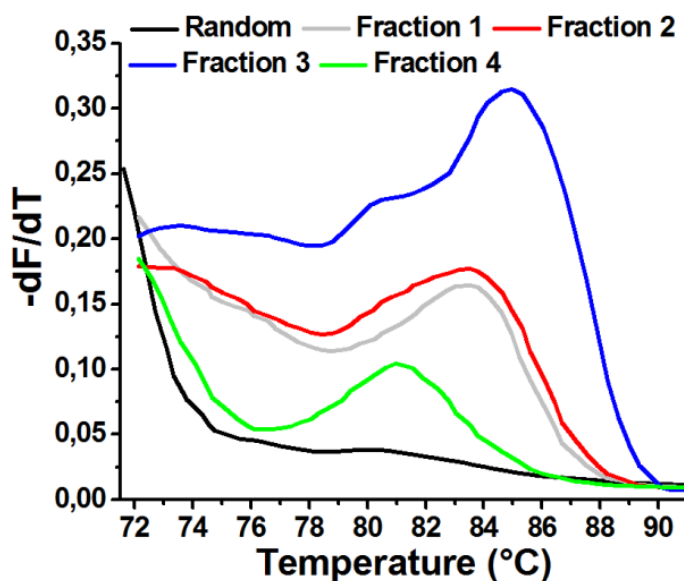


**Fig. 3.4. rMCA data after SELEX round 10 for CRP – clear differentiation between DNA compositions of different fractions.**

At this point, the selection procedure is continued in parallel with these four DNA fractions separately. As all elutions are analyzed separately, it is possible to monitor the whole SELEX procedure and progress in these fractions in detail, from round 1 to round 16 (Full plate-SELEX progress in four fractions: Fig. 3.5 to Fig. 3.8). This shows the progress of selection and shifts of the average remelting temperature of the analyzed ssDNA pools as enrichment takes place. Sequencing analysis of the 4 fractions after 16 rounds of selection confirms enrichment for 4 oligonucleotides, occurring in all fractions (Table 2.2). Nucleotide sequences of the most enriched oligonucleotides are given in Chapter 2.

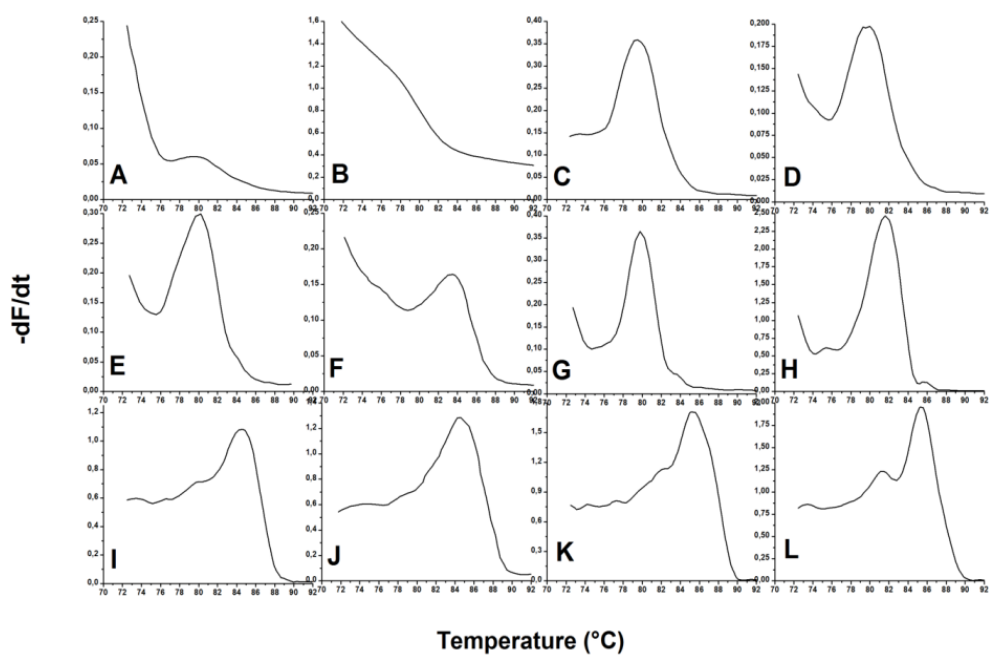


**Fig. 3.5. Full SELEX rMCA of fraction 1. (A) round 1; (B) round 3; (C) round 5; (D) round 7; (E) round 9; (F) round 10; (G) round 11; (H) round 12; (I) round 13; (J) round 14; (K) round 15; (L) round 16. Y-axis on graphs represents  $-dF/dt$ , the decrease in Fluorescence or dsDNA melting or denaturation with increasing temperature from 72 to 95°C (on x-axis).**

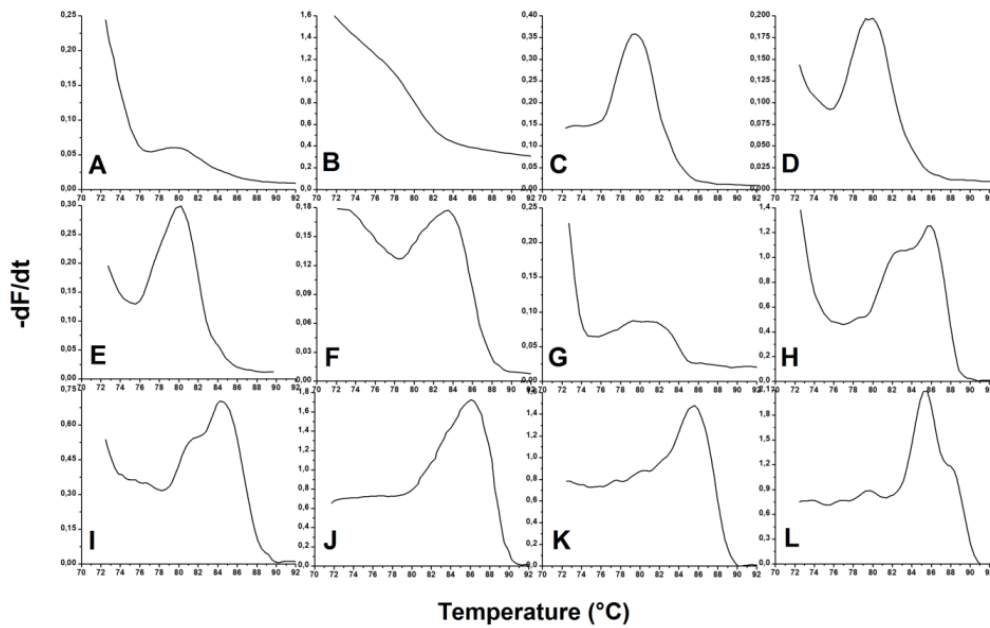
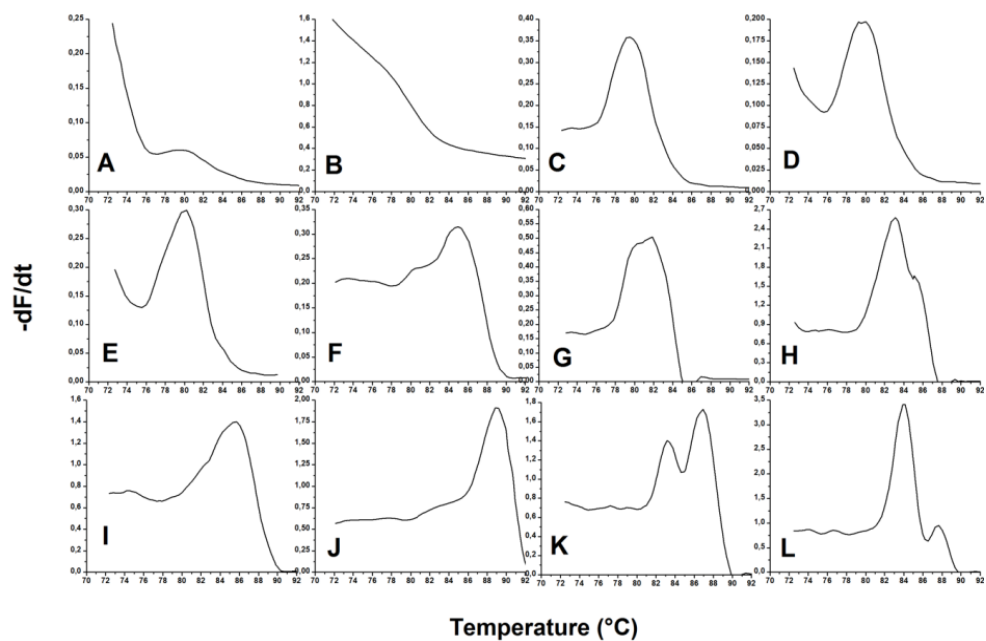


**Fig. 3.6. Full SELEX rMCA of fraction 2. (A) round 1; (B) round 3; (C) round 5; (D) round 7; (E) round 9; (F) round 10; (G) round 11; (H) round 12; (I) round 13; (J) round 14; (K) round 15; (L) round 16. Y-axis on graphs represents  $-dF/dt$ , the decrease in Fluorescence or dsDNA melting or denaturation with increasing temperature from 72 to 95°C (on x-axis).**



Temperature (°C)

**Fig 3.7. Full SELEX rMCA of fraction 3. (A) round 1; (B) round 3; (C) round 5; (D) round 7; (E) round 9; (F) round 10; (G) round 11; (H) round 12; (I) round 13; (J) round 14; (K) round 15; (L) round 16. Y-axis on graphs represents  $-dF/dt$ , the decrease in Fluorescence or dsDNA melting or denaturation with increasing temperature from 72 to 95°C (on x-axis).**

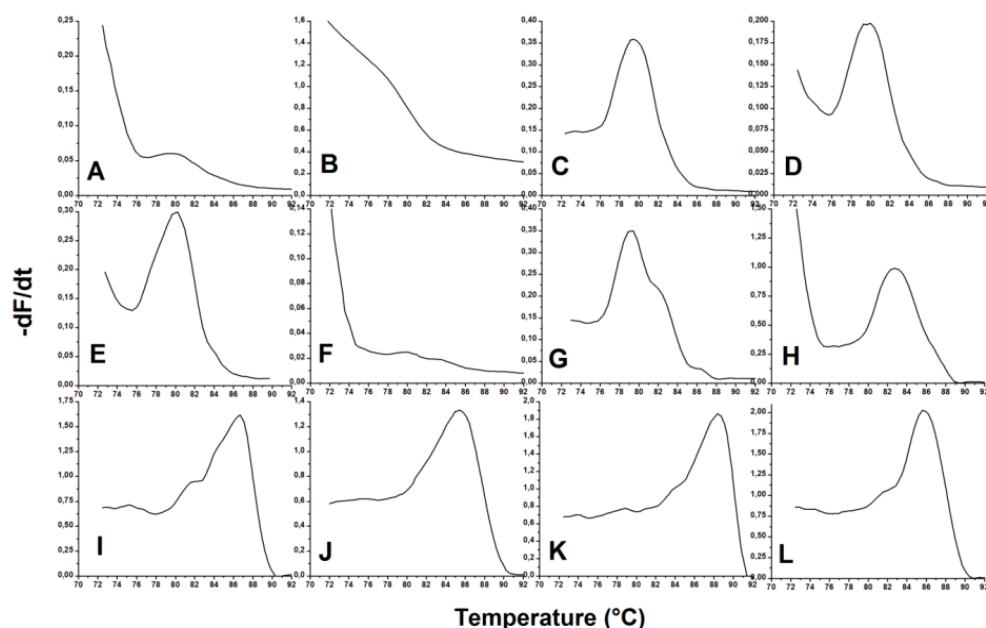


**Fig. 3.8. Full SELEX rMCA of fraction 4. (A) round 1; (B) round 3; (C) round 5; (D) round 7; (E) round 9; (F) round 10; (G) round 11; (H) round 12; (I) round 13; (J) round 14; (K) round 15; (L) round 16. Y-axis on graphs represents  $-dF/dt$ , the decrease in Fluorescence or dsDNA melting or denaturation with increasing temperature from 72 to 95°C (on x-axis).**

The selection of ssDNA aptamers for  $17\beta$ -estradiol (Figure 3.9.1) is performed on sepharose beads. Fractions of the remaining DNA pools after each positive selection are analyzed with rMCA, after an amplification step of 35 cycles and a reannealing phase of 1 min at 72 °C. After 8 rounds, the melting peak of the DNA pool is evolved from a broad random peak at 73 °C (Figure 3.9.1.A) to two specific peaks at 84 and 87 °C (Figure 3.9.1.H). Sequencing of the pool after selection round 8 confirms enrichment of specific oligonucleotides. In both selections, the melting peaks shift gradually from a broad early-melting zone to higher melting temperatures and the proportion of early melting DNA gradually decreases as enrichment proceeds.



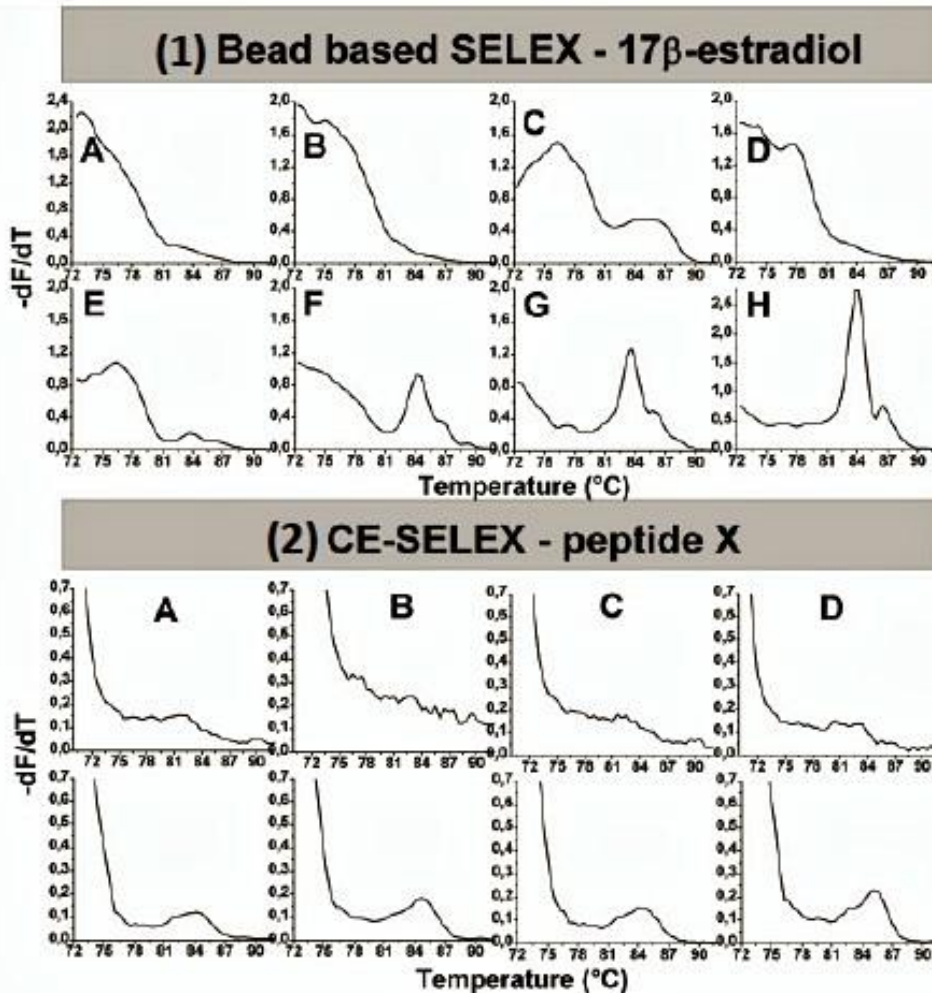


**Fig. 3.9. (1) rMCA of bead based SELEX round for 17 $\beta$ -estradiol; round 1 (A); round 2 (B); round 3 (C); round 4 (D); round 5 (E); round 6 (F); round 7 (G) and round 8 (H). (2) rMCA of CE-SELEX rounds for peptide X on 2 devices; Up: analysis on Rotor Gene-Q; Down: analysis on Lightcycler $^{\circledR}$ ; round 1 (A); round 4 (B); round 6 (C); round 11 (D). Y-axis on graphs represents  $-dF/dT$ , the decrease in Fluorescence or dsDNA melting or denaturation with increasing temperature from 72 to 95 $^{\circ}C$  (on x-axis).**

CE-SELEX on peptide X (Fig. 3.9.2) is challenging because of the lack of a ssDNA-X complex peak in the CE separation. rMCA is performed on a different real-time PCR device, the Rotor-Gene Q (Qiagen) to test the general applicability of this diversity analysis method. rMCA after 1 min reannealing at 70  $^{\circ}C$  indicates there still is a large fraction of random DNA present, illustrated by the large melting zone at low temperatures; 70-74  $^{\circ}C$ . CE-SELEX pools are also analyzed on the Lightcycler $^{\circledR}$  to compare the results. In Fig. 3.9.2, both rMCAs

are compared. In both analyses, the large remelting zone which correlates with random DNA (72-75 °C) remains present throughout the whole selection procedure. Nevertheless, library evolution and changes in DNA composition are clear when one focuses on higher temperatures, correlating for enriched oligonucleotides. rMCA with a higher reannealing temperature of 75 °C (Fig. 3.10), changing the rMCA window, elucidates changes in the DNA pool better and indicates that enrichment is occurring yet at a slow rate. In the onset of the procedure, rMCA only results in a broad melting zone. When the procedure continues, after round 4, there is a growing remelting peak appearing at higher temperatures. Since no discrete ssDNA-X complex peak can be discriminated, the collection window is chosen to be sufficiently broad, reducing separation efficiency of specific and non-specific oligonucleotides. Although rMCA on the Rotor-Gene Q and the Lightcycler® give the same empirical results, the Lightcycler® and the SYBR Mix appear more sensitive in fluorescence acquisition in the remelting phase. In the Rotor Gene Q temperature transition rate needs to be increased from 0.1 °C/s to 0.5 °C/s to produce conclusive data. rMCA enables monitoring of the SELEX progress regardless of target properties. When direct monitoring of affinity of the SELEX pools for the target is not possible, as demonstrated above or due to lack of extra functional groups for labeling or attachment, rMCA provides an interesting tool.

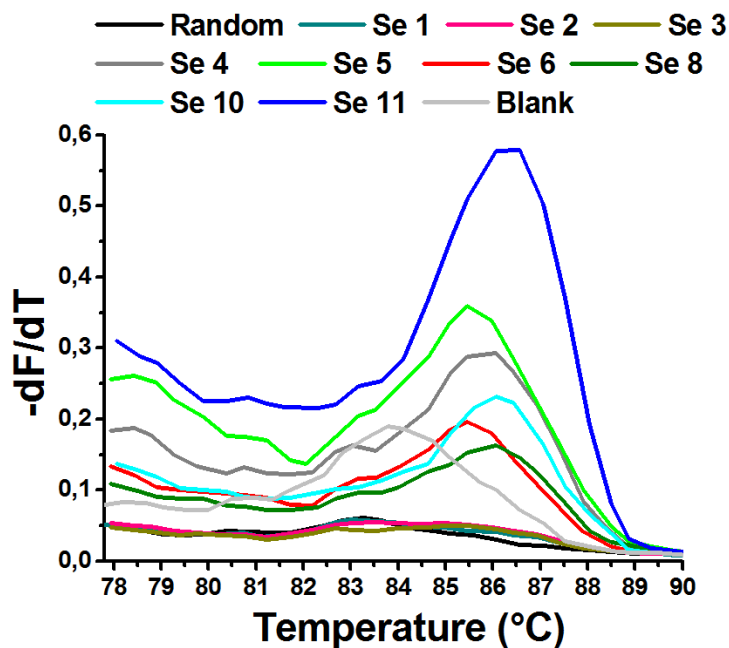
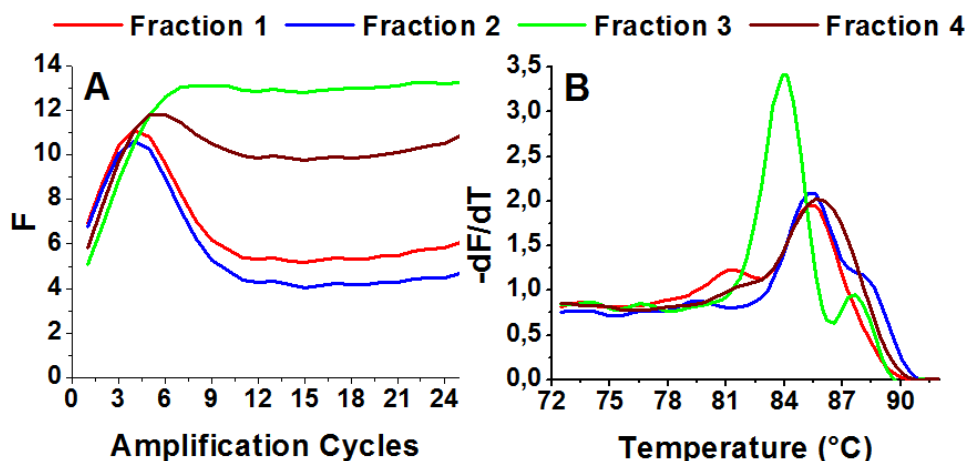


Fig. 3.10. rMCA of consecutive CE-SELEX rounds for peptide X after 1 min reannealing at 75 °C.

#### 3.3.4. Optimizing and monitoring the SELEX progress – SELEX design and contamination detection

As mentioned in the selection protocol for CRP aptamers, sequential elutions are analyzed separately by rMCA. After SELEX round 10, the selection procedure is continued in parallel with these four DNA fractions separately, because rMCA illustrated different DNA compositions (Fig. 3.4). These differences can be explained by selection stringency differences: the oligonucleotides that are eluted in fraction 4 have survived the three previous elutions. After 16 rounds of parallel selection, both amplification and remelting data indicate enrichment in the four fractions. Moreover, these fractions still differ from each other, demonstrated by both the amplification curves and rMCA data (Fig. 3.11). The melting peaks of rMCA (Fig. 3.11.B) have shifted from 72 °C to higher temperatures in all of them. The position and form of these peaks differ for each fraction. Fraction 3 forms a clearly distinct peak at 84 °C, whereas fraction 1 and 2 form broader peaks from 80-86 °C. The difference is reflected in the amplification curves as well (Fig. 3.11.A), with a drop in fluorescence after 4 amplification cycles for fraction 1 and 2 and absence of this drop for fraction 3. Fraction 4 demonstrates an intermediate enrichment and an intermediate drop.

Sequencing results reflect these differences, with one aptamer highly enriched in fraction 3, whereas the other fractions contain enrichment of multiple sequences (Table 3.1). Following enrichment in different elutions results in selection for CRP aptamers in four fractions of different stringencies, which each have their own aptamers enriched (Fig. 3.11). The presented method can be used to optimize conditions for selection steps. It may be useful to assess the effect of negative or stringent positive selection steps on the DNA library before starting the SELEX procedure. Both quantitative and qualitative analysis of DNA pools provide valuable information to take into account when setting up a SELEX procedure. Moreover, in the onset of selection, rMCA detects possible contaminations very quickly as they appear as a large, narrow melting peak in an otherwise broad melting zone.



**Fig. 3.11. (A) Amplification curve of 4 SELEX fractions after SELEX round 16 and (B) rMCA data of 4 SELEX fractions after SELEX round 16.**

*3.3.5. Importance of DNA quantity for rMCA*

Monitoring the ssDNA aptamer selection procedure for CRP by real-time PCR shows that the eluted fractions contain low amounts of DNA. When performing the remelting analysis on low copy number samples, the remelting data shows a peak at the same position as the blank sample, indicating that primer dimers are melted here. When analyzing the same sample with a pre-amplification step, the remelting data changes to a melting peak at 72 °C, corresponding to the melting peak of random library (Fig. 3.12).

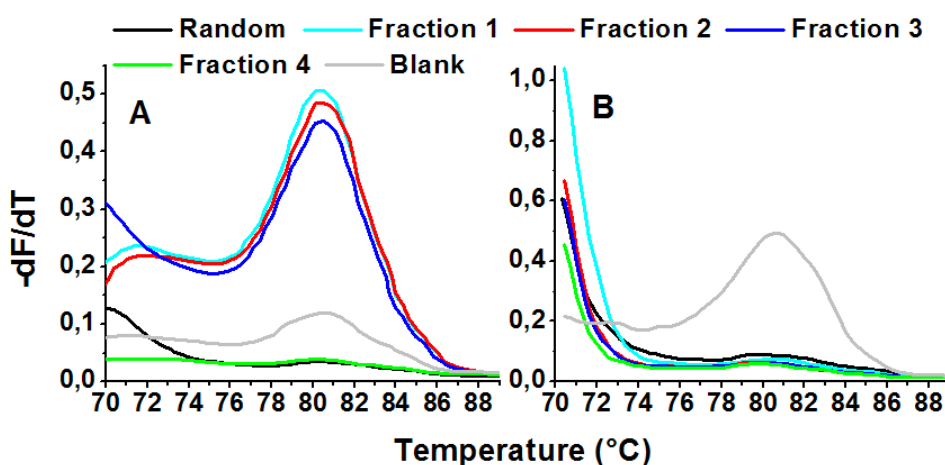


**Fig. 3.12. (A) rMCA data of four low copy fractions of SELEX pools before amplification and (B) after amplification.**

### **3.4. Conclusion and future prospects**

Expansion on the repertoire of rMCA will further demonstrate the power of this remelting method for assessing enrichment in various SELEX designs, on different real-time PCR platforms and for different targets and DNA libraries. Effects of the primer binding regions are to be determined. As these regions are equal for all sequences in the pool, they may reduce rMCA resolution capacity. Studying the effect of primer removal on the outcomes and resolution of diversity analysis by rMCA can result in more sensitive analysis or more insight on the role of these identical regions.

rMCA enables monitoring of the SELEX progress, regardless of target properties. When direct monitoring of affinity of the selection pools for the target is not possible, rMCA provides an interesting tool. The method is used to detect enrichment for target binding sequences during the SELEX process, but can also be used to optimize selection conditions. rMCA does not require a lot of input material, no supplementary target is needed and no extra labeling and incubation steps are involved. Monitoring by rMCA makes use of the characteristics of the selected ssDNA as such in terms of amplification and denaturation and is therefore independent of SELEX approach, target properties and different real-time PCR devices, as demonstrated in this chapter.



# 4

## Binding assays for selected aptamers

*In this chapter, the selected aptamer candidates for CRP are tested in a set of binding assays with ranging properties. This chapter explores assays with increasing complexities and costs, and highlights the challenges of using immobilized or labeled aptamers. Binding properties are defined and both kinetic and affinity constants for CRP are analyzed.*

### 4.1. Introduction

When an aptamer selection procedure is finished and sequencing identifies enriched oligonucleotides in the SELEX pool, the next step is to determine their functionality: do they specifically interact with the target they are selected for and what is the strength of this interaction? By means of a set of binding assays, aptamer characteristics and binding properties can be tested and defined.

As explained in the introduction of this dissertation, validation or binding assays can be classified in different ways: labeled or label-free, in solution or immobilized on a surface or according the signal generation mechanism. Binding assays exist in a range of properties, from simple and quit cheap to sophisticated, expensive and with highly specialized instrumentations. In this chapter, the selected aptamers for CRP will be tested in a series of binding assays, starting with assay designs that mimic the selection design in set-up and ending with real-time label-free screening of the aptamer-target interactions and determining the affinity of this interaction.

In a first set of binding assays that are tested, aptamer sequences and target are incubated in the same way they are selected. The analyte CRP is coated on NucleoLink™ Immobilizer 96 Well plates and incubated with the selected aptamers instead of random library. The amount of binding aptamer is quantified and compared with negative binding conditions (*i.e.* the binding of non-specific ssDNA to CRP and of selected aptamers to other compounds than CRP). The amount of binding ssDNA is measured by means of various signal amplification strategies.

As the aptamer sequences are equipped with primer binding regions and RT-PCR of ssDNA selection pools is optimized from the SELEX monitoring, the aptamers themselves can serve as a signal amplifier (Liao *et al.*, 2010; Avci-Adali *et al.*,

2013). The method is based on SYBR Green I real-time PCR technology and uses an aptamer standard curve to determine the accurate aptamer amount on CRP and negatively coated wells. As PCR is a very sensitive and robust amplification method, the slightest non-specific adsorption of DNA causes signal. Therefore, negative controls with non-specific sequences are of high importance. Moreover, additives can be added to reduce the non-specific binding by saturating the unoccupied binding sites with a blocking reagent (NSB agent) without taking active part in specific assay reaction (HS-ssDNA, BSA, ethanolamine) or by disrupting non-specific complexes (ionic detergents, dextran sulfate or aspecific HS-ssDNA; Gold *et al.*, 2010), provided that they do not interfere with efficient real-time PCR amplification. As these additives were not part of the SELEX procedures of the tested aptamers, one should keep in mind that adding these additives in detection assays may disrupt or inhibit aptamer-CRP binding and hence false negative results may be observed.

Enzyme-linked aptamer assays (ELAA) use aptamers directly conjugated to signal generating and amplifying enzymes, such as HRP and AP. Aptamers can also be tagged with a label specifically recognized by an enzyme-linked detector e.g. biotin-tagged aptamers are detected and quantified by means of streptavidin-conjugated HRP signal generation (Tanaka *et al.*, 2009). Sandwich assays with fluorescein-labeled aptamers that are detected by fluorescein-specific antibodies also belong to this category (Drolet *et al.*, 1996). In these assays, negative binding studies are of key importance since enzyme-linked aptamer assays are prone to non-specific binding and false positives. Non-specific interaction of the enzyme-linked detector to any other compound than its ligand results in signal generation in negative binding conditions (Kenna *et al.*, 1985). To tackle non-specific binding of signal generating compounds, a set of NSB (Non – Specific Binding) agents can be added to the assay by blocking of unsaturated binding spaces, by disruption of weak interactions between non-specific agents or by inhibition of enzyme substrate reactions (Farajollahi *et al.*, 2012). Detergent blockers such as Tween<sup>®</sup>20 disrupt weak interactions, but can also inhibit aptamer-target recognition as Tween<sup>®</sup>20 was not part of the selection buffer. Protein blockers like casein, BSA, Marvel or whole sera can be used to block binding positions, but can also decrease aptamer selectivity and specificity.

Moreover, altering the chemistry of an aptamer by labeling or tagging can cause increased background noise or change aptamer functionality and specificity for the target (Rowe *et al.*, 2009). The label or tag can alter the aptamer secondary structure, reducing aptamer functionality. On the other hand, the tag or label may be incorporated in the secondary structure of the aptamer, so it is not available for recognition or signal generation. Therefore, labels and tags are attached to the aptamer sequences with a linker between the tag or label and the actual aptamer sequence, to reduce the risk for incorporation in or inhibition of the secondary structure needed for binding. This can be an oligonucleotide



linker of several nucleotides (mostly a variably number of thymidine (T) groups) or another structure. For example, Biotin can be added to the 5'- or 3'-end of an oligonucleotide using either a C6 (standard) or a TEG (tetra-ethylene glycol) spacer arm (IDT, 2013a). Various types of spacers are available for incorporation in oligonucleotides, ranging from the short C3 Spacer phosphoramidite to the 18-atom hexa-ethylene glycol spacer, which is the longest spacer arm that can be added as a single modification (Fig. 4.1, IDT, 2013b).

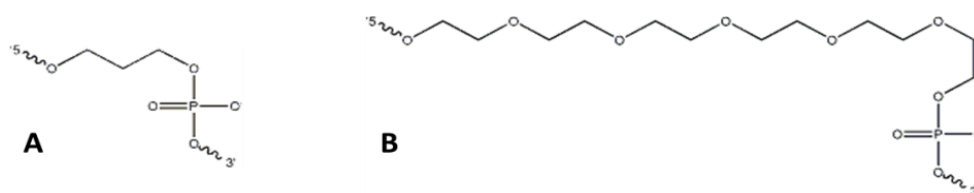


**Fig. 4.1. Examples of different spacers available in ssDNA synthesis (IDT, 2013).**

In another type of validation assay, the selected aptamer provides the molecular recognition unit that is required as the first step in an assay (Balamuragan *et al.*, 2008). The aptamer is immobilized as a receptor on a solid surface that can be utilized in a diverse array of analytical formats (Table 4.1). Immobilization leads to easy recovery of the aptamer and repeated use of the sensor or support after regeneration of the surface. Furthermore, immobilization allows the construction of array devices, to increase target specificity or for parallel detection of several targets simultaneously. However, one should keep in mind that immobilized aptamers were modified with functional groups for immobilization purposes and that grating of the selected oligonucleotides possibly reduces their mobility, flexibility and hence aptamer functionality (Rowe *et al.*, 2009). Therefore, testing the binding properties of immobilized aptamers is needed for later sensor applications, where the target can be measured without extra target preparations or immobilization procedures.

The proper design of immobilization procedures to fix an aptamer to the surface is of high importance to ensure a nicely oriented layer of receptors, without decrease of mobility and affinity for the target molecule (Centi *et al.*, 2007). There are several chemical methods for aptamer immobilization, all originating from DNA hybrids immobilization methods and all requiring a specific aptamer label or modification. Direct attachment to a gold surface is achieved by using a thiol-alkane linked to the aptamer sequence, forming a self-assembled monolayer (SAM) (Balamuragan *et al.*, 2006). Covalent attachment of aptamers to functionalized active layers on substrates is another option. The three most common groups employed for surface attachment are hydroxyl, amine and carboxylic acid surface functional groups, interacting with amine or thiol termini of modified aptamers (Heise & Bier, 2006). The EDC/NHS coupling procedure (Fig. 4.2) attaches amine-modified aptamers to carboxylic acid modified substrates by forming a reactive ester group, stabilized by NHS. This reactive

ester efficiently couples to the amine group of the aptamer (Hermanson, 2008). The highly specific interaction between streptavidin (or its derivatives avidin and neutravidin) and biotin is also exploited for aptamer immobilization with biotin-tethered aptamers readily available from DNA providers (Smith *et al.*, 2005). This method is operationally easy, as it mainly requires incubation at room temperature in a suitable buffer solution. Moreover, Ostadna *et al.* (2008) investigated the effect of the immobilization method on the interaction between thrombin and its DNA aptamers. Immobilization of aptamers by means of streptavidin-biotin system yields the best results in terms of sensor specificity and sensitivity.

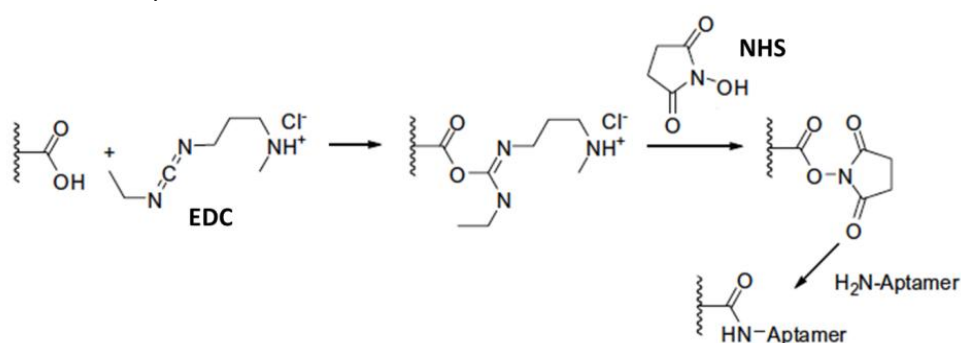


**Fig. 4.2. EDC/NHS coupling procedure of amine-labeled aptamer to carboxylic acid surfaces.**

Key features of immobilization procedures are receptor orientation, immobilization density and the use of appropriate linkers to maintain aptamer functionality. The function of the linker is to present the aptamer above the surface to promote target accessibility and to ensure full aptamer mobility. Linkers can consist of different modular components, such as an alkyl group, an oligo-ethylene glycol unit and an oligonucleotide spacer (Balamurugan *et al.*, 2008). The incorporation of an oligo-ethylene glycol spacer is chosen because of decreased non-specific adsorption of proteins to surfaces modified with oligo-ethylene glycol (Balamurugan *et al.*, 2006). Thymidine groups also exhibit the least non-specific adsorption to various surfaces in comparison to other bases (Kimura-Suda *et al.*, 2003). Longer linkers in combination with a low immobilization density ensure full flexibility of the aptamer structure and no steric hindrance for target binding.

The effect of aptamer orientation, immobilization to the support at the 5'- or 3'-end, depends on the particular aptamer sequence and structure confirmation. When the 3'-end is more involved in target recognition than the 5'-end, 3'-end availability will increase target binding. Cho *et al.* (2006) compared several biotin-terminated aptamers at different orientations. The anti-IgE (Wiegand *et al.*, 1996) aptamer showed 14-30 % higher sensitivity following 3'-end

immobilization, while the anti-thrombin aptamer (Tasset *et al.*, 1997) showed higher sensitivity following 5'-end immobilization.

All post-SELEX modifications to increase the stability of the selected aptamers, to optimize binding parameters to the target or for further applications are tested in binding assays before application. Truncation or miniaturization of the aptamer to the relevant binding sequence can be useful to reduce size, but has been shown both to increase or decrease target affinity (Wilson & Szostak, 1998; Strehlitz *et al.*, 2012).

Furthermore, changing the binding conditions of selected aptamers can elucidate what forces drive the binding events. Sandwich assays or incubation with tagged or modified target can increase the understanding of where the aptamer binds on the target and allows for epitope mapping. Changing the Na<sup>+</sup> concentration for example has elucidated that the 15-mer thrombin binding aptamer (TBA; Bock *et al.*, 1992) needs Na<sup>+</sup> for the formation of the typical G-quadruplex structure, whereas the newer 29-mer aptamer (TBA2; Tasset *et al.*, 1997) is Na<sup>+</sup> independent to maintain the same affinity for thrombin (Fig. 4.3) (Lin *et al.*, 2011). While this aptamer again forms a G-quadruplex, the longer ends of the quadruplex form a duplex that stabilizes the structure and further improves its binding affinity (Hall *et al.*, 2009). Moreover, competition assays with TBA1 and TBA2 have shown that both aptamers bind on different exosites of the thrombin, the fibrinogen (TBA1) and heparin (TBA2) binding sites. Real-time assays have shown that TBA1 has affinity for both sites, but TBA2 demonstrates higher affinity for the heparin binding site, caused by minimal structural differences along with the longer DNA sequence (Daniel *et al.*, 2013).

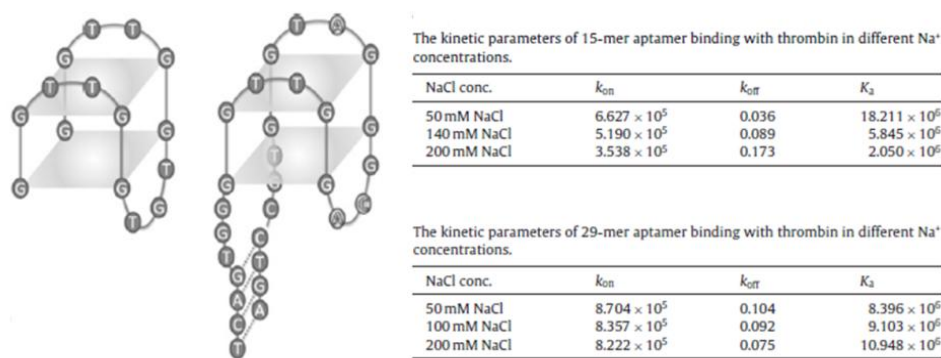


**Fig. 4.3. Secondary structure of TBA1 and TBA2 and the effect of different NaCl buffer concentrations on affinity constants for thrombin ( $k_{on}$ : association rate constant [ $M^{-1} \cdot s^{-1}$ ];  $k_{off}$ : dissociation rate constant [ $s^{-1}$ ];  $K_a$ : association constant [ $M^{-1}$ ]) (Adapted from Lin *et al.*, 2011)**

In order to have a complete view on the binding characteristics of a selected aptamer, one needs a highly informative assay system to intensively test the

aptamer functionality and the effects of changing binding conditions and immobilization or labeling of the aptamer.

The most informative systems to perform binding analysis of selected aptamers to their analytes are systems based on Surface Plasmon Resonance (SPR), which allow label-free, real-time investigation of biomolecular interactions (Hahnefeld *et al.*, 2003). SPR analysis allows a complete determination of binding conditions, specificity and selectivity. The aptamer or target is covalently coated to the sensor surface for real-time, label-free binding analysis with a concentration range of analyte and other competitor biomolecules. This allows assessing receptor specificity and concentration dependency of the response. Optimization of the binding conditions (buffer and incubation conditions, immobilization procedure, linker optimization...) and performing competition and sandwich assays gives important information about the interaction for epitope mapping.

Affinity analysis (Fig. 4.4) at binding equilibrium learns about the strength of the interaction in saturation and allows ranking of the selected aptamers. The concentration at which the response is half of the saturation response or  $R_{max}$  is defined as the equilibrium dissociation constant ( $K_d$ ).

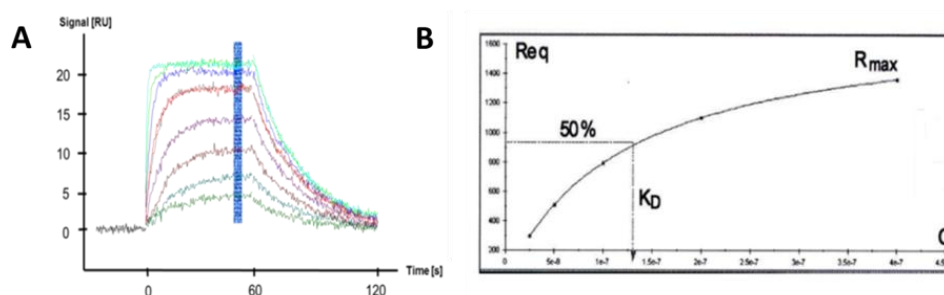


**Fig. 4.4. Affinity analysis at equilibrium (Biacore Technology Brochure). (A) sensorgram of concentration range (B) equilibrium  $K_d$  determination ( $R_{eq}$ =binding response at equilibrium;  $K_a$ = association constant; C= concentration ;  $R_{max}$  = maximum binding response. Adapted from Goodrich & Kugel, 2007).**

Kinetic analysis determines the association and dissociation rate constants  $k_a$  and  $k_d$ . Binding curves are measured and fit according a mathematical equation describing a binding model of choice (1:1 binding, heterogeneous ligand or analyte, two-state reaction...) which results in assessment of  $R_{max}$ , the kinetic rate constants  $k_a$  ( $M^{-1}s^{-1}$ ) and  $k_d$  ( $s^{-1}$ ) and hence the affinity dissociation constant  $K_d$  (M). Furthermore, analysis of residuals and  $\chi^2$  (*Chi-square*) statistics allows quality determination of the fittings and the estimated values.

In the following parts, a panel of binding assays is performed to test binding specificity and selectivity of the 4 aptamer candidates discussed in Chapter 2. Immunosorbent-like assays are tested with immobilization of both the target

and the selected aptamers and by applying different signal generation and amplification mechanisms such as chemiluminescence, fluorescence and real-time PCR amplification. During the performance of this PhD, the biosensor lab acquired an SPR T200 Instrument (Biacore, Uppsala, Sweden) on which surface plasmon resonance (SPR) analysis is performed for an extensive binding analysis for aptamer functionality and affinity and kinetic analysis to gain insight in the binding strength and the rates of association and dissociation to CRP.

## 4.2. Experimental section

For full description of the applied buffers and reagents, please see the abbreviations and buffer composition list in the appendix of this dissertation. Unless stated otherwise, buffers are made with reagents purchased from Sigma Aldrich.

### 4.2.1. Modified aptamer sequences for immobilization and detection

The aptamer sequences (Chapter 2) are modified by 5'-end labeling with an amine group for covalent attachment, with a fluorescein for detection or with biotin as an affinity tag. All labels are tethered with different spacer lengths. A dummy aptamer sequence is used with the same labels for negative control purposes (Table 4.1). All sequences are purchased from IDT.

**Table 4.1. Dummy sequence and aptamer modifications for different binding assays.**

<b>Dummy</b>	5'-GCACCAGCATATTCGATTGGGAGGTGTGAACGTTATGTGGTAGAG AGATGGGTGGTGGGGCTAGTAGGTGCATCAG-3'						
<b>Label</b>	NH <sub>2</sub>		Biotin		FITC	Alexa488	
<b>Spacer</b>	C6-5T	C6-10T	C6-5T	C6-10T	10T	5T	10T
<b>Application</b>	ALISA SPR		ALISA ELAA SPR		ELAA Fluorescence Microscopy		Fluorescence Microscopy

### 4.2.2. Sandwich assays: ALISA and ELAA

Immunosorbent-like assays are tested in two general assay designs (Fig. 4.5), with different modifications in substrate, immobilization method and detecting agent. As shown in the left, 167 nM CRP is covalently immobilized on

NucleoLink™ Immobilizer plates as described in Chapter 2 or captured by an immobilized anti-CRP monoclonal antibody (by the instruction provided by the manufacturer, BBI Solution, Cardiff, UK). The surface is blocked by 200 mM ethanolamine and/or different concentrations of BSA (0.1-1 %). 200 nM Aptamer incubation in 10 mM HEPES + 5 mM CaCl<sub>2</sub> for 30 min is followed by triple washings with 1x PBS. Detection of the aptamer by FITC-label recognition by HRP-conjugated pFITC-antibodies (Abcam Ab6656, Cambridge, UK) in conjugation buffer for 45 min is quantified by chemiluminescence after triple washings with 1x PBS. In another case, the aptamer is detected by interaction of the 5'-biotin tag and SA-HRP (Life Technologies) in conjugation buffer, resulting in chemiluminescence measurement at 450 nm in an absorbance plate reader after washing with 1x PBS and TMB addition.

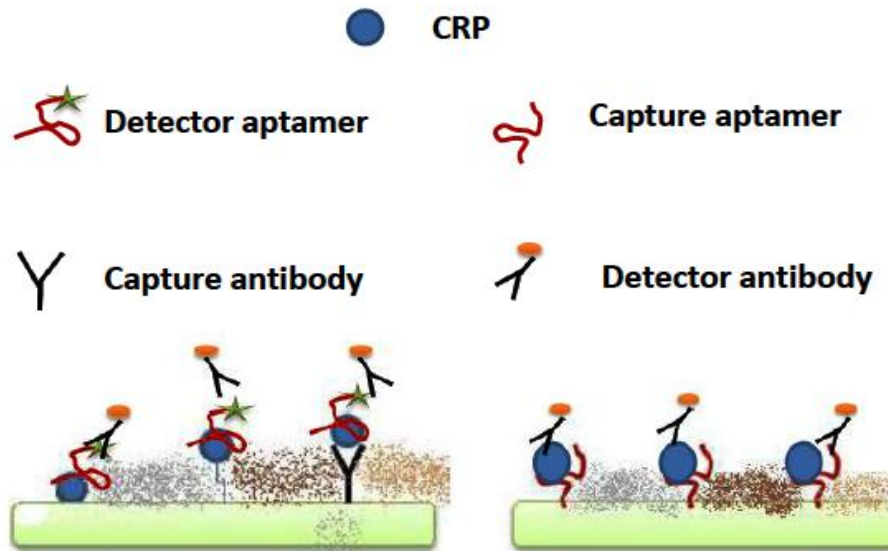


**Fig. 4.5. Schematic representation of sandwich binding assays. Left: CRP is adsorbed, covalently linked or captured on the substrate. Binding aptamer is detected by HRP-conjugated pFITC-AB or a Biotin tag.(ELAA) Right: CRP binding on covalently immobilized aptamer is detected by HRP-conjugated mCRP-AB (ALISA).**

As shown in the right part of Fig. 4.5., selected aptamers are also immobilized on the solid surface. Reaction of 10 nM amine-labeled aptamer with the free electrophilic group at the Nunc™ Immobilizer is achieved at room temperature for 2 hours in 100mM Carbonate buffer pH 9.6 After triple washing with 2x SSC + 0.1 % Tween®20, the surface is blocked with 100 mM ethanolamine (Jacobsen & Skouw, 2010). In another test, 1 μM, 100 nM and 10 nM 5'-Biotin tagged DNA is coated on Streptavidin-coated plates (Thermo Scientific) by 2 h incubation in 1x TBS + 0.05 % Tween®20 and washing with 1x TBS + 0.05 % Tween®20 + 0.1 % BSA. Remaining binding spots are blocked with Biotin. After 30 min incubation with 0-10 μM CRP in 10 mM HEPES + 5 mM CaCl<sub>2</sub> and washing as

before, CRP is detected by means of HRP-conjugated mCRP-AB in conjugation buffer.

All these binding assays are referenced with the (modified) dummy sequence and/or the same assay conditions without CRP. The addition of HS-ssDNA and 0.1 % - 0.5 % dextran sulfate (Sigma Aldrich) is tested to reduce non-specific binding.

#### 4.2.3. Quantitative PCR assay

The quantitative PCR assay is done as a selection step in the SELEX procedure. Predenatured 83 pM aptamer and dummy sequences are incubated for 30 min in 10 mM HEPES + 5 mM CaCl<sub>2</sub> on positively coated (1.67 nM CRP + 100 mM ethanolamine) and negatively coated (100 mM ethanolamine) Nunc™ Immobilizer plates. After triple washing with PBS, the bound ssDNA is eluted 4 times by hot TE + urea addition. After extraction and purification, quantitative PCR (as described in Chapter 2 and 3) allows comparison of bound ssDNA quantities. A concentration range of aptamer (8.3 nM - 0.083 pM) is also amplified for calibration purposes. Real-time quantitative PCR data analysis allows DNA quantification by comparing the reported C<sub>t</sub> or threshold cycle value (number of qPCR cycles that are performed before a threshold fluorescence value is measured) of unknown samples with the calibration cycles.

#### 4.2.4. Fluorescence assays

Fluorescence microscope assays are executed with FITC- and Alexa488- labeled aptamers on NucleoLink™ MicroArray Slides (Thermo Scientific) coated with CRP. EDC mediates the formation of amide bonds between carboxylic acids or phosphates and amines by activating carboxyl or phosphate groups to form an O-urea derivate. This derivate reacts readily with nucleophiles like the free amines of CRP (Hermanson, 2008). According instructions provided by the manufacturer, the microarray slides are activated by 10 mM EDC, coated with 2 μM of CRP, washed three times in 100 mM TRIS-HCl (pH 7.5) + 150 mM NaCl + 0.1 % Tween® 20 and blocked with 5x SSC + 0.1 % Tween® 20. Predenatured fluorescent aptamers are incubated 30 min in 10 mM HEPES + 5 mM CaCl<sub>2</sub> and washed three times with 1x PBS.

#### 4.2.5. Surface Plasmon Resonance

SPR analysis of the binding interaction between selected aptamers and CRP is done on the Biacore T200 SPR device (Biacore, Uppsala, Sweden). Different assay designs are tested using different SPR chips. (Types and specifications are shown in Fig. 4.6), buffers and instruction manuals for ligand immobilization, preconcentration testing and kinetic analysis. All reagents used for SPR analysis are purchased from Biacore, unless stated otherwise.

Receptor coating is achieved by 200 nM 5'-biotin aptamer immobilization on a Biacore SA-chip in 1x HBS-buffer + 350 mM NaCl in 1 min pulses at 20 $\mu$ L/min flow rate until a binding level of 1000 RU is reached. Biotinylated dummy sequence is immobilized on the reference flow cell. Both flow cells are blocked with 5'-biotin primer. DNA immobilization on C1-chips is achieved by covalent linkage in 1 min pulses of 1  $\mu$ M 5'-NH<sub>2</sub>-ssDNA in HBS + 750 mM NaCl to mitigate electrostatic repulsion between negatively charged DNA and the chip surface. Blocking of the surface is done with 100mM ethanolamine pH 8.

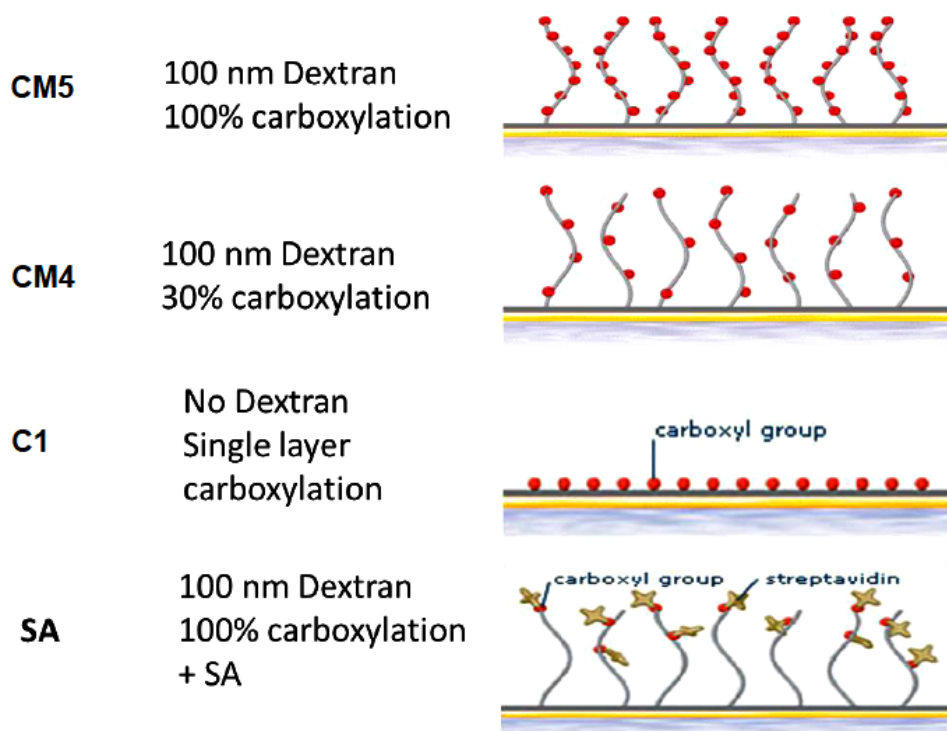


**Fig. 4.6. Overview of used SPR chips and their usage in this dissertation (Biacore Surface Handbook, 2003). CM5 and 4 chips are coated with Dextran matrix but with different levels of carboxylation for different immobilization levels of target protein. CM1 chips for low immobilization levels by a single layer of carboxylation. SA chips for streptavidin-biotin mediated functionalization of biotinylated ssDNA aptamers.**

Immobilization of CRP is executed on CM5 and CM4 chips by covalent amine coupling after EDC/NHS activation in MES buffer pH 6. Coating of 45 nM CRP is done in Na-Acetate buffer pH 5 until the desired binding response is reached. The flow cells are also inactivated with ethanolamine pH 8.



Running buffers are SELEX binding buffer with a concentration range of NaCl, but 1x TBS and 1x HBS + CaCl<sub>2</sub> is tested as well. Regeneration of the surface is achieved by 30 s pulses with 2 M NaCl or 50 mM NaOH.

### **4.3. Results and discussion**

In this section the results of different aptamer binding assays are shown and discussed, starting with the ELISA-like assays by detection of selected aptamers or CRP through HRP mediated chemiluminescence. Biotinylated aptamers, bound on immobilized CRP are detected by SA-HRP and CRP, bound on immobilized aptamers is detected by HRP-conjugated mAbs for CRP. In the next parts, the ssDNA is used as the quantitative signal generator in real-time PCR assays and fluorescently labeled aptamer binding is measured in fluorescence measurements. Target and aptamer sequence are also functionalized on various gold SPR chips to measure and quantify the binding events by means of surface plasmon resonance.

#### 4.3.1. Sandwich assays: ALISA and ELAA

ELISA-like assays suffer from high noise due to non-specific interactions and cross-talk effects with the applied labels and antibodies. The detection of bound FITC-labeled aptamer with HRP-conjugated pFITC-antibodies gives no differential responses and indicates an interaction between the antibodies and coated CRP which disappears after washing with 1x PBS + 0.5 % Tween<sup>®</sup>20. Detection of biotinylated aptamers by SA-HRP on CRP-immobilized plates shows false positive results, due to interaction between SA-HRP and CRP (illustrated in Appendix Fig. 5). Washing with 1 % Tween<sup>®</sup> 20 addition reduces ssDNA adhesion to the plate surface significantly but the non-specific interaction between SA-HRP and CRP is not altered much. Further analysis of binding and washing conditions shows that washing with 0.5 % dextran sulfate reduces aspecific interaction of SA-HRP and CRP, as does the addition of low concentrations (10 and 50 mM) of ethanolamine during SA-HRP incubation. Further analysis however indicates equal binding levels and an equal decrease in signal whether CRP is incubated with aptamer, dummy sequence or no ssDNA at all (Appendix Fig. 6).

The best result for this assay set-up is obtained when washings are performed with 1x PBS + 1 % Tween<sup>®</sup>20 and SA-HRP incubation with 10 mM ethanolamine addition (Fig. 4.7). Although the absorbance levels are low, the condition with aptamer A1 incubated with CRP shows higher levels as the other control conditions. However, large concentrations of target and aptamer are applied in these assays (200 nM). Conclusion to be made from these analyses is that there is a substantial non-specific interaction between CRP and ssDNA and between

SA-HRP and CRP. Selected aptamer A1 does have a binding effect on CRP, but this is masked by the non-specific interactions. Moreover, the binding of biotinylated aptamer A1 to CRP seems not strong enough to endure the stringent washings needed in this assay. The labeling of the aptamer with FITC or Biotin can inhibit the aptamer functionality.

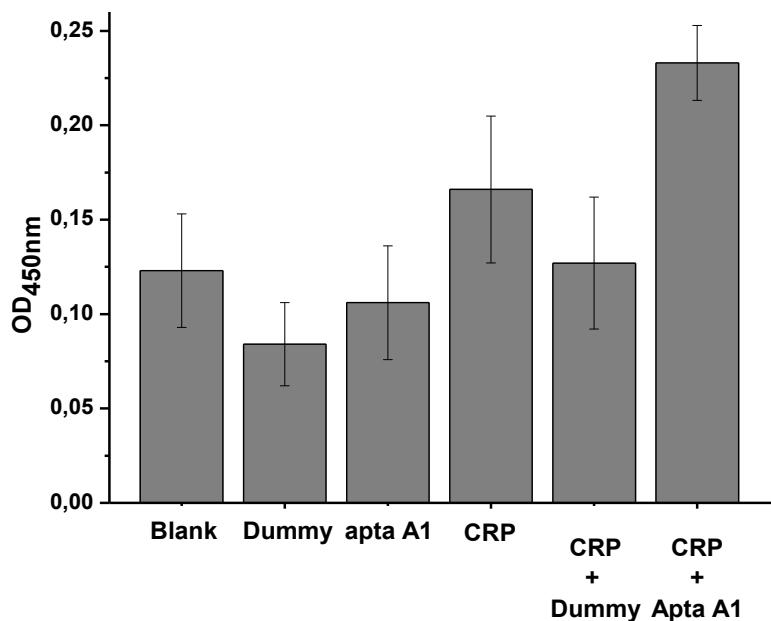


**Fig. 4.7. ELAA-assay with SA-HRP: (OD measured at 450 nm) in different assay conditions (n=3). Plots shows mean OD values with indicated standard deviations (error bars).**

Amine-labeled aptamer immobilization is performed with the NH<sub>2</sub>-C6-10T-sequences to maintain mobility of the aptamer. Bound CRP detection by means of HRP-conjugated-mCRP-Abs is not possible since the antibodies interact non-specifically with the immobilized DNA, as shown in Appendix Fig. 7. In this in triplo performed experiment, OD<sub>450</sub> measurements in A1, A2 and A3 immobilized wells are of the same level, whether there is CRP incubated in the wells or not. There is binding of the antibodies to the Nunc™ plates as well, as shown by the absorbance values in the blank condition.

The immobilization of Biotin-C6-10T-A4 on SA-plates gives the best results and allows to set-up a partial dose-response curve for various immobilized aptamer and dummy concentrations and for various applied CRP concentrations (Fig. 4.8). Reference values with equal immobilization levels of Biotin-C6-10T-dummy sequence are subtracted from the positive data. The SA-surface in this assay is blocked with Biotin-primer to block all remaining free Streptavidin. There is still substantial CRP binding to the dummy aptamer which results in low signal values.

These ALISA and ELAA assays indicate non-specific binding of detector reagents or of CRP to ssDNA. Using these approaches we could not demonstrate that the selected aptamers bind CRP more specifically and selectively than random ssDNA, but functionalities of the aptamers may be inhibited by immobilization and labeling procedures, changing the aptamer characteristics. On the other hand, non-specific interactions by detector reagents result in high stringency washings that can disrupt the aptamer-CRP complexes.

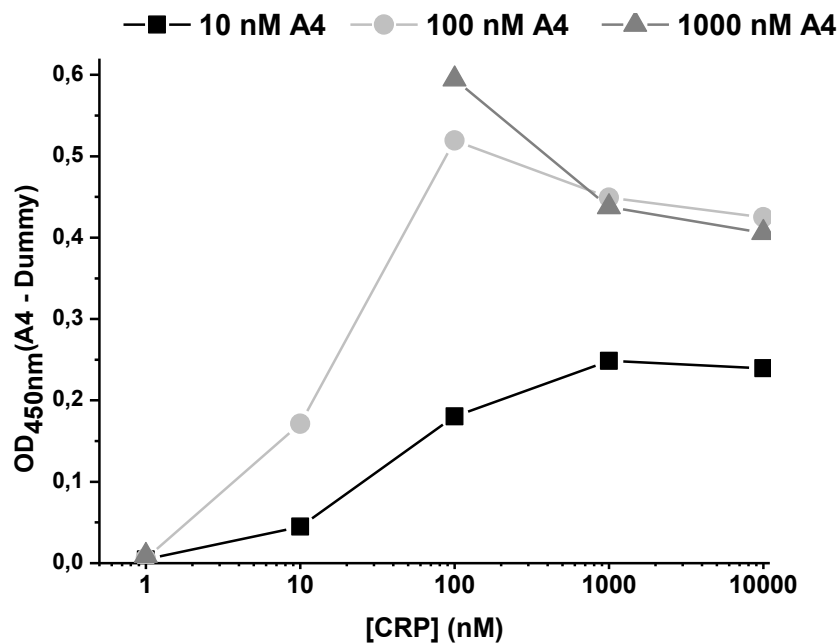


**Fig. 4.8. ALISA-assay on SA-plates: dose-response curves for increasing concentrations of CRP incubated on different concentrations of aptamer A4 (10, 100 & 1000 nM). Reference values for 0 nM CRP and CRP binding on Dummy ssDNA are subtracted.**

#### 4.3.2. Quantitative PCR assays

DNA quantification of eluted aptamer and dummy conditions in the real-time PCR assay shows a higher binding level on CRP than on ethanolamine alone for all selected aptamer conditions. Furthermore, the difference with the dummy sequence is clear as well. Amplification curves are shown in appendix (Appendix Fig. 8), but Fig. 4.9 shows the calibration curve that was used for quantification of the ssDNA pools. An amount of 83 pM equal to  $10^{10}$  aptamer or dummy oligonucleotides was incubated in the wells coated with CRP or only ethanolamine. Average  $C_t$  values for all conditions are calculated and plotted on the calibration curve which results in quantification of the elutions of A1-A4 and the dummy sequence. In this analysis, selected aptamer ( $10^{9.1}$ - $10^{9.6}$ ) sequences

bind to CRP a 100 fold more than the dummy ( $10^{7.1}$ ) sequences. Nevertheless, there is still substantial binding to ethanolamine of both the dummy ( $10^{7.8}$ ) and selected aptamer ( $10^{8.4}$ - $10^{8.7}$ ) sequences.

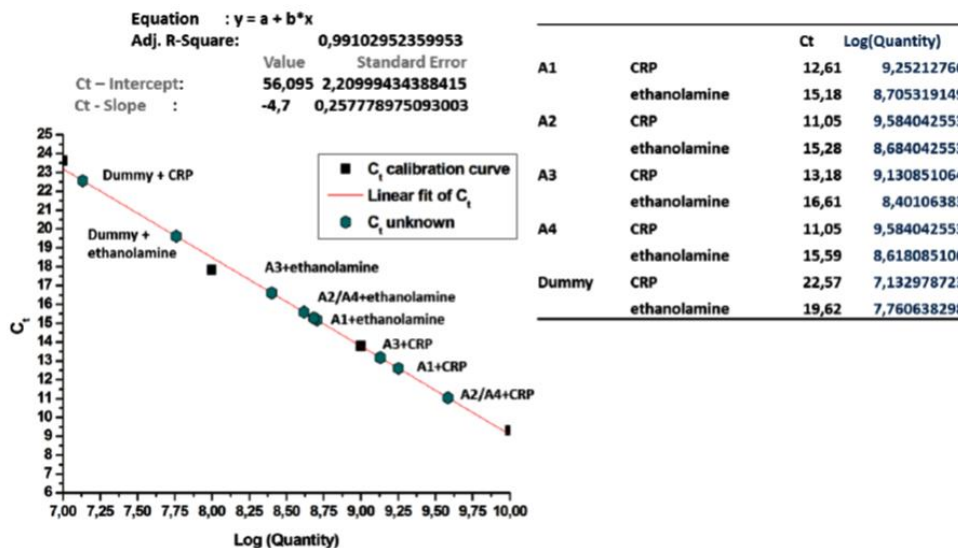


**Fig. 4.9. Linear fitted calibration curve for qPCR DNA quantification of eluted pools on CRP and ethanolamine, with reported R-square value of 0.99. Inset table shows the calculated number of DNA sequences for each condition in log scale, based on the reported  $C_t$  (threshold cycle value) and fitted linear equation.**

The observed non-specific binding can explain the signals measured in the ELAA-assays negative controls, where every remaining aptamer sequence results in signal generation and further amplification. Increasing the stringency of the washing step with 0.5 % dextran sulfate results in the loss of specific interaction.

#### 4.3.3. Fluorescence Microscopy

Fluorescent microscopy measurement of FITC-labeled ssDNA gives no result, as detection of Alexa488-labeled aptamer (Fig. 4.10) indicates non-specific binding of the labeled ssDNA to the Nunc™ Microarray slides. These microarray slides are taken out of production because of this reason.

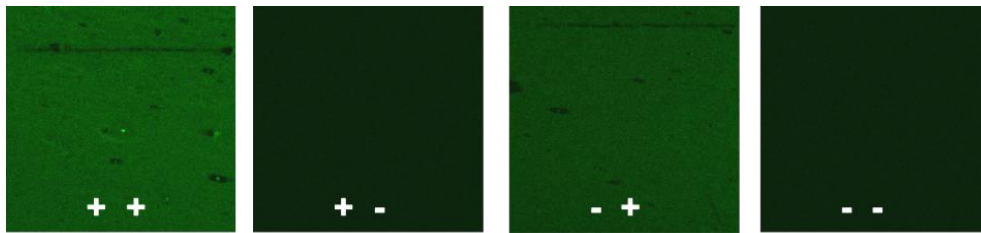


**Fig. 4.10. Alexa488-aptamer detection on CRP coated microarray slides. (++) CRP + aptamer; (+-) CRP; (-+) aptamer; (--) blank.**

#### 4.3.4. Surface Plasmon Resonance

Biotinylated aptamer and dummy sequences are immobilized on SA-chips in 1x HBS + 350 mM NaCl to a binding response of 1000 RU and further immobilized with biotin. Association for 20 min with 50 nM CRP in SELEX binding buffer at 30  $\mu$ L/min and 10 min dissociation indicates a non-specific binding interaction on both flow cells that slowly dissociates from the cell surface and is washed off by 2 M NaOH regeneration (Fig. 4.11). The binding Response of CRP in both flow cells is high and corresponds to 4800 RU. The non-specific CRP interaction is influenced by the immobilized ssDNA: the longer the ssDNA immobilized on the reference flow cell, the more non-specific CRP interaction occurs. However, non-immobilized SA reference flow cells still show a CRP binding response of 3000 RU. Immobilization with high amounts of biotin reduces this non-specific interaction to 2000 RU.

Buffer analysis with increasing ionic strength indicates an electrostatic interaction between both ssDNA immobilized and non-immobilized cell surfaces and CRP, as increasing NaCl concentrations in the SELEX binding buffer reduce this interaction. Addition of 750 mM NaCl in the SELEX binding buffer decreased CRP binding to zero, in the reference flow cell, but in the measuring flow cell with immobilized aptamers as well.

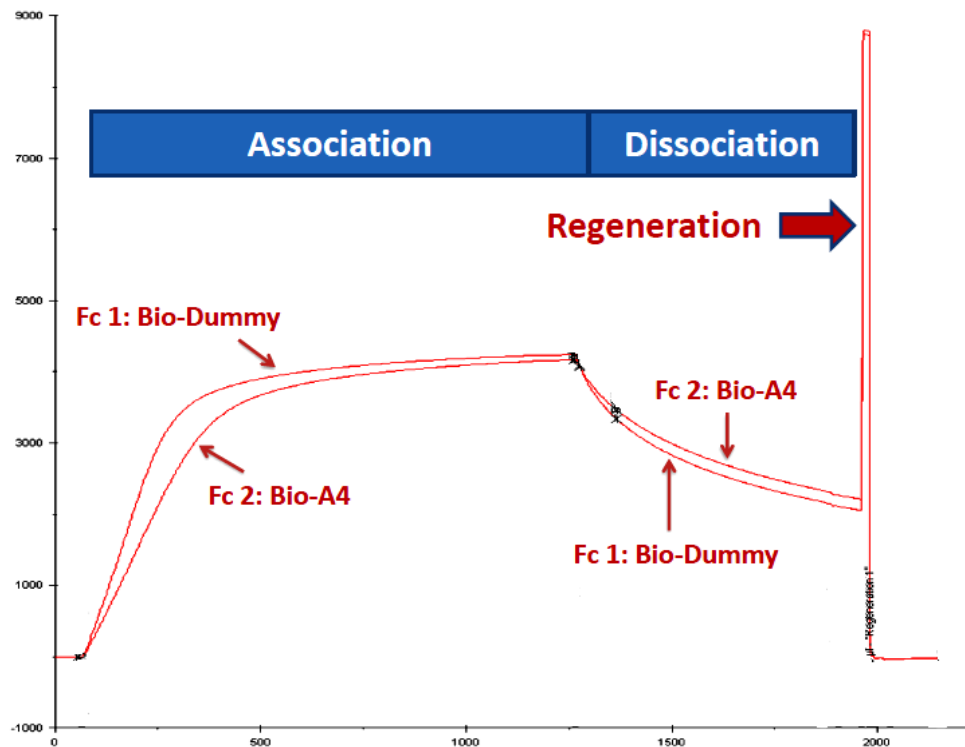


**Fig. 4.11. Sensorgram of 50 nM CRP on the reference flow cell (Bio-Dummy) and measuring flow cell (Bio-A4) of an SA-chip in 10 mM HEPES + 5 mM CaCl<sub>2</sub>. 20 min association and 10 min dissociation. Regeneration with a 30 s 2 M NaCl flush. x-axis = time (s); y-axis = response units (RU).**

These findings indicate there are multiple unwanted interactions of the ssDNA immobilized flow cell surfaces with CRP which are of an electrostatic nature. Increasing the ionic strength of the binding buffer is no solution, since this reduces the ability of the selected aptamers to bind CRP in a specific way as well. The selected aptamers lose functionality when applied in changed buffer characteristics, as they are not selected in high ionic strength conditions.

The possibility of immobilizing high amounts of selected aptamer on a SA-chip was used to test non-specific binding of other compounds on immobilized aptamer A3 & A4. Consecutive binding cycles of CRP and other molecules show there is no interaction on an equal amount of human plasminogen (50 nM – 100 nM – 500 nM) and low binding to 75 and 150  $\mu$ M BSA in SELEX running buffer and referenced by a biotin-immobilized flow cell, as visualized in Fig. 4.12. Between each binding cycle, the surface is regenerated with a 60 s flush of 1 M NaCl.

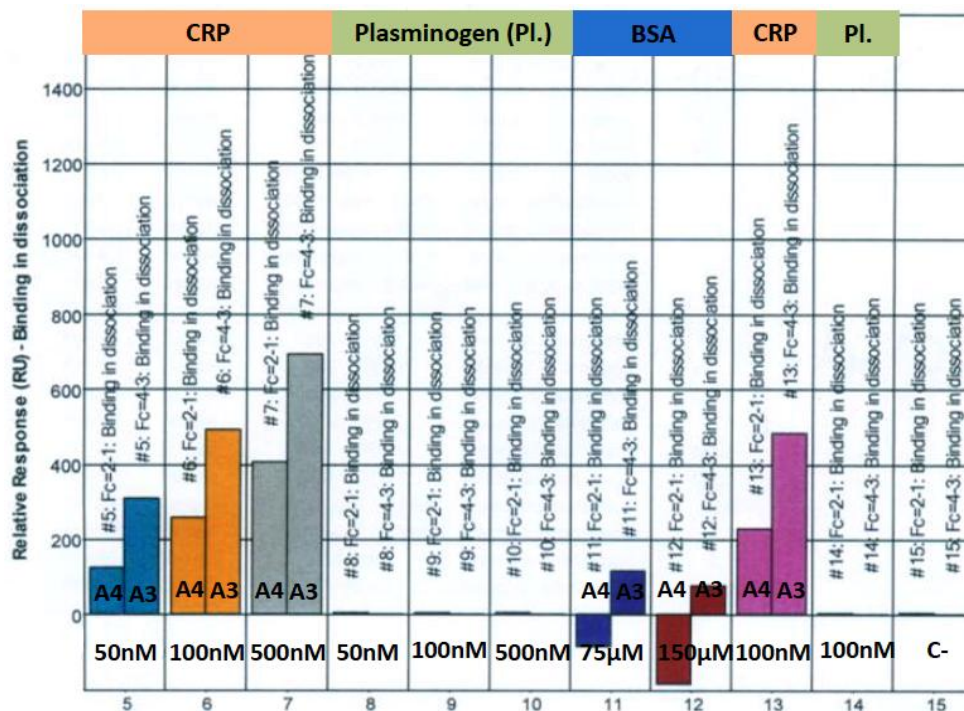


**Fig. 4.12. Bar chart of relative (reference subtracted) binding responses at the start of the dissociation phase in consecutive binding cycles (x-axis: 5 – 15) of different concentrations of CRP, Human Plasminogen and BSA in 10 mM HEPES + 5 mM CaCl<sub>2</sub> over an A4 & A3 immobilized flow cell (reference flow cell blocked with biotin); (5) 50 nM CRP; (6) 100 nM CRP; (7) 500 nM CRP; (8) 50 nM Plasminogen; (9) 100 nM Plasminogen; (10) 500 nM Plasminogen; (11) 75 μM BSA; (12) 150 μM BSA (13) 100 nM CRP; (14) 100 nM Plasminogen in (15) 10 mM HEPES + 5 mM CaCl<sub>2</sub>.**

As CRP association on other chip types (Fig. 4.6) is checked, it is clear that there is an electrostatic interaction between the activated carboxylic groups and the dextran layer (both net negatively charged in pH 7.4) on the chip surface. Equal concentrations (100 nM) of CRP in SELEX binding buffer is tested on unmodified SA, CM5, CM4 and C1 chips in 10 min association and 5 min dissociation experiments at 10 μL/min flow rates (Table 4.2).

SA chips illustrate the highest CRP association which slowly dissociates to a lower level of RU signal. The interaction between CRP and a CM5 chip dissociates much faster to an RU of zero. CM4 chips contain lower levels of carboxylation which results in lower responses in the association phase and immediate dissociation. CRP interaction on C1 chips, chips with a lower amount of carboxylic groups directly on the surface, in absence of the dextran matrix, is reduced to only 50 RU, and dissociates immediately after buffer change. These

results show a highly non-specific interaction of CRP with the chip types that use a dextran matrix and high levels of carboxylation.

**Table 4.2. 100 nM CRP in SELEX buffer responses on different unmodified chip types at 10 $\mu$ L/min flow rates.**

	<b>Binding response (RU) after 10 min association</b>	<b>Binding response (RU) after 5 min dissociation</b>
<b>SA</b>	<b>3500</b>	<b>1800</b>
<b>CM5</b>	<b>3000</b>	<b>200 – 0</b>
<b>CM4</b>	<b>200</b>	<b>0</b>
<b>C1</b>	<b>50</b>	<b>0</b>

Amine-labeled aptamers and dummy sequence are immobilized on EDC/NHS activated C1 chips to a binding response of 100 RU in 1x HBS + 750 mM NaCl. As the non-specific binding of CRP to the flow cell is reduced, there still is an electrostatic interaction between negatively charged DNA and CRP as well, as CRP also interacts with the DNA coated reference flow cell. The longer the phosphate backbone of the tested ssDNA strand, the more non-specific binding of CRP. When the dummy sequence of the same length (76 bp + 10T) is applied in the reference flow cell, there is higher binding on aptamer functionalized surfaces which results in a corrected positive, but irregular binding response (Fig. 4.13). Different buffers (SELEX buffer, 1x TBS, 1x HBS) with increasing KCl and NaCl concentrations (50-100-200 mM) are tested and shows decreased binding levels in both the reference and measuring flow cell in higher salt concentrations. Addition of 0.1 % Tween<sup>®</sup> 20 has no effect as 0.5 % disrupts every interaction on the flow cells.



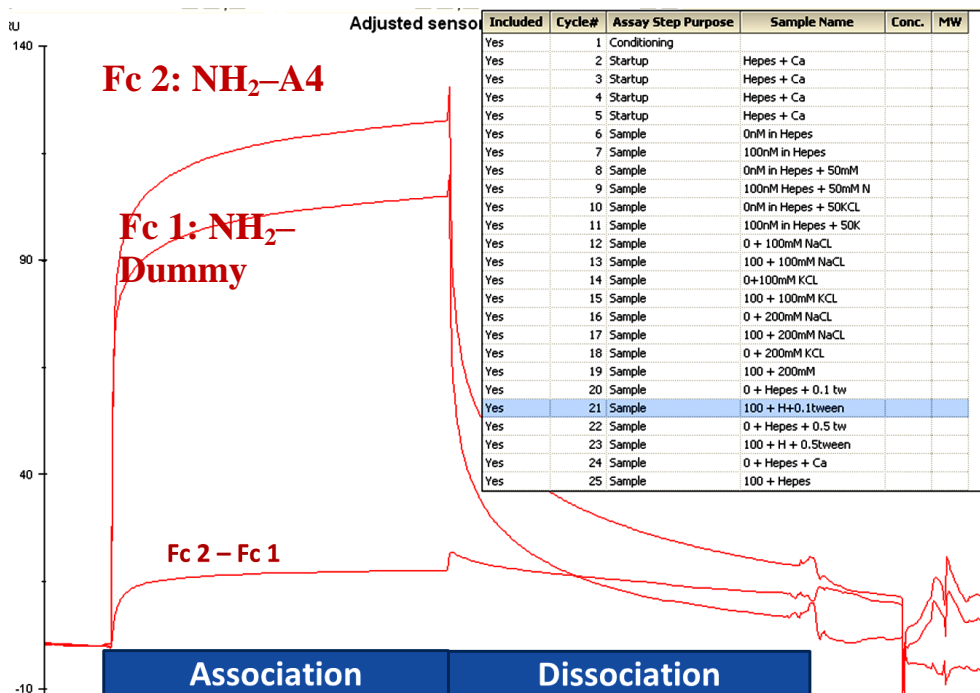


**Fig. 4.13. 100 nM CRP Binding sensorgrams on Aptamer A4 or dummy-functionalized C1 flow cells in SELEX binding buffer + 0.1 % Tween®20. (300 s association and 300 s dissociation at 30 µL/min). In this assay, SELEX binding buffer was tested with addition of 50 – 100 – 200 mM NaCl or KCl and 0.1-0.5 % Tween®20 (Inset table shows other tested buffers).**

As the binding responses on the measuring and reference flow cell are irregular, with high levels of non-specific binding and bulk contributions, the resulting corrected binding curves for kinetic analysis are irregular too, which make kinetic analysis and data fitting unreliable. Multy-cycle kinetic analysis of increasing CRP concentrations (5 – 200 nM) in SELEX binding buffer with 180 s of association & dissociation, a flow rate of 30 µL/min and regeneration by 2 M NaCl indicates problematic fitting and high bulk contributions and residuals (Fig. 4.14). Because of these warnings, the estimated kinetic dissociation constant ( $K_d$ ) of 20 nM for aptamer A4 is not readily accepted and further measurements are performed.

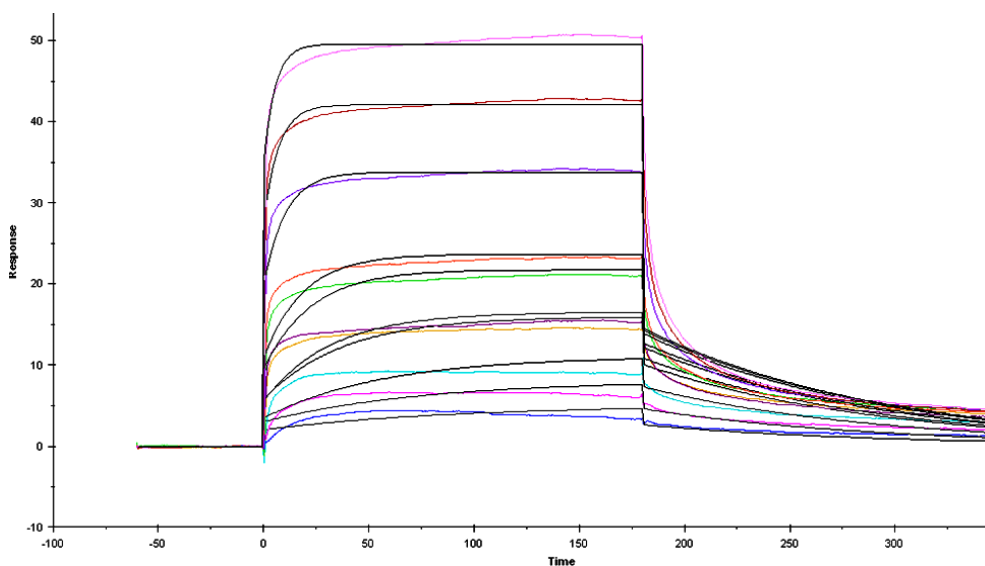


**Fig. 4.14. Multi-cycle kinetic analysis of 5-10-20-40-50-80-100 and 200 nM CRP in SELEX buffer on aptamer A4 functionalized C1 flow cells indicates problematic fitting and high bulk contributions. The red circle indicates the unreliable  $K_D$  estimation of 20 nM.**

In the following part of the SPR analysis of selected aptamers, the assay design is changed to be more similar to the SELEX design with surface-immobilized CRP and ssDNA in solution. As the aptamers are selected in this way, they should have a substantially higher affinity for CRP than randomly chosen ssDNA.

CRP is immobilized to a level of 600 RU on EDC/NHS-activated CM4-chips in Sodium-Acetate buffer pH 5, after preconcentration analysis for buffer pH. This chip type is chosen for lower immobilization levels than on a CM5-chip by lower carboxylation which is important for kinetic analysis to be optimally performed with low interaction responses of maximum 100 RU (Goodrich & Kugel, 2007). CRP-immobilized C1-chips do not allow ssDNA binding on the chip surface in the applied SELEX binding buffer, due to high electrostatic repulsion. The reference flow cell is immobilized with human Plasminogen and both flow cells are immobilized with ethanolamine. Binding analyses of 100 nM A1-A4 aptamers in SELEX binding buffer indicate show high association levels ( $\approx 100$  RU) compared to dummy sequence ( $\approx 0 - 10$  RU) and slow dissociation. Moreover, these binding responses are in accordance with the theoretical calculated  $R_{max}$  of 125 from the equation  $R_{max} = (MW_{analyte} / MW_{ligand}) \times R_{ligand} \times S_r$  where MW is the molecular weight of the immobilized ligand CRP (125000 Da) or aptamer analyte (24000 Da),  $R_{ligand}$  is the immobilization level of CRP (600 RU) and the stoichiometric ratio ( $S_r$ ) between aptamer and CRP is one, assuming each aptamer binds one CRP protein.

Multi-cycle kinetic analysis of 0 - 500 nM A1 in SELEX binding buffer is performed with 450 s association and 300 s dissociation at 30  $\mu\text{L}/\text{min}$  and 60 s 1 M NaCl regeneration (Fig. 4.15). Biacore Evaluation Software allows affinity rate constant estimation by fitting the acquired binding curves by mathematical equations of 5 different binding models (1:1 Langmuir binding, bivalent analyte model, heterogeneous ligand or heterogeneous analyte model and a two-state reaction binding model) (BIAevaluation 3.0 Software Handbook, 1997). Fitting of the binding curves gives best results (lowest *chi-square* value) with the model for heterogeneous ligand and reports two estimated  $K_d$  values ( $K_{d1}$ = 0.59 nM and  $K_{d2}$  = 19.0 nM) for aptamer A1 affinity for CRP. Kinetic analysis of Aptamer A2 is shown in Appendix Fig. 9 and indicates similar binding behavior and kinetic constants ( $K_{d1}$ = 0.62 nM and  $K_{d2}$ = 16.6 nM).

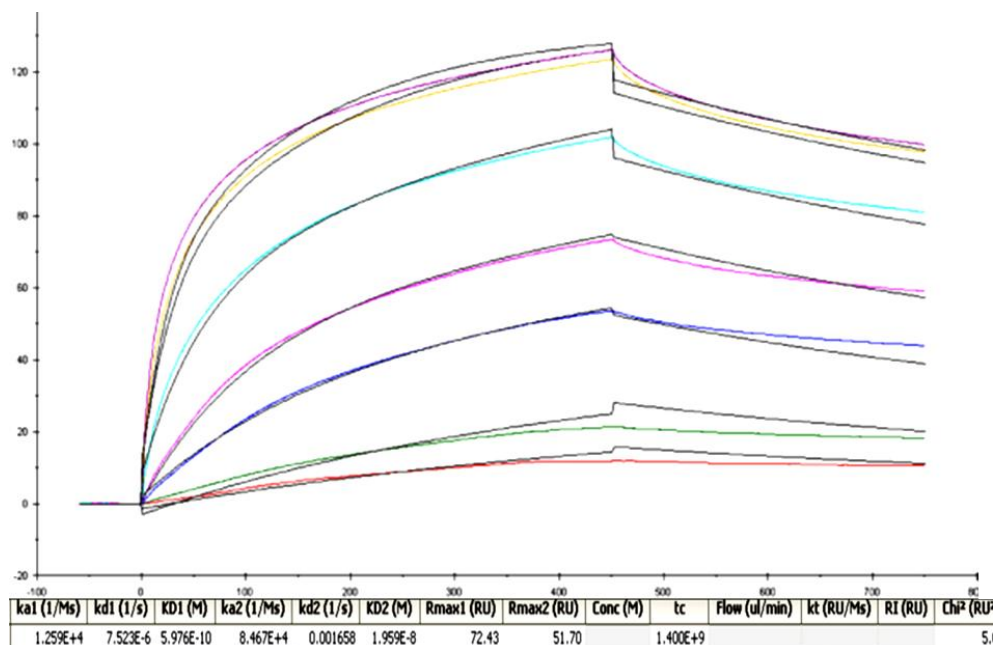


**Fig. 4.15. Multi-cycle kinetic analysis of 450s association and 300s dissociation of different concentrations (10-20-50-100-200-400-500 nM) of A1 in SELEX binding buffer on CRP-coated CM4-chip. Data fitting with model for heterogeneous ligand indicates two  $K_d$  values: 0.6 nM and 19.6 nM respectively. (Chi-square value = 5  $\text{RU}^2$ )**

Kinetic analysis of the aptamers A3 and A4 for 600 s association and 300 s dissociation at the same flow rate of 30  $\mu\text{L}/\text{min}$  show an inverse binding pattern, with a higher estimated  $K_{d1}$  value than the estimated  $K_{d2}$  values (Fig. 4.16). For aptamer A4 these values are  $K_{d1}$ = 13.2 nM and  $K_{d2}$ = 0.3 nM and for aptamer A3 (Appendix Fig. 10) the estimated affinities are lower, with  $K_{d1}$ = 77.6 nM and  $K_{d2}$ = 9.0 nM.

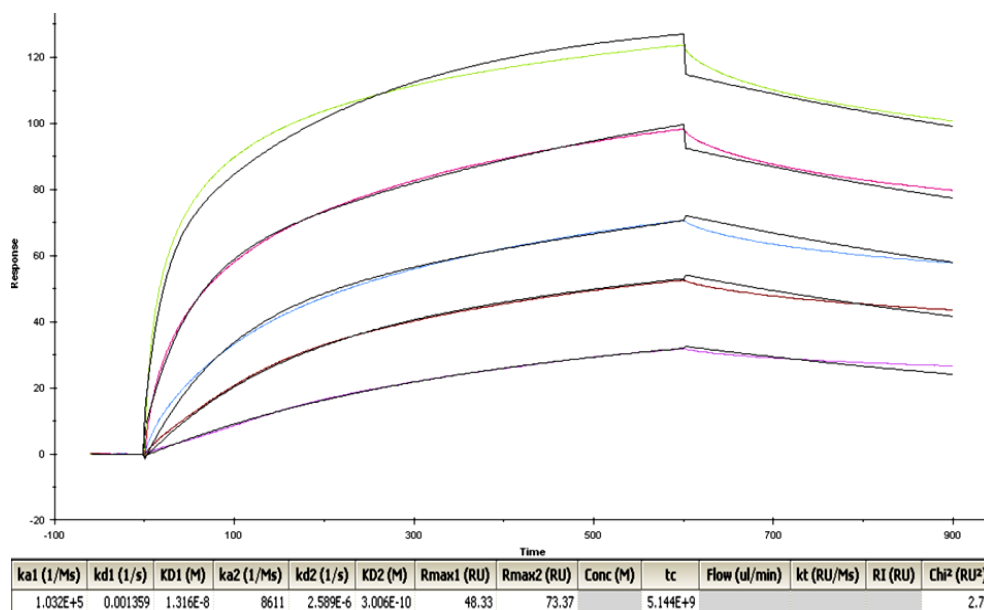


**Fig. 4.16. Multi-cycle kinetic analysis of 600s association and 300s dissociation of different concentrations (20-50-100-200-500 nM) of A4 in SELEX binding buffer on CRP-coated CM4-chip. Data fitting with model for heterogeneous ligand indicates two  $K_d$  values: 13.2 nM and 0.3 nM respectively (Chi-square value = 2.76  $\text{RU}^2$ ).**

The different binding behavior of aptamers A1 & 2 and aptamers A3 & 4 indicates a different binding mechanism with CRP. When looking at the sequence (Fig. 2.11) and structure information (Fig. 4.17) of these aptamer couples, it is clear that couple A1/2 and couple A3/4 have similar secondary structures that are different between each couple.

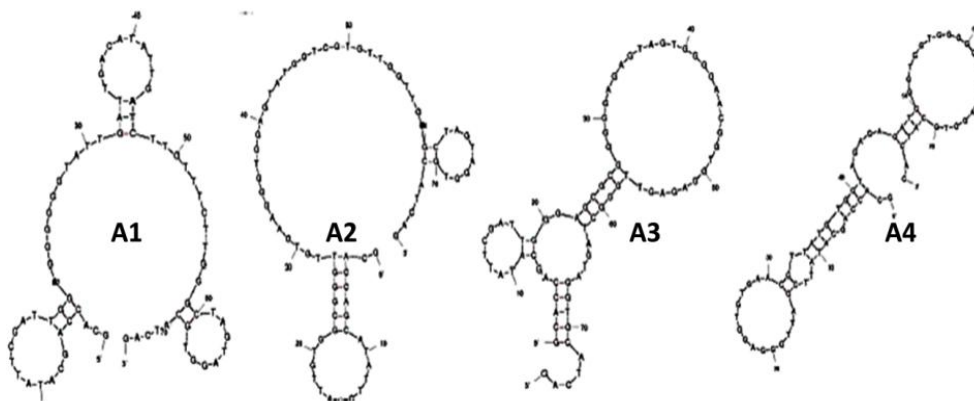


**Fig. 4.17. Secondary structure analysis of aptamer candidates A1 – A4.**

The real time label-free SPR analysis elucidates interesting features of the selected aptamers A1 to A4 and helps to understand and interpret the other binding assays that are performed.

It is clear that the immobilization of aptamers to the chip surface decreases the ability of all 4 selected aptamers to bind CRP in a selective way. In all SPR binding assays that involve immobilized aptamer, CRP binding was of a non-specific electrostatic nature, either to the applied flow cell surface or to negatively charged ssDNA as such. The use of a 10T-spacer does not ensure full aptamer mobility or functionality, and reduces affinity for CRP of the aptamers to the affinity levels of random ssDNA. Fluorescence labeling of the aptamers has a similar effect on the CRP binding ability than immobilization, reduction of CRP affinity to the level of random DNA.

CRP shows a high tendency to bind non-specifically in the applied SELEX binding buffer, as shown by the binding analysis on different kinds of SPR chips. The high interaction between CRP and SA may also explain the false positive results that are obtained in ELISA experiments, using SA-HRP as a detector for Biotin-labeled aptamers or using SA-modified plates for Biotin-labeled ssDNA immobilization. Changing the ionic strength of the buffers in SPR or addition of reagents to reduce non-specific in ALISA and ELAA have only marginal effects or completely disrupt the CRP interaction.

SPR data fitting of the aptamer-CRP interaction on CM4 chips indicates best fits when a binding model for a heterogeneous ligand is applied. This model describes an interaction between one analyte and two independent forms of the ligand and therefore reports two  $K_d$  values. Heterogeneous ligand situations frequently arise in practice through heterogeneous immobilization of ligand (e.g. amine coupling of proteins, where the ligand has multiple attachment points), as well as through heterogeneity in the ligand preparation itself (BIAevaluation 3.0 Software Handbook, 1997). This indicates heterogeneity of CRP on the CM4-surface, reflecting the possibility of having two forms of CRP, a pentamer and a decamer form, attributed to the recently reported CRP decamer formation in the applied SELEX buffer (Okemefuna *et al.*, 2010). Moreover, kinetic analysis reports aptamer A1 and 2 having higher affinities for CRP form 1 and aptamer A3 and 4 having higher affinities for CRP form 2. As stated in Chapter 2 as well, testing the binding affinities of selected aptamers on the known occurring forms of CRP (mCRP, pCRP and dCRP) can elucidate interesting features of the selected aptamers or of CRP behavior in various buffer conditions.

The selected aptamers have their maximum functionality in the SELEX binding buffer and changing the buffer characteristics (additives, increased ionic strength) seriously decreases the binding abilities of the aptamers. Attempts to mitigate electrostatic interactions by increasing the ion concentrations have no effect in low concentrations (extra 50-200 mM NaCl or KCl) or disrupt interaction with both the aptamer and the reference dummy sequence in high

concentrations (>250 mM addition). As CRP has an isoelectric point (pI) of 5.3 - 7.4 (Tsujiimoto *et al.*, 1983), it is expected to be neutral or slightly net negatively charged in the SELEX buffer pH 7.4. However, there is an interaction with negatively charged ssDNA, dextran or carboxylic surfaces, indicating a positive charge of CRP in the used binding conditions. Changing the pH of the SELEX buffer (pH 5) to change the net electric charge of CRP to positive has little effect on CRP binding on aptamer (A3 and A4) and dummy immobilized C1-chips (Fig. 4.18), with slightly higher binding levels on all flow cells. As the net charge of CRP is more positively charged, higher interaction levels are expected. Increasing the pH of the buffer (pH 8) results in no binding or preconcentration of CRP at the C1 flow cell surface at all, as expected by electrostatic repulsion of two negatively charged molecules.

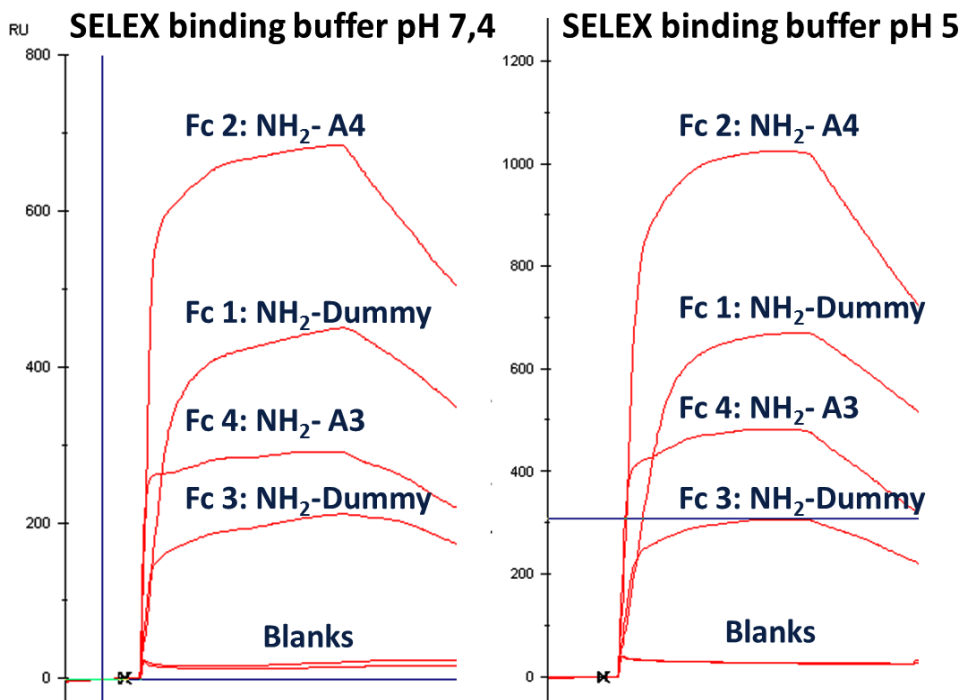


**Fig. 4.18.** 100 nM CRP injections in SELEX binding buffer pH 7.4 and 5. Flow cell (Fc) 1 & 2 of an activated C1 chip are immobilized to a level of 200 RU and Flow cell 3 & 4 to a level of 100 RU. CRP binding levels are higher on all flow cells in SELEX binding buffer pH 5.

The best results for CRP binding analysis come from binding assays that are similar to the SELEX design *i.e.* with the target immobilized on a surface and unmodified aptamers in solution. This is clear from the SPR analyses on CRP coated CM4 chips and from the qPCR assay which are the only assays where the selected aptamers display a clear higher affinity for CRP. In other types of assays, the ability of selected aptamers to bind CRP is reduced to the level of random ssDNA electrostatic interactions.

#### 4.4. Conclusion and recommendations

The research presented in this Chapter shows that the 4 selected aptamer candidates in Chapter 2 display high affinities for CRP which are in the low nanomolar (nM) range, provided they are used in the right set-up. Application of the unmodified aptamers as they are selected results in selective and specific CRP interaction. After optimization of the assay conditions, SPR binding and kinetic analysis of the 4 selected aptamers shows sensitive (nM affinities) and specific (no binding of plasminogen or BSA) CRP binding. Any deviation of these binding conditions (aptamer labeling or immobilization, changed buffer properties) results in the loss of aptamer functionality and reduces the affinity for CRP to the level of random ssDNA affinity for CRP. The aptamers demand the right binding conditions, which seriously decreases possible binding designs for aptamer application.

ALISA and ELAA designs suffer from non-specific interactions and reduced aptamer performance caused by labeling or immobilization, which is necessary for signal generation or target capture. Consequently, fluorescence measurements that imply fluorescent labeling of the aptamers are difficult to perform as well. The qPCR assay and SPR analysis have the best results for CRP binding specificity and selectivity because they are both real-time and allow the application of unlabeled aptamer sequences in solution, similar as they are selected.

The SPR analysis is the most informative assay that was performed in this study. It allows estimation of kinetic equilibrium constants but also allows assessing the binding properties of the selected aptamers in detail. Most interestingly, changing chip types allowed to identify possible causes of non-specific interactions of CRP that are experienced with other assay compounds such as SA. Changing buffer characteristics as pH and ionic strength gains insights about the causes of electrostatic interaction to random ssDNA and shows the sensitivity of the aptamer to buffer deviations.

This research clearly illustrates that an aptamer is only as good and versatile as it is selected. Efforts can be made in future selection procedures to build in some sort of flexibility of the aptamers to maintain full functionality in different applications. If a highly informative but expensive system such as a real-time SPR device is available a lot of the difficulties faced in this chapter can be checked *a priori*. Optimal buffer conditions for minimal non-specific interactions of the target with cell surfaces or other compounds can be tested. Moreover, the selection of aptamers can be performed with a random library that already contains modifications that are needed in later binding assays. Performing a selection procedure with fluorescently labeled random sequences can result in successful aptamers to be applied in fluorescence assays. Selection with an immobilized random library can be applied to select aptamers that serve as an

immobilized capturing agent. Performing a SELEX procedure with different buffer conditions in each round may result in highly flexible aptamers, not demanding specific buffer agents or ionic concentrations for full functionality.



# 5

## **Application of aptamers in a new label-free read-out system**

*This chapter explores the application of the selected aptamers in a new label-free read-out system, measuring changes in heat-transfer resistance which is proven to be useful in DNA denaturation experiments for SNP detection. Several assay designs are explored which highlights some key features of this read-out method and their consequences for sensitive protein detection on this platform by means of aptamers.*

### **5.1. Introduction**

As the previous chapter clearly indicates, the use of a post-SELEX modified aptamer structure has certain risks in regard to target selectivity and specificity. Attachment of fluorescent dyes, affinity tags or other compounds to the 5'- or 3'-terminus of the ssDNA strand can seriously alter the structural confirmation and the folding properties of a selected aptamer. As other chemical compounds are tethered to the ssDNA, this also changes the chemical characteristics of the ligands (e.g. net electric charge, molecular weight, etc.) which can disrupt the specific interaction mechanism between aptamer and the target or induce non-specific interactions of other compounds than the target to the labeling compound or to the whole aptamer sequence.

Real-time label-free read-out systems and mechanisms that do not require the modification or labeling of the aptamers after their selection are very interesting to be investigated because they have some obvious advantages over read-out platforms that do:

- *Reduced time and costs of binding analysis:* No need for costly labeling dyes and procedures or for specialized instrumentations for signal detection and quantification. The labeling process makes the experiments complex and affects the bioaffinity between the probes and their targets (Deng *et al.*, 2013).
- *Highly informative output:* As the aptamer is an unmodified structure, detailed information about the binding abilities of the aptamer is

obtained, without the loss of aptamer functionality. By comparing the properties of the aptamer as a capturing or detecting agent, the effect of aptamer immobilization can also be assessed.

- *Effect determination of labeling procedures:* Labeled aptamers can be applied and evaluated by these label-free methods to assess the effect of tethered labels on the affinity for the target in condition that the label does not interfere with the signal generation of the method.
- *Real-time analysis:* Signal generation by labeled aptamers is often measured in an 'end-point' reaction, after the interaction between the aptamer and target has taken place. The possibilities of real-time analysis can provide crucial information about molecular recognition.

Label-free platforms make use of intrinsic characteristics of the compounds to be analyzed, such as electrical charge, molecular weight, size vs. charge ratio and conformational changes and are focused on optical and electrochemical signal generation platforms such as impedance spectroscopy (Park & Park, 2009; Tran *et al.*, 2011; van Grinsven *et al.*, 2011; Luo *et al.*, 2013; Gao *et al.*, 2013) electric field-effect based devices (Stern *et al.*, 2008; Kawarada & Ruslinda, 2011), SPR, SPRi (Chen *et al.*, 2012) and LSPR (Guo & Kim, 2011) and linear (electric) conductivity measurements (Guo *et al.*, 2008b). All of these methods measure a change in mechanical rigidity, changes in the total charge or the redistribution of counter-ions and make use of differentiations of the dielectric or optic interfacial features near the surface or electrode onto which the ligand or analyte is attached (Deng *et al.*, 2013).

A recently developed read-out platform makes use of the change of heat-transfer resistance ( $R_{Th}$ ) at a solid-liquid interface (van Grinsven *et al.*, 2012) to measure the dsDNA melting temperatures of dsDNA brushes at this interface. This method is proven useful for fast, label-free, denaturation-based SNP detection and is explained in the following paragraph.

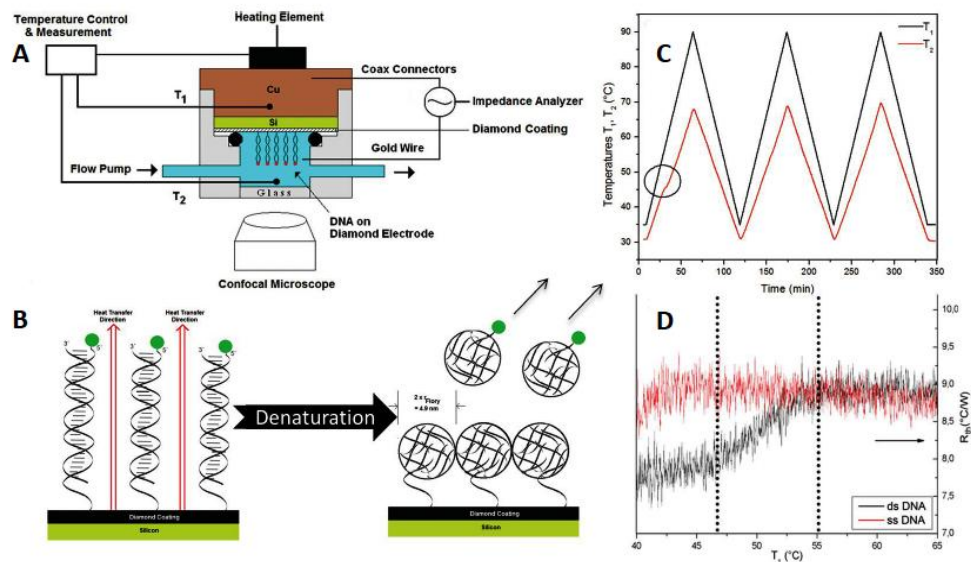


**Fig. 5.1. (A) Principle of a heat-transfer measurement at a copper Solid-Liquid interface. (B) Effect of dsDNA denaturation on Heat-transfer direction. (C) Measured effect in the flow cell temperature  $T_2$  upon denaturation (D) Translated  $R_{Th}$  values and shift for dsDNA and ssDNA. (Figure adapted from van Grinsven *et al.*, 2012)**

van Grinsven *et al.* (2012) observed that a molecular brush of dsDNA grafted onto synthetic diamond surfaces does not notably affect the heat-transfer resistance at the solid-to-liquid interface. In contrast to this, molecular brushes of ssDNA cause a higher heat-transfer resistance and behave like a thermally insulating layer (Fig. 5.1). Upon denaturation at the dsDNA specific  $T_m$  ( $^{\circ}\text{C}$ ), a thermal effect is measured in the liquid phase flow cell, confirmed by impedance spectroscopy and confocal microscopy measurements. This effect is translated to the heat-transfer resistance or  $R_{Th}$  value ( $^{\circ}\text{C}/\text{W}$ ), defined in (eq.1) below. In this way, mismatch dsDNA strands are detected and identified, which is useful for SNP detection.

$$R_{Th} = (T_1 - T_2) / P \quad (\text{eq.1})$$

$T_1$  = internal temperature ( $^{\circ}\text{C}$ ) of the solid phase copper block,  $T_2$  = temperature ( $^{\circ}\text{C}$ ) measured in the liquid phase flow cell,  $P$  = electrical heating power  $P$  (W), required to achieve the linear increase of  $T_1$  according to the applied heating rate (Fig. 5.1).

This new read-out device for dsDNA denaturation and SNP detection makes use of the structural conformational change of the DNA at a solid-liquid interface and measures the effect on thermal conductivity or resistance over this interface. In this part of the dissertation, this label-free read-out platform is tested for

aptamer applicability in two ways. In a first approach, the thermal insulation effects of CRP binding and the conformational changes of the immobilized aptamer sequences is evaluated. Since the selected aptamers suffer from immobilization constraints, as shown in Chapter 4, the assay design is also switched to be more similar to the SELEX design, with immobilized CRP and the evaluation of the effect of aptamer binding on heat-transfer resistance over the solid-liquid interface. Furthermore, the insulating effects of target binding on immobilized aptamer sequences are evaluated with an immobilized validated aptamer sequence for human  $\alpha$ -thrombin (Tasset *et al.*, 1997) and the detection of  $\alpha$ -thrombin by means of  $R_{Th}$  analysis at the solid-liquid interface, to investigate the general applicability of aptamers with this method.

## 5.2. Experimental section

### 5.2.1. Design of the sensor cell and the thermal read-out system.

The sensor set-up shown in Fig. 5.1.A is described in detail in van Grinsven *et al.* (2012). As the same set-up is applied here, the most important features for understanding are repeated. The flow cell has an inner volume of 110  $\mu$ L, and liquids are exchanged with a syringe-driven flow system (ProSense, model NE-500, The Netherlands) that automatically injects the applied buffers or reagents solutions. This is not a stopped-flow system. Two thermocouples (type K, diameter 500  $\mu$ m, TC Direct, The Netherlands) monitor the temperature  $T_1$  of the copper backside contact and the liquid temperature  $T_2$  in the center of the flow cell at 1.7 mm above the solid-liquid interface surface. The heat flow is generated with a power resistor (22  $\Omega$ , MPH 20, Farnell, Belgium) glued onto the copper block with heat conductive paste. To regulate  $T_1$ , the thermocouple signal is led to a data acquisition unit (Picolog TC08, Picotech, United Kingdom) and from there processed into a PID controller (parameters: P = 10, D = 5 I = 0.1). The calculated output voltage was sent via a second controller (NI USB 9263, National Instruments, USA) to a power operational amplifier (LM675, Farnell, Belgium) and fed into the power resistor. Sampling of the  $T_1$ ,  $T_2$  and the voltage values is done at a rate of one measurement per second.

The central element through which the heat transfer passes is a silicon chip ( $\pm 10 \times 10$  mm<sup>2</sup>) covered with a thin layer of nanocrystalline diamond (NCD) (Janssens *et al.*, 2011). This diamond layer serves as the immobilization surface for the selected aptamers or CRP proteins via the photochemical fatty acid & EDC coupling mechanism, which is well described for NCD (Christiaens *et al.*, 2006; Vermeeren *et al.*, 2008) Furthermore, NCD is chosen as interface material for the high thermal conductivity and chemical, electrochemical and thermal stability it displays (Vermeeren *et al.*, 2009). The functionalized NCD sensor chip is glued with the back-side to the copper block by means of conductive silver paste, to minimize possible heat loss. The front-side of the sensor chip is

exposed to the applied buffer in the flow cell, with a contact area of 28 mm<sup>2</sup>, sealed by an O-ring seal.

This general sensor and flow system set-up is used for the following described assay designs: aptamer immobilization and direct CRP binding detection, aptamer immobilization with indirect CRP binding detection and target immobilization with direct aptamer binding detection.

#### 5.2.2. Aptamer immobilization and direct CRP binding detection

Amine-tethered aptamer and dummy sequence with a 10T-spacer are covalently immobilized on fatty acid-functionalized NCD surface by EDC/NHS chemistry in 25 mM MES buffer pH 6. A 50  $\mu$ L mixture of 25 mg/mL EDC and NHS is incubated 30 min at RT on a fatty acid functionalized NCD sample. After rinsing the sample in MES buffer pH 6, 300 pmol of NH<sub>2</sub>-A4 or NH<sub>2</sub>-dummy sequence in 100 mM MES pH 5.5 is incubated 2 hours at 4 °C. After a triple wash in 1x PBS pH 7.4, 200 mM ethanolamine in carbonate buffer pH 9.6 is incubated 1 hour for deactivation of the carboxylic groups. Non-reacted ssDNA or ethanolamine is rinsed off by washing the samples for 30 min in 2x SSC + 0.5 % SDS at room temperature. After ssDNA functionalization, the NCD samples are stored in SELEX binding buffer at 4 °C.

Since the heat-transfer device is operated in a temperature-stabilized environment at 19.3 ( $\pm$  0.1 °C), a higher temperature  $T_1$  is needed to ensure substantial heat transfer over the interface. Therefore, the copper block temperature  $T_1$  is set at 37 °C. Flow cell injections are programmed as 3 mL injections at a 250  $\mu$ L/min flow rate followed by 30 min stabilization (Fig. 5.2). A typical binding assay is programmed as three injections of SELEX binding buffer and consecutive injection of 25, 50 and 100 nM of CRP in the same buffer. After stabilization, the sample is regenerated by 50 mM NaOH injection and 30 min stabilization in SELEX binding buffer.

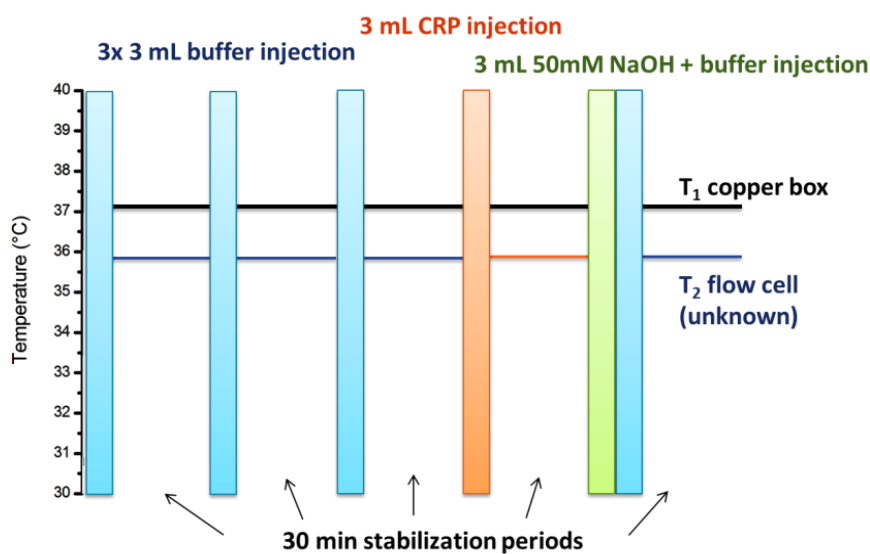


**Fig. 5.2. Diagram of the assay for CRP binding on A1-functionalized NCD with indicated injections and a temperature  $T_1$  of 37 °C. Flow rate for all injections is 250  $\mu$ L/min.**

5.2.3. Aptamer immobilization, target binding and detection of conformational changes at increasing temperature.

NCD samples are ssDNA-functionalized as above and are expected to form an insulating layer that affects the heat-transfer resistance over this surface, in analogy to the findings of van Grinsven *et al.* (2012). To investigate whether the secondary structure formation of selected aptamers upon target binding affects the insulating properties of the ssDNA layer, any secondary structure or complex formation is disrupted by thermal denaturation of the ssDNA strand. The copper box temperature  $T_1$  and consequently flow cell temperature  $T_2$  is increased slowly from 30 °C to 80 °C at a 1 °C/min temperature transition rate to induce secondary structure or complex disruption for the aptamer- or dummy-functionalized NCD sample incubated with a 0 or 100 nM CRP SELEX binding buffer solution in the flow cell (Fig. 5.3).

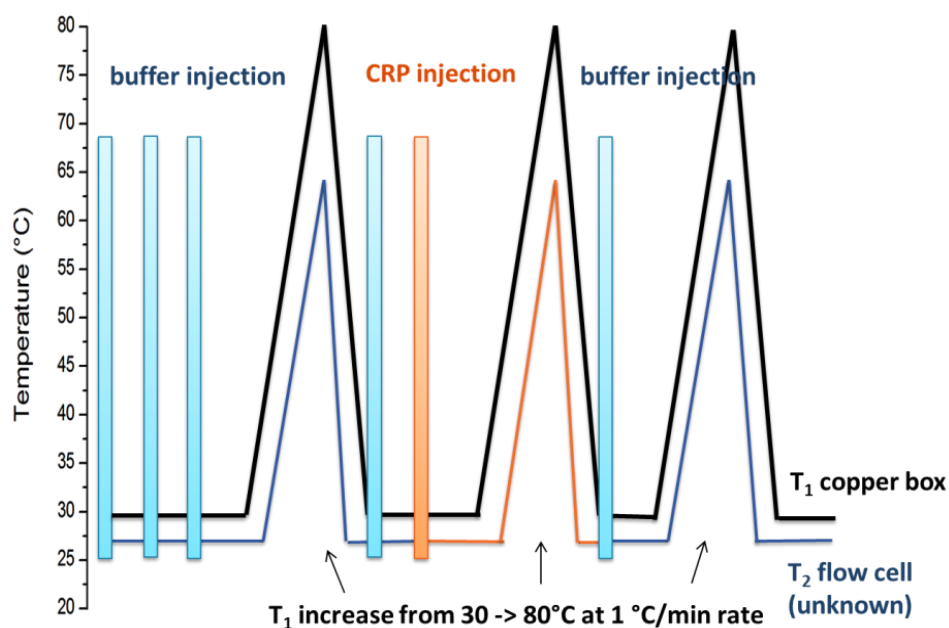


**Fig. 5.3. Diagram of the assay for CRP binding on A1-functionalized NCD with indicated injections and increasing temperatures  $T_1$  to 80 °C. Flow rate for all injections is 250  $\mu\text{L}/\text{min}$**

The same analysis is also performed with a generally validated aptamer for human  $\alpha$ -thrombin TBA2 (Tasset *et al.*, 1997) with a 5'-NH<sub>2</sub>-10T modification purchased from IDT and thrombin from Haematologic Technologies Inc. (HTI, Essex Junction, Vermont, USA). The aptamer sequence and modifications are shown in Table 5.1.

Aptamer functionality and affinity for  $\alpha$ -thrombin is checked by kinetic analysis on the Biacore™ T200 SPR device. 5'-Biotin-10T-functionalized TBA2 (IDT) is immobilized on a SA-Chip (Biacore) to a binding level of 800 RU. Biotinylated dummy sequence (as described in Table 4.2.) is immobilized on the reference flow cell. Multi-cycle kinetic analysis is performed with 2, 5, 10, 20, 40, 50, 80 and 100 nM concentrations of  $\alpha$ -thrombin in 50 mM Tris-HCl (pH 7.5) + 100 mM NaCl + 1 mM MgCl<sub>2</sub> at 37 °C for 5 minutes at a 30  $\mu\text{L}/\text{min}$  flow rate. After 180 s of association and 240 s of dissociation, the surface is regenerated with a 30 s 2 M NaCl flush.

**Table 5.1. Aptamer sequences of (modified) TBA2 (IDT).**

5'-ATTCCGTGGTAGGGTAGGTTGGGGTGAAT-3'
5'-NH <sub>2</sub> -10T-ATTCCGTGGTAGGGTAGGTTGGGGTGAAT-3'
5'-Biotin-10T-ATTCCGTGGTAGGGTAGGTTGGGGTGAAT-3'

#### 5.2.4. CRP capture and aptamer binding detection.

For the heat-transfer measurement of the aptamer binding event on captured CRP in the flow cell, the validated and in-house CRP-mAB 4DG2 is immobilized on the NCD-surface by EDC/NHS chemistry in a similar way as amine-tethered ssDNA. After activation the surface is incubated with 10 µg/mL 4DG2 in 100 mM MES pH 5 for 2 h at 4 °C, washed three times in 1x PBS + 0.2 % Tween®20 and deactivated with 200 mM ethanolamine in carbonate buffer e.6. This functionalization is checked in an ELISA sandwich assay by 100 nM CRP incubation and detection with HRP-conjugated hsCRP-mABs (apDia bvba, Turnhout, Belgium) in SELEX binding buffer.

CRP binding in the heat-transfer set-up is double-checked by dismantling the system after 100 nM CRP incubation and rinsing and by performing the ELISA sandwich assay as described above. Aptamer A1 binding ability on the immobilized mAB 4DG2-CRP complex is checked by performing an identical binding assay on the Biacore™ T200 SPR device at 25 °C. Therefore, 4DG2 is covalently immobilized on an activated C1-chip by injecting 1 µg/mL in Sodium acetate buffer pH 5 for 5 min. The immobilization is optimized to reach a final binding response of 200 RU. After binding of 100 nM CRP in SELEX binding buffer is checked, aptamer binding on the mAB-CRP complex is checked by 240 s injection of 20 nM and 100 nM of aptamer A1 or 100 nM dummy sequences in SELEX binding buffer. The flow cell is regenerated by a 60 s flush with 1 M NaCl and a 60 s 10 mM NaOH flush to dissociate aptamer and/or CRP. As a double-check, 200 nM CRP is preincubated with 200 nM A1 or dummy sequence at room temperature in SELEX binding buffer before a 240 s injection over the mAB-functionalized flow cell. The surface is regenerated in the same way as stated above.



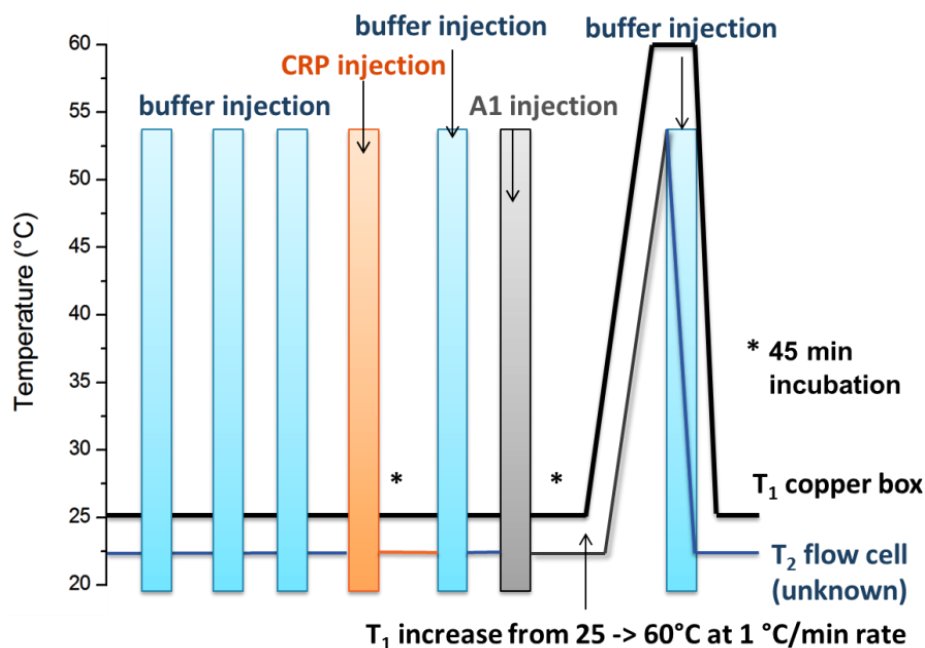


**Fig. 5.4. Diagram of the assay for CRP binding on 4DG2-functionalized NCD and consecutive binding of A1 with indicated injections and increasing temperature  $T_1$  to 60 °C for denaturation purposes. Flow rate for all injections is 250  $\mu\text{L}/\text{min}$ .**

The capturing AB functionalized NCD is mounted in the heat-transfer set-up and the following consecutive injections (250  $\mu\text{L}/\text{min}$  flow rate) are performed at a copper box set temperature  $T_1$  of 25 °C (Fig. 5.4.):

- three injections of 3 mL SELEX binding buffer with 30 min stabilization time in between
- one injection of 3 mL 100 nM CRP in binding buffer followed by 45 min of incubation and a 3 mL rinse with binding buffer
- one injection of 3 mL 100 nM A1 aptamer in binding buffer followed by 45 min incubation

After these injections, the temperature of the copper box is increased to 60 °C for aptamer denaturation together with a 3 mL flush of binding buffer at elevated flow cell temperature to flush the aptamer out of the flow cell. A final stabilization of 30 min at 25 °C ends the assay.

Extended A1 aptamer sequences are applied as well for the same heat-transfer assay as described above to investigate whether extension of the binding ssDNA strand increases the insulating effect on the coated interface. To make sure no influence of a 20T or 40T extension at the 5'- or 3'-terminus on the aptamer A1 secondary structure is predicted by mfold (Zuker, 2003) and the extensions that cause no drastic structure deformation are selected for analysis. CRP binding

functionality of the selected extended aptamers is checked by SPR binding analysis of the oligonucleotides to captured CRP or of preincubated aptamer-CRP mixes to the immobilized mABs 4DG2 as described above.

### 5.3. Results & discussion

#### 5.3.1. Direct detection of the CRP binding event by heat-transfer resistance measurements

It is clear from Fig. 5.5 that system stabilization is crucial and multiple buffer injections are needed to have a stable base-line. The measured flow cell temperature  $T_2$  shows an irregular pattern, with the temperature decreasing every time new SELEX binding buffer is injected. This effect is expected since no pre-heating of the newly injected buffer to 37°C took place. However, unexplained temperature variations in the stabilization phases are also observed, when there was no flow of buffer in the flow system. The  $R_{Th}$  (°C/W) value shows a noisy pattern resulting from its calculation. This pattern is smoothed by Savitsky-Golay smoothing with 60 points of window in Origin Pro v.8 (OriginLab, Northampton, MA, USA) resulting in the red line in the  $R_{Th}$  graphs. As  $T_2$  decreases from 33.8 to 33.2 °C,  $R_{Th}$  is slowly increasing from 5.5 to 7.2 °C/W. These variations are not necessarily a problem, if the response upon CRP binding is substantially higher than these base-line variations.

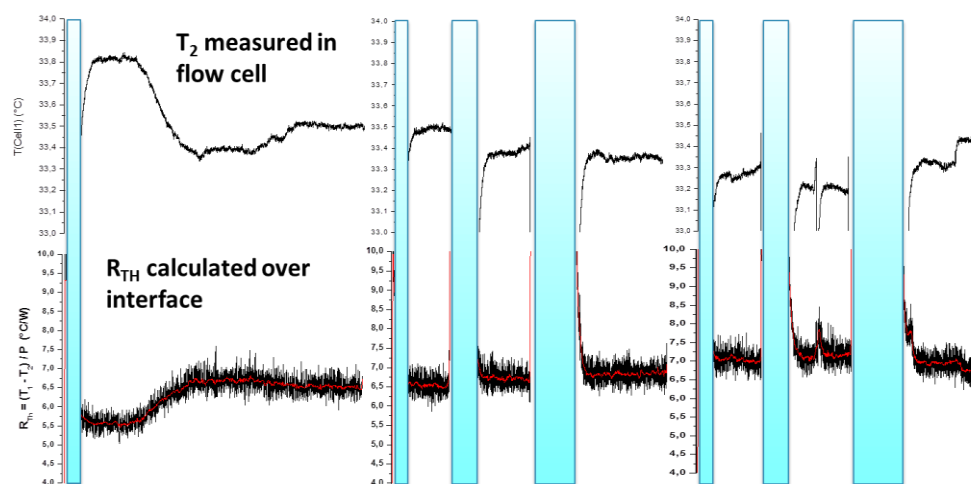


**Fig. 5.5. Real-time measurement of  $T_2$  (°C) in the flow cell and calculated  $R_{Th}$  (°C/W) (eq. 1 pg. 80) over consecutive SELEX buffer injections. Copper Temperature  $T_1$  is set as 37 °C. Red Line in  $R_{Th}$  data represent smoothed values (Savitsky-Golay smoothing; 60 points window).**

Both immobilized aptamer A1 and dummy sequences are incubated with increasing concentrations of CRP in SELEX binding buffer in the heat-transfer set-up. As shown in figure 5.6, these measurements indicate that the binding

event of CRP on aptamer A1 or dummy ssDNA coated NCD does not occur or has no measurable effect on the heat-transfer over the coated surface. Real-time flow cell temperature  $T_2$  data and the calculated  $R_{Th}$  values illustrate similar effects for both aptamer A1 and dummy functionalized NCD upon CRP addition (Fig. 5.6). In Fig.5.6.A and 5.6.D, the signal is stable but a measurable effect on  $R_{Th}$  is only measured upon 100nM addition on the dummy ssDNA functionalized NCD (Fig.5.6.D). In the other cases, despite of buffer flushes, the measured  $T_2$  and calculated  $R_{Th}$  values show an irregular pattern. These measurements are performed over the same NCD sample. Nevertheless, the absolute value of  $R_{Th}$  (inset table Fig. 5.6) also seems to differ from measurement to measurement, implying that other variables such as extent of NCD carboxylation and ssDNA functionalization influence the  $R_{Th}$  value as well.

These obtained results indicate there is no clear  $R_{Th}$  signal response upon CRP addition on aptamer functionalized NCD and a high non-specific variation of  $R_{Th}$  change, regardless of NCD functionalization with dummy or aptamer ssDNA. Or there is no CRP binding at all, and the changes in calculated  $R_{Th}$  are caused by undesired variations of other parameters than ssDNA functionalization and CRP interaction. Or CRP binding takes place on NCD, but this event cannot be measured by heat-transfer resistance. In this case, binding on aptamer or dummy ssDNA cannot be distinguished. The variations in  $R_{Th}$  upon CRP incubation are not substantially higher than upon SELEX buffer injections, so whether CRP is binding specifically or not, this event cannot be measured by calculating heat-transfer resistance over the interface.

Van Grinsven *et al.* (2012) observes that the functionalization of a molecular brush of dsDNA does not change the heat-transfer resistance notably and explains this by calculating that 65 % of the interface is in fact not coated with dsDNA, but stays unaltered. The low surface coverage of the interface with CRP receptor due to steric hindrance during aptamer functionalization of the NCD can also explain why binding of CRP on the functionalized ssDNA cannot be measured, as the low binding level over the whole NCD surface does not have sufficient impact on the overall insulation properties over the whole NCD surface. In other words, even if CRP binds specifically on the functionalized ssDNA and locally affects the insulation layer on the interface, the gaps between the bound CRP complexes through which the applied heat can escape are too large to have a substantial effect on the overall  $R_{Th}$  signal change. Moreover, the binding between an aptamer and its ligand is a dynamic process and not of an on-off nature which makes drastic insulating effects upon CRP binding on the interface unlikely. In the 30 min incubation time, CRP binding is dynamic and dispersed over the interface, which makes drastic, uniform  $R_{Th}$  changes over the whole NCD surface unlikely in this stabilization period. Whereas denaturation of dsDNA can be seen as one blanket of ssDNA that is put on the NCD surface, the binding of CRP can be seen as 100 mini-blankets that are put on dedicated spots

on the NCD surface and randomly are displaced to other dedicated spots, with a much lower effect on the overall insulation properties over the NCD surface.

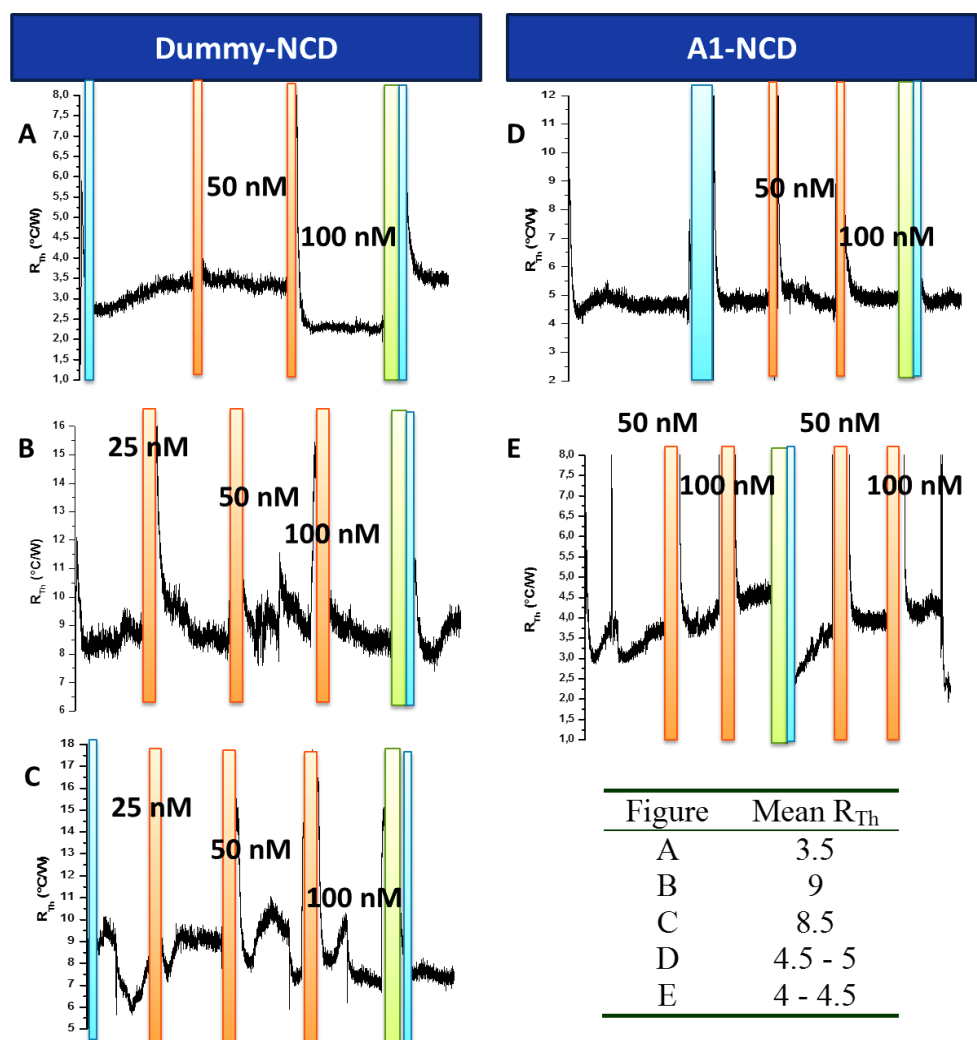


**Fig. 5.6.** Calculated real-time  $R_{Th}$  measurements over a dummy (A,B,C) or A1-functionalized (D, E) NCD sample. Bars indicate injections: blue = buffer; orange = CRP with indicated concentration; green = 50 mM NaOH followed by buffer. Inset table indicates mean base-line  $R_{Th}$  ( $^{\circ}\text{C}/\text{W}$ ) values (mean  $R_{Th}$  value of buffer injection before CRP injection).

### 5.3.2. Aptamer immobilization, target binding and detection of conformational changes at increasing temperature.

In an attempt to focus the  $R_{Th}$  measurement to an event that occurs on the whole interface at the same time, the denaturation of the assumed ssDNA-CRP complex is induced by increasing the copper box and flow cell temperature to the denaturation temperature of the functionalized ssDNA-CRP complexes and compared to the denaturation of the ssDNA oligonucleotides that were not incubated with CRP. By looking at the denaturation effect of assumed CRP complex *versus* uncomplexed ssDNA, analysis does not focus on the dynamic and dispersed CRP binding event but focusses on the more uniform denaturation effect of the ssDNA-CRP complex after CRP binding on the interface.

This analysis is performed on two different NCD samples, with both aptamer A1 and the dummy sequence functionalized.  $R_{Th}$  is compared in the stabilization periods and in the three temperature ramps from 30 °C to 80 °C for the functionalized ssDNA (ramp 1), after 100 nM CRP injection (ramp 2) and after SELEX buffer flush (ramp 3). As observed above, the incubation of 100 nM CRP does not have any effect on the  $R_{Th}$  values in the stabilization period (marked with \* in Fig. 5.7).

Fig. 5.7 shows the temperature data of these measurements (A) and the  $R_{Th}$  behavior during heating of the copper box ( $T_1$ ) and the flow cell ( $T_2$ ), which does not differentiate according the content of the flow cell. Whether A1 or dummy is incubated with SELEX binding buffer or 100 nM CRP in this buffer, the calculated  $R_{Th}$  has the same course, a reduction of the heat-transfer resistance as the copper box temperature rises. NCD sample A and B also display the same behavior of  $R_{Th}$  with sample A having a  $R_{Th}$  value of 7.5 °C/W (A) at 30 °C and sample B having a starting value of 7 °C/W (B). Sample B has a lower  $R_{Th}$  value when coated with the dummy sequence (C), but the course during heating is the same.

A minor jump in  $R_{Th}$  can be observed in ramp two of Fig. 5.7.B at a copper temperature of 52 °C, but Fig. D displays about the same jump in ramp 3, at a higher copper temperature. This means this is not a specific effect of CRP dissociating of aptamer A1 in the flow cell. Furthermore, Van Grinsven *et al.* observes a  $\Delta R_{Th}$  of  $1.3 - 1.5 \pm 0.2$  °C/W upon denaturation of the dsDNA to ssDNA or the formation of an insulating network on the interface. Here, the aptamer-CRP complex can be expected to denature during the heating to 80 °C, but this does not result in a large variation of the insulating properties at the interface which gradually decrease as the temperature increases, regardless of what is functionalized on the interface or what is incubated in the flow cell. This gradual decrease can be expected; the more heat applied on the copper box, the higher the heat transfer to the flow cell, and the lower the calculated heat-transfer resistance. From these results, it seems that aptamer A1 does not have any structural conformation change which affects the insulating properties, not

in SELEX binding buffer at 30°C and upon 100 nM CRP incubation and not upon thermal denaturation of any complex or secondary structure.

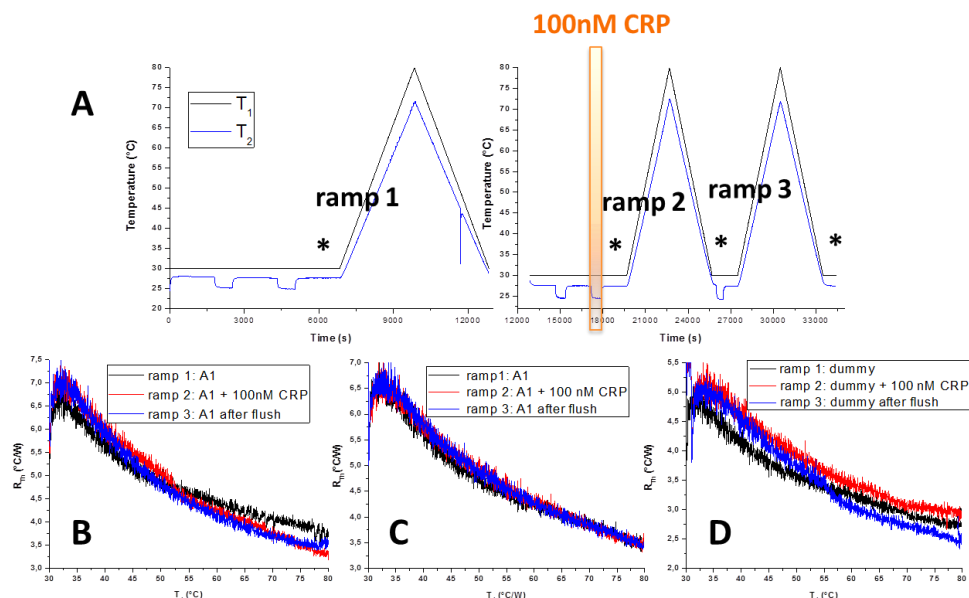


**Fig. 5.7. (A) Temperature data of the experiment. Orange bar indicates 100 nM CRP injections. R<sub>Th</sub> in stabilization period is equal in the three conditions (\*). (B) R<sub>Th</sub> course in three temperature ramps on NCD sample A, coated with A1. (C) R<sub>Th</sub> course in three temperature ramps on NCD sample B, coated with A1. (D) R<sub>Th</sub> course in three temperature ramps on NCD sample B, coated with dummy.**

The same heat-transfer assay is also performed with a well validated aptamer sequence and target, TBA2 and human  $\alpha$ -thrombin (Fig 5.8), to test whether binding interaction cannot be measured by heat transfer resistance measurement or that binding simply does not take place in the measurement flow cell. Immobilized aptamer functionality of TBA2 is tested by SPR analysis and indicates an aptamer kinetic affinity for thrombin of 2 nM, as estimated by a repeated multi-cycle kinetic analysis on TBA2-functionalized flow cells at 37 °C (Fig. 5.8.A). This experiment was repeated two times and indicated a  $K_d$  of 2-3 nM in both analyses.

The same analysis as illustrated above is performed with 3 mL injections of running buffer (50 mM Tris-HCl + 100 mM NaCl + 1 mM MgCl<sub>2</sub> pH 7.5) and 100 nM  $\alpha$ -thrombin in running buffer at 37 °C. Sample A and B both have a high initial heat-transfer resistance (9.5-10 and 9.5 °C/W, respectively) which gradually decreases to 8-8.5 and 8.7 °C/W respectively. Only on sample A (Fig 5.8.B) there is a difference between the first heating in running buffer and the two next denaturations, with a lower initial R<sub>Th</sub> at 45 °C and a higher R<sub>Th</sub> at 80 °C. As this is not repeated in the third heating to 80 °C or on sample B (Fig 5.8.C) this is not regarded as a positive effect. The gradual decrease in heat-

transfer resistance dependent on applied copper box temperature  $T_1$  is lower in this assay than in the previous one with CRP. This can be explained by the net upwards movement of heat. In this assay, the heat transfer set-up was turned over (as in Fig. 5.1.A), with the heated copper box on top and the upside down NCD sample and flow cell below. The lower decrease in heat-transfer resistance shows that the applied heat now is mainly transferred upwards into the air instead of over the interface into the flow cell. In this way, the change in heat-transfer resistance over the interface is less dependent of the applied temperature  $T_1$ , but more of what happens on the interface surface. Nevertheless, no effect on  $R_{Th}$  is observed in both assays on NCD sample A and B, although immobilized TBA2 functionality is proven by SPR analysis. This indicates that direct target binding on aptamer-functionalized NCD cannot be investigated by measuring heat-transfer upon complex denaturation and ssDNA conformational change.

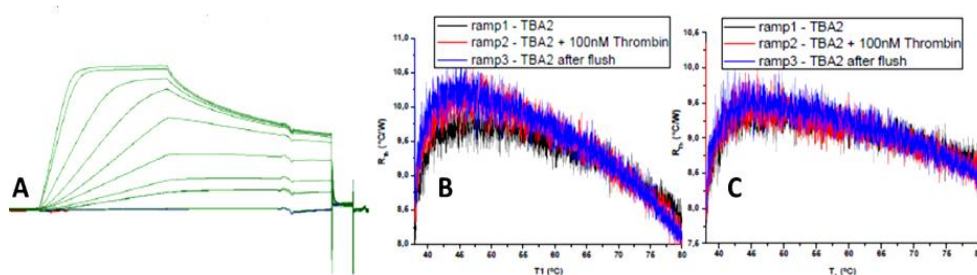


**Fig. 5.8. (A) SPR analysis of increasing thrombin concentrations over a TBA2-functionalized SA-chip. (B) Heat-transfer analysis of TBA2-functionalized NCD sample A. (C) Heat-transfer analysis of TBA2-functionalized NCD sample B.**

### 5.3.3. CRP capture and aptamer binding detection.

In analogy with chapter 4, where the selected aptamers demonstrated reduced aptamer functionality upon immobilization, the heat transfer assay is also tested in a design more similar to the SELEX design, with immobilized CRP on the NCD and the evaluation of the effect of aptamer binding on heat-transfer resistance over the solid-liquid interface.

CRP antibody immobilization and CRP capture capability on NCD is tested in- and outside the heat-transfer set-up, by performing a hsCRP ELISA sandwich assay outside the set-up, and with CRP incubation and flushing with the applied flow rate (250  $\mu$ L/min) inside the measurement flow cell. UV/Vis Spectrophotometer measurements indicate high absorbance values at 450 nm on both CRP incubated NCD samples, generated by specific HRP-conjugated hsCRP-antibody, whereas negative controls do not (Table 5.2). This proves that the CRP capturing mAB 4DG2 is efficiently immobilized on the NCD surface and that specific CRP detection is allowed after incubation in the heat-transfer set-up at the applied conditions. CRP binds after 3 mL injection of 100 nM CRP at a flow rate of 250

$\mu\text{L}/\text{min}$  and, more importantly, it is not removed by a SELEX binding buffer flush at the same flow rate.

**Table 5.2. Absorbance values of ELISA on 4DG2-functionalized NCD sample (1) with no CRP incubated; (2) with CRP incubation outside the flow cell set-up; (3) with CRP incubation inside the assay set-up.**

(1) OD <sub>450nm</sub> blank	(2) OD <sub>450nm</sub> outside set-up	(3) OD <sub>450nm</sub> in set-up
0.16	2.06	1.82

The aptamer functionality for covalently bound CRP is proven in Chapter 4 by SPR analysis on CRP-functionalized CM4 chips and here aptamer binding on mAB-captured CRP is shown as well. Antibody immobilization is optimized to reach binding levels of about 200 RU (Appendix Fig. 11). Fig 5.9 shows the 10 nM CRP injection and consecutive A1 (Fig. 5.9.A) or Dummy (Fig. 5.9.B) incubations and their respective binding responses (Table inset). A binding response of 57 RU is reached after 20 nM (+ 16 RU) and 100 nM (+ 41 RU) aptamer A1 incubation whereas incubated dummy sequences result in a net response loss of 10 RU (See inset table Fig. 5.9). As the 1 M NaCl flush has a larger effect on the A1 bound flow cell (-80 RU) than on the dummy bound flow cell (-26 RU), 1 M NaCl injection is expected to wash off loosely bound CRP from the mAB surface and to disrupt aptamer interaction on CRP. These results confirm that dummy sequence does not bind on immobilized CRP, whereas selected aptamer A1 does.



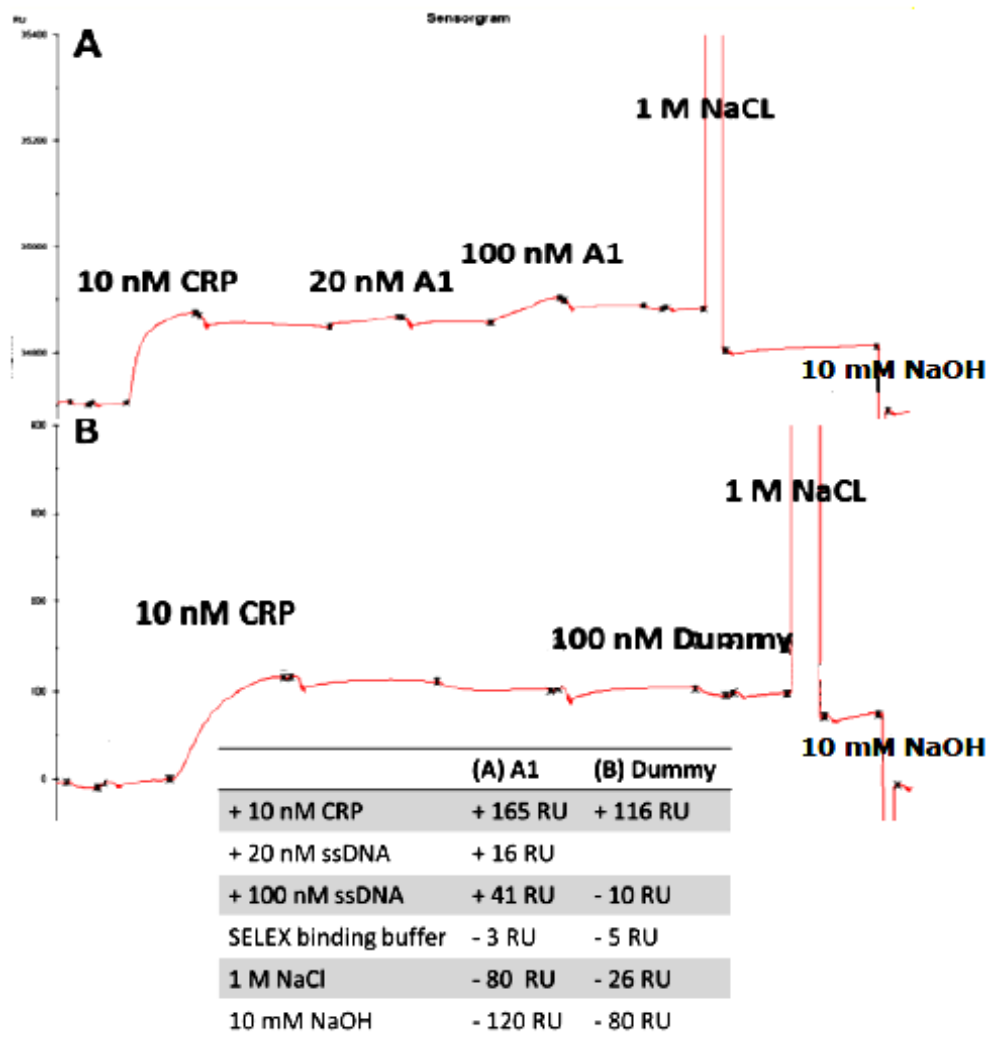


**Fig. 5.9. (A) CRP and A1 binding analysis on 4DG2. 20 nM A1 incubation results in 16 RU response and 100 nM A1 incubation results in 41 RU binding response (B) CRP and dummy binding analysis on 4DG2. Resulting binding responses are summarized in the inset table for both conditions. All injections are identified on the figure except SELEX binding buffer flushes.**

Preincubated mixes of CRP and aptamer A1 or dummy sequence are also evaluated for mAB 4DG2-functionalized chip binding (Fig. 5.10). Incubations and their responses of only CRP and CRP/dummy sequence complexes are comparable but preincubated CRP/aptamer A1 complexes show a clearly slower association to 4DG2 (green curve in Fig. 5.10) but a higher resulting binding response (+ 243 RU, inset table Fig. 5.10) which indicates a larger complex is bound on the flow cell surface. Moreover, the 1M NaCl flush results in the largest RU loss for the condition with preincubated complex of aptamer A1 and CRP

(122 RU vs. 60 RU), which can be contributed to the disruption of the aptamer A1/CRP complex, while CRP stays bound to the mAB 4DG2. In analogy with the experiment performed above, injection of 1 M NaCl washes off loosely bound CRP in all three conditions and disrupts the interaction of aptamer A1 and CRP for the preincubated aptamer A1 and CRP condition. A final flush with 10 mM NaOH removes bound CRP from the chip surface in all three conditions.

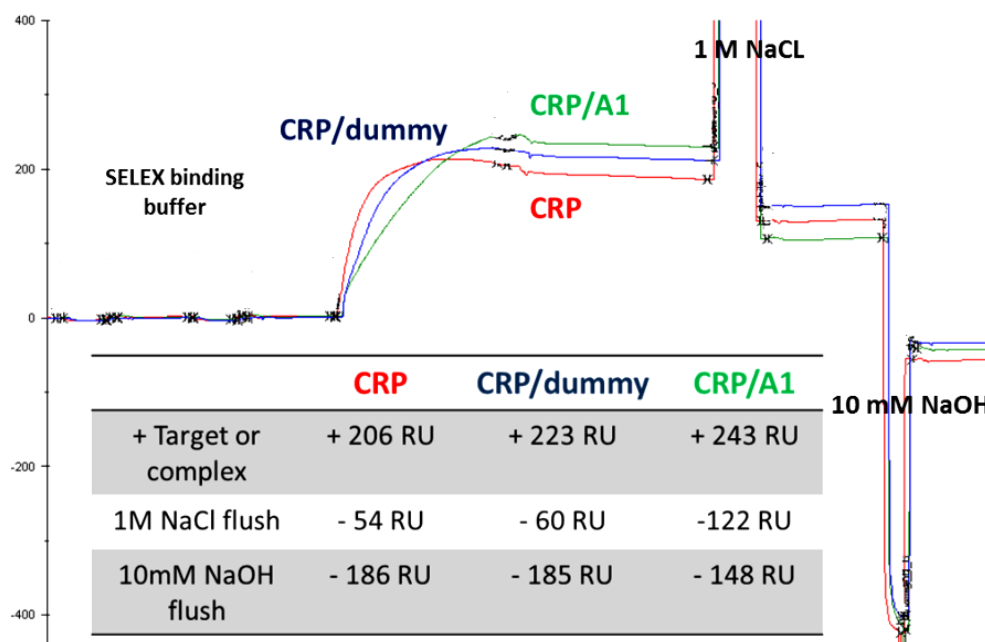


**Fig. 5.10. Reference subtracted binding responses (RU) of CRP and complex binding analysis on 4DG2-immobilized flow cell with binding responses (inset table) of indicated injections (Red curve = CRP; Blue curve = CRP + dummy; Green = CRP + aptamer A1).**

As CRP is a pentameric protein, it is not sure whether mAB and aptamer A1 bind on a different epitope, or bind on the same epitope of a different CRP monomer. Nevertheless, the heat-transfer assay design is validated for aptamer functionality, since SPR analysis reveals clear binding of the aptamer A1 to captured CRP and binding of the complex aptamer A1+CRP to the capturing mAB 4DG2.

When the same consecutive CRP and aptamer A1 binding assay is performed in the heat-transfer set-up, no noticeable signal is observed in the heat-transfer resistance response (Fig. 5.11). Even though binding of CRP to the antibody is proven by ELISA and SPR analysis, this binding event does not result in measurably changed insulation properties at the solid-liquid interface. Moreover, incubation of 100 nM aptamer A1 in binding buffer has no effect on the heat-transfer resistance which is stable at 11.2 °C/W throughout the consecutive

analyte and ligand incubations. Only after thermal denaturation and buffer flush a minimal increase in  $R_{Th}$  is observed which can be addressed to changes of the immobilized mAB 4DG2 after heating of the system.

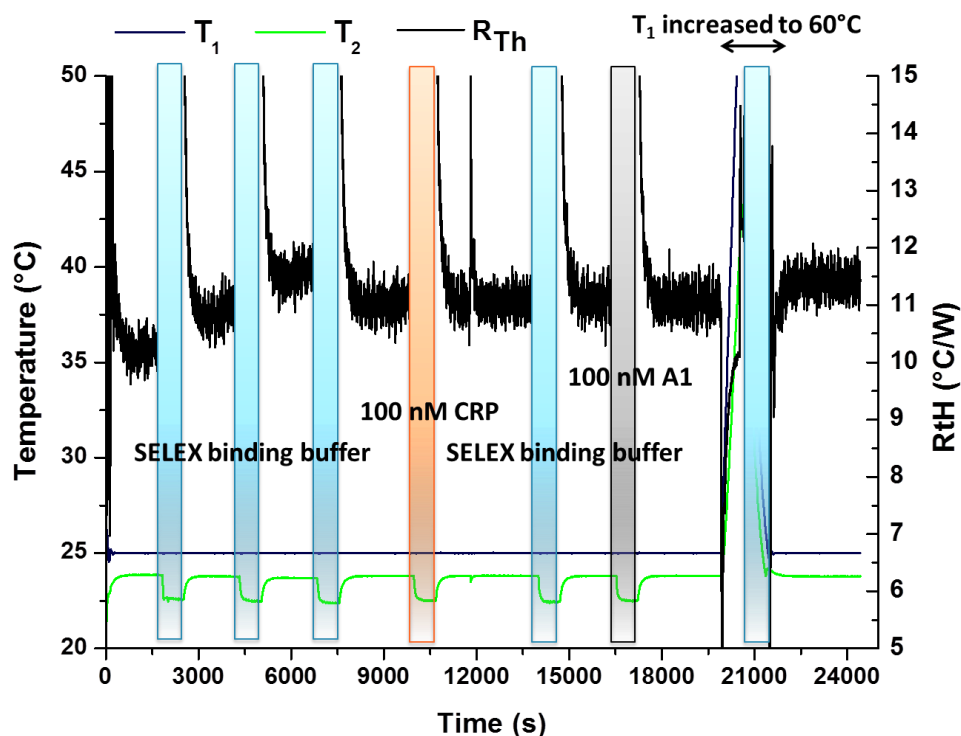


**Fig. 5.11. CRP and A1 binding assay in heat-transfer set-up: temperature data (left axis) and  $R_{Th}$  data (right axis). Bars indicate 3 mL injections at 250  $\mu$ L/min flow rate of SELEX binding buffer (blue), 100 nM CRP (orange) and 100 nM A1 (gray) in SELEX binding buffer.**

These findings indicate that heat-transfer measurements cannot detect binding of biomolecules onto the solid-liquid interface surface, not of CRP to the immobilized antibodies and not of ssDNA aptamer sequences onto the captured analyte CRP.

Van Grinsven *et al.* (2012) does not observe effects on the insulation properties at the interface upon immobilization of a 29 *bp*. dsDNA molecular brush which supports this statement. The heat-induced denaturation of this 29-mer however does result in a notable change in heat-transfer resistance over the interface by the formation of a 29-mer insulating ssDNA network right at the NCD surface. In other words, the formation of an insulating ssDNA layer of 29 *nt* on the NCD surface can be measured by heat transfer resistance over that surface, whereas binding of a 76 *nt* ssDNA insulating layer has no measureable effect on the insulating properties over the surface. This could be explained by the fact that the applied detecting aptamers do not bind as close to the solid-liquid interface

surface, as the applied dsDNA strands are covalently coupled directly to the NCD surface, whereas the 76 nt aptamer sequences bind on CRP, captured on the 4DG2 functionalized NCD surface. Because of the higher distance to the solid-liquid interface surface, the insulating effect of this aptamer ssDNA insulating layer is lower. Another explanation could be that the ssDNA binding and network density over the interface is much lower compared to the coupling density of the covalently coupled dsDNA, due to the reduced number of binding sites on a large protein like CRP, steric hindrance or secondary structure formation of the aptamer sequences. Because of the lower density of the applied aptamer insulating layer, the insulating effect is lower and cannot be detected by measuring the heat transfer resistance in this set-up.

To increase the ssDNA network density on captured CRP, extended aptamer sequences are tested for this binding assay. However, one should keep in mind that these aptamer modifications should not alter the CRP binding properties. Different sequence extensions are checked for maintaining the predicted aptamer A1 secondary structure in mfold, which results in the selection of a 3'-40T-extended aptamer for SPR binding analysis since extension of the 5'-terminus has on larger effect on the structure confirmation (Appendix Fig. 12), changing it to a halter-like structure. Unchanged aptamer functionality is proven by performing similar SPR analyses as described above, comparing the binding responses to captured CRP of A1 and 3'-40T-A1 (Fig. 5.12.A) and the binding responses of preincubated CRP/A1 and CRP/3'-40T-A1 (Fig. 5.12.B). Whereas less CRP (140 RU vs. 165 RU) is captured on the flow cell, extended aptamer association results in higher binding responses (77 RU vs. 57 RU), which is completely washed off by 1 M NaCl regeneration. Association of preincubated CRP/3'-40T-A1 is slower but results in an increased binding response compared to preincubated CRP/A1 mixes (258 RU vs. 180 RU) and in an increased loss of binding when disrupting the CRP-A1 interaction by flushing 1 M NaCl (-110 RU vs. -59 RU). These results confirm that 3'-40T extended A1 can bind to captured CRP, which is important for validation of the heat-transfer experiment with extended aptamer sequences.

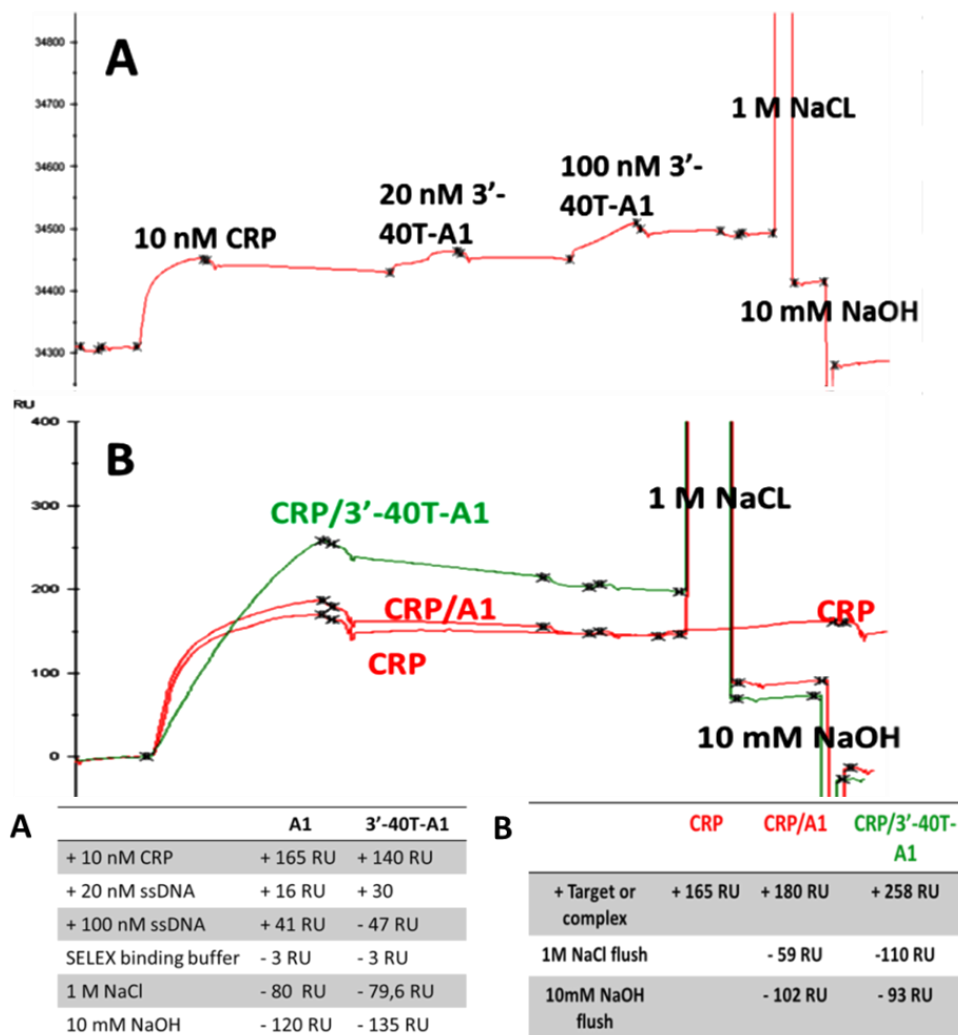


**Fig. 5.12. (A) SPR binding analysis of 3'-40T-A1 on captured CRP. Inset table below compares binding responses of the unmodified aptamer A1 and the 3'-extended A1. (B) Preincubated CRP/ssDNA complex binding analysis with binding responses of indicated injections for CRP/A1 and CRP/3'-40T-A1 in inset table below.**

Since the dissociation of CRP/3'-40T-A1 is faster than for the CRP/A1 complex (Fig. 5.12.B), the injection flow rates are lowered to 100  $\mu\text{L}/\text{min}$  in the heat-transfer assay to reduce the dissociation of the complex on the liquid-solid interface during buffer pump injections. Despite the proven binding capabilities of extended aptamer to captured CRP, there is no detected binding signal observed in the heat-transfer resistance upon binding of CRP to immobilized 4DG2 and 3'-40T-A1 to CRP (Fig. 5.13). Moreover, after thermally induced

denaturation and flow cell wash the  $R_{Th}$  value is still at the level of 13.9 °C/W. This measurement confirms the findings of previous measurements with non-extended A1 that both CRP and ssDNA binding on the interface surface does not notably alter the measured heat-transfer resistance in this set-up. The extension of the applied ssDNA sequence with 40 nt, which increases the size of A1 with 150%, has no effect on the insulation properties of the aptamer layer on the surface.

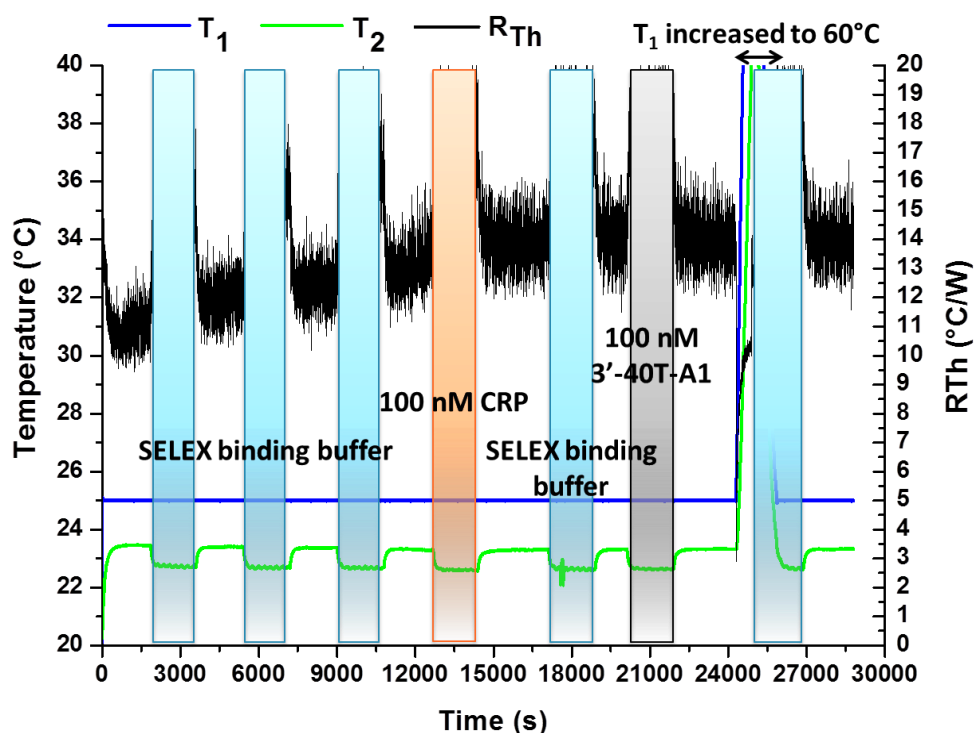


**Fig. 5.13. CRP and 3'-40T-A1 binding assay in heat-transfer set-up: temperature data (left axis) and  $R_{Th}$  data (right axis). Bars indicate 3 mL injections at 100  $\mu$ L/min flow rate of SELEX binding buffer (blue), 100 nM CRP, (orange) and 100 nM 3'-40T-A1 (gray).**

The heat-transfer resistance assay is proven to be a valuable label-free read-out platform for the detection of SNPs in the form of a DNA sensor (van Grinsven *et al.*, 2012) and for the detection of L-nicotine, histamine, and serotonin using molecularly imprinted polymers (MIPs) as biomimetic receptors (Peeters *et al.*, 2013). For the former, the change in heat-transfer resistance in response to dsDNA denaturation is analyzed in function of hybridization surface coverage (Bers *et al.*, 2013). This shows that the measurable change in  $R_{Th}$  is dependent of the amount of hybridized dsDNA. Lower dsDNA concentrations (and hence higher ssDNA) result in less pronounced changes of heat-transfer resistance. Although ssDNA and certainly aptamers are assumed to exhibit conformational changes as well, they do not result in measurable changes of  $R_{Th}$ . In the latter,

heat-transfer resistance over the solid-liquid interface is increased with  $\approx 0.4 - 0.9$  °C/W which can be explained by the "poreblocking model." MIPs contain nanopores which can specifically rebind their target based on its size and functionality. Upon rebinding, the heat flux through one cavity is strongly reduced due to the presence of the template. The more L-nicotine is bound, the more cavities exhibit this behavior leading to an ultimately higher effect size. The two validated heat-transfer assays have in common that the heat-transfer resistance is altered upon a change in the geometrical configuration of the dsDNA or receptor, directly bound to the interface surface. In the assay designs that are evaluated in this dissertation, the binding of analyte to the immobilized aptamer or *vice versa* does not result in sufficient conformational change close to the interface surface to significantly affect the analyzed heat-transfer properties over that interface. Forming an extra insulating layer of ssDNA aptamers over the target-bound interface does not result in detectable changes due to low surface coverage, caused by low binding epitope availability and high steric hindrance. Expansion of the applied insulation layer by increasing the length of the applied ssDNA or by minimization of the interface surface can increase the effect of ssDNA layer formation on the heat-transfer properties but is to be further investigated. Bers *et al.* (2013) applied a compartmentalized flow cell which can also be tested for these purposes.

Adaptation of the aptamer assay design to the validated dsDNA denaturation design of van Grinsven *et al.* (2012) in the form of target induced strand displacement is an interesting option to get this read-out system operational for aptamer applications. Strand displacement assays in many forms are extensively studied for electrochemical read-out systems and charge-based ultrasensitive detection of biomolecules. The following examples all have in common that the starting point of the assay is a dsDNA strand tethered to the read-out platform which consists of an immobilized ssDNA probe and hybridized aptamer or *vice versa*.

- Target induced displacement of a  $\text{Ru}(\text{bpy})_3^{2+}$  doped ssDNA probe measured by electrogenerated chemiluminescence (ECL) (Wang *et al.*, 2007)
- Target induced displacement of complementary aptamer strand measured by Faradic Impedance Spectroscopy (Peng *et al.*, 2009). A partial complementary DNA (pcDNA)-lysozyme binding aptamer (LBA) duplex is tethered on the surface of a gold electrode. The introduction of target lysozyme induces the displacement of the LBA from the pcDNA-LBA duplex on the electrode into the solution, decreasing the electron transfer resistance of the aptasensor.
- Target induced displacement of a redox-modified aptamer from the aptamer - capture DNA duplex bound on an electrode, measured by differential pulse voltammetry (DPV) (Yoshizumi *et al.*, 2008).

- Universal neutralizer displacement assay measured by differential pulse voltammetry (DPV) (Das *et al.*, 2012): Immobilized aptamer probe is hybridized to a neutralizer strand. When analyte binding occurs the neutralizer is displaced, which results in a dramatic change in the surface charge for all types of analytes.

As the set-up in this chapter is able to detect dsDNA thermal denaturation and allows measuring the denaturation event electrochemically by measuring impedance over the interface at the same time, target induced strand displacement measurements are a readily available strategy to investigate.

#### **5.4. Conclusions and future recommendations**

The results in this chapter clearly indicate that the application of aptamers as target capturing or detection agent in the heat-transfer set-up cannot be used as it is performed in this dissertation. Binding of target (CRP and  $\alpha$ -thrombin) to the immobilized aptamer or binding of aptamer to the immobilized target does not result in sufficient conformational change on the interface surface to significantly affect the heat-transfer properties over that interface. Different explanations for having no effect on the heat-transfer resistance at the solid-liquid interface are selectively eliminated by changing the assay design or by performing control experiments on other read-out platforms (ELISA and SPR) or with other analytes (TBA2 for  $\alpha$ -thrombin).

Lost CRP aptamer functionality caused by NCD-immobilization is addressed by exchanging the applied aptamer and target and by exchanging the assay design to the one that has proven selected CRP aptamer specificity and selectivity. Moreover, aptamer functionality in the applied assay design was investigated by SPR kinetic analysis of immobilized TBA2 and SPR binding analysis of selected aptamer A1 in the captured CRP approach.

Focusing the heat-transfer measurement on complex denaturation instead of complex formation does not result in a significant change of the heat-transfer resistance, as is observed for dsDNA denaturation in van Grinsven *et al.* (2012). Comparison of the  $R_{Th}$  value during or before and after complex denaturation indicates no detectable denaturation event of aptamer structure or aptamer-target complex. Extension of the detecting aptamer sequence to enlarge the network formation and hence insulating properties upon aptamer binding on captured target has no measured effect as well, but can be further explored. Mfold analysis indicates a 3'-80T and -120T extension for A1 is feasible in terms of secondary structure formation, although target functionality still needs to be tested by *e.g.* SPR analysis.

Lowering the surface area of the solid-liquid interface in combination with binding of extended aptamer sequences will increase the effect of target recognition on the insulating properties over that interface and hence will



increase detection ability of the binding or denaturation event. Alternatively, a measurable heat transfer resistance signal upon target binding can be reached by formation of a dense insulating layer of oligonucleotides using the specifically bound aptamer sequences as scaffold for nanostructure formation. Further extension of the target binding aptamer sequences on the target-functionalized interface can be reached by specific linkage of multidimensional DNA nanostructures to the target bound aptamers that are extended with DNA probes for specific recognition. This nanostructure assembly occurs through the specific and highly controlled base-pairing of complementary bases. Unique geometries can be formed when complementary single-stranded DNA molecules anneal together to form double-stranded DNA molecules by design (Zadegan and Norton, 2012). This complementary binding only happens if the strands are complementary over a sufficient number of bases, the temperature is appropriate and the required ions are present at the optimum concentration. Construction of large one dimensional (1D) and two dimensional (2D) DNA arrays have been demonstrated by using DNA probes with sticky ends and the application of DNA ligases and DNA elongases (Seeman, 2007). This approach can be used to connect the ends of bound aptamers on the solid-liquid interface that are situated closely together, hereby closing the gaps between them and increasing the insulating properties over the interface. Moreover, by the aptamer specific hybridization of so-called DNA building blocks or DNA tiles, self-assembly of complex insulating 2D and 3D DNA nanostructures can be achieved (Zadegan and Norton, 2012). In extension, the application of highly controlled folding of a large hybridized ssDNA strand (so-called 2D- and 3D-DNA origami, Endo *et al.*, 2013) on the solid-liquid interface into a dense nanostructure of DNA is an interesting option to increase the insulating properties over that interface.

Great potential of aptamer application in the heat-transfer set-up lies within the target induced strand displacement of one of the ssDNA strands that forms a dsDNA brush on the NCD surface. Whether the aptamer is displaced by means of target injection under flow conditions or the complementary probe is displaced by binding of the target, this target induced denaturation should be detectable by means of heat-transfer measurement. Testing this assay design with the well validated aptamer sequences and (partially) complementary DNA probes from electrochemical assays can result in successful application of aptamers in this set-up. Moreover, the use of the built-in impedance analyzer as a validated control for target binding, dsDNA denaturation or strand displacement would enable to use the full potential of this read-out set-up.



# 6

## General discussion, conclusions and perspectives

*In this concluding chapter, the results of this dissertation are summarized and evaluated. Suggestions are made for further research and for further improvements of aptamer selection procedures, validation assays and read-out applications.*

### 6.1. Synopsis

The outline of this dissertation has more or less a linear work-flow, as was illustrated in Fig. 1.14. In the first introductory **chapter 1**, the definition and composition of biosensors and the application of aptamers in these measuring devices is elaborated. An insight in the various aptamer selection procedures and the myriad of bio-assays and read-out applications using aptamers is illustrated. Concluding this chapter, the performance of so called aptasensors is discussed.

**Chapters 2** and **3** describe the knowledge that is gained of the start of any aptamer application for any target: the specific aptamer selection procedure. In this case, CRP was chosen as the selection target for selective ssDNA oligonucleotide binders. This was not chosen with a specific diagnostic test or application in mind, although commercial partners as NXP Semiconductors (Eindhoven, NL) and apDia bvba (Turnhout, BE) are interested in developing such tests. Nevertheless, being an acute-phase protein, examined in every standard blood test and being proposed as predictive marker for cardiovascular disease, highly sensitive diagnostic CRP tests have a high commercial interest. Chapters 2 and 3 have clearly contributed to the first aim of this dissertation: a better understanding of the selection procedure. By the detailed optimization of a SELEX procedure for CRP aptamers, general pitfalls are identified and general solutions to these problems are proposed. By providing a new method for SELEX progress monitoring that can be incorporated in any SELEX procedure without much extra labeling or analysis procedures, chapter three is a step forward in informed decision making during the SELEX procedure and increased control on SELEX dynamics.

In **Chapter 2**, different aspects of the SELEX selection procedure were explored in detail to obtain successful aptamer candidates selection for the applied target CRP. As the selection design was mainly tailored for CRP aptamer selection, conclusions of this chapter can be divided in CRP-specific findings and more general findings about the SELEX procedure.

As there is a general concern to introduce selection bias due to library amplification and non-specific binders, the optimizations that were performed in this respect may be applied in every SELEX procedure. An increased number of negative selections were introduced to cope with the observed high non-specific binding of ssDNA. Performing an initial series of negative selections may be applied for every random library to purge these selection pools from non-specific binding oligonucleotides before they are amplified. As negative selections outnumber the positive ones, the addition of non-amplifiable ssDNA can also be considered to block ssDNA binding places in the set-up and to minimize the risk of losing target specific oligonucleotides. The changed timing of amplification and moreover, the reduced cycle number results in a reduction of amplification by PCR to minimize confounding amplification effects and by-product formation. The post-PCR size purification is proposed as a crucial purification step to purge the selection pool from unwanted by-products like primer-dimers and product-dimers and to guarantee an unbiased selection procedure.

The CRP-specific finding that CRP immobilization on magnetic bead results in bead aggregation illustrates that all conditions of the selection design need to be closely evaluated. Preferably, this needs to be done by a set of different assays that have different signal generation or signal amplification systems, such as flow cytometry and ELISA tests, providing information of different aspects of the applied selection conditions and set-ups. Monitoring of the selection procedure steps and applied conditions before and during the SELEX procedure is of crucial importance for a succeeding selection procedure. In this respect, real-time SPR analysis of applied target immobilization and selection conditions, such as buffer pH and ionic strength can be a highly informative tool to tune and optimize the selection procedure.

**Chapter 3** explores a new method for monitoring the SELEX procedure and progress in terms of ssDNA selection pool diversity and enrichment by means of performing a remelting curve analysis after every selection round. This rMCA method is proven reproducible and irrespective of target properties and SELEX design. Next to the CRP SELEX, this method is applied and studied for two other SELEX designs (bead based SELEX and CE-SELEX) on two other targets ( *$\beta$ -estradiol* and a peptide, respectively). rMCA is shown to be a universal and useful tool for monitoring the effect of different SELEX conditions on the ssDNA pool and for enrichment monitoring during the selection procedure, in order to decide when to stop selection and start sequencing. In this way, chapter three has clearly contributed to the first aim of this dissertation: a better understanding and increased control on the selection procedure.

The applied SELEX procedure on CRP-coated well plates in combination with rMCA analysis resulted in selective enrichment of different ssDNA oligonucleotides. Dividing the selection pool in four pools according to elution resistance after the 10<sup>th</sup> SELEX cycle resulted in four different selected aptamer candidates.

In **Chapter 4**, the selected aptamers were carefully evaluated for CRP binding selectivity and specificity by means of different binding assays on different read-out platforms. The findings of this chapter contributed to the second aim of this dissertation, validation of the selected aptamers and their functionalities, as detailed binding analyses have investigated the binding behavior of labeled or immobilized aptamers and the affinities of original aptamer sequences as well. Application of the unmodified aptamers as they are selected resulted in selective and specific CRP interaction. Any deviation of these binding conditions (aptamer labeling or immobilization, changed buffer properties) causes the loss of aptamer functionality which seriously decreases possible binding designs for aptamer application. The quantitative PCR assay and SPR analysis have the best results for CRP binding specificity and selectivity because they allow the application of unlabeled aptamer sequences in solution, similar as they are selected. SPR analysis showed that the four selected aptamer candidates in Chapter two display high (nM) affinities for CRP. However, these aptamers demand the right binding conditions or their CRP binding abilities drop to the level of random ssDNA of the same length.

**Chapter 5** explores the feasibility of selected aptamer application as target capturing or detection agent in a new label-free read-out system, measuring the change in heat-transfer resistance over a functionalized solid-liquid interface. This application was the third aim of this dissertation and has been addressed in detail but not been fulfilled as the direct binding of selected aptamers or CRP did not result in successful application of the selected aptamers. The tested direct binding assays were referenced by application of a SPR validated aptamer TBA2 and  $\alpha$ -thrombin or successful SPR simulation of CRP capturing and aptamer association. In the assay designs that are evaluated in this dissertation, the binding of analyte to the immobilized aptamer or vice versa does not result in sufficient conformational change close to the interface surface to significantly affect the analyzed heat-transfer properties. Adaptation of the aptamer assay design in the form of target induced strand displacement is an interesting option to get this read-out system operational for aptamer applications.

## **6.2. Future considerations and perspectives**

Aptamer selection and binding strategies are carefully evaluated in this dissertation and important lessons can be learnt from the difficulties that were faced during this research. As stated in the introduction of this thesis, despite

the advantages of aptasensors and the potential of aptasensing technologies, their impact up-to-date is very limited (Baird, 2010). Since their discovery, many have predicted that aptamers represented a technology with the potential to rival the antibody revolution in molecular diagnostic testing (Jayasena, 1999; Carlson, 2007). Years have passed, and while performance limiting patents have expired and many aptamers have been reported in academic journals, the aptamer-based diagnostic revolution has not materialized (Baird, 2010). The problems that are discussed in this dissertation are a good illustration of some of the flaws of aptamer research. At all stages from aptamer discovery to aptamer application in a diagnostic assay, there is room for improvement. Recent advances in aptamer technology contribute to increase performance of these bioreceptors that are finally coming of age (Bunka & Stockley, 2006).

Optimization of a SELEX procedure for CRP specific ssDNA aptamers has shown that the aptamer identification process is still highly target specific and not routine. The reliance on polymerase chain reaction (PCR) based amplification of very small concentrations of short target DNA molecules can easily lead to artifacts. In addition, without effective counter measures, the immobilization of the analyte onto resin for selection purposes can easily lead to the identification of aptamers for components of the resin, rather than the analyte (Mann *et al.*, 2005). Published aptamers often display non-specific interactions with other compounds, when not carefully tested and corrected for. As the selection method is laborious and prone to induced bias, efforts are made to change the separation approach for higher efficiencies or to perform a more smart selection, ideally without the need for amplification (Berezovski *et al.*, 2006). The following part clearly illustrates that many of the limitations that slowed the growth of SELEX are beginning to be addressed in terms of affinity, stability and throughput (Bowser, 2005).

Methods of CE-SELEX display the highest separation efficiencies in solution, which severely decreases the risk for non-specific interactions (Berezovski *et al.*, 2005) and allows successful aptamer selection in only a few rounds of selection (Mensdonsa & Bowser, 2004). Moreover, Drabovich *et al.* (2006) uses kinetic capillary electrophoresis to develop 'Smart' aptamers with predefined binding parameters as  $K_D$  and  $k_{off}$ . These methodologies provide a robust tool for the fast generation of ligands that exhibit desired binding parameters.

More efforts have been made to change the SELEX procedure to a fast, highly efficient procedure that can be performed in a few selection rounds using a single microbead (Tok & Fisher, 2008) to only one single selection step (Fan *et al.*, 2008; Lauridsen *et al.*, 2012).

A different approach is changing the sequencing analysis that is used to examine the resulting DNA pool after target incubation and elution to high-throughput screening of the sequence space. Schütze *et al.* (2011) shows the high affinity aptamers can be identified by copy number enrichment in the first selection rounds. Based on these results, a new selection scheme is suggested that avoids

a high number of iterative selection rounds while reducing time, PCR bias, and artifacts. Hoon *et al.* (2011) describes a method for selecting high-affinity DNA aptamers based on a single round of selection followed by high-throughput sequencing and bioinformatic analysis. Aptamer sequences are identified by selecting variable k-mer length sequences that are enriched in the sequenced library in a method termed Aptamer Selection by K-mer Analysis of Sequences (ASKAS).

Performing less selection rounds in a more automated way can significantly decrease selection time, non-specific binding and manually induced bias which contributes to a more controlled and routine aptamer identification process. Efforts have been made to modify robotic workstations to perform the entire procedure, including selection, purification and amplification (Cox & Ellington, 2001; Eulberg *et al.*, 2005). Wochner *et al.* (2007) have developed a semi-automatic selection design employing a robotic workstation for magnetic particle handling. At SomaLogic® (Boulder, CO, USA) a fully automated assay is implemented for the selection of high affinity aptamers against new proteomic targets. This set-up is successfully used as a multiplexed proteomic discovery platform (Keeney *et al.*, 2009; Gold *et al.*, 2010)

In order to enhance aptamer stability and affinity, modified aptamer sequences are used in an expanding number of applications. In the past, modifications aimed to increase aptamer stability and enhance nuclease resistance and were applied in so-called post-SELEX modifications (Eaton, 1997). Nowadays, selections are performed with chemically modified nucleotides already present in the selection library, as newly identified polymerases allow incorporation in the selection procedure (Keefe & Cload, 2008; Vaught *et al.* 2010). The extended functionality of the libraries allows the generation of new aptamers with exceptional affinities that recognize a whole new range of epitopes, broadening the repertoire of aptamers to whole new levels (Gold *et al.*, 2010).

The selected aptamer sequences in this dissertation show high dependency of the right conditions, which seriously limits future application possibilities. Due to the highly specific nature of the aptamer performance, unique for each aptamer structure under very specific binding conditions, the analysis and documentation of (new) aptamer sequences and assays needs to be precise and accurate. Cho *et al.* (2009) have suggested standards for aptamer research and reporting as experiments should be reported in sufficient detail that other scientists can potentially reproduce the results themselves. If an aptamer sequence or reference (Rodriguez *et al.*, 2005) is not reported, then the experiment cannot be independently repeated. Aptamers are typically selected in a single buffer, and their performance may be very specific for that buffer. Nucleic acid structures are particularly sensitive to both the type and the amount of monovalent and divalent cations. By leaving out or changing the concentration of a given ion during the assay development, a researcher may greatly

compromise aptamer function. Any deviation from the original selection buffer requires a re-assay of function. Since many other variables (buffer conditions, temperature, purification method and conformational state) affect the function of an aptamer, all of these variables need to be reported. Cho *et al.* (2006) shows how aptamers can be adapted to operate under standard buffer conditions by screening a number of common buffer conditions with four sets of aptamer-protein complexes selected under very different buffer conditions in order to find a universal buffer where the selected aptamers retain their affinity and selectivity.

A particular example of aptamer selectivity was encountered with the aptamer TBA2 for human  $\alpha$ -thrombin (Tasset *et al.*, 1997). SPR analysis of immobilized TBA2 on a Biacore SA-chip (Chapter 5) only indicated a binding response when thrombin was applied that was from the same company as used in the cited publication. Injection of human  $\alpha$ -thrombin ordered from another company (Sigma) did not result in any binding. Moreover, the TBA2 functionality was highly temperature dependent, as a temperature of 25°C instead of 37°C did not result in any binding.

The selected aptamers in this dissertation were prone to loss of functionality by immobilization and labeling with detection or capturing agents, which is also reported in literature (Rowe *et al.*, 2009). The increased development of label-free assays and read-out systems addressed this problem as strategies are developed for sensing without the need of labeling or modification of the aptamer or any compound of the assay to generate the binding signal.

Moreover, aptamers have specific characteristics which make them particularly interesting for label-free applications. The inherent net negative charge of ssDNA strands make aptamers very attractive for electrochemical sensing, as illustrated by the increased development of analytical electrochemical applications (Cho *et al.*, 2009). If this characteristic is combined with the significant conformational changes upon binding to their cognate ligands (Hermann & Patel, 2000), structure-switching sensor designs are developed as for optical read-out systems, without the need for labeling (Patolsky *et al.*, 2006; Drummond *et al.*, 2008). In these assays, the aptamer probe is tethered to an electrode and the charge of the sensor is determined by the probe. After analyte binding, the state of the charge is changed by the analyte charge and hence the signal is analyte dependent (Das *et al.*, 2012).

As the aptamers are ssDNA strands, they are easily incorporated in target-induced displacement assays. Aptamers or their complementary sequences are employed as anchors. After incubation with targets, the complementary strands or the formed target-aptamer complexes will be liberated into the solution (respectively), which leads to the changes of detectable signals (Han *et al.*, 2010). This approach is used in a faradic impedance spectroscopy (FIS) for lysozyme assay as the release of the aptamer due to the formation of target-aptamer complex decreases the interfacial electron transfer resistance, which was utilized to quantify the concentration of lysozyme (Peng *et al.*, 2009). Label-



free electrogenerated chemiluminescence (ECL) measurement of thrombin is achieved due to displacement of a doped complementary probe (Wang *et al.*, 2007). Moreover, Das *et al.* (2012) proposed Neutralizer Displacement Assays (NDA) that allows charge-based label-free sensing irrespective of the analyte charge. In this assay, the aptamer probe is joined by a (mismatched) neutralizer strand that neutralizes the charge. As target-induced strand displacement of the neutralizer occurs, in dramatic change in surface charge is detected for all types of analytes with high sensitivities, irrespective of the nature, the charge or the size of the analyte.

Aptamer research has made great leaps forward during the performance of this dissertation. In terms of SELEX efficiency and output, automated SELEX procedures and instruments are emerging. In terms of affinities for new targets, aptamer sequence space has expanded massively with the development of highly diverse, chemically modified random libraries. In terms of read-out technologies, label-free detection systems allow ultra-sensitive detection, irrespective of the analyte characteristics and without the need for aptamer or target modifications. From these advances, it is clear that aptamers are finally being applied at their full potential. When reported and documented well, aptamers can still fulfill the high expectations of being revolutionary biosensor receptors.



## References

- Abe K. & Ikebukuro K. (2011). Aptamer Sensors Combined with Enzymes for Highly Sensitive Detection, In: *Biosensors - Emerging Materials and Applications*. (Ed. Prof. Pier Andrea Serra) InTech Europe, Croatia. ISBN: 978-953-307-328-6, DOI: 10.5772/19708.
- Adler M., Wacker R. & Niemeyer C.M. (2003) A real-time immuno-PCR assay for routine ultrasensitive quantification of proteins. *Biochem. Biophys. Res. Commun.* **308**: 240-250.
- Affymetrix Inc. (2011) USB<sup>®</sup> ExoSAP-IT<sup>®</sup> PCR Product Cleanup Protocol. [http://media.affymetrix.com/support/technical/usb/brief\\_proto/78200B.pdf](http://media.affymetrix.com/support/technical/usb/brief_proto/78200B.pdf) (Accessed 04/09/2013).
- AptaGen (2013) Product Page DNA aptamer for C-reactive protein. [http://www.aptagen.com/customize\\_product.aspx?id=353](http://www.aptagen.com/customize_product.aspx?id=353) (Accessed 06/09/2013).
- Arun Kumar R.N. & Arrowsmith J.E. (2006) Point of care testing. *Surgery (Oxford)* **24**(10): 341.
- Avci-Adali M., Paul A., Wilhelm N, Ziemer G. & Wendel H.P. (2010) Upgrading SELEX Technology by Using *Lambda* Exonuclease Digestion for Single-Stranded DNA Generation. *Molecules* **15**: 1-11.
- Avci-Adali M., Wilhelm N., Perle N., Stoll H., Schlensak C. & Wendel H.P. (2013) Absolute Quantification of Cell-Bound DNA Aptamers During SELEX. *Nucleic Acid Ther.* **23**(2): 125-130.
- Bairakova I.V., Kazachek I.V., Gruzdeva O.V., Sergeeva T.I., Grigor'ev A.M. & Ivanov S.V. (2013) The dynamics of C-reactive protein in the process of coronary artery bypass grafting in patients with ischemic heart disease. *Klin. Lab. Diagn.* **3**: 3-6.
- Baird G. S. (2010) Where Are All the Aptamers? *Am. J. Clin. Pathol.* **134**: 529-531.
- Balamurugan S., Obubuafo A., Soper S.A., McCarley R.L. & Spivak D.A. (2006) Designing highly specific biosensing surfaces using aptamer monolayers on gold. *Langmuir* **22**(14): 6446-6453.
- Balamurugan S., Obubuafo A., Soper S.A. & Spivak D.A. (2008) Surface immobilization methods for aptamer diagnostic applications. *Anal. Bioanal. Chem.* **390**: 1009-1021.
- Baldrich E., Restrepo A. & O'Sullivan C.K. (2004) Aptasensor development: Elucidation of critical parameters for optimal aptamer performance. *Anal.Chem.* **76**: 7053-7063.
- Baum P.D. & McCune J.M. (2006) Direct measurement of T-cell receptor repertoire diversity with AmpliCot. *Nat. Methods* **3**: 895-901.
- Berezovski M., Drabovich A., Krylova S.M., Musheev M., Okhonin V., Petrov A. & Krylov, S.N. (2005) Nonequilibrium Capillary Electrophoresis of Equilibrium Mixtures: A universal tool for Development of Aptamers. *J. Am. Chem. Soc.* **127**: 3165-3171.
- Berezovski M.V., Lechmann M., Musheev M.U., Mak T.W. & Krylov S.N. (2008) Aptamer-facilitated biomarker discovery (AptaBiD). *J. Am. Chem. Soc.* **130**(28): 9137-9143.
- Berezovski M.V., Musheev M.U., Drabovich A.P., Jitkova J.V. & Krylov S.N. (2006) Non-SELEX: selection of aptamers without intermediate amplification of candidate oligonucleotides. *Nat. Prot.* **1**: 1359 -1369.
- Bers K., van Grinsven B., Vandenryt T., Murib M., Janssen W., Geerets G., Ameloot M., Haenen K., Michiels L., De Ceuninck W. & Wagner P. (2013) Implementing heat transfer resistivity as a key element in a nanocrystalline diamond based single nucleotide polymorphism detection array. *Diam. Relat. Mater.* **38**: 45-51.
- Biacore (1997) BIAevaluation 3.0 Software Handbook. Biacore AB (Uppsala, Sweden)

- Biacore (2001) *An introduction to Biacore Technology* Edition June 2001 (Version 1) (Accessed 29-08-2013) <http://www.biotech.iastate.edu/facilities/protein/seminars/BIACore/TechnologyNotes/TechnologyBrochure.pdf>
- Biacore (2003) *Sensor Surface Handbook* Edition October 2003 (Version AA) (Accessed 12/09/2013) [http://www.biophysics.bioc.cam.ac.uk/wp-content/uploads/2011/02/SensorSurface\\_Handbook.pdf](http://www.biophysics.bioc.cam.ac.uk/wp-content/uploads/2011/02/SensorSurface_Handbook.pdf)
- Biacore. *An introduction to Biacore Technology* brochure. Accessed 29-08-2013: <http://www.biotech.iastate.edu/facilities/protein/seminars/BIACore/TechnologyNotes/TechnologyBrochure.pdf>
- Bianchini M., Radrizzani M., Brocardo M.G., Reyes G.B., Gonzalez S.C. & Santa-Coloma T.A. (2001) Specific oligobodies against ERK-2 that recognize both the native and the denatured state of the protein. *J. Immunol. Methods* **252**: 191-197.
- Bini A., Centi S., Tombelli S., Minunni M. & Mascini M. (2008) Development of an optical RNA-based aptasensor for C-reactive protein. *Anal. Bioanal. Chem.* **390**: 1077-1086.
- Bittker J.A., Le B.V. & Liu D.R. (2002) Nucleic acid evolution and minimization by nonhomologous random recombination. *Nat. Biotechnol.* **20**(10): 1024-1029.
- Bobrow M.N., Shaughnessy K.J. & Litt, G.J. (1991). Catalyzed reporter deposition, a novel method of signal amplification. II. Application to membrane immunoassays. *J. Immunol. Methods* **137**: 103-112.
- Bock L.C., Griffin L.C., Latham J.A., Vermaas E.H. & Toole J.J. (1992) Selection of single-stranded DNA molecules that bind and inhibit human thrombin. *Nature* **355**: 564-566.
- Bowser M.T. (2005) SELEX: just another separation? *Analyst* **130**: 128-130.
- Britten R.J., Graham D.E. & Neufeld B.R. (1974) Analysis of repeating DNA sequences by reassociation. *Methods Enzymol.* **29**: 363-418.
- Britten R.J. & Kohne D.E. (1968) Repeated sequences in DNA. *Science* **161**: 529-540.
- Bunka D.H. & Stockley P.G. (2006) Aptamers come of age - At last. *Nat. Rev. Microbiol.* **4**: 588-596.
- Burmeister, P. E., Wang C., Killough J.R., Lewis S.D., Horwitz L.R., Ferguson L., Thompson K.M., Pendergrast P.S., McCauley T.G., Kurz M., Diener J., Cload S.T., Wilson C. & Keefe A.D. (2006) 2'-Deoxy purine, 2'-O-methyl pyrimidine (dRmY) aptamers as candidate therapeutics. *Oligonucleotides* **16**: 337-351.
- Cadwell R.C. & Joyce G.F. (1992) Randomization of genes by PCR mutagenesis. *PCR Methods Appl.* **2**(1): 28-33.
- Cao X., Li S., Chen L., Ding H., Xu H., Huang Y., Li J., Liu N., Cao W., Zhu Y., Shen B. & Shao N. (2009) Combining use of a panel of ssDNA aptamers in the detection of *Staphylococcus aureus*. *Nucleic Acids Res.* **37**: 4621-4628.
- Carlson, B. (2007). Aptamers: The New Frontier In Drug Development? *Biotechnol Healthc.* **4**(2): 31-32,34-36.
- Centi S., Tombelli S., Minunni M. & Mascini M. (2007) Aptamer-Based Detection of Plasma Proteins by an Electrochemical Assay Coupled to Magnetic Beads. *Anal. Chem.* **79** (4): 1466-1473.
- Charlton J. & Smith D. (1999) Estimation of SELEX pool size by measurement of DNA renaturation rates. *RNA* **5**: 1326-1332.
- Chen C. B., Chernis G.A., Hoang V.Q. & Landgraf R. (2003) Inhibition of heregulin signaling by an aptamer that preferentially binds to the oligomeric form of human epidermal growth factor receptor-3. *Proc. Natl Acad. Sci. USA* **100**: 9226-9231.
- Chen S., Deng T., Wang T., Wang J., Li X., Li Q. & Huang G. (2012) Visualization of high-throughput and label-free antibody-polypeptide binding for drug screening based on

- microarrays and surface plasmon resonance imaging. *J. Biomed. Opt.* **17**(1), 015005 (Feb 03, 2012). doi:10.1117/1.JBO.17.1.015005
- Cho E.J., Collett J.R., Szafranska A.E. & Ellington A.D. (2006) Optimization of aptamer microarray technology for multiple protein targets. *Anal. Chim. Acta* **564**: 82-90.
- Cho E.J., Lee J. & Ellington A.D. (2009) Applications of Aptamers as Sensors. *Annu. Rev. Anal. Chem.* **2**: 241-264.
- Christiaens P., Vermeeren V., Wenmackers S., Daenen M., Haenen K., Nesládek M., vandeVen M., Ameloot M., Michiels L. & Wagner P. (2006) EDC-Mediated DNA Attachment to Nanocrystalline CVD Diamond Films. *Biosens. Bioelectron.* **22**: 170-177.
- Citartan M., Tang T.H., Tan S.C. & Gopinath S.C. (2011) Conditions optimized for the preparation of single-stranded DNA (ssDNA) employing lambda exonuclease digestion in generating DNA aptamer. *World J. Microb. Biotechn.* **27**(5): 1167-1173.
- Conrad R.C., Baskerville S. & Ellington A.D. (1995) *In vitro* selection methodologies to probe RNA function and structure. *Mol. Div.* **1**: 69-78.
- Cowperthwaite M.C. & Ellington A.D. (2008) Bioinformatic Analysis of the Contribution of Primer Sequences to Aptamer Structures. *J. Mol. Evol.* **67**(1): 95-102.
- Cox J.C. & Ellington A.D. (2001) Automated selection of anti-protein aptamers. *Bioorg. Med. Chem.* **9**: 2525-2531.
- Daniel C., Mélaïne F., Roupioz Y., Livache T. & Buhot A. (2013) Real-time monitoring of thrombin interactions with its aptamers: insights into the sandwich complex formation. *Biosens. Bioelectron.* **40**: 186-192.
- Das J., Cederquist K.B., Zaragoza A.A., Lee P.E., Sargent E.H. & Kelley S.O. (2012) An ultrasensitive universal detector based on neutralizer displacement. *Nat. Chem.* **4**: 642-648.
- Dausse E., Taouji S., Evadé L., Di Primo C., Chevet E. & Toulmé J. (2011) HAPIScreen, a method for high-throughput aptamer identification. *J. Nanobiotechn.* **9**: 25. DOI: 10.1186/1477-3155-9-25
- Dehghan A., Kardys I., de Maat M.P., Uitterlinden A.G., Sijbrands E.J., Bootsma A.H., Stijnen T., Hofman A., Schram M.T. & Witteman J.C. (2007) Genetic variation, C-reactive protein levels, and incidence of diabetes. *Diabetes* **56**(3): 872-878.
- Deng D., Shi Y., Feng H., Chen Q., Li D. & Liu L. (2013) Label-free Electrochemical Sensing Platform for the detection of Protease. *Int. J. Electrochem. Sci.* **8**: 6933-6940.
- Djordjevic M. (2007) Selex experiments: New prospects, applications and data analysis in inferring regulatory pathways. *Biomol. Eng.* **24**: 179-189.
- Drabovich A., Berezovski M. & Krylov S.N. (2005) Selection of Smart Aptamers by Equilibrium Capillary Electrophoresis of Equilibrium Mixtures (ECEEM). *J. Am. Chem. Soc.* **127**: 11224-11225.
- Drabovich A.P., Berezovski M., Okhonin V. & Krylov S.N. (2006) Selection of Smart Aptamers by Methods of Kinetic Capillary Electrophoresis. *Anal. Chem.* **78**: 3171-3178.
- Drolet D.W., Moon-McDermott L. & Romig T.S. (1996) An enzyme-linked oligonucleotide assay. *Nat. Biotechnol.* **14**: 1021-1025.
- Drummond T.G., Hill M.G. & Barton J.K. (2008) Electrochemical DNA sensors. *Nature Biotechnol.* **21**: 1192-1199.
- Dynabeads® (2010) Dynabeads® MyOne™ Carboxylic Acid product page - Two-step protocol with NHS. <http://www.lifetechnologies.com/be/en/home/references/protocols/proteins-expression-isolation-and-analysis/protein-isolation-protocol/dynabeads-myone-carboxylic-acid.html> (Accessed 4/09/2013)

- Eaton B.E. (1997) The joys of *in vitro* selection: chemically dressing oligonucleotides to satiate protein targets. *Curr. Op. Chem. Bio.* **1**: 10-16.
- Ellington A.E. & Szostak J.W. (1990) *In vitro* Selection of RNA Molecules that Bind Specific Ligands. *Nature* **46**: 818-822.
- Ellington A.E. & Szostak J.W. (1992) Selection *in vitro* of single-stranded DNA molecules that fold into specific ligand binding structures. *Nature* **355**: 850-852.
- Endo M., Yang Y., Sugiyama H. (2013) DNA origami technology for biomaterials applications. *Biomater. Sci.* **1**: 347-360.
- Eulberg D., Buchner K., Maasch C. & Klusmann S. (2005) Development of an automated *in vitro* selection protocol to obtain RNA-based aptamers: identification of a biostable substance P antagonist. *Nucleic Acid Res* **33**(4): e45.
- Fan M., McBurnett S.R., Andrews C.J., Allman A.M., Bruno J.G. & Kiel J.L. (2008) Aptamer Selection Express: A Novel Method for Rapid Single-Step Selection and Sensing of Aptamers. *J. Biomol. Tech.* **19**: 311-321.
- Farajollahi M.M., Cook B., Hamzehlou S. & Self C.H. (2012) Reduction of non-specific binding in immunoassays requiring long incubations. *Scand. J. Clin. Lab. Invest.* **72**: 531-539.
- Fischer N., Tarasow T. & Tok J. (2008) Protein detection via direct enzymatic amplification of short DNA aptamers. *Anal. Biochem.* **373**(1): 121-128.
- Fredriksson S., Gullberg M., Jarvius J., Olsson C., Pietras K., Gústafsdóttir S., Östman A. & Landegren U. (2002). Protein detection using proximity-dependent DNA ligation assays. *Nat. Biotechnol.* **20**(5): 473-477.
- Gao Z., Deng H., Shen W. & Ren Y. (2013) A Label-Free Biosensor for Electrochemical Detection of Femtomolar MicroRNAs. *Anal. Chem.* **85**(3): 1624-1630.
- Genelink™ Product Profile V3.1: *Oligo Modifications for Increased Duplex Stability & Nuclease Resistance.* <http://www.genelink.com/literature/ps/duplexstability.pdf> (Accessed 26/08/2013).
- Geng X., Zhang D., Wang H. & Zhao Q. (2013) Screening interaction between ochratoxin A and aptamers by fluorescence anisotropy approach. *Anal. Bioanal. Chem.* **405**: 2443-2449.
- Giovannoli C., Baggiani C., Anfossi L. & Giraudi G. (2008) Aptamers and molecularly imprinted polymers as artificial biomimetic receptors in affinity capillary electrophoresis and electrochromatography. *Electrophoresis* **29**(16): 3349-3365.
- Gokulrangan G., Unruh J.R., Holub D.F., Ingram B., Johnson C.K. & Wilson G.S. (2005) DNA Aptamer-Based Bioanalysis of IgE by Fluorescence Anisotropy. *Anal. Chem.* **77**: 1963-1970.
- Gold L., Ayers D., Bertino J., Bock C., Bock A., *et al.* (2010) Aptamer-Based Multiplexed Proteomic Technology for Biomarker Discovery. *PLoS ONE* **5**(12): e15004. doi:10.1371/journal.pone.0015004.
- Goodrich J.A. & Kugel J.F. (2007) *Binding and Kinetics for Molecular Biologists*. First edition. Cold Spring Harbor Laboratory Press, Cold Spring Harbor, New York, USA. ISBN-10: 0879697369.
- Gopinath S.C. (2007) Methods developed for SELEX. *Anal. Bioanal. Chem.* **387**: 171-182.
- Gragoudas E. S., Adamis A.P., Cunningham E.T., Feinsod M. & Guyer D.R. (2004) Pegaptanib for neovascular age-related macular degeneration. *N. Engl. J. Med.* **351**: 2805-2816.
- Guo K. T., Paul A., Schichor C., Ziemer G. & Wendel H.P. (2008a) CELL-SELEX: novel perspectives of aptamer-based therapeutics. *Int. J. Mol. Sci.* **9**: 668-678.

- Guo X.F., Gorodetsky A.A., Hone J., Barton J.K. & Nuckolls C. (2008b) Conductivity of a Single DNA Duplex Bridging a Carbon Nanotube Gap. *Nat. Nanotechnol.* **3**: 163-167.
- Guo L. & Kim DH (2011) Reusable plasmonic aptasensors: using a single nanoparticle to establish a calibration curve and to detect analytes. *Chem. Comm.* **47**: 7125-7127.
- Guo L., Xu Y., Ferhan A.R., Chen G., Kim D.-H. (2013) Oriented Gold Nanoparticle Aggregation for Colorimetric Sensors with Surprisingly High Analytical Figures of Merit. *J. Am. Chem. Soc.* **135**(33): 12338-12345.
- Gupta B.D. & Verma R.K. (2009) Surface Plasmon Resonance-Based Fiber Optic Sensors: Principle, Probe Designs, and Some Applications. *Journal of Sensors*. Article ID 979761, 12 pages, 2009. doi:10.1155/2009/979761
- Hahnefeld C., Drewianka S. & Herberg F.W. (2003) Determination of Kinetic Data Using Surface Plasmon Resonance Biosensors *Methods Mol. Med.* **94**: 299-320.
- Hall B., Cater S., Levy M. & Ellington A.D. (2009) Kinetic Optimization of a Protein-Responsive Aptamer Beacon. *Biotechn. Bioeng.* **103**: 1049-1059.
- Han K., Liang Z. & Zhou N. (2010) Design Strategies for Aptamer-Based Biosensors. *Sensors* **10**: 4541-4557.
- Healy J. M., Lewis S.D., Kurz M., Boomer R.M., Thompson K.M., Wilson C. & McCauley T.G. (2004) Pharmacokinetics and biodistribution of novel aptamer compositions. *Pharm. Res.* **21**: 2234-2246.
- Heise C. & Bier F.F. (2006) Immobilization of DNA on Microarrays. *Topics in current chemistry* **261**: 1-25. In: Immobilisation of DNA on chips II. (Ed. Wittmann C.) Springer, Berlin Heidelberg New York. ISBN 978-3-540-28436-9.
- Hermann T. & Patel D.J. (2000) Adaptive recognition by nucleic acid aptamers. *Science* **287**: 820-825.
- Hermanson G.T. (2008) Bioconjugate Techniques (Second Edition). Elsevier Inc., London, UK. ISBN 978-0-12-370501-3
- Hianik T., Ostatna V., Sonlajternova M. & Grman I. (2007) Influence of ionic strength, pH and aptamer configuration for binding affinity to thrombin. *Bioelectrochemistry* **70**(1): 127-133.
- Hoon S., Zhou B., Janda K.D., Brenner S. & Scolnick J. (2011) Aptamer selection by high-throughput sequencing and informatic analysis. *BioTechniques* **51**: 413-416.
- Huang C.J., Lin H.I., Shiesh S.C., Lee G.B. (2010) Integrated microfluidic system for rapid screening of CRP aptamers utilizing systematic evolution of ligands by exponential enrichment (SELEX). *Biosens Bioelectron.* **25**: 1761-1766.
- Hwang B. & Lee S.I. (2002) Aptamer activity against myasthenic autoantibodies by Extended Sequence Selection. *Biochem. Biophys. Res. Commun.* **290**: 656-662.
- IDT (2013a) IDT catalogue - Attachment Chemistry / Linkers Modifications. (Accessed 9/9/2013) <http://eu.idtdna.com/catalog/Modifications/Modifications.aspx?catid=2>
- IDT (2013b) IDT catalogue - Spacer Modifications. (Accessed 9/9/2013) <http://eu.idtdna.com/catalog/Modifications/Modifications.aspx?catid=6>
- Jacobsen N. & Skouw J. (2010) Custom-made Thermo Scientific Nunc Immobilizer for DNA binding. *Technical Note* **56**. <http://static.thermoscientific.com/images/D19606~.pdf> (Accessed 12/09/2013)
- Janssens S.D., Pobedinskas P., Vacik J., Petráková V., Ruttens B., D'Haen J., Nesládek M., Haenen K. & Wagner P. (2011) Separation of the Intra- and Intergranular

- Magnetotransport Properties in Nanocrystalline Diamond Films on the Metallic Side of the Metal-Insulator Transition. *New J. Phys.* **8**: 083008.
- Jauho E.S., Boas U., Wiuff C., Wredström K., Pedersen B., Anresen L.O., Heegaard P.M.H. & Jakobsen M.H. (2000) New technology for regiospecific covalent coupling of polysaccharide antigens in ELISA for serological detection. *J. Immunol. Methods* **242**: 133-143.
- Jayasena S. D. (1999) Aptamers: an emerging class of molecules that rival antibodies in diagnostics *Clin. Chem.* **45**(9): 1628-1650.
- Jing M. & Bowser M.T. (2011) A Review of Methods for Measuring Aptamer-Protein Equilibria. *Anal. Chim. Acta* **686**(1-2): 9-18.
- Kawarada H. & Ruslinda A. R. (2011) Diamond Electrolyte Solution Gate FETs for DNA and Protein Sensors Using DNA/RNA Aptamers. *Phys. Status Solidi A* **208**: 2005-2016.
- Keefe A.D. & Cload S.T. (2008) SELEX with modified nucleotides. *Curr. Opin. Chem. Biol.* **12**: 448-456.
- Keefe A.D., Pai S. & Ellington A.D. (2010) Aptamers as therapeutics. *Nat. Rev. Drug Discov.* **9**: 537-550.
- Keeney T.R., Bock C., Gold L., Kraemer S., Lollo B., Nikrad M., Stanton M., Stewart A., Vaught J.D. & Walker J.J. (2009) Automation of the SomaLogic Proteomics Assay: A platform for Biomarker Discovery. *JALA* **14**: 360-366.
- Kenna J.G., Major G.N. & Williams R.S. (1985) Methods for reducing non-specific antibody binding in enzyme-linked immunosorbent assays. *J. Immunol. Methods* **85**(2): 409-419.
- Kheiss T., Jozsef L., Potempa L.A. & Filep J.G. (2004) Conformational rearrangement in C-reactive protein is required for pro-inflammatory actions on human endothelial cells. *Circulation* **109**: 2016-2022.
- Kirby R., Cho E.J., Gehrke B., Bayer T., Park Y.S., Neikirk D.P., McDevitt J.T. & Ellington A.D. (2004) Aptamer-based sensor arrays for the detection and quantitation of proteins. *Anal. Chem.* **76**: 4066-4075.
- Kimura-Suda H., Petrovykh D.Y., Tarlov M.J. & Whitman L.J. (2003) Base-dependent competitive adsorption of single-stranded DNA on gold. *J. Am. Chem. Soc.* **125**: 9014-9015.
- Krylov S.N. (2006) Nonequilibrium Capillary Electrophoresis of Equilibrium Mixtures (NECEEM): A Novel Method for Biomolecular Screening. *J. Mol. Screen.* **11**: 115-122.
- Kuang H., Yin H., Liu L., Xu L., Ma W. & Xu C. (2014) Asymmetric Plasmonic Aptasensor for Sensitive Detection of Bisphenol A. *ACS Appl. Mater. Interfaces* **6**(1): 364-369.
- Kusser W. (2000) Chemically modified nucleic acid aptamers for *in vitro* selections: evolving evolution. *J. Biotechnol.* **74**(1): 27-38.
- Lakowicz J.R. (2006) *Principles in Fluorescence Spectroscopy* Third Edition. Kluwer Academic/Plenum, New York. ISBN 978-0-387-46312-4
- Lamoureux D., Peterson D.G., Li W., Fellers J.P. & Gill B.S. (2005) The efficacy of C<sub>6</sub>t-based gene enrichment in wheat (*Triticum aestivum* L.). *Genome* **48**(6): 1120-1126.
- Larkin M.A., Blackshields G., Brown N.P., Chenna R., McGettigan P.A., McWilliam H., Valentin F., Wallace I.M., Wilm A., Lopez R., Thompson J.D., Gibson T.J. & Higgins D.G. (2007) Clustal W and Clustal X version 2.0. *Bioinformatics* **23**(21): 2947-2948.
- Lauridsen L.H., Shamaileh H.A., Edwards S.L., Taran E. & Veedu R.N. (2012) Rapid One-Step Selection Method for Generating Nucleic Acid Aptamers: Development of a DNA Aptamer against  $\alpha$ -Bungarotoxin. *PLoS ONE* **7**(7): e41702. doi:10.1371/journal.pone.0041702



- Lee J.F., Hesselberth J.R., Meyers L.A. & Ellington A.D. (2004) Aptamer Database. *Nucleic Acids Res.* **32**: D95-100.
- Li L., Zhao T., Chen Z., Mu X. & Guo L. (2011) Aptamer biosensor for label-free impedance spectroscopy detection of thrombin based on gold nanoparticles. *Sensors Actuat. B-Chem.* **157**: 189-194.
- Li N. (2010) Detection of Non-Nucleic Acid Targets with an Unmodified Aptamer and a Fluorogenic Competitor. *J. Lab. Autom.* **15**: 189-197.
- Li W., Yang X., Wang K., Tan W., Li H. & Ma C. (2008) FRET-based aptamer probe for rapid angiogenin detection. *Talanta* **75**(3): 770-774.
- Liao S., Liu Y., Zeng J., Li X., Shao N., Mao A., Wang L., Ma J., Cen H., Wang Y., Zhang X., Zhang R., Wei Z. & Wang X. (2010) Aptamer-Based Sensitive Detection of Target Molecules via RT-PCR Signal Amplification. *Bioconjugate Chem.* **21**(12): 2183-2189.
- Life Technologie (2012) TOPO® TA Cloning® Kit – User Guide. *MAN0000047*. [http://tools.lifetechnologies.com/content/sfs/manuals/topota\\_man.pdf](http://tools.lifetechnologies.com/content/sfs/manuals/topota_man.pdf) (Accessed 04/09/2013).
- Lin P., Chen R., Lee C., Chang Y., Chen C. & Chen W. (2011) Studies of the binding mechanism between aptamers and thrombin by circular dichroism, surface plasmon resonance and isothermal titration calorimetry. *Colloid Surface B* **88**: 552-558.
- Liu J.J. & Stormo G.D. (2005) Combining SELEX with quantitative assays to rapidly obtain accurate models of protein–DNA interactions. *Nucleic Acids Res.* **33**: e141.
- Luo X., Xu M., Freeman C., James T. & Davis J. J. (2013) Ultrasensitive Label Free Electrical Detection of Insulin in Neat Blood Serum. *Anal.Chem.* **85**: 4129-4134.
- Mann D., Reinemann C., Stoltenburg R., Strehlitz B. (2005) *In vitro* selection of DNA aptamers binding ethanolamine. *Biochem. Biophys. Res. Comm.* **338**: 1928-1934.
- Mantovani A., Garlanda C. , Doni A. & Bottazzi B. (2008). Pentraxins in innate immunity: from C-reactive protein to the long pentraxin PTX3. *J. Clin. Immunol.* **28**(1): 1-13.
- Mantovani A., Valentino S., Gentile S., Inforzato A., Bottazzi B. & Garlanda C. (2013) The long pentraxin PTX3: a paradigm for humoral pattern recognition molecules. *Ann. N.Y. Acad. Sci.* **1285**: 1-14.
- Marshall K.A. & Ellington A.D. (2000). *In vitro* selection of RNA aptamers. *Methods Enzymol.* **318**: 193-214.
- Mendonça S.D. & Bowser M.T. (2004) *In vitro* selection of high-affinity DNA ligands for human IgE using capillary electrophoresis. *Anal. Chem.* **76**: 5387-5392.
- Meyer Z.C., Schreinemakers J.M.J., Mulder P.G.H., de Waal R.A.L., Ermens A.A.M. & van der Laan L. (2013) The Role of C-Reactive Protein and the SOFA Score as Parameter for Clinical Decision Making in Surgical Patients during the Intensive Care Unit Course. *PLoS ONE* **8**(2): e55964.
- McGinness K.E., Wright M.C. & Joyce G.F. (2002) Continuous *in vitro* evolution of a ribozyme that catalyzes three successive nucleotidyl addition reactions. *Chem. Biol.* **9**: 585-596.
- Ming Xu M., Zhu M., Du Y., Yan B., Wang Q, Wang C. & Zhao J. (2013) Serum C-reactive protein and risk of lung cancer: a case-control study. *Med Oncol.* **30**(1): 319-325.
- Miramontes Espino M.V. & Romero-Prado M.M. (2013) Patented Aptamers For C-reactive protein Detection: A Review About Their Use In Clinical Diagnostics. *Recent Pat. DNA Gene Seq.* **7**(3): 195-206.
- Misono T.S. & Kumar P.K.R. (2005) Selection of RNA aptamers against human influenza virus hemagglutinin using surface plasmon resonance. *Anal.Biochem.* **342**: 312-317.
- Morgan C.L., Newman D.J. & Price C.P. (1996) Immunosensors: technology and opportunities in laboratory medicine. *Clin. Chem.* **42**(2): 193-209.

- Müller J., El-Maarri O., Oldeburg J., Pötzsch B. & Mayer G. (2008) Monitoring the progression of the *in vitro* selection of nucleic acid aptamers by denaturing high-performance liquid chromatography. *Anal. Bioanal. Chem.* **390**: 1033-1037.
- Musheev M.U. & Krylov S.N. (2006) Selection of aptamers by systematic evolution of ligands by exponential enrichment: Addressing the polymerase chain reaction issue. *Anal. Chim. Acta* **564**: 91-96.
- Nagata K. & Handa H. (2000) Real-Time Analysis of Biomolecular Interactions: Applications of Biacore. Springer-Verlag, ISBN 40431-70289-X, Tokyo
- Naimuddin M., Kitamura K., Kinoshita Y., Honda-Takahashi Y., Murakami M., Ito M., Yamamoto K., Hanada K., Husimi Y. & Nishigaki K. (2007) Selection-by-function: efficient enrichment of cathepsin E inhibitors from a DNA library. *J. Mol. Recognit.* **20**: 58-68.
- Nakamura T., Grimer R.J., Gaston C.L., Watanuki M., Sudo A. & Jeys L. (2013) The prognostic value of the serum level of C-reactive protein for the survival of patients with a primary sarcoma of bone. *Bone Joint J.* **95-B(3)**: 411-418.
- New England Biolabs (2013) Lambda Exonuclease Product Sheet. <http://www.neb.com/products/m0262-lambda-exonuclease?device=pdf> (Accessed 04/09/2013).
- Niazi J.H., Lee S.J., Kim Y.S. & Gu M.B. (2008) ssDNA aptamers that selectively bind oxytetracycline. *Bioorg. Med. Chem.* **1**: 1254-1261.
- Nudler E. & Mironov A.S. (2004). "The riboswitch control of bacterial metabolism". *Trends Biochem. Sci.* **29**(1): 11-17.
- Nutiu R. & Li Y.F. (2003) Structure-switching signaling aptamers. *J. Am. Chem. Soc.* **125**(16): 4771-4778.
- Okemefuna A.I., Stach L., Rana S., Buetas A.J.Z., Gor J. & Perkins S.J. (2010) C-reactive protein Exists in an NaCl Concentration-dependent Pentamer-Decamer Equilibrium in Physiological Buffer. *J. Biol. Chem.* **285**(2): 1041-1052.
- O'Neil, M.J. (ed.) (2006) *The Merck Index - An Encyclopedia of Chemicals, Drugs, and Biologicals*. Merck & Co., Inc., Whitehouse Station, N.J.
- Orito N., Umekage S., Sato K., Kawauchi S., Tanaka H., E Sakai E., Tanaka T. & Kikuchi Y. (2012) High-affinity RNA aptamers to C-reactive protein (CRP): newly developed pre-elution methods for aptamer selection. *J. Phys. Conf. Ser.* **352**: 012042. doi:10.1088/1742-6596/352/1/012042.
- Ostatná V., Vaisocherová H., Homola J. & Hianik T. (2008) Effect of the immobilization of DNA aptamers on the detection of thrombin by means of surface plasmon resonance. *Anal. Bioanal. Chem.* **391**: 1861-1869.
- Pan W. & Clawson G.A. (2009) The Shorter the Better: Reducing Fixed Primer Regions of Oligonucleotide Libraries for Aptamer Selection. *Molecules* **14**: 1353-1369.
- Park J.Y. & Park S.M. (2009) DNA Hybridization Sensors Based on Electrochemical Impedance Spectroscopy as a Detection Tool. *Sensors* **9**: 9513-9532.
- Patolsky F., Zheng G. & Lieber C.M. (2006) Fabrication of silicon nanowire devices for ultrasensitive, label-free, real-time detection of biological and chemical species. *Nature Protocols* **1**: 1711-1724.
- Peeters M., Csipai P., Geerets B., Weustenraed A., van Grinsven B., Thoelen R., Gruber J., De Ceuninck W., Cleij T.J., Troost F.J. & Wagner P. (2013) Heat-transfer-based

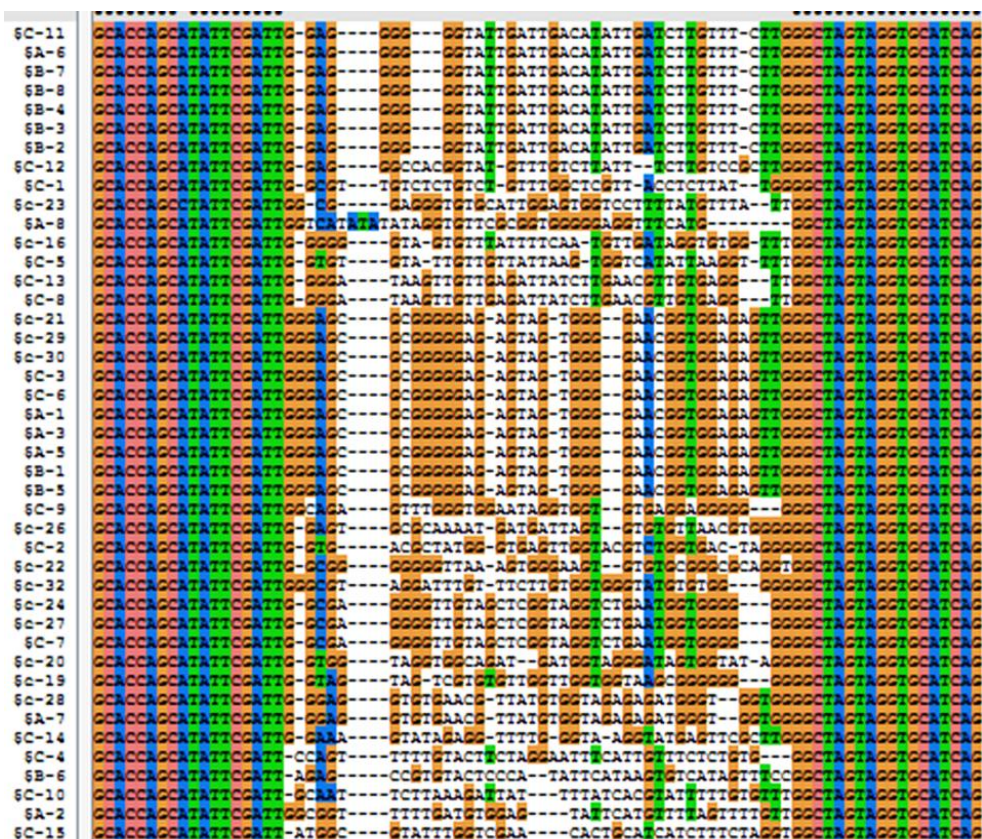
- detection of L-nicotine, histamine, and serotonin using molecularly imprinted polymers as biomimetic receptors. *Anal. Bioanal. Chem.* **405**(20): 6453-6460.
- Peng Y., Zhang D., Li Y., Qi H., Gao Q. & Zhang C. (2009) Label-free and sensitive faradic impedance aptasensor for the determination of lysozyme based on target-induced aptamer displacement. *Biosens. Bioelectron.* **25**: 94-99.
- Pepys M.B. (1999) The Lumleian Lecture. C-reactive protein and amyloidosis: from proteins to drugs? In: *Horizons in medicine*. (Ed. G. Williams.) Royal College of Physicians of London. London, UK **10**: 397-414.
- Pepys M.B. & Hirschfield G.M. (2003) C-reactive protein: a critical update. *J. Clin. Invest.* **111**: 1805-1812.
- Perkin Elmer™ (2007) ELAST® ELISA Amplification System Manual. *PC2578-1008*. [http://www.perkinelmer.com/BE/CMSResources/Images/44-73589MAN\\_NEP116ELASTELISAManual.pdf](http://www.perkinelmer.com/BE/CMSResources/Images/44-73589MAN_NEP116ELASTELISAManual.pdf) (Accessed 12/09/2013).
- Potyrailo R.A., Conrad R.C., Ellington A.D. & Hieftje G.M. (1998) Adapting Selected Nucleic Acid Ligands (Aptamers) to Biosensors. *Anal. Chem.* **70**: 3419-3425.
- Radom F., Jurek P.M., Mazurek M.P., Otlewski J. & Jeleń F. (2013) Aptamers: molecules of great potential. *Biotechnol. Adv.* **31**(8): 1260-1274.
- Rhie A., Kirby L., Sayer N., Wellesley R., Disterer P., Sylvester I., Gill A., Hope J., James W. & Tahiri-Alaoui A. (2003) Characterization of 20-fluoro-RNA aptamers that bind preferentially to disease-associated conformations of prion protein and inhibit conversion. *J. Biol. Chem.* **278**: 39697-39705.
- Rodriguez M.C., Kawde A.N. & Wang J. (2005) Aptamer biosensor for label-free impedance spectroscopy detection of proteins based on recognition-induced switching of the surface charge. *Chem. Commun.* **2005**: 4267-4269.
- Rodriguez-Mozaz S., Marco M.P., Lopez de Alda M.J. & Barcelo D. (2004a) Biosensors for environmental monitoring of endocrine disruptors: a review article. *Anal. Bioanal. Chem.* **378**(3): 588-598.
- Rodriguez-Mozaz S., Marco M.P., Lopez de Alda M.J. & Barcelo D. (2004b) Biosensors for environmental applications: Future development trends. *Pure Appl. Chem.* **76**(4): 723-752.
- Rowe W., Platt M. & Day P.J.R. (2009) Advances and perspectives in aptamer arrays. *Integr. Biol.* **1**: 53-58.
- Sano T., Smith C.L. & Cantor C.R. (1992) Immuno-PCR: very sensitive antigen detection by means of specific antibody-DNA conjugates. *Science* **258**(5079): 120-122.
- Scheller F.W., Wollenberger U., Warsinke A., Lisdorf F. (2001) Research and development in biosensors. *Curr. Opin. Biotechnol.* **12**: 35-40.
- Schütze T., Arndt P.F., Menger M., Wochner A., Vingron M., Volker A.E., Lehrach H., Kaps C. & Glökler, J. (2010) A calibrated diversity assay for nucleic acid libraries using DiStRO – a Diversity Standard of Random Oligonucleotides. *Nucleic Acids Res.* **38**(4): e2. DOI: 10.1093/nar/gkp1108
- Schütze T., Wilhelm B., Greiner N., Braun H., Peter F., Mörl M., Erdmann V.A., Lehrach H., Konthur Z., Menger M., Arndt P.F. & Glökler J. (2011) Probing the SELEX Process with Next-Generation Sequencing. *PLoS ONE* **6**(12): e29604. doi:10.1371/journal.pone.0029604.
- Seeman N.C. (2007) An Overview of Structural DNA Nanotechnology. *Mol. Biotechnol.* **37**(3): 246-257.

- Serna-Cock L. & Perenguez-Verdugo J.G. (2011) "Biosensors Applications in Agri-food Industry." In: *Environmental Biosensors* (ed. Prof. Vernon Somerset). InTech Europe, Croatia. ISBN: 978-953-307-486-3 DOI: 10.5772/16744.
- Sepúlveda B., Angelomé P.C., Lechuga L.M. & Liz-Marzán L.M. (2009) LSPR-based nanobiosensors. *Nano Today* **4**: 244-251.
- Shao K., Ding W., Wang F., Li H., Ma D. & Wang H. (2011) Emulsion PCR: A high efficient way of PCR amplification of Random DNA libraries in aptamer selection. *PLoS One* **6**(9): e24910.
- Smith C.L., Milea J.S. & Nguyen G.H. (2005) Immobilization of Nucleic Acids Using Biotin-(Strept)avidin Systems. *Topics in current chemistry* **261**: 1-25. In: Immobilisation of DNA on chips II. (Ed. Wittmann C.) Springer, Heidelberg New York. ISBN 978-3-540-28436-9
- Smuc T, Ahn I & Ulrich H. (2013) Nucleic acid aptamers as high affinity ligands in biotechnology and biosensorics. *J. Pharmaceut. Biomed.* **81–82**: 210-217.
- Song K., Lee S. & Ban C. (2012) Aptamers and Their Biological Applications. *Sensors* **12**: 612-31.
- Song S., Wang L., Li J., Zhao J. & Fan C. (2008) Aptamer-based biosensors. *Trends Anal. Chem.* **27**(2): 108-117.
- Stern E., Steenblock E.R., Reed M.A. & Fahmy T.M. (2008) Label-free Electronic Detection of the Antigen-Specific T-Cell Immune Response. *Nano Lett.* **8**(10): 3310-3314.
- Stoltenburg R., Reinemann C. & Strehlitz B. (2005) FluMag-SELEX as an advantageous method for DNA aptamer selection. *Anal. Bioanal. Chem.* **383**(1): 83-91.
- Stoltenburg R., Reinemann C. & Strehlitz B. (2007) SELEX-A (r)evolutionary method to generate high-affinity nucleic acid ligands. *Biomol. Eng.* **24**(4): 381-403.
- Stoltenburg R., Nikolaus N. & Strehlitz B. (2012) Capture-SELEX: Selection of DNA Aptamers for Aminoglycoside Antibiotics. *J. Anal. Methods . Chem.* Published online 2012 December 30. doi: 10.1155/2012/415697
- Strehlitz B., Reinemann C., Linkorn S. & Stoltenburg R. (2012) Aptamers for pharmaceuticals and their application in environmental analytics. *Bioanal Rev.* **4**(1): 1-30.
- Tanaka Y., Honda T., Matsuura K., Kimura Y. & Inui M. (2009) *In vitro* Selection and Characterization of DNA Aptamers Specific for Phospholamban. *J. Pharmacol. Exp. Ther.* **329**(1): 57-63.
- Tang J.J., Xie J.W., Shao N.S. & Yan Y. (2006) The DNA aptamers that specifically recognize ricin toxin are selected by two *in vitro* selection methods. *Electrophoresis* **27**: 1303-1311.
- Tasset D.M., Kubik M.F. & Steiner W. (1997) Oligonucleotide inhibitors of human thrombin that bind distinct epitopes. *J. Mol. Biol.* **272**: 688-698.
- Thermo Scientific Plate Guide (2009) BRLSPPLATES/74059 0709.
- Thompson D., Pepys M.B. & Wood S.P. (1999) The physiological structure of human C-reactive protein and its complex with phosphocholine. *Structure* **7**: 169-177.
- Tok J. B.-H. & Fischer N.O. (2008) Single microbead SELEX for efficient ssDNA aptamer generation against botulinum neurotoxin. *Chem. Commun.* **16**: 1883-1885.
- Tuerk C. & Gold L. (1990) Systematic evolution of ligands by exponential enrichment: RNA ligands to bacteriophage T4 DNA polymerase. *Science* **249**: 505-510.
- Tran D. T., Janssen K., Pollet J., Lammertyn E., Anné J., Van Schepdael A. & Lammertyn J. (2010) Selection and Characterization of DNA Aptamers for Egg White Lysozyme. *Molecules* **15**: 1127-1140.

- Tran D. T., Vermeeren V., Grieten L., Wenmaeckers S., Wagner P., Pollet J., Janssen K., Michiels L. & Lammertyn J. (2011) Nanocrystalline diamond impedimetric aptasensor for the label-free detection of human IgE. *Biosens. Bioelectr.* **26**(6): 2987-2993.
- Tran D. T., Knez K., Janssen K., Pollet J., Spasic D. & Lammertyn, J. (2013) Selection of aptamers against Ara h 1 protein for FO-SPR biosensing of peanut allergens in food matrices. *Biosens. Bioelectron.* **43**: 245-251.
- Tsai R.Y.L. & Reed R.R. (1998) Identification of DNA recognition sequences and protein interaction domains of the multiple-Zn-finger protein Roaz. *Mol. Cell. Biol.* **18**: 6447-6456.
- Tsujimoto M., Inoue K. & Nojima S. J. (1983) Purification and characterization of human serum C-reactive protein. *J. Biochem.* **5**: 1367-1373.
- Turner A.P.F., Karube I. & Wilson G.S. (1987) "The biological component" In: *Biosensors: Fundamentals and Applications* pp. 30-59. (Eds. Turner A.P.F., Karube I. & Wilson G.S.) Oxford Science Publication, Oxford. ISBN 0198547242
- van Grinsven B., Vanden Bon N., Grieten L., Murib M., Janssens S. D., Haenen K., Schneider E., Ingebrandt S., Schöning M.J., Vermeeren V., Ameloot M., Michiels L., Thoelen R., De Ceuninck W. & Wagner P. (2011) Rapid Assessment of the Stability of DNA Duplexes by Impedimetric Real-Time Monitoring of Chemically Induced Denaturation. *Lab Chip* **11**: 1656-1663.
- van Grinsven B., Vanden Bon N., Strauven H., Grieten L., Murib M., Monroy K.L.M., Janssens S.D., Haenen K., Schöning M.J., Vermeeren V., Ameloot M., Michiels L., Thoelen R., De Ceuninck W. & Wagner P. (2012) Heat-Transfer Resistance at Solid-Liquid Interfaces: A Tool for the Detection of Single-Nucleotide Polymorphisms in DNA. *ACS Nano* **6**(3): 2712-2721.
- Vartanian J.P., Henry M. & Wain-Hobson S. (1996) Hypermutagenic PCR involving all four transitions and a sizeable proportion of transversions. *Nucleic Acids Res.* **24**: 2627-2631.
- Vaught J.D., Bock C., Carter J., Fitzwater T., Otis M., Schneider D., Rolando J., Waugh S., Wilcox S.K. & Eaton B.E. (2010) Expanding the Chemistry of DNA for *in vitro* Selection. *J. Am. Chem. Soc.* **132**: 877-888.
- Vermeeren V., Wenmackers S., Daenen M., Haenen K., Williams O. A., Ameloot M., vandeVen M., Wagner P. & Michiels L. (2008) Topographical and Functional Characterisation of the ssDNA Probe Layer Generated through EDC Mediated Covalent Attachment to Nanocrystalline Diamond Using Fluorescence Microscopy. *Langmuir* **24**: 9125-9134.
- Vermeeren V., Wenmackers S., Wagner P. & Michiels L. (2009) DNA Sensors with Diamond as a Promising Alternative Transducer Material. *Sensors* **9**(7): 5600-5636.
- Vivekananda J. & Kiel J.L. (2006) Anti-*Francisella tularensis* DNA aptamers detect tularemia antigen from different subspecies by Aptamer-Linked Immobilized Sorbent Assay. *Lab Invest.* **86**: 610-618.
- Vo-Dinh T. & Cullum B. (2000) Biosensors and biochips: advances in biological and medical diagnostics. *Fresenius J. Anal. Chem.* **366**: 540-551.
- Wang C., Yang G., Luo Z. & Ding H. (2009) *In vitro* selection of high affinity DNA aptamers for Streptavidin. *Acta. Biochim. Biophys. Sin.* **41**(4): 335-340.
- Wang H.W., Wu Y., Chen Y. & Sui S.F. (2002) Polymorphism of structural forms of C-reactive protein. *Int. J. Mol. Med.* **9**: 665-671.

- Wang M.S. & Reed S.M. (2012) Direct visualization of electrophoretic mobility shift assays using nanoparticle-aptamer conjugates. *Electrophoresis* **33**(2): 348-351.
- Wang X., Zhou J., Yun W., Xiao S., Chang Z., He P. & Fang Y. (2007) Detection of thrombin using electrogenerated chemiluminescence based on Ru(bpy)<sub>3</sub><sup>2+</sup>-doped silica nanoparticle aptasensor via target protein-induced strand displacement. *Anal.Chim. Acta* **598**: 242-248.
- Wang Y., Bao L., Liu Z. & Pang D.W. (2011) Aptamer biosensor based on fluorescence resonance energy transfer from upconverting phosphors to carbon nanoparticles for thrombin detection in human plasma. *Anal Chem.* **83**(21): 8130-8137.
- Werner A. & Hahn U. (2009) Fluorescence Correlation Spectroscopy (FCS)-Based Characterisation of Aptamer Ligand Interaction. In: *Nucleic Acid and Peptide Aptamers*. (Ed. Mayer G.) *Methods in Molecular Biology*<sup>TM</sup> **535**: 107-114. ISBN 978-1-934115-89-3.
- Wiegand T.W., Williams P.B., Dreskin S.C., Jouvin M.H., Kinet J.P. & Tasset D. (1996) High-affinity oligonucleotide ligands to human IgE inhibit binding to FcεR1 receptor I. *J. Immunol.* **157**: 221-230.
- Wiegand T.W. (2000) Fluorescence correlation microscopy: Probing molecular interactions inside living cells. *Am. Lab.* **September**: 44-47.
- Wilson C. & Szostak J.W. (1998) Isolation of a fluorophore-specific DNA aptamer with weak redox activity. *Chem. Biol.* **5**: 609-617.
- Wochner A., Cech B., Menger M., Erdmann V.A. & Glöckler J. (2007) Semi-automated selection of DNA aptamers using magnetic particle handling. *BioTechniques* **43**: 344-353.
- Wu L.H. & Curran J.F. (1999) An allosteric synthetic DNA. *Nucleic Acids Res.* **27**:1512-1516.
- Yamamoto R. & Kumar P.K.R. (2000) Molecular beacon aptamer fluoresces in the presence of Tat protein of HIV-1. *Genes Cells* **5**(5): 389-396.
- Yang X.B., Li X., Prow T.W., Reece L.M., Bassett S.E., Luxon B.A., Herzog N.K., Aronson J., Shope R.E., Leary J.F. & Gorenstein D.G. (2003) Immunofluorescence assay and flow-cytometry selection of bead-bound aptamers. *Nucleic Acids Res.* **31**: e54.
- Yanga Y., Yanga D., Schluesenerb H.J. & Zhang Z. (2007) Advances in SELEX and application of aptamers in the central nervous system. *Biomol. Eng.* **24**(6): 583-592.
- Yoshida W., Mochizuki E., Takase M., Hasegawa H., Moritaa Y., Yamazakib H., Sodea K. & Ikebukuroa K. (2009) Selection of DNA aptamers against insulin and construction of an aptameric enzyme subunit for insulin sensing. *Biosens. Bioelectron.* **24**(5): 1116-1120.
- Yoshizumi J., Kumamoto S., Nakamura M. & Yamana K. (2008) Target-induced strand release (TISR) from aptamer-DNA duplex: A general strategy for electronic detection of biomolecules ranging from a small molecule to a large protein. *Analyst* **133**(3): 323-325.
- Zadegan R.M. & Norton M.L. (2012) Structural DNA Nanotechnology: From Design to Applications. *Int. J. Mol. Sci.* **13**: 7149-7162.
- Zhu J., Wang J., Su Z., Li Q., Cheng M. & Zhang J. (2008) Identification of ssDNA Aptamers Specific for Anti-neuroexcitation Peptide III and Molecular Modeling Studies: Insights into Structural Interactions. *Arch. Pharm. Res.* **31**(9): 1120-1128.
- Zuker M. (2003) Mfold web server for nucleic acid folding and hybridization prediction. *Nucleic Acids Res.* **31**(13): 3406-3415.

## Appendix A: Figures



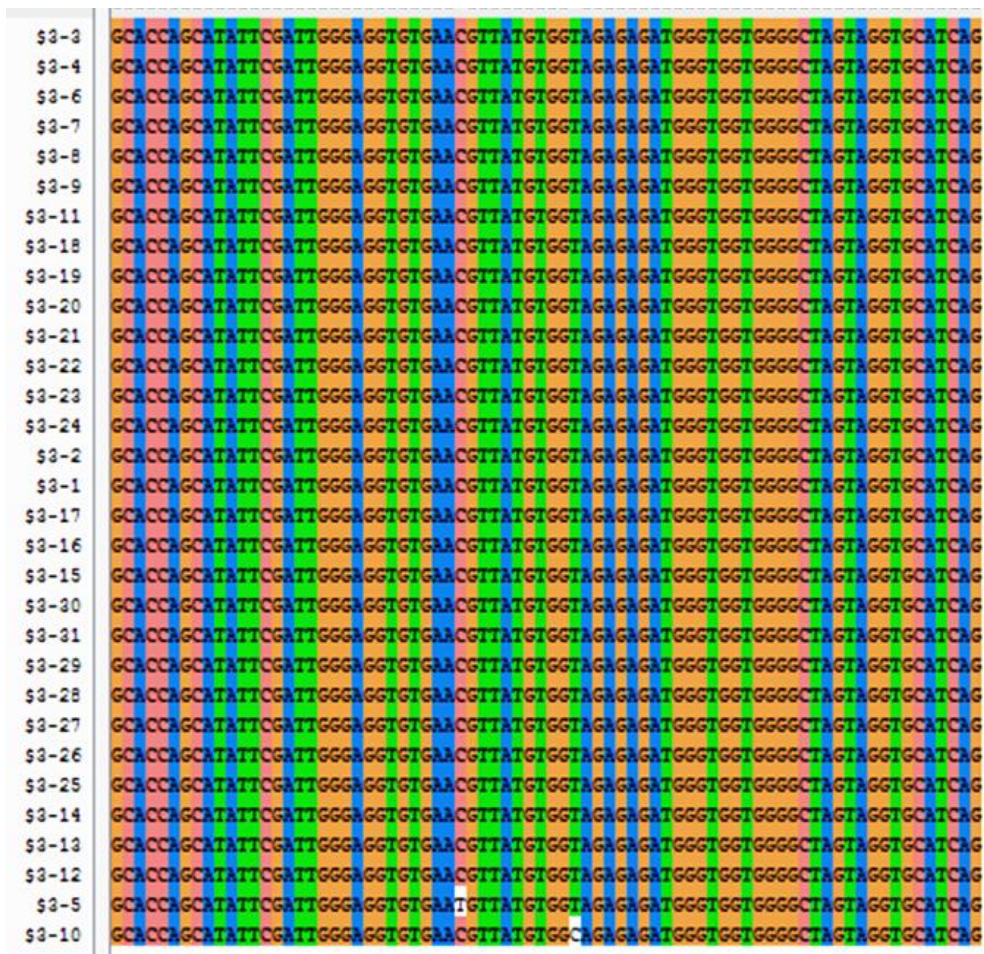
```

$2-1 GCACCAGCATAATTCGATTGGGAGGCGGGGGAGAGTAGTGGGGAACGGTGGAG--AGTTGG-G-CTAGTAGGTGCATCAG
$2-19 GCACCAGCATAATTCGATTGGGAGGCGGGGGAGAGTAGTGGGGAACGGTGGAG--AGTTGG-G-CTAGTAGGTGCATCAG
$2-23 GCACCAGCATAATTCGATTGGGAGGCGGGGGAGAGTAGTGGGGAACGGTGGAG--AGTTGG-G-CTAGTAGGTGCATCAG
$2-17 GCACCAGCATAATTCGATTGGGAGGCGGGGGAGAGTAGTGGGGAACGGTGGAG--AGTTGG-G-CTAGTAGGTGCATCAG
$2-10 GCACCAGCATAATTCGATTGGGAGGCGGGGGAGAGTAGTGGGGAACGGTGGAG--AGTTGG-G-CTAGTAGGTGCATCAG
$2-13 GCACCAGCATAATTCGATTGGGAGGCGGGGGAGAGTAGTGGGGAACGGTGGAG--AGTTGG-G-CTAGTAGGTGCATCAG
$2-16 GCACCAGCATAATTCGATTGTG-GGG-GGTTGTGAAGGGTGGAGTATGGTCGTCTTGGTTGG-G-CTAGTAGGTGCATCAG
$2-18 GCACCAGCATAATTCGATTGTG-GGG-GGTTGTGAAGGGTGGAGTATGGTCGTCTTGGTTGG-G-CAAGTAGGTGCATCAG
$2-15 GCACCAGCATAATTCGATTGTG-GGG-GGTTGTGAAGGGTGGAGTATGGTCGTCTTGGTTGG-G-CTAGTAGGTGCATCAG
$2-24 GCACCAGCATAATTCGATTGTG-GGG-GGTTGTGAAGGGTGGAGTATGGTCGTCTTGGTTGG-G-CTAGTAGGTGCATCAG
$2-25 GCACCAGCATAATTCGATTGTG-GGG-GGTTGTGAAGGGTGGAGTATGGTCGTCTTGGTTGG-G-CTAGTAGGTGCATCAG
$2-26 GCACCAGCATAATTCGATTGTG-GGG-GGTTGTGAAGGGTGGAGTATGGTCGTCTTGGTTGG-G-CTAGTAGGTGCATCAG
$2-9 GCACCAGCATAATTCGATTGTG-GGG-GGTTGTGAAGGGTGGAGTATGGTCGTCTTGGTTGG-G-CTAGTAGGTGCATCAG
$2-14 GCACCAGCATAATTCGATTGTG-GGG-GGTTGTGAAGGGTGGAGTATGGTCGTCTTGGTTGG-G-CTAGTAGGTGCATCAG
$2-12 GCACCAGCATAATTCGATTGTG-GGG-GGTTGTGAAGGGTGGAGTATGGTCGTCTTGGTTGG-G-CTAGTAGGTGCATCAG
$2-8 GCACCAGCATAATTCGATTGTG-GGG-GGTTGTGAAGGGTGGAGTATGGTCGTCTTGGTTGG-G-CTAGTAGGTGCATCAG
$2-6 GCACCAGCATAATTCGATTGTG-GGG-GGTTGTGAAGGGTGGAGTATGGTCGTCTTGGTTGG-G-CTAGTAGGTGCATCAG
$2-4 GCACCAGCATAATTCGATTGTG-GGG-GGTTGTGAAGGGTGGAGTATGGTCGTCTTGGTTGG-G-CTAGTAGGTGCATCAG
$2-7 GCACCAGCATAATTCGATTGTG-GGG-GGTTGTGAAGGGTGGAGTATGGTCGTCTTGGTTGG-G-CTAGTAGGTGCATCAG
$2-3 GCACCAGCATAATTCGATTGTG-GGG-GGTTGTGAAGGGTGGAGTATGGTCGTCTTGGTTGG-G-CTAGTAGGTGCATCAG
$2-22 GCACCAGCATAATTCGATTCCGGGGGATTAAAGCGGAGTGT-GGAGACCGCTCGTG-TGG--GGCTAGTAGGTGCATCAG
$2-27 GCACCAGCATAATTCGATT-GAGGTGGICTTAGGGGCAGTGT-CTATGATGTGGTA-TGGG--GGCTAGTAGGTGCATCAG
$2-2 GCACCAGCATAATTCGATTGGC-GTG-GATTGTATTGGATGGCGAGCGGAGGTGGCGTTGGG-G-CTAGTAGGTGCATCAG
$2-11 GCACCAGCATAATTCGATTGGG---AGGTGTGAACGTTATGTGCTAGAGAGATGGGTGCTGG-GGCTAGTAGGTGCATCAG
$2-20 GCACCAGCATAATTCGATTGGG---AGGTGTGAACGTTATGTGCTAGAGAGATGGGTGCTGG-GGCTAGTAGGTGCATCAG
$2-5 GCACCAGCATAATTCGATTGTI-GTAGTAGGGCCGATGTTG--TTTAGGAAGTGGGGGGGG-GGCTAGTAGGTGCATCAG
$2-21 GCACCAGCATAATTCGATTG---GGGGTTAATGGGAGTTAG-CTTGGGATCGGGTCCGGAGGCTAGTAGGTGCATCAG

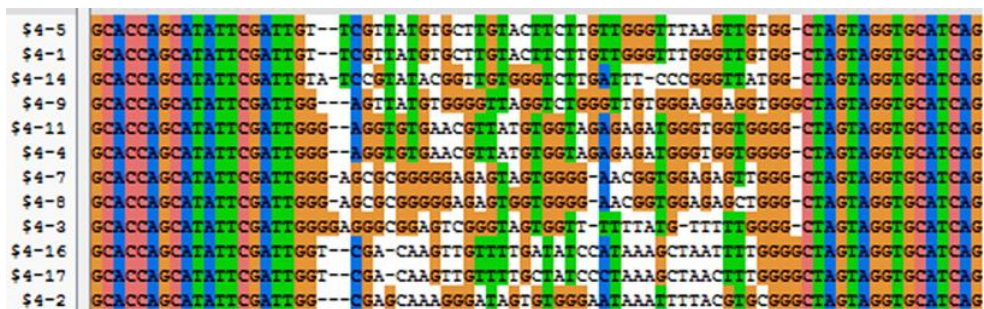
```

**Appendix Fig. 2. Sequence alignment of oligonucleotides in fraction 2 after 16 SELEX rounds**

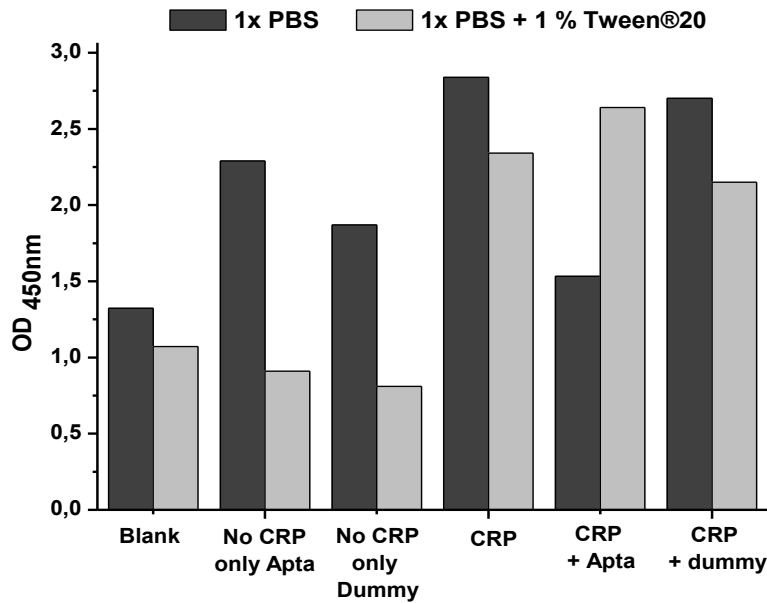




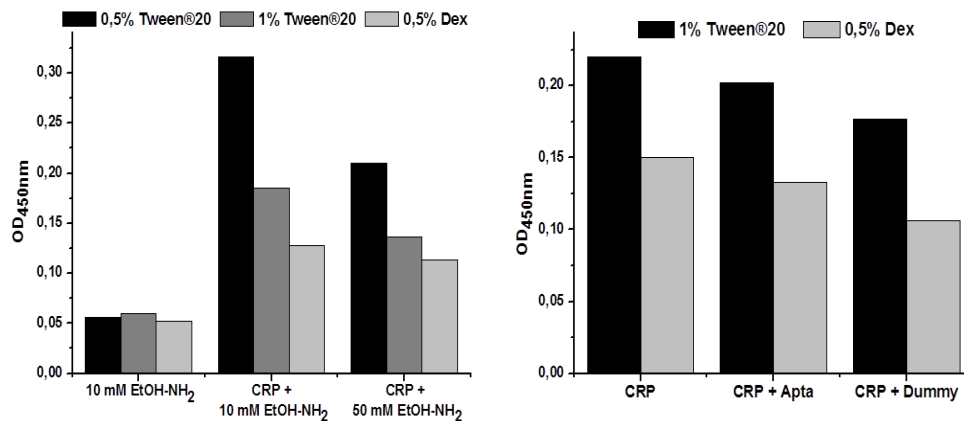
**Appendix Fig. 3. Sequence alignment of oligonucleotides in fraction 3 after 16 SELEX rounds**



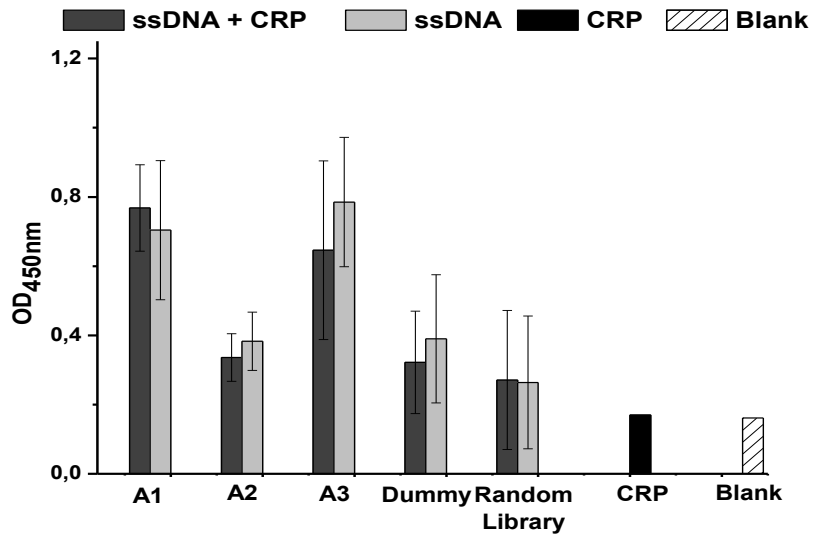
**Appendix Fig. 4. Sequence alignment of oligonucleotides in fraction 4 after 16 SELEX rounds**



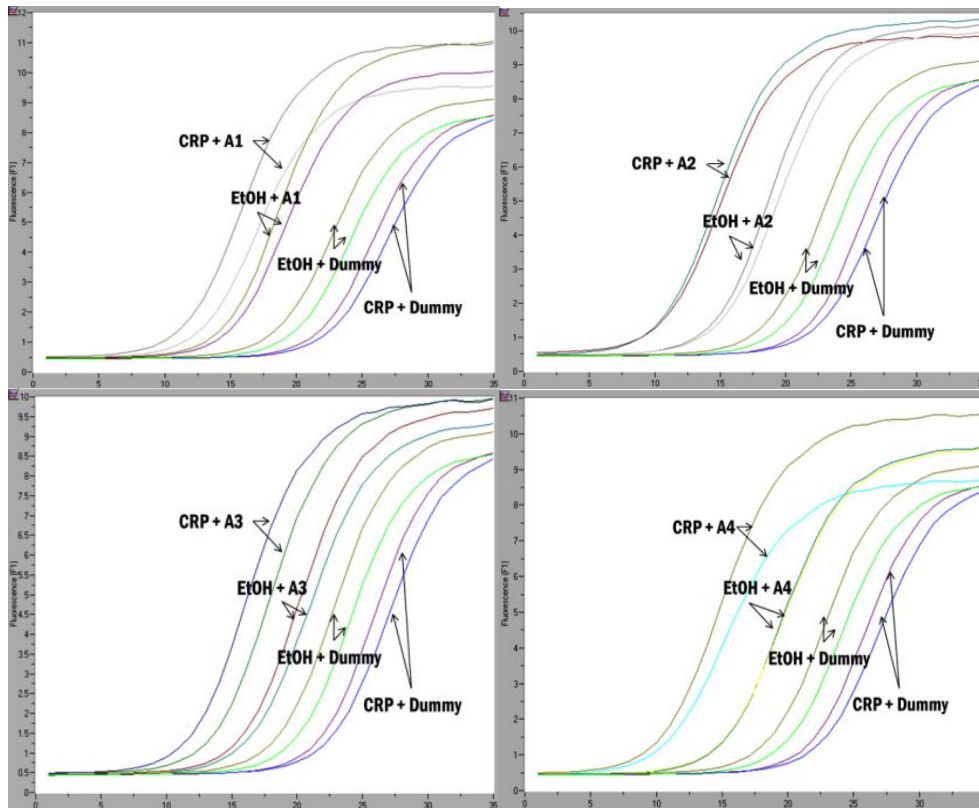
**Appendix Fig. 5. UV/Vis absorbance measurement (at 450 nm) after SA-HRP detection of biotinylated aptamer A1 and dummy sequence incubated on CRP-immobilized plates with triple washing (1x PBS and 1x PBS + 1% Tween@20). Measurements with other selected aptamers A2, A3 and A4 give similar results.**



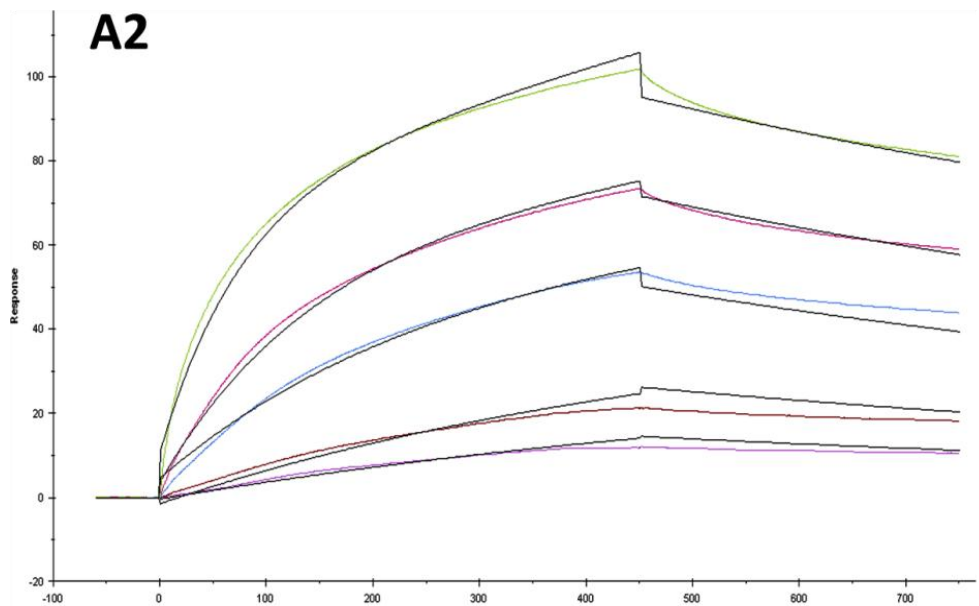
**Appendix Fig. 6. Left: Interaction of SA-HRP and CRP with different washing conditions (1x PBS + 0.5 and 1 % Tween@20; 1x PBS + 0.5% Dextran sulfate) and 10 mM and 50 mM ethanolamine addition during incubation. Right: The effect of washing with 1x PBS + 1% Tween@20 or 0.5% dextran sulfate on CRP-ssDNA interaction and CRP-SA-HRP interaction. Experiments performed with aptamer A3. Experiments with aptamers A1, A2 and A4 give similar results.**



**Appendix Fig. 7. Absorbance read at 450 nm of CRP detection by HRP-conjugated mAbs for CRP, bound on selected aptamers A1, A2 & A3 and non-selected ssDNA in Nunc™ Immobilizer plates (n = 3). Error bars are standard deviations of the calculated mean absorbance values.**

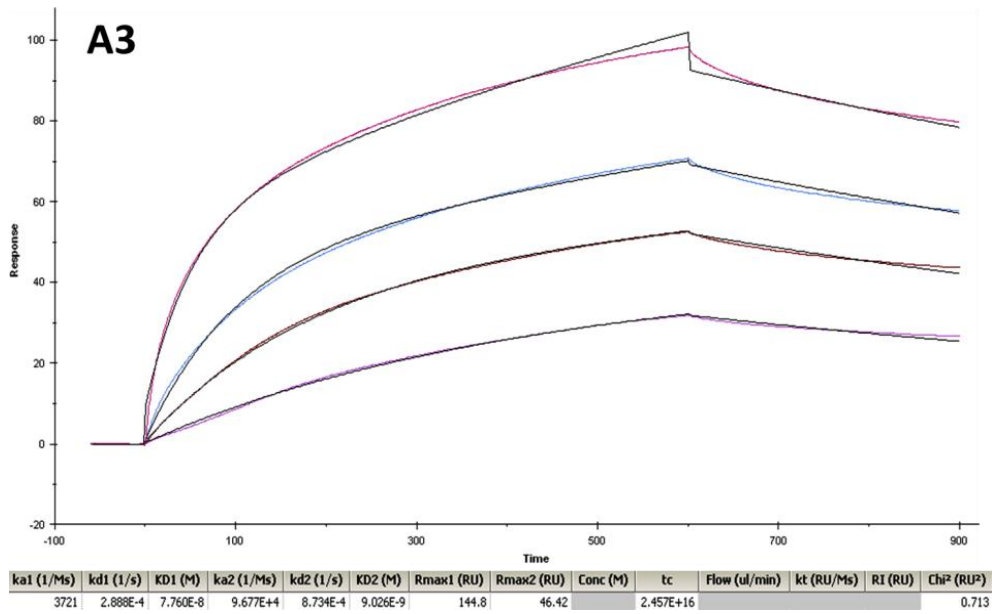


**Appendix Fig. 8. RT-PCR amplification curves of 83pM selected aptamers A1-A4 vs dummy sequence incubated on CRP vs ethanolamine coated NucleoLink™ plates.**

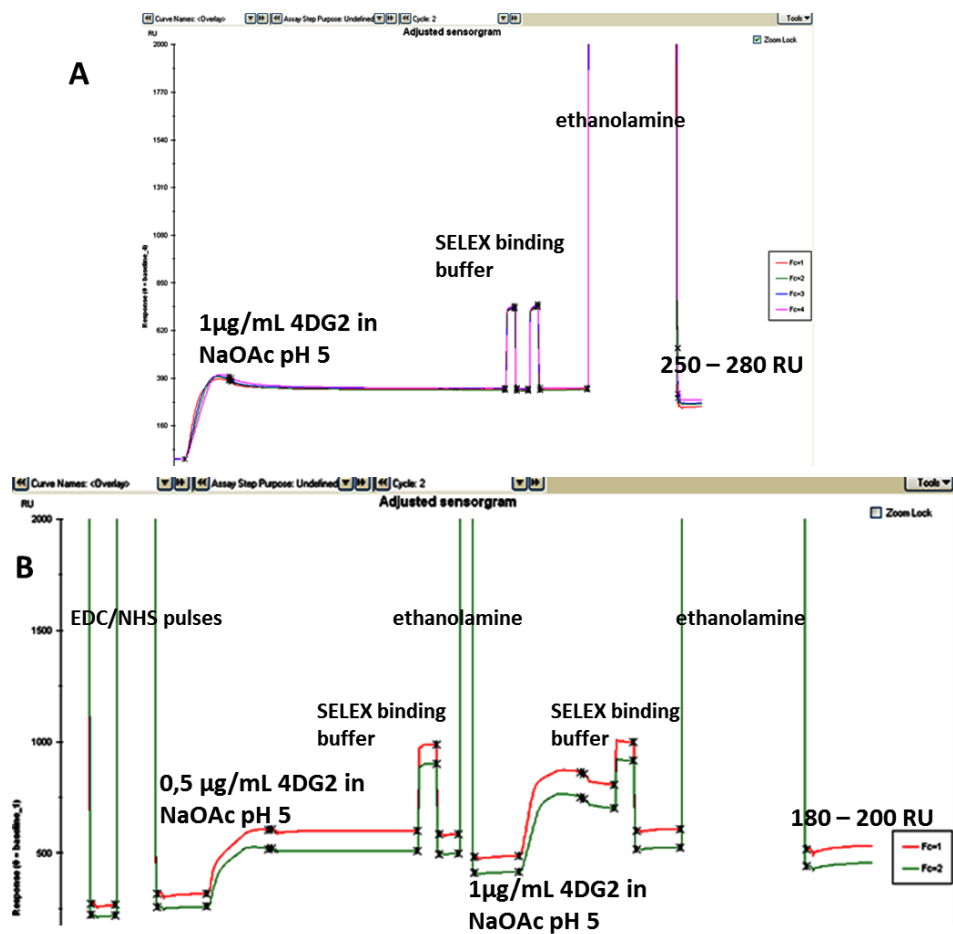


Time													
ka1 (1/Ms)	kd1 (1/s)	KD1 (M)	ka2 (1/Ms)	kd2 (1/s)	KD2 (M)	Rmax1 (RU)	Rmax2 (RU)	Conc (M)	tc	Flow (ul/min)	kt (RU/Ms)	RI (RU)	Chi² (RU²)
2650	1.634E-6	6.165E-10	6.276E+4	0.001042	1.661E-8	176.0	62.70		6.747E+8				3.49

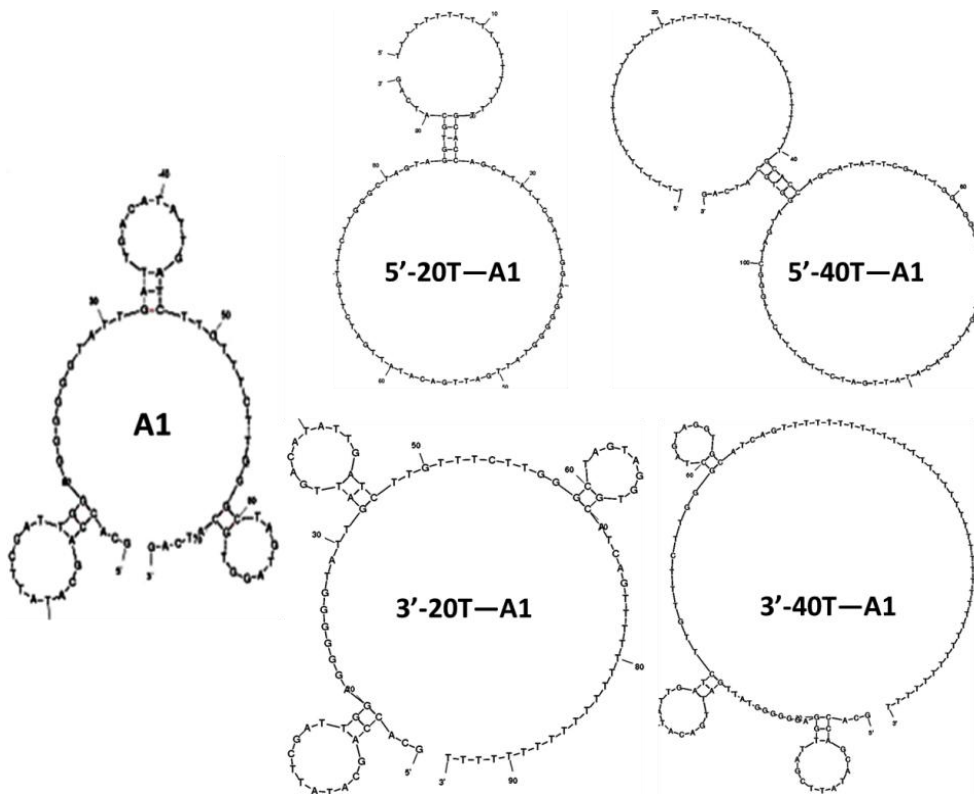
**Appendix Fig. 9. Multi-cycle kinetic analysis of 600s association and 300s dissociation of different concentrations (20-50-100-200 nM) of A2 in SELEX binding buffer on CRP-coated CM4-chip. Data fitting with model for heterogeneous ligand indicates two  $K_d$  values:  $K_{d1}=0.62\text{nM}$  and  $K_{d2}=16.6\text{nM}$  (Chi-square value is  $3.49\text{ RU}^2$ )**



**Appendix Fig. 10. Multi-cycle kinetic analysis of 600s association and 300s dissociation of different concentrations (20-50-100-200 nM) of A3 in SELEX binding buffer on CRP-coated CM4-chip. Data fitting with model for heterogeneous ligand indicates two  $K_d$  values:  $K_{d1}=77.6\text{nM}$  and  $K_{d2}=9.0\text{nM}$  (Chi-square value is  $0.71\text{ RU}^2$ )**



**Appendix Fig. 11. Immobilization optimization of mAb 4DG2. (A) 1 µg/mL mAb incubation results in rapid immobilization. (B) More controlled immobilization of mAb by incubation of lower concentrations in pulses on EDC/NHS activated C1 flow cells.**



**Appendix Fig. 12. Structure prediction of extended A1 sequences in mfold indicate 5'-extensions having a larger impact on secondary structure that 3' modifications. The 3'-40T extension is chosen for application.**



## Appendix B: Buffer and reagent list

### EDC/NHS coupling buffer: MES pH 6 (pH adjusted with HCL and NaOH)

25 mM MES:

*5.3 g MES (2-[N-morpholino]ethane sulfonic acid) / 1L*

100 mM MES:

*21.3 g MES (2-[N-morpholino]ethane sulfonic acid) / 1L*

### Coatingsbuffer: Sodium Bicarbonate Buffer pH 9.6

100 mM Na<sub>2</sub>CO<sub>3</sub> • 10H<sub>2</sub>O pH 9.6:

*Mix of 300 mL 0.1 M Na<sub>2</sub>CO<sub>3</sub> + 700 mL 0.1 M NaHCO<sub>3</sub>*

0.1M-solution contains 28.62 g/l

### 1x PBS: phosphate buffered saline pH 7.4 (pH adjusted with HCL and NaOH)

*8 g NaCl + 0.2 g KCl + 1.44 g Na<sub>2</sub>HPO<sub>4</sub> + 0.24 g K<sub>2</sub>HPO<sub>4</sub> in 1 L MQ, pH adjusted*

### 1x TBS: Tris buffered saline pH 7.4 (pH adjusted with HCL and NaOH)

50 mM Tris-HCl + 150 mM NaCl:

*6.05 g Tris + 8.76 g NaCl in 1 L MQ*

### 1x PBST / TBST: 1x PBS/TBS + 0.5 % Tween® 20 (Polyoxyethylenesorbitan monolaurate)

### CRP-buffer, pH 8

*20 mM Tris-HCl + 280 mM NaCl + 5 mM CaCl<sub>2</sub> + 0.09 % NaN<sub>3</sub>*

### SELEX binding buffer:

*10 mM HEPES + 5 mM CaCl<sub>2</sub>, pH 7.4*

### SELEX elution buffer:

1x TE-buffer + 2M urea pH 8:

*10mM Tris-HCL + 2mM EDTA + 2 M urea*

### AB conjugation buffer:

*1x PBS + 0.01 % Tween®20 + 0.05% BSA*

### Electrophoresis buffer:

1x TAE + 4% agarose:

*4.84 g Tris-Base + 1.14 mL glacial acetic acid + 0.37 g EDTA + 4% agarose*

### Crush & Soak buffer:

*300 mM C<sub>2</sub>H<sub>3</sub>NaO<sub>2</sub> + 500 mM NH<sub>4</sub>C<sub>23</sub>O<sub>2</sub> + 1 mM EDTA + 0.1 % SDS*

### Agar medium:

*32 g/L LB Broth with agar + 0.1 % X-Gal and Ampicillin*

### Growth medium:

*20 g/L LB Broth + 0.1 % Ampicillin*

### 2x SSC + 0.5 % SDS:

*300 mM NaCl + 30 mM Na<sub>3</sub>C<sub>6</sub>H<sub>5</sub>O<sub>7</sub> + 0.5 % SDS*

**10x PCR pH 8.3**

*15 mM MgCl<sub>2</sub> + 500 mM KCl + 100 mM Tris-HCl*

**1x HBS: HEPES buffered saline pH 7.4:**

*0.01 M HEPES + 0.15 M NaCl + 3 mM EDTA*

**Thrombin Running buffer:**

*50 mM Tris-HCl + 100 mM NaCl + 1 mM MgCl<sub>2</sub> pH 7.5*

**Sodium Acetate buffer pH 5**

*Mix of 700 mL 0.2 M NaOAc and 300 mL 0.2M HOAc (27.22 g/L)*



